KTH Industrial Engineering and Management

Secondary Fluids Impact on Ice Rink Refrigeration System Performance

Willem

Mazzotti

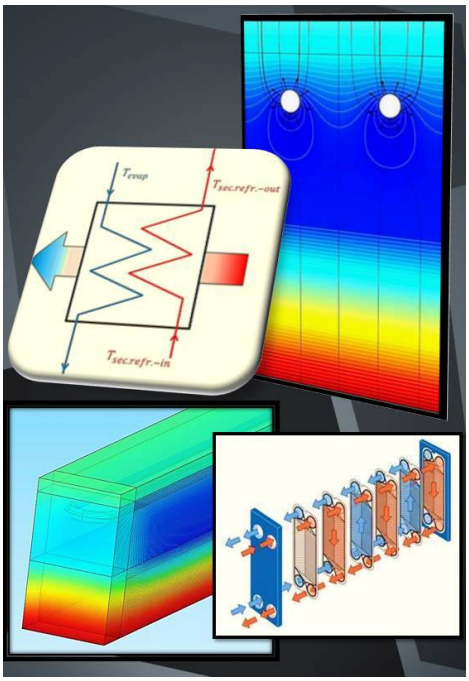

Master of Science Thesis

KTH School of Industrial Engineering and Management
Energy Technology EGI-2013-156MSC
Division of Applied Thermodynamics and Refrigeration
SE-100 44 STOCKHOLM

Master of Science Thesis EGI 2013: 156MSC

KTH Industrial Engineering and Management

Secondary Fluids Impact on Ice Rink Refrigeration System Performance

Willem Mazzotti

Approved	Examiner	Supervisor
2014-01-27	Björn Palm	Monika Ignatowicz
	Commissioner	Contact person

ABSTRACT

Sweden has 350 ice rinks in operation which annually use approximately 1000 MWh each. The refrigeration system usually accounts for about 43 % of the total energy consumption which is the largest share of the major energy systems. Besides improving the facilities one-by-one, it is important to distinguish common features that will indicate the potential energy saving possibilities for all ice rinks. More than 97 % of the Swedish ice rinks use indirect refrigeration systems with a secondary fluid. Moreover, the thermo-physical properties of secondary fluids directly impact the heat transfer and pressure drop. Thus, assessing and quantifying their influence on the refrigeration system performance is important while estimating the energy saving potential for the ice rinks.

A theoretical model as well as two case studies focusing on the importance of the secondary fluid choice are investigated. The theoretical model calculations are performed assuming the steady-state conditions and considering a fixed ice rink design independently on the secondary fluid type. Hence, they can be compared on the same basis. According to this theoretical model, the refrigeration efficiency ranking starting from the best to the worst for secondary fluid is: ammonia; potassium formate; calcium chloride; potassium acetate; ethylene glycol; ethyl alcohol; and propylene glycol. Secondary fluids can be ranked in exactly the same order starting from the lowest to the highest value in terms of the dynamic viscosity. It was shown that potassium formate has the best heat transfer properties while ammonia leads to the lowest pressure drops and pumping power. Propylene glycol shows the worst features in both cases. Ammonia and potassium formate show respectively 5% and 3% higher COP than calcium chloride for typical heat loads of 150 kW. When controlling the pump over a temperature difference ΔT, the existence of the optimum pump control or optimum flow was highlighted. For common heat loads of 150 kW this optimum pump control ΔT is around 2,5 K for calcium chloride while it is around 2 K for ammonia. It is shown that the secondary fluids having laminar flow in the ice rink floor pipes have a larger share in the convection heat transfer resistance (~20-25 %) than the secondary fluids experiencing turbulent flow (~3 %).

One of the case studies shows a potential energy saving of 12 % for the refrigeration system when increasing the freezing point of the secondary fluid. An energy saving of 10,8 MWh per year was found for each temperature degree increase in the secondary fluid freezing point.

KEYWORDS

Ice rink, secondary fluid, refrigeration system, thermo-physical properties, heat transfer, pressure drop, model

ACKNOWLEDGEMENTS

For her patience, help, support and availability I would like to thank Monika Ignatowicz who has supervised this work at the Applied Thermodynamics and Refrigeration Division at Royal Institute of Technology (KTH).

Special thanks to Jörgen Rogstam for the valuable and numerous advices kindly given during this thesis. I am also very grateful towards him for financing this project via his company Energi & Kylanalys.

I also would like to express my gratitude to Dr. Carmen Vasile-Muller who was my supervisor at the National Institute of Applied Science (INSA) of Strasbourg.

I am grateful to Chadi Beaini from Energi & Kylanalys for helping me with *COMSOL Multiphysics software*.

Thank you to Göran Hammarson from the company Alfa Laval for introducing and letting me use one of the company's calculation software.

Many thanks to all the people in the KTH Applied Thermodynamics and Refrigeration division who made this project a pleasant time.

My last thanks go to my family, friends and Elena for supporting me during this thesis work.

Table of Contents

INDEX OF FIGURES

INDEX OF TABLES

NOMENCLATURE

A	Cross sectional area	m^2
$A_{ceiling}$	Ceiling area	m^2
A_{ht}	Heat transfer area	m^2
A_{ice}	Ice pad surface	m^2
b	Pressing depth	m
$\overline{C_{p,0-T_{ice}}}$	Mean specific heat cap. of water between 0°C and T_{ice}	$J.kg^{-1}.K^{-1}$
$\overline{C_{p,T_f-0}}$	Mean specific heat cap. of water between T_f and 0°C	$J.kg^{-1}.K^{-1}$
$\bar{c}$	Mean molecular speed	$m.s^{-1}$
c_f	Fanning friction factor	-
C_p	Specific heat capacity	$J.kg^{-1}.K^{-1}$
$CaCl_2$	Calcium chloride – water secondary fluid	-
CC	Cooling capacity	W
COP	Coefficient Of Performance	-
COP_{is}	Coefficient Of Performance for isentropic compression	-
COP_{pure}	Coefficient Of Performance for pure secondary fluid	
COP_{real}	Coefficient Of Performance for real secondary fluid	
COP_{refr}	Coefficient Of Performance of the refrigeration system	-
d_h	Hydraulic diameter	M
D_{in}	Inner diameter	m
D_{port}	Port diameter	m
$D_{spacing}$	Spacing distance between consecutives pipes	m
DHW	Domestic Hot Water	-
DX	Direct expansion	-
$\dot{E}_{p,header}$	Pumping power associated with header	W
$\dot{E}_{comp}$	Compressor power	W
e_{pump}	Pump efficiency	-
EA	Ethyl alcohol – water secondary fluid	
EG	Ethylene glycol – water secondary fluid	-
f	Moody friction factor	-
f_{ci}	Gray body configuration factor	-
F_{ci}	View factor (radiation)	-
F_p	Freezing point	°C
G	Mass flux	$kg.m^{-2}.s^{-1}$
Gz	Graetz number	-
h	Convection heat transfer coefficient	$W.m^{-2}.K^{-1}$
$h_{sec.fl.}$	Convection heat coefficient of the secondary fluid	$W.m^{-2}.K^{-1}$
h_{boil}	Boiling hea transfer coefficient	$W.m^{-2}.K^{-1}$
h_{cd}	Condensation heat transfer coefficient	$W.m^{-2}.K^{-1}$
$h_{comp,in/out}$	Enthalpy of the refrigerant before/after compressor	$J.kg^{-1}$
h_{cv}	Convection heat transfer coefficient	$W.m^{-2}.K^{-1}$
h_g	Enthalpy at saturated vapor state	$J.kg^{-1}$
h_l	Enthalpy at saturated liquid state	$J.kg^{-1}$
h_{lg}	Latent heat of evaporation	$J.kg^{-1}$
$h_{subcool}$	Enthalpy of the subcooled fluid	$J.kg^{-1}$
$h_{superheat}$	Enthalpy of the superheated fluid	$J.kg^{-1}$

K	Minor loss coefficient	-
k	Thermal conductivity	$W.m^{-1}.K^{-1}$
k_l	Thermal conductivity at saturated liquid state	$W.m^{-1}.K^{-1}$
k_{ice}	Thermal conductivity of ice	$W.m^{-1}.K^{-1}$
k_{plate}	Thermal conductivity of plates	$W.m^{-1}.K^{-1}$
$K-acetate$	Potassium acetate – water secondary fluid	-
$K-formate$	Potassium formate – water secondary fluid	-
L	Length	m
L_{comp}	Compressor losses	W
L_{Cr}	Rotor core or iron losses	W
L_{Cs}	Stator core or iron losses	W
L_{eff}	Effective channel length	m
L_{fc}	Frequency converter losses	W
L_{Jr}	Rotor Joule losses	W
L_{Js}	Stator Joule losses	W
$LMTD$	Log Mean Temperature Difference	K
m	Mass	kg
$\dot{m}$	Mass flow	$kg.s^{-1}$
$\dot{m}_{tot}$	Total mass flow	$kg.s^{-1}$
M_{H_20}	Molar mass of water	$g.mol^{-1}$
M_{air}	Molar mass of air	$g.mol^{-1}$
$N_{U-pipes}$	Number of U-pipes	-
N_C	Number of channels	-
N_P	Number of plates	-
N_{pass}	Number of pass in PHE	-
NH_3	Ammonia – water secondary fluid	-
Nu	Nusselt number	-
P	Atmospheric pressure	Pa
P	Wet perimeter	m
P_0	Reference pressure	Pa
P_{crit}	Critical pressure	Pa
P_{elec}	Electrical power	W
P_m	Mechanical power provided to the compressor shaft	W
P_{refr}	Effective power provided to the refrigerant	W
P_s	Power provided to the stator	W
P_{sat}	Saturation pressure	Pa
$P_{sat,ice}$	Saturation pressure at the ice temperature	Pa
P_T	Triple point pressure	Pa
P_{tr}	Power transmitted to the rotor (from the stator)	W
P_v	Vapor partial pressure	Pa
PG	Propylene glycol – water secondary fluid	-
PHE	Plate Heat Exchanger	-
Pr	Prandtl number	-
$\dot{q}$	Internal heat generation rate	$W.m^{-2}$
$\dot{Q}$	Heat flow / Cooling capacity	W
$\bar{\dot{Q}}_{resurfacing}$	Average ice resurfacing heat flow	kW
$\dot{Q}_0$	Cooling capacity	W

$\dot{Q}_{condensation}$	Condensation heat flow	W
$\dot{Q}_{conduction}$	Conduction heat flow	W
$\dot{Q}_{convection}$	Convection heat flow	W
$\dot{Q}_{radiation}$	Radiation heat flow	W
R	Heat transfer resistance	$K.W^{-1}$
R	Distance between surfaces (radiation)	m
r	Bend radius	m
$R_{ice-floor}$	Ice rink floor total resistance	$K.W^{-1}$
R_{cond}	Conduction heat transfer resistance	$K.W^{-1}$
R_v	Vapor gas constant	$J.kg^{-1}.K^{-1}$
R^2	Coefficients of determination of the least square method	-
Re	Reynolds number	-
Re_l	Reynolds number at saturated liquid state	-
RTD	Resistance Temperature Detector	-
T	Temperature	°C or K
t	Time taken to solidify the water	s
T_{air}	Air temperature	°C
T_{av}	Secondary fluid average temperature	°C
$T_{ceiling}$	Ceiling temperature	K
T_{evap}	Evaporation temperature	
T_f	Temperature of flooded water	°C
T_{ice}	Ice temperature	°C or K
$T_{sec.fl.-in/out}$	Secondary fluid temperature in or out the evaporator	°C or K
T_T	Triple point temperature	K
U	Overall heat transfer coefficient	$W.m^{-2}.K^{-1}$
u	Velocity	$m.s^{-1}$
V	Volume	m^3
$\dot{V}$	Volume flow	$m^3.s^{-1}$
V_{air}	Air velocity	$m.s^{-1}$
$\dot{V}_{tot}$	Total volume flow	$m^3.s^{-1}$
V_f	Total volume of flooded water	m^3
v_l	Specific volume at saturated liquid state	$m^3.kg^{-1}$
W	Plate width	m
W_{ice}	Ice width	m
$x_{fd,h}$	Hydraulic entry length	m
$x_{fd,max}$	Maximum thermal and hydraulic entry length	m
y	Corrugation function	m
β	Reverse chevron angle	°
δ	Inverted mass transfer coefficient	$s.m^{-1}$
δ	Plate thickness	m
Δh	Enthalpy difference	$J.kg^{-1}$
Δh_{fusion}	Water latent heat of fusion	$J.kg^{-1}$
Δp	Pressure drop	Pa
Δp_f	Major head loss	Pa
Δp_{header}	Pressure drop in a header	Pa
Δp_{ports}	Pressure drop in the PHE ports	Pa
Δp_s	Minor head loss	Pa

ΔT	Temperature difference	K
ΔT	Temperature difference (pump control)	K
ΔT_{LMTD}	Log mean temperature difference	K
$\varepsilon_{ceiling}$	Ceiling emissivity factor (radiation)	-
ε_{ice}	Ice emissivity factor (radiation)	-
η_{el}	Electrical efficiency	-
θ	Bend angle	°
Λ	Corrugation pitch	m
λ_{mfp}	Molecular mean free path	m
μ	Dynamic viscosity	Pa.s
μ_l	Dynamic viscosity at saturated liquid state	Pa.s
μ_w	Viscosity at the wall temperature	Pa.s
ν	Kinematic viscosity	$m^2.s^{-1}$
ρ	Density	$kg.m^{-3}$
σ	Stefan Boltzmann's constant	$W.m^{-2}.K^{-4}$
τ	Shear stress	$N.m^{-2}$
Φ	Surface enlargement factor	-
Φ	Heat flow	W
φ	Chevron angle	°
φ	Relative humidity	%

1 INTRODUCTION

In a worldwide society where energy is increasingly used, reducing global energy consumptions has become a necessity. While constantly trying to discover smarter and more sustainable ways of producing energy, refrigeration systems have become a matter of concern for industrial and household applications. Therefore, the optimization and reliability of refrigeration systems used in different applications need to be investigated (Granryd, et al., 2011).

Amongst those applications, ice rinks must be particularly considered since they present high annual energy consumptions. In Sweden, ice rinks use around 1000 MWh per year, and refrigeration accounts for the largest energy share as shown in Figure 1 (Rogstam, 2010). Moreover, the energy saving potential can be significant and more detailed investigations of different ice rink refrigeration systems need to be performed.

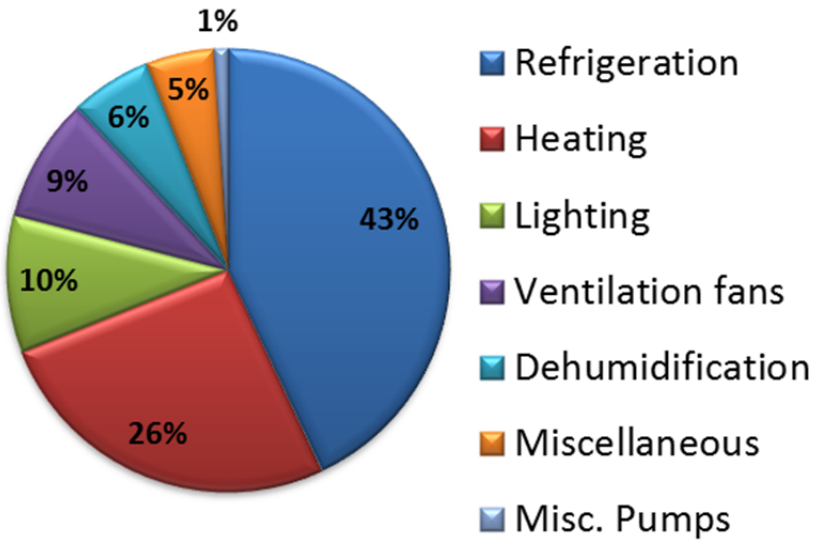

Figure 1: Energy consumption shares in ice rinks (Rogstam, 2010)

In 2010, around 6700 indoor ice rinks have been recorded all over the world. Countries having most ice rinks are Canada and United States of America with 2703 and 2500 facilities, respectively (IIHF, 2010). 352 ice rinks are currently in operation in Sweden and the number is still growing. Altogether, those ice rinks account for 300 GWh.yr^{-1}. According to the figures given by the International Energy Agency (2008), it represents around 1,2 % of the total energy used for public and commercial services. That is a significant part considering the low amount of ice rinks in comparison to other commercial and public facilities.

In order to estimate the ice rinks' energy saving potential in Sweden, a project called *STOPPSLADD* has been developed. The *STOPPSLADD*´s aim is to gather useful information and data; and to expand the know-how base about ice rink refrigeration systems. The *STOPPSLADD* project particularly focuses on the ice hockey arenas. Data from hundreds of ice rinks have been collected within the project scope including building design; site information; ice rink floor; heating; ventilation and air-conditioning system; lighting and cooling system (Makhnatch, 2011). Due to the fact that each ice rink's refrigeration system is different, as many ice rinks as possible should be included in study so that every system type is overviewed. Thus, the statistical data base and overall design information can be as complete as possible.

Besides improving the ice rink refrigeration system designs one-by-one, it is essential to find a common feature applicable to all ice rinks which would help in decreasing their energy consumption. Therefore, secondary fluids' thermo-physical properties have become significant to estimate more accurately the

performance of refrigeration systems. Indeed, as it will further be explained in chapter 2, most of those systems are indirect type. A refrigeration system is characterized as indirect when the refrigerant does not chill directly the cooling target or heat source. This implies the use of another medium or fluid which carries heat from the heat source to the refrigeration unit. Many terms have been employed to describe this fluid such as *secondary working fluid, brine, secondary fluid, secondary coolant, secondary fluid, heat carrier, heat transfer fluid,* and *antifreeze* (Marvillet, 2003; Melinder, 2007). Since this thesis focuses on the refrigeration side of ice rinks, the term *secondary fluid* will be used when referring to the fluid circulating from the heat source to the cooling machine. This is one of the terms used by the International Institute of Refrigeration (IIR).

The thermo-physical properties of secondary fluids impact directly the heat transfer and pressure drop phenomena.

1.1 Objectives

The objectives of this study may be split into several sub-objectives:

- Reveal the energy saving potential associated with secondary fluids in the ice rinks
- Analyze the heat transfer and pressure drop related to different secondary fluids used for the ice rink application
- Evaluate the influence of the secondary fluids' thermo-physical properties in both theory and case studies
- Find control strategy of the real ice rink refrigeration systems
- Compare theoretical and case study results

1.2 Methodology

In order to fulfill the previously mentioned objectives, a theoretical model has been developed and two case studies have been conducted.

The theoretical model allows comparing the different secondary fluids that may be used in the ice rinks. The modeling needs to be as detailed as possible so that the influence of each thermo-physical property can be accurately assessed. The model has been performed using *Microsoft Excel* and its programming interface *Visual Basic* as well as *COMSOL Multiphysics* simulation software.

The two case studies have been conducted using the ClimaCheck tool. It is a performance analyzer measuring parameters (temperatures, pressures, etc.) at different points of the refrigeration systems. From the measurements accessible online, the refrigeration system operations and performance can be evaluated. However, the ClimaCheck analyzer does not allow assessing the influence of the secondary fluid used in the refrigeration system. Therefore, with the kind help of QTF and Energi & Kylanalys samples from the real facilities have been collected. Thus, the thermo-physical properties could be tested in the laboratory and it has been possible to link the refrigeration system performance to secondary fluid properties.

A literature review on the refrigeration systems and secondary fluids used in ice rinks had led to as comprehensive overview as possible.

1.3 Scope and limitations

The scope and limitations of this study are as following:

- The theoretical model developed is suitable only for the steady-state condition.
- A typical refrigeration system design is investigated.
- The control strategies of the compressors and pumps may be further investigated.
- The model is only simulating the refrigeration system.
- Only two case studies have been conducted.
- Some measurements from the real installations were missing.
- Some thermo-physical properties (density, specific heat capacity) were partly or not measured at all.

The scope and limitations of the theoretical comparison are presented in part 4.10.

2 ICE RINK REFRIGERATION SYSTEMS

A multitude of different ice rinks exist. Depending on the main activity taking place in the ice rink, it can be: indoor or outdoor; running half or all year round; with or without grandstands, etc. The main activities held in ice rink buildings are (ASHRAE, 2010):

- Ice hockey
- Curling
- Figure skating
- Speed skating
- Recreational skating
- Public arenas / Auditoriums / Coliseums

Each ice rink has its special features although common features can be found. Figure 2 shows the main geometrical features of a common ice pad used for the ice hockey. The geometrical dimensions are generally the same for all ice rinks. Ice pads will be considered 60 m long and 30 m wide throughout this study, according to the recommendation of the International Ice Hockey Federation (IIHF, 2010). In public arenas though, ice rinks are slightly longer (61 m) than in smaller buildings (IIHF, 2010).

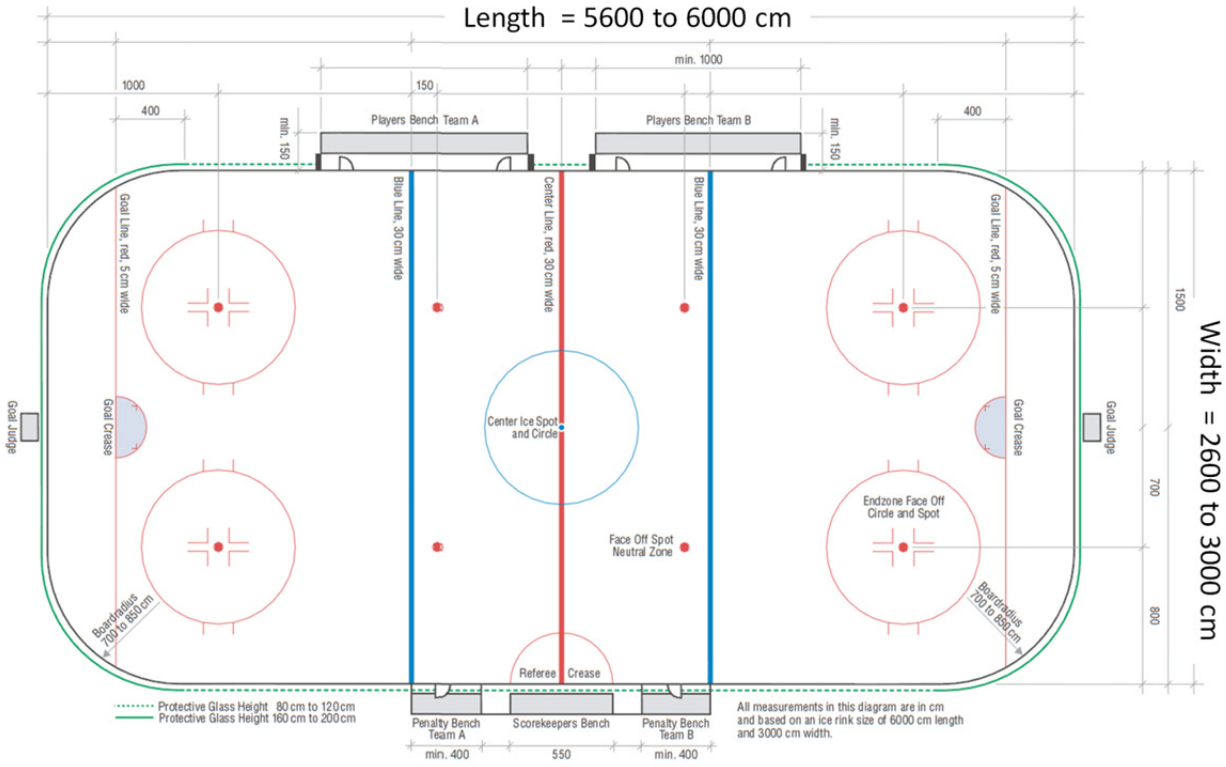

Figure 2: Top view of an ice rink meant for ice hockey and its significant features (IIHF, 2010)

Likewise, energy demands are similar from one ice rink to another but the energy system design and energy consumption may be different. Among the various energy systems used in ice rinks, this study particularly focuses on the refrigeration system. The performance of a general refrigeration system and two case studies are assessed.

The energy consumption, operating costs and maintenance, as well as indoor climate control are common concerns in all ice rinks. Ice rink design and operation are totally unique and differ in many ways from the common residential or office buildings. For instance, indoor temperatures vary from -5°C on the ice pad to 30°C in the ventilation system.

2.1 Energy demand in ice rinks

Figure 1 gives an overview of the different energy needs in ice rinks. Ice rinks are unique since both cooling and heating demands may occur simultaneously. Figure 3 presents the spatial distribution of those demands in the ice rink and the energy system devices that may be used.

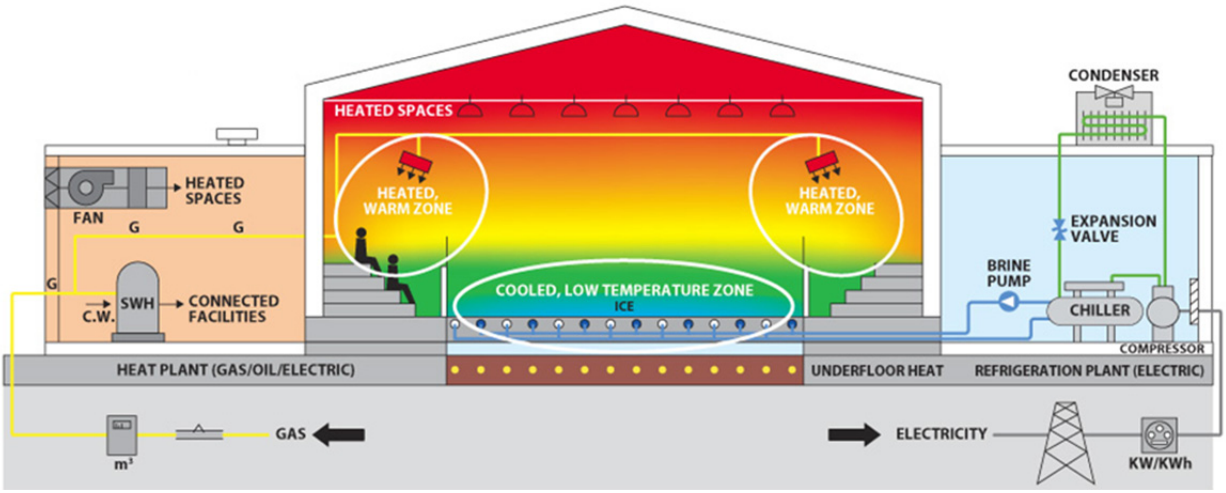

Figure 3: Energy demands and their spatial distribution in ice rinks (RETscreen, 2005)

2.1.1 Cooling demand

The cooling demand is the most important demand, accounting in average for 43% of the total energy consumption due to the fact that around 1800 m² ice surface that needs to be cooled down constantly. The ice temperature can vary between -2°C, for recreational skating, to -7°C, for ice hockey (ASHRAE, 2010). The cooling demand is directly affected by the heat loads and gains which are presented in part 2.3. Reducing the cooling demand is an important step while trying to decrease the overall energy consumption of an ice rink.

The cooling capacity generally reaches 300 to 350 kW. In some cases, one refrigeration system is used to chill two ice rinks simultaneously, one indoor and one outdoor for example. In this case, the total cooling capacity may be even higher. Cooling may also be needed in the dehumidification process, explained in part 2.1.4.

In general, the refrigeration system is an electricity powered vapor compression indirect system. The refrigeration system is further described in part 2.2.

2.1.2 Heating demand

Ice rinks have several heating requirements which all together account for the total heating demand. The heating demand is the second largest energy demand in ice rinks. In a given ice rink the following heating requirements may be found

- Space heating
- Domestic hot water (DHW)
- Ground heating
- Ice resurfacing
- Snow melting

Space heating is needed to provide comfortable temperatures in areas meant to receive public, like the stands. It can be carried out using Heating, Ventilation and Air-Conditioning (HVAC) system or radiating panels installed above the stands for instance. Other public areas such as locker rooms and offices need space heating. The space heating should be sufficient to provide a temperature of 10°C in the stands and 20°C in other public areas (Nguyen, 2012).

Domestic hot water (DHW) is used in all water devices (faucets) that can be found in the bathroom, toilets or other rooms. The heating requirement for DHW depends on the volume of hot water used per day.

Ground heating is necessary to avoid the ground permanent frost, called permafrost, which can cause structural damages to the ice pad and the building (Seghouani, et al., 2011).

Ice resurfacing is a process used to restore the ice surface condition (flatness, gliding friction). Hot water, which temperature is normally between 55 and 80 °C according to ASHRAE (2010), is flooded over the ice sheet. However, temperatures down to 10°C may also be sufficient for the ice resurfacing process (Karampour, 2011). The water used for ice resurfacing needs to be heated up; therefore it is part of the total heating demand.

Snow melting may be a part of the heating demand if a snow melting pit is installed by the ice rink.

The heating device(s) installed to meet the heating requirements may be furnace(s), additional heat pump(s), or other traditional equipment using gas, fuel, electricity or district heating. However the most energy-efficient method is to use the heat rejected by the condensation (and desuperheating) of the refrigeration system (see part 2.2) whenever possible. This heat recovery process can fulfill several heating requirements, sometimes up to 100% of the total need (ASHRAE, 2010). Even high temperature applications can be covered by the heat recovery, using high temperatures available from the desuperheater heat exchanger as shown in Figure 4 (Sawalha & Chen, 2010). This figure emphasizes the condensation and desuperheating processes in a pressure-enthalpy (P, h) diagram. If the desuperheat is not sufficient to fulfill all the high-temperature needs, a cascade solution may be set up with two heat pumps working in parallel.

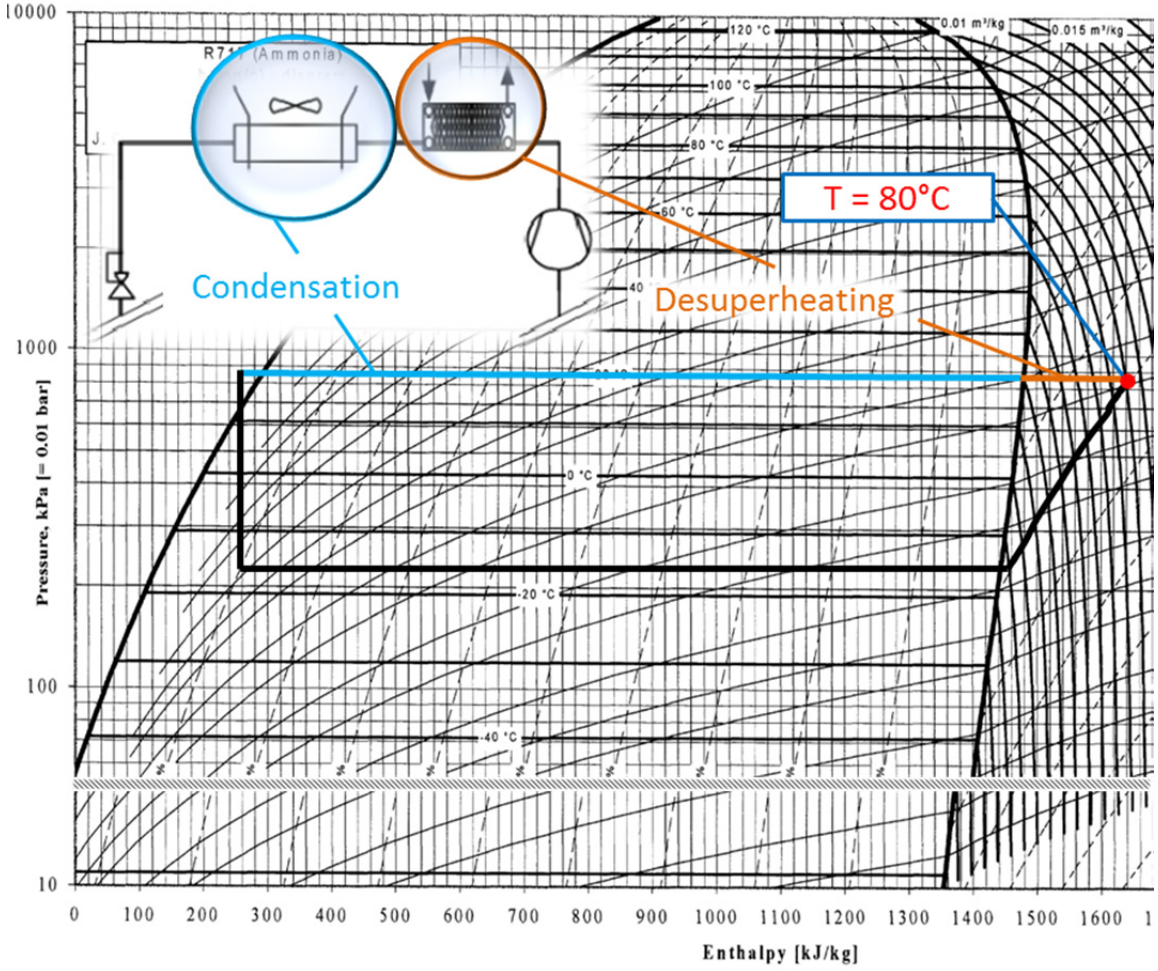

Figure 4: Air-cooled condenser and desuperheater in a common refrigeration cycle

In case the heat from the condenser is not recovered, the condensation temperature should not be too high since it leads to lower energy efficiency (Granryd, et al., 2011). The heat recovery is particularly suitable for ventilation when it is used for the space heating; indeed, yearly energy savings of more than 20% of energy used can be performed using warm air from the condenser (Piché & Galanis, 2010). Figure 5 gives an example of the waste heat recovery and Figure 7 schematically shows the refrigeration unit with its main components. A more complete (P, h) diagram giving details on a whole refrigeration cycle is presented in Figure 25.

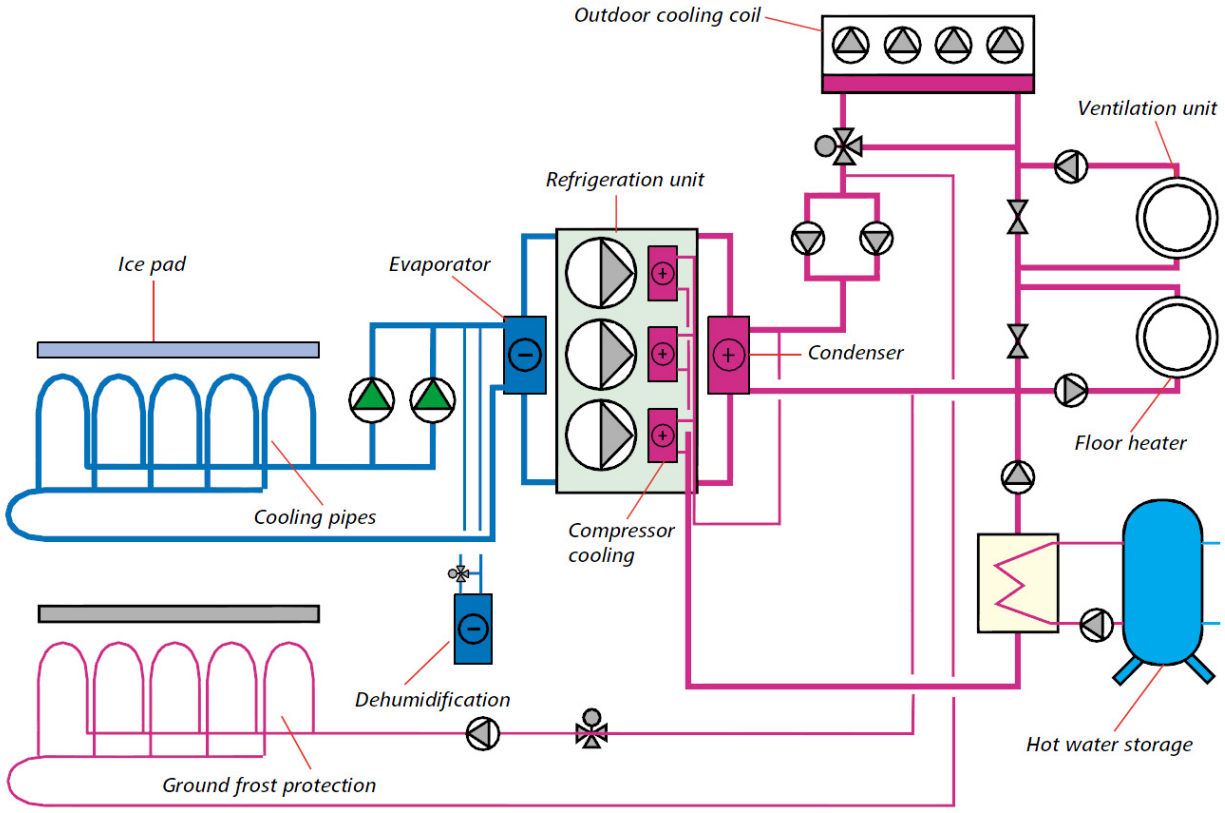

Figure 5: Example of a complete heat pump system with waste heat recovery process (IIHF, 2010)

2.1.3 Ventilation

Ventilation's primary purpose is to guarantee a good indoor air quality by maintaining standard air change rate. It should avoid high airborne pollutant or contaminant concentration and the health problems like asthma or allergies (Masters & Ela, 2008). In the ice rink case, the ventilation systems are often associated with the dehumidification systems. Moreover, the supply air may be used for the space heating as previously evoked. When ventilation carries out all those functions, the term HVAC system may be used. Figure 6 shows an example of a HVAC facility called *DryCool*™ (*Munters*) and used in the ice rinks.

The supply of fresh air is carried out by fans. Thus, the electricity is used to power the ventilation system. Even when ventilation does not ensure the space heating, the air may need to be heated up or cooled down to provide the specific indoor comfort. An air-to-air heat exchanger between the make-up air and the exhaust air may be installed to reduce the ventilation heating or cooling need as it is presented in Figure 6 under the name "Energy recovery wheel" (Munters, 2011).

2.1.4 Dehumidification

Dehumidification in the ice rinks is more important than in common buildings. A lack of dehumidification system may cause higher energy consumption, discomfort issues and the metallic structure corrosion (or wood-rotting) due to the humidity level increase. Indeed, the people, ice resurfacing process and ventilation system generate humidity inside the building.

Additionally, the average indoor temperature is rather low (10°C) implying a lower saturated pressure of the water vapor in air, which in turn implies higher relative humidity, φ, as given (Egolf, et al., 2000)

$$\varphi = \frac{P_v}{P_{sat}} \quad (1)$$

where P_v and P_{sat} are the partial and the saturated pressure of water vapor in air, respectively, in Pa, at the air temperature.

The saturated pressure of water vapor in air P_{sat} at temperature T $[K]$ depends on the latent heat Δh involved, the gas constant of vapor R_v and an integration constant P_0 (Egolf, et al., 2000)

$$P_{sat} = P_0 \cdot \exp\left(-\frac{\Delta h}{R_v} \cdot \frac{1}{T}\right) \quad (2)$$

The numerical value of R_v is 461,5 J.kg^{-1}.K^{-1}. P_0 may be expressed with the pressure and temperature at the water triple point, P_T (610,4 Pa) and T_T (273,17 K) respectively as

$$P_0 = P_T \cdot \exp\left(\frac{\Delta h}{R_v} \cdot \frac{1}{T_T}\right) \quad (3)$$

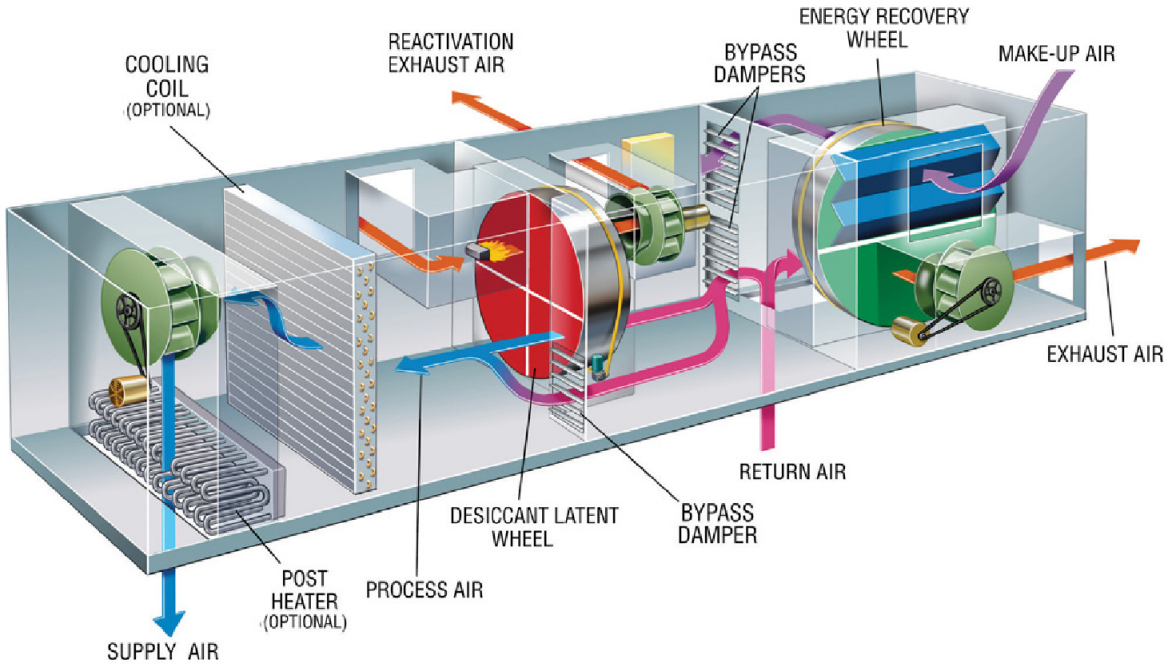

Figure 6: Example of HVAC system (*DryCool*™) used in ice rink (Munters, 2011)

High relative humidity may cause an undesirable fog formation. Moreover, the air having high relative humidity tends to condensate more easily since the dew point is higher. Condensation on metallic structure may be the source of corrosion phenomena or rotting in case of the wooden structures (IIHF, 2010). High relative humidity increases the condensation on the ice surface, leading to higher heat loads (see part 2.3.1 for condensation equations).

To dehumidify air two methods may be employed. The first one reduces humidity by condensing the water contained in the make-up and return air; hence the air supplied has low water content. Cooling coils placed in the HVAC system are used to condensate the water vapor. This method is similar to the method used for air-conditioning in the typical buildings.

The second method uses an adsorption process. The most conventional device using this technique for the ice rink application is the desiccant wheel as shown in Figure 6. The wheel contains an adsorbent material e.g. silica gel. When rotating, the wheel passes through separated warm and cold air streams. The cold air stream is the one needed to be dehumidified and hence has higher relative humidity. While being on the cold side, the adsorbent material is moist-less and adsorbs humidity from the air as a consequence. When the adsorbent passes on the warm side, the warm air absorbs its water content. Since the air is warm its saturated pressure is high meaning that it can absorb more humidity. The air circulating on the warm side may need to be heated up and could then account for the heating demand (Karampour, 2011).

2.1.5 Lighting

The lighting system consumes around 10% of the total energy. The lighting intensity (lux) should be sufficient to provide good visibility for the skaters and spectators, but at the same time lights are a source of the radiation and too high lighting intensity increases heat loads on the ice. Different type of lighting may be used in ice rinks: fluorescent lamps, metal halide lamps, high-pressure sodium lamps, induction lamps and halogen lamps (Karampour, 2011).

2.1.6 Yearly energy consumption

The energy consumption is variable from one ice rink to another. In Sweden, statistical studies show an average yearly consumption of 1000 MWh per year (Rogstam, 2010). The inefficient ice rinks may use up to 2000 MWh per year whereas the most efficient ones may present energy consumptions as low as 700 MWh per year. (Karampour, 2011). In contrast, the average energy consumption of ice rinks in Quebec province in Canada reaches 1500 MWh per year with highest energy consumptions of 2400 MWh per year (Nichols, 2009).

2.2 Ice rink refrigeration system

Since the cooling demand is the most important energy demand in the ice rinks, the refrigeration system plays an important part in the overall energy consumption. Furthermore, the refrigeration system absorbs the energy required to maintain the ice in its most desired form. This system is sometimes referred to as "the heart" of the ice rink because of its importance. In most cases, the refrigeration system is an electricity powered vapor compression system, commonly known as a heat pump system. These refrigeration systems are composed of the following elements: evaporator, condenser, compressor, expansion device and the refrigerant. To avoid any confusion with the term "secondary refrigerant", the refrigerant used in the refrigeration unit will be called the "primary refrigerant". The most common primary refrigerant used in Swedish ice rinks is ammonia (R717), which accounts for about 85% of all facilities. The remaining 15% use R404A, R134a or other HFC refrigerants (Makhnatch, 2011). Figure 7 shows the main components of a typical refrigeration unit used in the ice rinks having a flooded type evaporator. Several compressors in parallel may be used to stagger the cooling demand and improve the refrigeration system performance. Most of the ice rinks refrigeration systems in Sweden have two compressors (Rogstam, 2013).

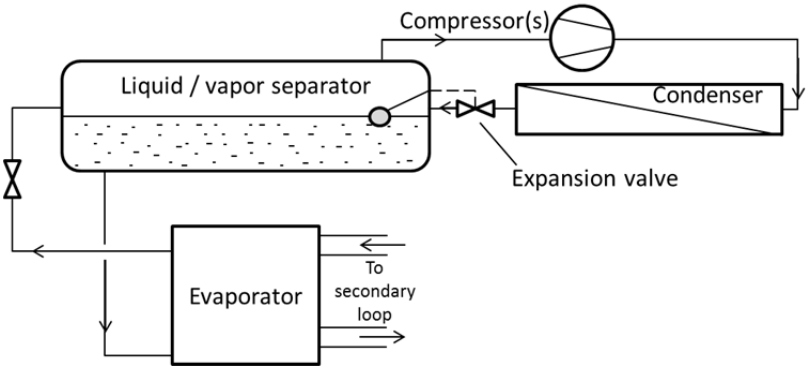

Figure 7: A conventional ice rink refrigeration unit using a flooded evaporator

The performance of refrigeration systems is often expressed in terms of the coefficient of performance, COP, which depends on the power supplied to the compressor, $\dot{E}_{comp}$, and the cooling capacity provided at the evaporator, $\dot{Q}_0$

$$COP = \frac{\dot{Q}_0}{\dot{E}_{comp}} \quad (4)$$

Besides the heat pump, three different system designs may be found in ice rinks: direct, indirect or partly indirect systems. In a direct refrigeration system (DX- system), the evaporator with primary refrigerant directly cools down the ice pad. In fact, the overall under-ice piping layout is used as the evaporator. The direct systems mostly use R22 or ammonia as primary refrigerant. R22 is now banned due to its global warming potential and pure ammonia solution may be dangerous for human beings (Calm, 2008). A high exposure to ammonia may cause airway soreness, eye-irritations, chemical burns and mucus membrane oedema (CSST, 2009). In the ice rinks, having the direct refrigeration system involves using a large amount of primary refrigerant; that can increase either the global warming potential or the health hazard potential. Moreover, a charge minimization is recommended in case of the hazardous primary refrigerants like ammonia, which is limiting the applications for direct systems (Melinder, 2009).

In an indirect refrigeration system, the secondary fluid is used to transfer and remove the heat from the heat source and the heat sink, respectively. Besides the basic components of the heat pump, indirect systems imply the use of two secondary loops with tubes, circulation pump and an additional heat exchanger. Figure 8 shows the main components of the secondary loop on the evaporator-cooling side (Melinder, 2009).

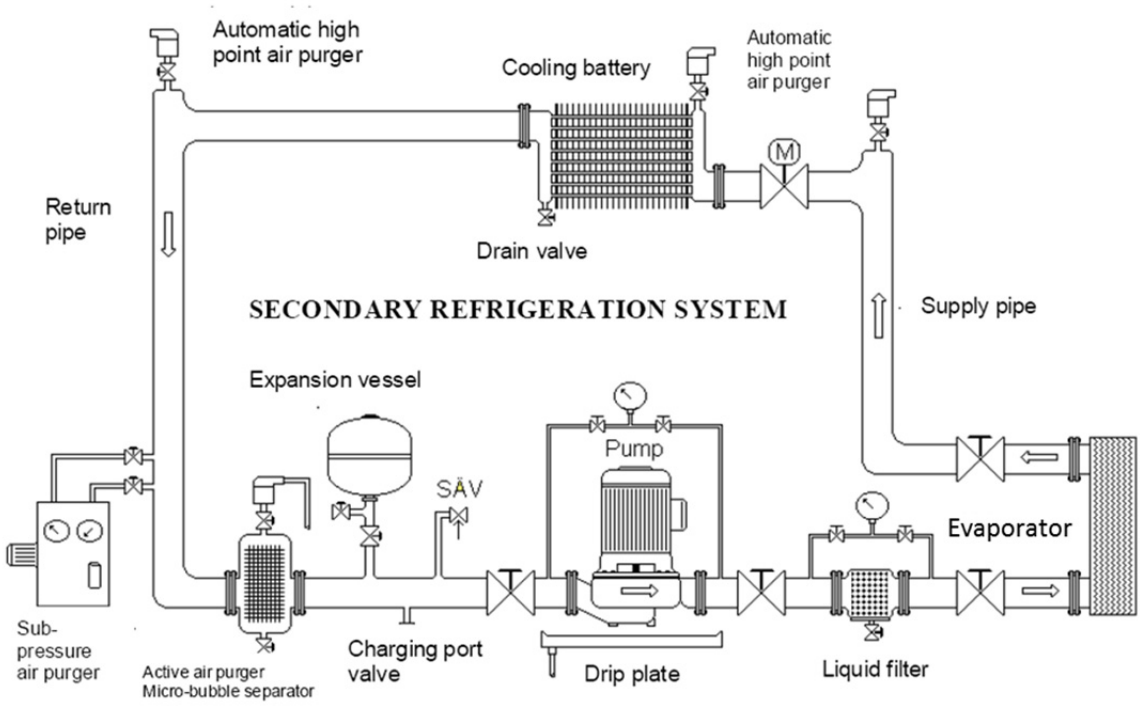

Figure 8: Main components of a secondary loop with single-phase secondary fluid on the evaporator side (Melinder, 2009)

The partly-indirect systems are refrigeration systems in which either the condenser or the evaporator is not connected to the secondary loop. Either the condenser or the evaporator heats up or cool down a secondary fluid. In Sweden more than 97% of the ice rinks refrigeration systems are designed as indirect system or partly-indirect system on the evaporator side (Makhnatch, 2011). Figure 5 shows a fully indirect system and Figure 9 shows the difference between direct and indirect systems. The "cooling battery" mentioned in Figure 8 is the equivalent of the ice rink floor shown in the left part of Figure 9. The ice rink works in fact as a huge heat exchanger between the ice and the secondary fluid.

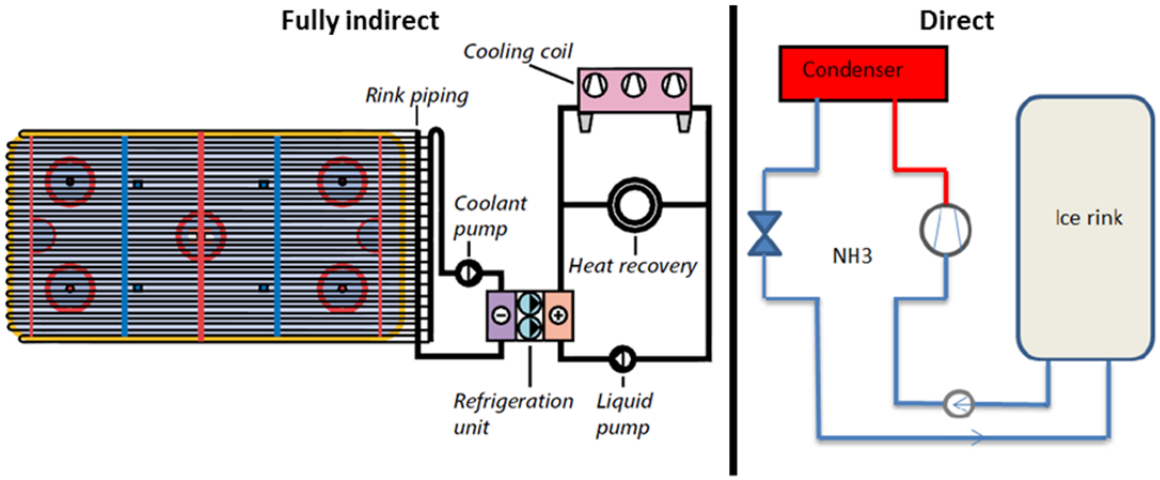

Figure 9: Fully indirect (left) and direct (right) refrigeration system in ice rink application (IIHF, 2010; Nguyen, 2012)

Details about the secondary fluids are further given in part 3. The single-phase or two-phase secondary fluids (like CO_2) may be used in the ice rink application. However, only single-phase secondary fluids are considered in this study.

2.2.1 Advantages and drawbacks of indirect systems

The main drawbacks of using indirect systems are: the higher investment costs due to the secondary loop components; the additional temperature difference introduced by the additional heat exchanger leading to lower evaporation temperature and somewhat lower performance; and the added pumping power implied by the secondary fluid circulation (Melinder, 2007). Additional maintenance and possible corrosion problems depending on the corrosive character of secondary fluid in the secondary loop may also be accounted as drawbacks.

Nevertheless, the indirect refrigeration systems become more and more popular because of their positive environmental effects. Moreover, due to increasing knowledge about the indirect systems, they may soon compete with traditional DX-systems in terms of the energy consumption, investment cost and environmental aspects (Wang, et al., 2010). The main advantages of indirect systems are: local construction of primary refrigerant piping is avoided leading to less primary refrigerant leakage; the primary refrigerant is confined in the machine room; the primary refrigerant charge is lower and, as a consequence, high performing refrigerants may be used; and efficient flooded evaporators may be used while thermostatic expansion valves may limit the effective evaporator surface down to 70 % (Melinder, 2007). Wang et al. (2010) also claimed that using the indirect systems was leading to lower operating costs and reducing the hazards linked to the primary refrigerant. Table 1 summarizes the main advantages and drawbacks of the ice rink indirect systems in comparison to the direct systems.

Table 1: Advantages/Drawbacks of ice rink indirect systems in comparison to direct systems

Advantages	Drawbacks
Less primary refrigerant charge	Higher investment costs
Leakage risks reduced	Higher temperature differences
Primary refrigerant confined in the machine room	Added pumping power
Possibility to use flooded evaporator	Maintenance / corrosion (2ndary loop)
Possibility to use high-performing refrigerant (hazards' reduction)	
May lead to lower operating costs	

2.2.2 Ice rink floor layout

As previously mentioned, the ice rink floor works as a huge heat exchanger between the ice top and the secondary fluid. The ice rink floor is composed of several layers as shown in Figure 10. The layout may be different from one ice rink to another but most of them have: ice as the topmost layer, concrete with in-slab pipes as the second layer and insulation as the bottom layer before the ground. Moreover, a heated concrete layer, as well as a sand-and-gravel layer with water drain may be found (Karampour, 2011).

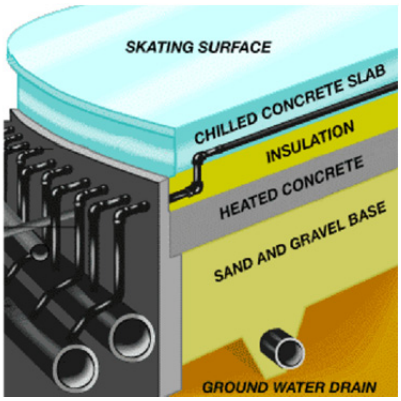

Figure 10: Ice rink floor cross section (Karampour, 2011)

Pipes embedded in the ice rink floor where the secondary fluid circulates are organized in U-shapes as shown in Figure 11. The left drawing shows the case where the U-pipes cross each other. Each U-pipe is connected to two headers: the supply and the return headers. U-pipe arrangement may also be called two-pass arrangement. In Figure 11, it is possible to see the diameter reduction along the headers. This may be done to even the flow distribution in all U-pipes as much as possible. Another way of accomplishing this is to use a reverse-return header concept. In this case, each U-pipe has the same resistance to the flow leading to evenly distributed flows.

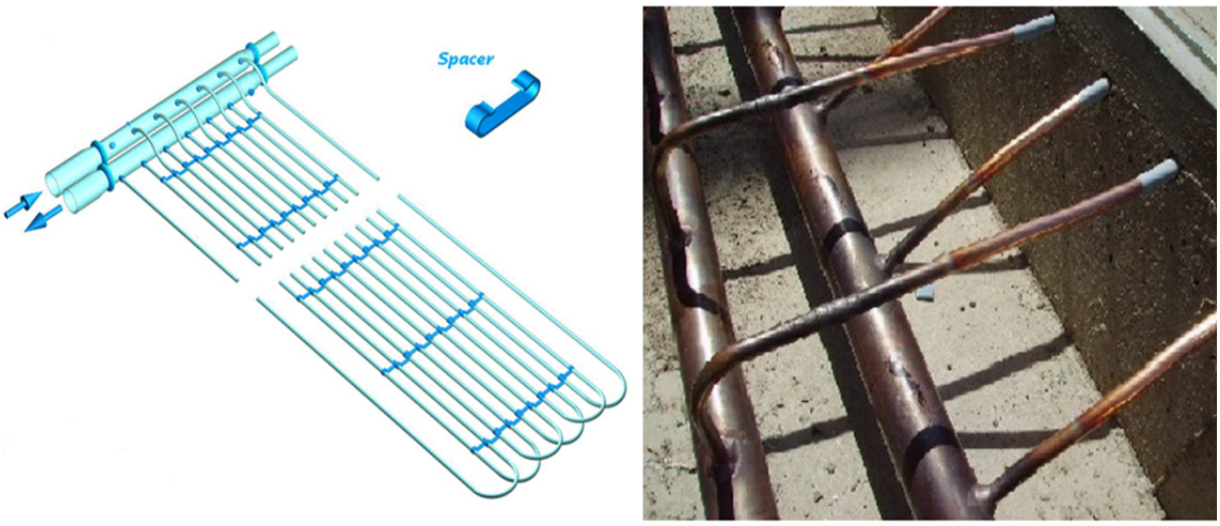

Figure 11: In-slab pipes arrangement in U-shapes (Ingvar, 2007; Nguyen, 2012)

Three different pipe materials may be used: plastic, steel and copper. The most popular type of pipe installed in the ice rinks is plastic pipe because of its light weight, ease of and low installation cost. Steel and copper pipes have higher thermal conductivity but the investment cost linked to these types of pipes is also higher. In Sweden, only few, rather old ice rinks use steel pipes. Copper pipes are used when carbon dioxide is used as the secondary fluid (Nguyen, 2012). Plastic pipes may let oxygen enter the secondary loop due to oxygen diffusion through the pipe wall, causing corrosion in the system (Ignatowicz, 2008).

2.3 Heat loads and heat gains characterization

The sum of the heat loads and heat gains represents the total cooling demand at a given moment. This instantaneous cooling demand is referred to as the cooling capacity.

2.3.1 Heat loads

The term "heat loads" is used while describing the heat power involved on the ice sheet surface. The heat loads involve the three heat transfer mechanisms:

- Convection
- Radiation
- Conduction

Condensation phenomenon also happens on the ice sheet. Condensation may be considered as convection involving the latent heat transfer (Granryd, et al., 2011). The ice resurfacing process is also part of the total heat loads.

Convection heat transfer is occurring between the ice sheet and the surrounding air. Both air and ice temperatures, as well as air velocity, influence the rate of this heat transfer process. The convection heat load rate may be calculated as

$$\dot{Q}_{convection} = h_{cv} \cdot A_{ice} \cdot (T_{air} - T_{ice}) \quad (5)$$

where

- h_{cv} is the convection heat transfer coefficient in $W.m^{-2}.K^{-1}$.
- A_{ice} is the ice sheet area in m^2.
- T_{air} and T_{ice} are the air and the ice temperature in K, respectively.

The convection heat transfer coefficient h_{cv} may be defined using the boundary condition at the ice surface ($y = 0$) by (Incropera, et al., 2007)

$$h_{cv} = \frac{-k_{ice} \cdot \left(\frac{dT}{dy}\right)_{y=0}}{T_{ice} - T_{air}} \quad (6)$$

where

- k_{ice} is the thermal conductivity of ice in $W.m^{-1}.K^{-1}$.
- $\left(\frac{dT}{dy}\right)_{y=0}$ is the temperature gradient at the ice surface in $W.m^{-1}$.
- y is the vertical axis.
- T_{air} and T_{ice} are as defined in eq.(5).

ASHRAE (2010) gives a correlation to calculate the convection heat transfer coefficient h_{cv} in regard to the air velocity V_{air} *[m.s⁻¹]*

$$h_{cv} = 3{,}41 + 3{,}55 \cdot V_{air} \quad (7)$$

Condensation phenomena also occur at the ice pad surface. The driving force for condensation is the partial pressure difference of water vapor between saturated air at the ice-air limit and the air surrounding the ice sheet. On the contrary, the temperature difference between those two is the driving force of convection process. Condensation phenomena occur whenever a surface temperature is below the dew point temperature and the general condensation equation may be expressed likewise the convection one, eq.(5), (Granryd, et al., 2011)

$$\dot{Q}_{condensation} = h_{cd} \cdot A_{ice} \cdot (T_{air} - T_{ice}) \quad (8)$$

where h_{cd} is the heat transfer coefficient referring to condensation in $W.m^{-2}.K^{-1}$. This depends directly on the partial pressure difference presented previously

$$h_{cd} = \frac{\delta \cdot \Delta h}{T_{air} - T_{ice}} (P_v - P_{sat,ice}) \quad (9)$$

where

- Δh is the enthalpy difference between vapor water in air and condensate water in $J.kg^{-1}$.
- P_v is the partial pressure of water vapor in the surrounding air, in Pa.
- $P_{sat,ice}$ is the saturated pressure of water vapor at the ice temperature, in Pa.
- T_{air} and T_{ice} are as defined in eq.(5).

Since the ice temperature is below 0°C, both the latent heat of fusion and vaporization should be taken into account for the enthalpy difference Δh.

δ is the mass transfer coefficient expressed as

$$\delta = \frac{M_{H_2O}}{M_{air}} \cdot \frac{1}{P \cdot C_p} \cdot h_{cv} \quad (10)$$

where

- M_{H_2O} and M_{air} are the molar mass of water and air, respectively, in $g.mol^{-1}$.
- P is the atmospheric pressure in Pa.
- C_p is the specific heat capacity of air in $J.kg^{-1}.K^{-1}$.
- h_{cv} is the convection heat transfer coefficient as calculated in eq.(6).

Combining eq.(8), (9) and (10), and taking numerical values of 1.10^5 Pa, 18 g.mol^{-1}, 29 g.mol^{-1}, 1,006 kJ.kg^{-1}.K^{-1} and 2835 kJ.kg^{-1} for P, M_{H_2O}, M_{air}, C_p and Δh respectively, we obtain

$$\dot{Q}_{condensation} = 1{,}75.10^{-2} \cdot A_{ice} \cdot h_{cv} \cdot (P_v - P_{sat,ice}) \quad (11)$$

If the indoor air humidity is not controlled, the condensation phenomena may become important since the ice sheet temperature is almost always below the dew point of the indoor air.

Radiation is one of the most significant heat loads in ice rink (ASHRAE, 2010). Indeed, two large surfaces, the cold ice sheet and the relatively warm ceiling, face each other implying a high rate of radiation heat transfer. Besides the ceiling, lighting devices and radiating panels are also sources of radiation heat loads. Radiation heat transfer rate from the ceiling is calculated using the Stefan-Boltzmann's law

$$\dot{Q}_{radiation} = A_{ceiling} \cdot f_{ci} \cdot \sigma \cdot (T_{ceiling}^4 - T_{ice}^4) \quad (12)$$

where

- $A_{ceiling}$ is the ceiling area in m^2.
- σ is the Stefan-Boltzmann's constant, equal to 5,67 10^{-8} W.m^{-2}.K^{-4}.
- $T_{ceiling}$ and T_{ice} are the ceiling and ice temperatures, respectively, in K.

f_{ci} is the gray body configuration factor given by (Incropera, et al., 2007)

$$f_{ci} = \left(\frac{1}{F_{ci}} + \left(\frac{1}{\varepsilon_{ceiling}} - 1 \right) + \frac{A_{ceiling}}{A_{ice}} \cdot \left(\frac{1}{\varepsilon_{ice}} - 1 \right) \right)^{-1} \quad (13)$$

where

- F_{ci} is the view factor depending on the geometry, *dimensionless*.
- $\varepsilon_{ceiling}$ and ε_{ice} are the emissivity factors of the ceiling and the ice pad, respectively, *dimensionless*.
- $A_{ceiling}$ and A_{ice} are the areas of the ceiling and the ice pad, respectively, in m^2.

F_{ci} is the fraction of radiation leaving the ceiling that is intercepted by the ice surface, hence, the subscript used (ci). Figure 12 shows geometrical parameters used to calculate the angle factor for the ice rink case. The following equation refers to the parameters named on Figure 12 (Incropera, et al., 2007)

$$F_{ci} = \frac{1}{A_c} \cdot \int_{A_c} \int_{A_i} \frac{\cos(\theta_c) \cdot \cos(\theta_i)}{\pi \cdot R^2} dA_i dA_c \quad (14)$$

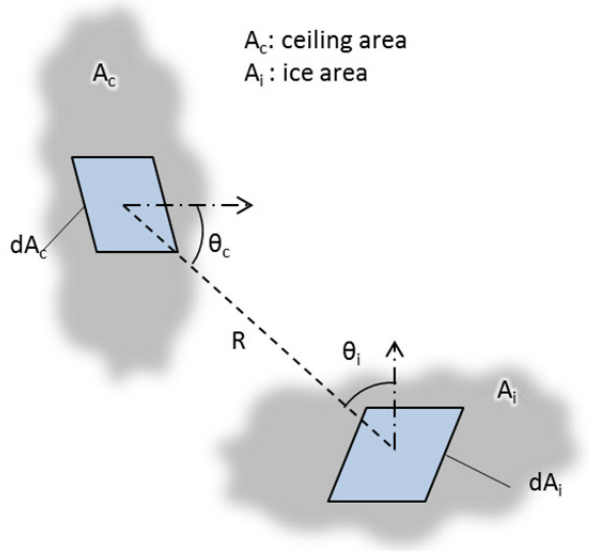

Figure 12: Parameters influencing the view factor in case of radiation between surfaces

Ice resurfacing is explained in part 2.1.2. It involves latent heat transfer and conduction. The mean heat flow rate $\bar{\dot{Q}}_{resurfacing}$ associated with ice resurfacing depends on the temperature of the flooded water T_f, the temperature of the ice T_{ice}, the total volume of water flooded on the ice pad V_f and the total time taken to solidify water t. The expression given by ASHRAE (2010) has been generalized, resulting in

$$\bar{\dot{Q}}_{resurfacing} = \frac{V_f}{t} \cdot \left(\overline{C_{p,T_f-0}} \cdot (T_f - 0) + \Delta h_{fusion} + \overline{C_{p,0-T_{ice}}} \cdot (0 - T_{ice}) \right) \quad (15)$$

where

- $\overline{C_{p,T_f-0}}$ is the mean specific heat capacity of water between T_f and 0°C, in $J.kg^{-1}.K^{-1}$.
- $\overline{C_{p,0-T_{ice}}}$ is the mean specific heat capacity of ice between 0°C and T_{ice}, in $J.kg^{-1}.K^{-1}$.
- Δh_{fusion} is the latent heat of fusion of water in $J.kg^{-1}$.

Generally, the ice resurfacing heat (kWh) is calculated instead of the heat rate (kW) since it is hard to define the time taken for water to solidify, t. The number of ice resurfacing processes depends on the type of activity practiced and the number of sessions. In general, the ice resurfacing is performed after each session. In eq.(15), it is considered that all the flooded water is transformed into ice. However, the flooded water may also partly evaporate to the ambient air. In this case, the ice resurfacing would increase the air humidity; and thus indirectly the condensation heat load.

Skaters and spectators contribute to the heat loads directly by radiation, and indirectly by convection. However, it is hard to quantify precisely their contribution to the heat loads. ASHRAE (2010) suggests considering that skaters represent 4% of the total heat loads. The skaters also indirectly contribute to the ice resurfacing frequency since skates' friction deteriorates the ice quality.

Conduction heat transfer is taking place within the ice pad floor but does not account as a part of the heat loads. Indeed, the conduction process is the way heat is transferred from the ice top to the secondary fluid circulating in the pipes. In case of the ice surface, the energy conservation equation (first law of thermodynamics) applies as (Daoud, et al., 2008)

$$\dot{Q}_{conduction} = \dot{Q}_{radiation} + \dot{Q}_{convection} + \dot{Q}_{condensation} + \dot{Q}_{resurfacing} \quad (16)$$

where $\dot{Q}$ represents a heat flow, the indexes indicating the process to which it refers. Figure 13 illustrates the energy balance at the ice surface. Since the conduction heat flow is the sum of all different heat loads, it represents the total amount of heat loads. Moreover, the resurfacing heat load should be included only during the resurfacing time. Heat gains may also be transmitted by conduction from the ground to the secondary fluid. The conduction heat transfer as expressed in eq.(16) should not be confused with the ground heat gains, also transmitted by conduction.

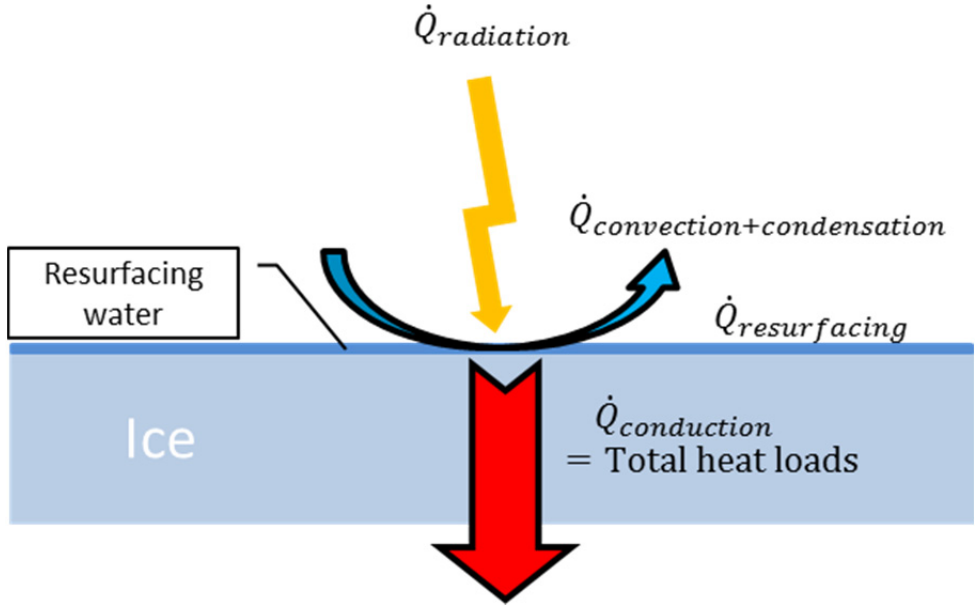

Figure 13: Energy balance at the ice surface

Conduction is generally characterized by two equations:

- the Fourier's law (Incropera, et al., 2007)

$$\dot{Q}_{conduction-x} = -k \cdot A \cdot \frac{\partial T}{\partial x} \quad (17)$$

- and the heat diffusion equation for an isotropic medium

$$\frac{\partial}{\partial x}\left(k\frac{\partial T}{\partial x}\right)+\frac{\partial}{\partial y}\left(k\frac{\partial T}{\partial y}\right)+\frac{\partial}{\partial z}\left(k\frac{\partial T}{\partial z}\right)+\dot{q}=\rho\cdot C_p\frac{\partial T}{\partial t} \quad (18)$$

where

- A is the heat transfer area in m^2.
- k is the thermal conductivity in $W.m^{-1}.K^{-1}$.
- T is the temperature in K.
- (x,y,z) is the Cartesian coordinate system.
- $\dot{q}$ is the internal heat generation rate in $W.m^{-2}$.
- ρ is the density in $kg.m^{-3}$.
- C_p is the specific heat capacity in $J.kg^{-1}.K^{-1}$.
- t is the time in s.

2.3.2 Heat gains

Similarly to the heat loads, heat gains increase the cooling demand, and thus the required cooling capacity. The heat gains are all the heat sources contributing to increase the cooling capacity but not happening above the ice sheet. These heat gains should be considered as part of the heat loads. The conventional heat gains are

- Conduction from the ground
- Heating up of the secondary fluid by the pump
- Ambient air heating through the distribution pipes and headers

If the ground has higher temperature than the ice rink floor, then the heat is transferred from the ground to the ice floor by conduction. The major part of the electrical energy transmitted to the secondary fluid by the pump is converted into heat. Finally, the ambient air heats up the pipes by convection which in turn, heat up the secondary fluid. Figure 14 shows the shares of the heat loads and heat gains in two North American ice rinks in winter and summer. The heat loads per ice surface unit is also given. In the literature source (Karampour, 2011), the pumping power was fully accounted as heat gains. If the pumps are of dry rotor type, part of the motor heat losses is however not transmitted to the secondary fluid.

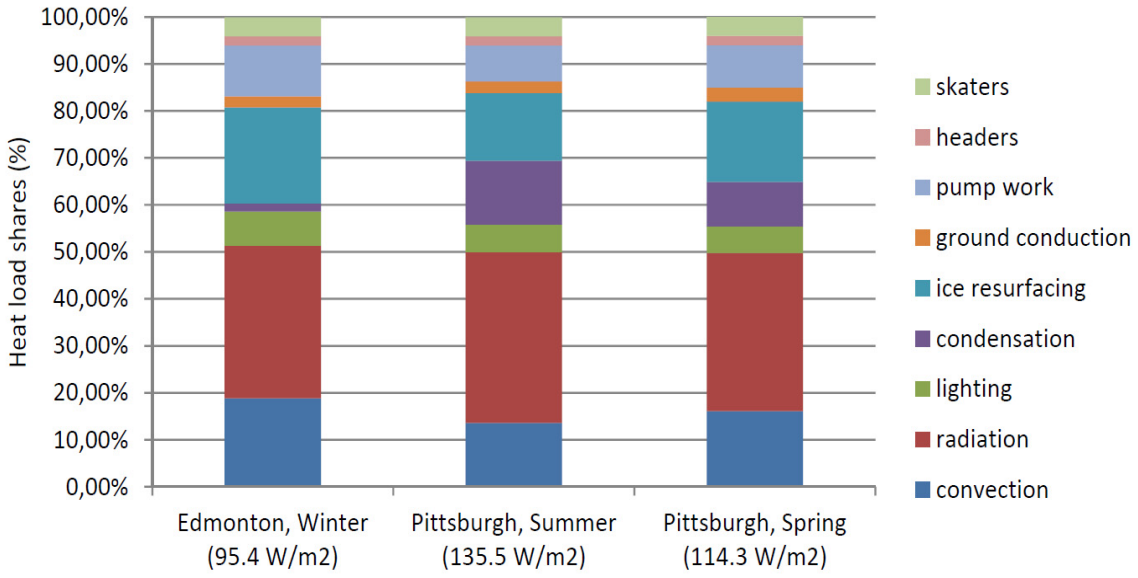

Figure 14: Daily heat loads and heat gains shares for two indoor ice rinks (Karampour, 2011)

2.4 Energy saving potential

Generally, two approaches are considered while trying to reduce the energy consumption in ice rink facilities. The first one is to reduce the cooling demand by decreasing the heat loads and/or heat gains. The second method is to improve the energy efficiency in ice rinks; that is simply decreasing the power supply for the same energy demand.

2.4.1 Heat loads and heat gains decrease

Low emissivity ceiling. The radiation may be the largest share in the heat loads as shown in Figure 14. As indicated in eq.(12) and (13), the ceiling emissivity, $\varepsilon_{ceiling}$, plays an important part in the radiation load rate; and the materials used for the ceiling structure (wood, steel) have an emissivity between 0,85 and 0,95 (Karampour, 2011). Therefore, a way to reduce the radiation is to cover the ceiling with a low-emissivity layer. This layer usually consists of low emissivity aluminum-based paints or hung ceilings. As the indirect effect, it may reflect the lighting and reduce the lighting demand but at the same time it may indirectly increase the radiation from the lights by reflection. The low radiating ceilings have an emissivity index between 0,05 and 0,25. Another way of reducing the radiation heat load would be to reduce the ceiling temperature; however it is hard to control since it depends on several factors e.g.: outdoor weather conditions, solar radiation, and normal stratification of indoor air (Blades, 1992). Hence, the low-emissivity ceiling solution is favored.

Lighting control. Reducing and controlling the lighting helps decreasing both the radiating loads and the electricity consumption. The lights should be as efficient as possible and the lighting intensity controlled according to the rink activity. Fluorescent lamps are efficient lamps used in ice rinks (Karampour, 2011). The use of LED lighting may be seen as an even more efficient solution.

Space heating control and position. If possible, space heating devices should strategically be positioned to avoid unnecessary heating while providing comfortable conditions. Although it does not allow using the heat recovery, radiating panels over the spectators' heads are a good solution since it provides spot heating. If the ventilation system is used for space heating, the air should be blown as close as possible to the stands. Under-stands ventilation heating may be a good solution if the blown air is not too warm; otherwise it may cause some discomfort problems. In some Swedish ice rinks which were visited as part of this study, the ventilation blowers were located close to the ceiling. In this case the warm air stays in the upper part of the building warming up the ceiling and thus indirectly increases the radiation heat loads. The space heating should also be controlled so it is working only when needed.

Dehumidification. As explained in part 2.1.4, dehumidification is important in the ice rinks. If the humidity is not controlled, a dehumidifier may be installed to reduce condensation loads on the ice sheet.

Ice resurfacing volume and temperature have significant effects on the respective heat load. Those two parameters should be reduced as much as possible while providing a good resurfacing. In Sweden, 30 to 40°C is the normal temperature range while in North American ice resurfacing water temperature can reach up to 80°C (Makhnatch, 2011).

Insulation beneath ice rink floor. The heat gains from the ground can be diminished if an insulation layer is initially included in the ice floor design. Somrani et al. (2008) stated that insulation reduces the time of charging the ice rink (i.e. converting water to ice) by more than 40 %. In general, it is not cost-efficient to replace the whole ice rink floor; especially in comparison to the low-emissivity ceiling energy saving solution.

Distribution pipes and headers insulation. The heat gains through the distribution pipes and headers can be reduced by insulating these pipes. If they are not insulated, the pipes covered with ice gives a natural insulating layer. However, this ice layer cannot be controlled and may create mechanical loads on the pipes. Moreover, the ice has a much higher thermal conductivity than any insulating material.

2.4.2 Energy efficiency improvement

In this part, energy efficiency improvements are discussed in a qualitative way. The different energy devices may interact with each other, thus, an integrated approach including all devices within the ice rink building should be considered if possible. In this case study only the efficiency of the refrigeration system has been considered due to the time constrains of the project. An overall efficiency may be defined as explained in part 2.5. The effects of the secondary fluids are quantitatively explained in part 4.

Waste heat recovery. The waste heat from the condenser and the desuperheater should be used whenever possible to fulfill the heating needs as explained in part 2.1.2. Using the waste heat recovery may lead to more than 24% of yearly savings (Piché & Galanis, 2010).

Variable speed pumps. Pumps working at full speed all the time may lead to high electricity consumption and inefficiency. Variable speed pumps may be installed to reduce the pumping power. However, these pumps are only efficient if a control strategy is set up to avoid too low flow leading to lower heat transfer performance. The variable speed pumps are often controlled by the secondary fluid temperature difference. For a given heat load, an optimum control (i.e. temperature difference) exists leading to better efficiency as it is further shown in part 4.6. Nevertheless, too high secondary fluid temperature difference may lead to uneven ice top temperature distribution. The field measurements of some Swedish ice rinks indicated around 50% saving potential in terms of the pumping power when using variable speed pumps instead of full-speed ones (Rogstam, 2010).

Air permeability and ventilation control. Air permeability is important in any building since the indoor conditions need to be controlled. Too high air infiltration may increase the air humidity inside the building; cause discomfort issues; reduce the ventilation system's efficiency as well as increase the heat loads. If the air tightness is sufficient enough, the installation of vapor retarders inside the building walls may be considered to avoid the humidity enter and letting it flow out instead. The control of the ventilation system is also important. The ventilation system can be turned off or the air flow can be adjusted when the ventilation needs are lower (in agreement with the space heating demand if HVAC system is used). Pollution controllers (e.g. using CO_2 concentration) may be a good solution to adjust the air flows to the ventilation demand. Free cooling may also be considered together with the ventilation system. In summer for example, the outdoor air may be blown at night when the temperature is lower to cool down the building. As mentioned in part 2.1.3, an air-to-air heat exchanger between exhaust and make-up air helps reducing the ventilation heating demand.

Ice temperature and thickness. The ice temperature should be as high as possible while giving good ice quality. Different temperatures are recommended depending on the activity type. For hockey -6.5 to -5.5°C, figure skating -4 to -3°C and recreational skating -3 to -2°C is satisfactory (ASHRAE, 2010). The ice temperature may also be leveled up at night or when the ice rink is not used. Increasing the ice temperature has two beneficial effects. Firstly, it leads to a higher evaporation temperature for the refrigeration system, leading to a better system performance. Secondly, it reduces the heat load rate on the ice sheet, lowering the cooling demand. The thickness of ice influences the ice rink floor's heat transfer resistance and should therefore not be chosen too big. The recommended ice thickness is 25 mm (ASHRAE, 2010).

Concrete thermal properties improvements. A concrete with better thermal conductivity improves the heat transfer rate within the rink floor leading to a higher evaporation temperature and better performance of the refrigeration system (Granryd, et al., 2011). Moreover, the pipes' depth within the concrete also influences the heat transfer rate, thus higher in-slab pipes depth leads to higher heat transfer resistances.

Secondary fluid choice and thermo-physical properties. The choice of the secondary fluid is important. Different secondary fluids have different thermo-physical properties (e.g. thermal conductivity, viscosity) leading to higher or lower energy consumption. Moreover, the anti-freeze additive concentration should not be too high since these liquids have worse thermo-physical properties than water in most cases. The properties of the secondary fluid have an effect on both the heat transfer and pumping power

in the secondary loop. Secondary fluids may have other negative effects on the refrigeration system (e.g. corrosion) that are not quantitatively discussed in this study. The type and concentration of secondary fluid should be considered when trying to find energy savings solutions common to most ice rinks due to the fact that most of them have indirect refrigeration system. The secondary fluids impact and effect are further discussed in parts 3 and 4.

Control strategy. The control strategy may significantly reduce energy consumption for a given device. The variable speed pump is an example and the same principle can be applied for variable speed/capacity or stages compressors. On the other hand, some control strategies may not present any benefits in terms of improved performance but in terms of quality or services. A study by Mun and Krarti (2011) investigated two different control strategies for the refrigeration system. The first one was using the secondary fluid average temperature as the main control parameter whereas the second one was using the ice surface temperature. It was shown that, while using slightly less refrigeration energy (< 1%) the secondary fluid temperature control strategy did not present the same ability to maintain constant ice temperature and better ice quality in comparison to the second one.

2.5 Overall energy efficiency of ice rinks

As any other facility using energy, the ice rinks may be evaluated in terms of performance. The overall efficiency is calculated as the coefficient of performance (COP) of a refrigeration system but should be assessed by considering the total power supplied to the building. The overall efficiency is expressed as the ratio of the power supplied and the useful / effective power.

$$Overall\ efficiency = \frac{Useful\ power}{Power\ supply} \quad (19)$$

Figure 15 is a general illustration of the integrated approach rather than a tool to calculate the overall energy efficiency. One interesting feature highlighted in Figure 15 is the beneficial effect of the heat recovery in terms of the energy efficiency. If the cooling demand is close to the heating demand, a large part of the heat from the condenser may be recovered. Hence, the part of condenser heat that is wasted is lower and the efficiency better. On the other hand, if the cooling capacity is larger, more heat from the condenser will be wasted since the condensation heat is the sum of the cooling capacity and the compressor power.

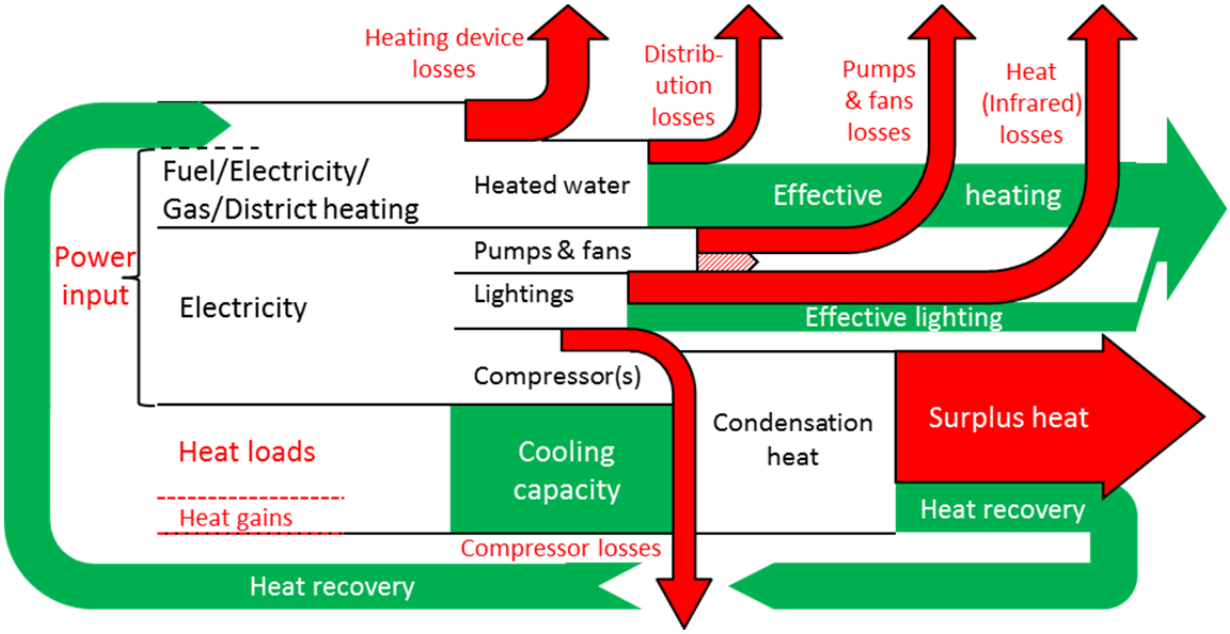

Figure 15: Simplified Sankey's chart illustrating energy losses in ice rink facilities

3 SECONDARY FLUIDS

As it was mentioned before in this study, the term *secondary fluid* refers to the working media transferring the heat from the cooling object to the evaporator in an indirect system. It circulates in the secondary loop; being both a heat sink for the cooling object (ice rink floor) and a heat source for the evaporation process.

The different types of secondary fluid that may be found are listed with some examples (Marvillet, 2003):

- Single-phase aqueous solutions (calcium chloride – water)
- Singe-phase non-aqueous solutions (diethylbenzene)
- Pure synthetic oils (hydro-fluoroether)
- Two-phase solutions (carbon dioxide, ice slurries)
- Gas (liquid nitrogen; low temperature applications)

The phase-changing secondary fluids have a big advantage over the single phase ones due to the high latent heat during the phase change process. However, there are still few indirect systems using two-phase secondary fluids (Wang, et al., 2010). Therefore, only single-phase aqueous solutions are considered in this study although carbon dioxide and ice slurries may be used in ice rink applications. Ice slurry is a phase changing refrigerant consisting of millions of ice micro-crystals suspended within a solution of water and a freezing point depressant. The single phase solutions are a mix between water and a freezing point depressant mixture (e.g. ethylene glycol) with additives (e.g. corrosion inhibitors). The good thermo-physical properties of water make it excellent as a secondary fluid as long as temperatures stay above 3°C.

The secondary fluids may be used in various engineering fields such as: air-conditioning, supermarket refrigeration, borehole heat exchanger, domestic heat pumps, solar panels or ice rinks (Wang, et al., 2010; Acuña, 2013; Norton & Edmonds, 1991).

3.1 Secondary fluid requirements

Ideally, a secondary fluid shall fulfill the following requirements (Melinder, 2007; Ignatowicz, 2008):

- Have a sufficiently low freezing point to avoid freezing in the system and yet not have too high freezing point depressant concentration to benefit the good properties of water.
- Give good heat transfer.
- Give small pressure drop.
- Transport as much heat as possible for low volumetric flows.
- Be environmentally acceptable, non-toxic, non-flammable or dangerous and biodegradable.
- Be non-corrosive, compatible with materials used in the secondary loop and chemically stable.
- Be inexpensive.

None of the existing secondary fluids fully fulfill the previous requirements. The secondary fluid is chosen depending on the application and the given system. The choice criteria may change from application to another but it is important to consider the thermo-physical properties in terms of the heat transfer, pressure drop and freezing protection.

3.2 Secondary fluid thermo-physical properties

When comparing secondary fluids in terms of the heat transfer, pressure drop and freezing protection, the following thermo-physical properties are of interest: freezing point, viscosity, thermal conductivity, specific heat capacity and density. For other concerns, like the thermal vessel design (Briley, 2004), the thermal volume expansion, the boiling point and the surface tension may be relevant properties to consider.

3.2.1 Freezing point

The freezing point temperature, or freezing point, is the temperature at which ice crystals starts to appear in equilibrium in the solution. The freezing point curve is the curve showing the freezing point variation with the freezing point depressant (additive) concentration. Since the secondary fluids are mixtures, eutectic transformations may happen as shown in the right side of Figure 16. Indeed, some mixtures have a well-defined eutectic point. If the mixture has the eutectic composition (concentration) the solution will form a fully-mixed solid solution (Marvillet, 2003). The eutectic temperature is the highest temperature at which full solidification can be achieved as illustrated in Figure 16. Hence, being below the freezing point does not necessarily imply that the fluid is fully solidified but rather that ice crystals are forming within the solution (van der Ham, et al., 1998). These ice-liquid mixtures are called ice slurries and may be used in refrigeration system as two-phase secondary fluid. Figure 16 schematically illustrates the eutectic transformation (right) and show a phase diagram for a mixture without eutectic composition (left).

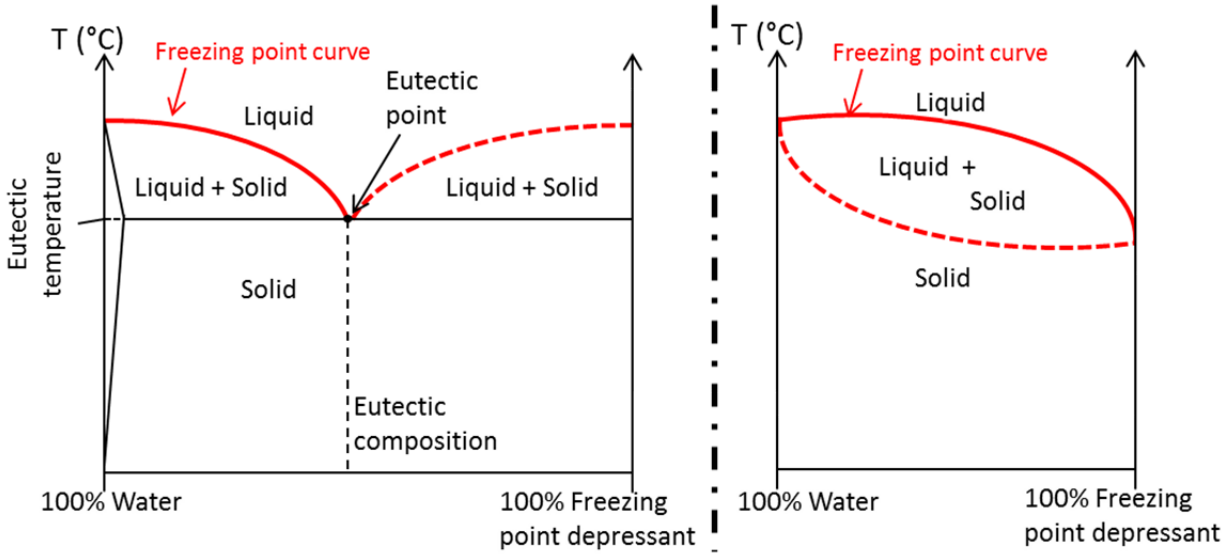

Figure 16: Water - freezing point depressant schematic phase-diagram with (left) and without (right) eutectic transformation

The freezing point should be below the lowest expected temperature and sufficiently below the normal operating temperature of the secondary fluid so that it can be pumped without difficulty through the system. However, the freezing point, or concentration, should not be too high to take advantages of the good thermo-physical properties of water. A temperature difference of 10K between the freezing point and the normal operating temperature is usually recommended.

3.2.2 Density

The density, ρ, may be defined as the concentration of matter measured in unit mass per unit volume. The density is expressed in kg.m^{-3}. It may be expressed as a ratio between mass, m, and volume, V

$$\rho = \frac{m}{V} \qquad (20)$$

3.2.3 Viscosity

The term viscosity may refer to two different physical properties: the dynamic viscosity, μ, and kinematic viscosity, ν. The relation between these two values involves the density, ρ,

$$\mu = \nu \cdot \rho \qquad (21)$$

In this study, the term viscosity only refers to the dynamic viscosity. The dynamic viscosity, may be defined as the ratio between the shear stress at the surface contact, τ, and the velocity gradient along the channel, $\frac{du}{dy}$

$$\tau = \mu \cdot \frac{du}{dy} \quad (22)$$

The viscosity is an important factor as it influences the pressure drop and the heat transfer. It should be as low as possible.

3.2.4 Specific heat capacity

The term specific heat capacity may refer to two different thermo-physical properties: the specific heat capacity at constant pressure, C_p, and the specific heat capacity at constant volume, C_v. Since we are dealing with non-compressible liquids in this study, those two physical parameters are undifferentiated. The specific heat capacity is the quantity of energy needed to raise by 1 K the temperature of 1 kg of a given substance (at constant pressure). Since the specific heat capacity is defined as the "*mean fluctuation of internal energy*", when the body does not undergo any phase changes, it may be given as the gradient of specific enthalpy, h, in J.kg^{-1}, versus the temperature, T, at constant pressure (Nishimori, 1981)

$$C_p = \left(\frac{\partial h}{\partial T}\right)_p \quad (23)$$

It is preferable to have high values of specific heat capacity since it leads to higher heat transfer rates and lower mass flow. A basic relation using the specific heat capacity is given in eq.(43).

The definitions given in parts 3.2.1, 3.2.2, 3.2.3 and 3.2.4 are based on Melinder (2007).

3.2.5 Thermal conductivity

The thermal conductivity, k, is usually defined with the Fourier's law as in eq.(17). Besides this definition, Incropera et al. (2007) give an alternative definition for species the liquid state

$$k = \frac{1}{3} \cdot C_p \cdot \rho \cdot \bar{c} \cdot \lambda_{mfp} \quad (24)$$

where

- C_p is the specific heat capacity in $J.kg^{-1}.K^{-1}$.
- ρ is the density in $kg.m^{-3}$.
- $\bar{c}$ is the mean molecular speed in $m.s^{-1}$.
- λ_{mfp} is the mean free path, in m, defined as "*the average distance traveled by an energy carrier (molecule) before experiencing a collision*".

3.3 Single-phase secondary fluids used in ice rinks

All secondary fluids considered in this part are aqueous solutions. To avoid repeating the term "water" each time a secondary fluid is mentioned, it is designated by its freezing point depressant name. For example, water – calcium chloride mixture will be referred to as calcium chloride solution (or its abbreviations: $CaCl_2$).

In Sweden, the major part of ice rinks use calcium-chloride based secondary fluids (Makhnatch, 2011). Besides calcium chloride, ASHRAE (2010) states that glycols (ethylene and propylene glycol), methanol or ethanol may be used as secondary fluids in ice rinks. However, methanol is now banned in Sweden and is therefore not included in this study. An article by Caliskan and Hepbasli (2010) and another one by Stegmann (2005) also consider ammonia as a potential secondary fluid for the ice rink application. Ethyl

alcohol (ethanol) was mentioned as a long-time used secondary fluid in Wang et al. (2010) and may be used in ice rinks. Potassium formate and potassium acetate are not widely used in ice rinks although they could be considered (Hillerns, 2001). Several commercial secondary fluids with additives for the ice rinks application exist on the market (Ignatowicz, 2008).

Figure 17 shows the main thermo-physical properties (density, thermal conductivity, specific heat capacity and viscosity) of: calcium chloride (*$CaCl_2$*); propylene glycol (*PG*); ethylene glycol (*EG*); ethyl alcohol (*EA*); ammonia (*NH_3*); potassium acetate (*K-acetate*) and potassium formate (*K-formate*); for a given concentration corresponding to the freezing point of -20°C. The data were retrieved from Melinder (2010) and the secondary fluids are considered as pure aqueous mixtures (without additives). The abbreviations used in Figure 17 and reminded previously will be used throughout this study.

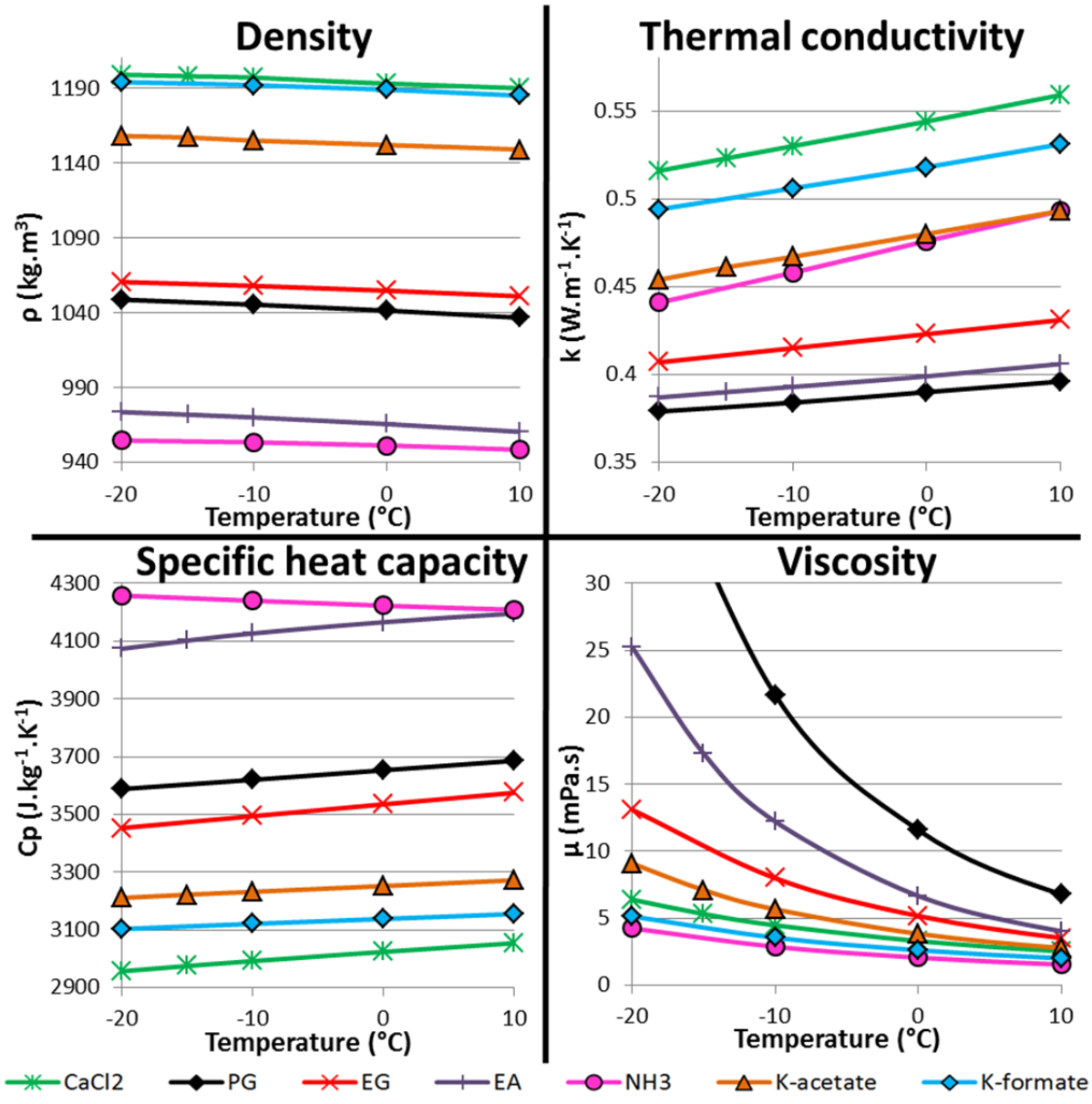

Figure 17: Basic thermo-physical properties of secondary fluids used in ice rink (freezing point -20°C)

It is interesting to notice that viscosity is increasing with decreasing temperature. For ethylene and propylene glycol, as well as for ethyl alcohol, it can reach high values (more than 10 mPa.s). This graph shows why viscosity is such an important factor at low temperatures applications in comparison to higher temperature applications (e.g. solar panels) for which the viscosity is rather low. The higher the viscosity the lower the heat transfer rate and higher the pumping power.

Ammonia-water is the only secondary fluid which specific heat capacity decreases with increasing temperature.

While Figure 17 gives quantitative data on the secondary fluids used in ice rinks, Table 2 lists the advantages and drawbacks of each secondary fluid in a qualitative way. Carbon dioxide was also included in this comparative table. The table also gives the chemical formula for the freezing point depressant of each secondary fluid.

The data shown in this table were mainly retrieved from Granryd et al. (2011) , Melinder (2007) and Ignatowicz (2008). Some data were taken from Marvillet (2003). Table 2 also mentions environmental, health and corrosion issues that may be associated with some secondary fluids.

Table 2: Advantages and drawbacks of secondary fluids used for ice rink application

2ndary fluids		Advantages	Drawbacks
Calcium Chloride ($CaCl_2$)	**$CaCl_2$**	✓ Non-toxic ✓ Non-flammable ✓ Rather low viscosity at low temperatures	▪ Highly corrosive ▪ Corrosion inhibitors used with $CaCl_2$ may cause health problems ▪ Source of scaling ▪ Low specific heat capacity
Ammonia (NH_3)	**NH_3**	✓ Low viscosity at low temperatures ✓ High specific heat capacity ✓ Environmentally-friendly	▪ Flammability risk ▪ Highly toxic ▪ Very low boiling point
Ethylene Glycol (EG)	**$C_2H_4(OH)_2$**	✓ Quasi non-corrosive ✓ Low fire hazard	▪ Highly toxic ▪ Environmental pollution risk ▪ Rather high viscosity at low temperatures
Propylene Glycol (PG)	**$C_3H_6(OH)_2$**	✓ Non-toxic ✓ Quasi non-corrosive ✓ Low fire hazard	▪ Very high viscosity at low temperatures ▪ Slightly water-polluting
Ethyl Alcohol (EA)	**C_2H_5OH**	✓ Non-toxic, unless ingested ✓ High specific heat capacity	▪ Flammability risk (concentration limit of 30% by weight) ▪ Low boiling point ▪ May be toxic if ingested ▪ High viscosity at low temperatures
Potassium Acetate (K-acetate)	**CH_3CO_2K**	✓ Low hazard potential ✓ Environmentally-friendly	▪ Long term effect not yet known ▪ Rather high pH-value
Potassium Formate (K-formate)	**CHO_2K**	✓ Environmentally-friendly ✓ Low viscosity at low temperatures	▪ Long term effect not yet known ▪ High pH-value that can cause eye damage
Carbon Dioxide	**CO_2**	✓ Environmentally-friendly ✓ Non-flammable ✓ Low toxicity ✓ Inexpensive ✓ Low pumping power	▪ Low heat transfer rate and specific heat capacity (compared to aqueous solutions) ▪ High pressures in the system

3.4 Secondary fluid maintenance

Due to corrosion problems, health and/or environmental issues caused by secondary fluids, an extra care and maintenance are needed. The effective maintenance operations may increase the life-time of the system, and may be considered in a Life-Cycle-Cost (LCC) investigation. The basic maintenance operations linked to secondary fluids are (QTF, 2012):

- Secondary fluid control and analysis
- System cleaning and filtration
- System degasing including dissolved oxygen removal.

The secondary fluids may have large quantities of dissolved oxygen since oxygen enters through plastic pipes and the solubility of oxygen in water increases with decreasing temperatures (Makhnatch, 2011).

Figure 18 shows a picture of corrosion phenomena on a pump of an ice rink refrigeration system. The secondary fluid used in the ice rink where the photography was taken is calcium chloride.

Figure 18: Corrosion phenomena due to a calcium chloride solution

4 HEAT TRANSFER AND PRESSURE DROP THEORETICAL COMPARATIVE STUDY

A theoretical comparative study has been conducted, in order to compare the secondary fluids commonly found in ice rinks in terms of their performance under certain operating conditions and design. The pump control is also investigated and results from this study will later be compared with measurements from two ice rink refrigeration systems. Neither investment nor running costs are accounted for in this study.

The results of this study are divided in five parts. In the first one, the secondary fluids are compared in terms of the heat transfer, pumping power and refrigeration overall efficiency. The second part highlights the existence of an optimum pump control (ΔT) while the third one focuses on the performance comparison of secondary fluids with calcium chloride. The fourth and fifth parts deal with the freezing point and real / pure secondary fluid comparisons, respectively.

The ice rink design is fixed throughout the study. The calculations are made assuming the steady-state condition. The study is conducted in the way that it is possible to choose one main input variable in a given range (secondary fluid average temperature, ice temperature, temperature difference / pump control). Fixing the ice temperature or the secondary fluid average temperature as the main input parameter may be considered as the control strategy. Figure 19 gives an example of the calculation process. Other parameters such as the heat loads or freezing point are taken constant for a given calculation although it is possible to change their value if needed. The assumptions are reminded for each presented result.

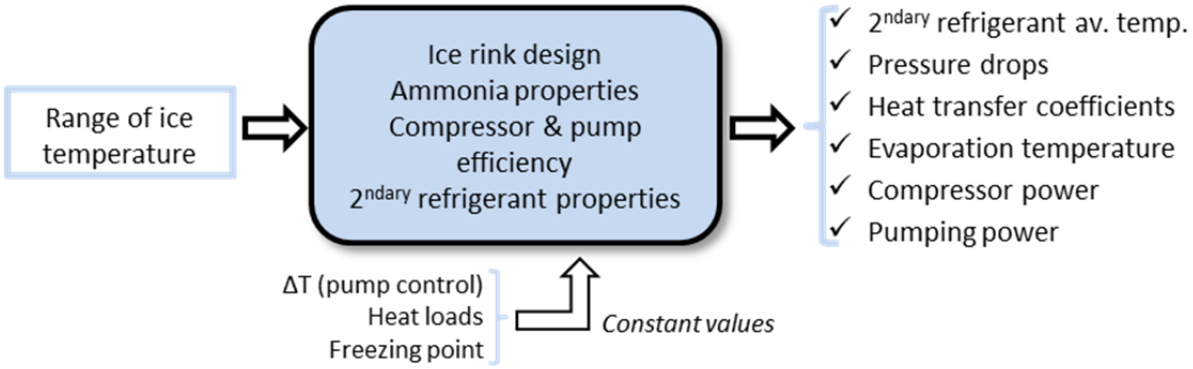

Figure 19: Calculation process with ice temperature as main input for the theoretical comparison

The study is made as a *Microsoft Excel* program to simplify the change of different parameters and make iterative calculations. A given ice rink design is chosen consisting of: the ice floor layout and piping arrangement; the evaporator design; and the ice rink and piping dimensions. All assumptions regarding the refrigeration system design and operating conditions are further described. An example of a *Visual Basic* (programming tool of *Microsoft Excel*) sub-routine is given in Appendix 4.

Ammonia is assumed to be the primary refrigerant used in the heat pump. The characteristics of ammonia as a primary refrigerant were retrieved from both Granryd, et al. (2011) and *EES property calculator software*. As for the secondary fluids properties, the data from Melinder (2010) are used. All secondary fluids listed in Table 2, except carbon dioxide, are compared. As part of this theoretical study, two and three dimensional models of the ice floor have also been developed using *COMSOL Multiphysics* software.

4.1 Assumptions on the evaporator side

The evaporation of the primary refrigerant is achieved by applying the heat source which, in case of ice rink indirect systems, is the secondary fluid. Thus, the evaporator is a simple heat exchanger which transfers heat between the primary and the secondary fluid.

In this study, it is assumed that this heat exchanger is a plate type. Indeed, plate heat exchangers (PHE's) have been increasingly used for the past two decades in refrigeration applications, from domestic heat pumps to large ammonia refrigeration installations. Nowadays, PHE's are widely employed due to their high efficiency, compactness and cost-competitiveness. (Huang, 2010; Sterner & Sunden, 2006).

4.1.1 Evaporator design and geometry

In order to be able to compare all secondary fluids on the same basis, the PHE design is assumed to be the same for each case. The evaporator features were chosen based on the literature study and simulations results from *Alfa Laval* calculation software. Results obtained from the software program are summed up in part 4.1.7 and an example of technical specifications for an *Alfa Laval* PHE can be found in Appendix 3.

The evaporator is considered to be a single-pass counter-flow heat exchanger which is the most common type for heat pump applications (Claesson, 2004). Figure 20 illustrates the flow principle for the chevron-type PHE which plates are corrugated. It is possible to see that the combination of two plates forms a channel in which either the primary or the secondary fluid circulates. The evaporator is considered to be a flooded type evaporator. In this study, the number of plates does not include the two boundary plates. Therefore, for a PHE having a number of plates, N_P, the number of channels, N_C, is

$$N_C = N_P + 1 \quad (25)$$

Figure 20 highlights the alternated flow distribution in the PHE, where each plate separates primary and secondary fluid. Hence, the convective heat transfer linked with the secondary fluid happens on one side whereas boiling heat transfer linked with the primary refrigerant happen on the other side of each plate. Those phenomena are further explained in parts 4.1.3 and 4.1.5.

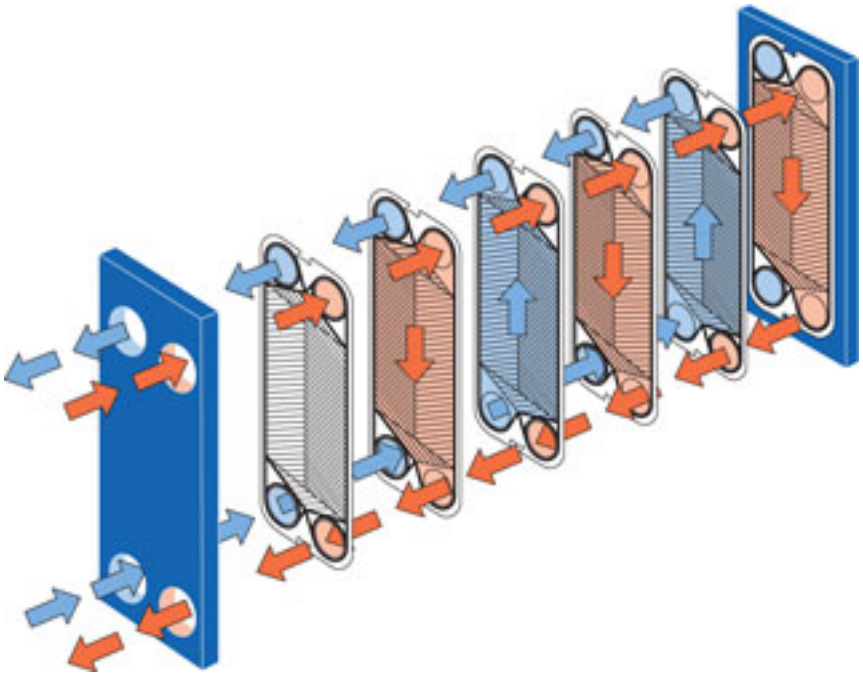

Figure 20: Flow configuration in a single-pass counter-flow PHE – Courtesy of ALFA LAVAL

The main geometrical features of the plates are: the effective channel length (L_{eff}) and width (W), the corrugation pitch (Λ), the plate thickness (δ), the chevron angle (φ), the pressing depth (b), the surface enlargement factor (Φ) and the hydraulic diameter (d_h). Further details on the first six ones are given in Figure 21. Φ and d_h depend directly on the other parameters, L_{eff}, W, Λ, δ, φ and b. Other number related to the PHE geometry, such as the Reynolds (Re) and the Nusselt (Nu) number are described in part 4.1.2. The surface enlargement factor, a dimensionless number is defined as (Claesson, 2004)

$$\Phi = \frac{2}{\Lambda}\int_0^{\frac{\Lambda}{2}} \sqrt{1 + \left(\frac{d}{dx}\left(y(x)\right)\right)^2}\, dx \qquad (26)$$

where

- y is the corrugation function
- the $x - axis$ is along with the plate width as shown in Figure 21.

Thus, the surface enlargement factor is the ratio between the corrugated width and the straight width of the plate. This ratio commonly varies from 1,15 to 1,25. Using a simple sinusoidal corrugation function, the surface enlargement factor equals 1,183 (Claesson, 2004).

The hydraulic diameter is known as

$$d_h = 4 \cdot \frac{A}{P} \qquad (27)$$

where

- A is the cross sectional area in m^2.
- P is the wet perimeter in m.

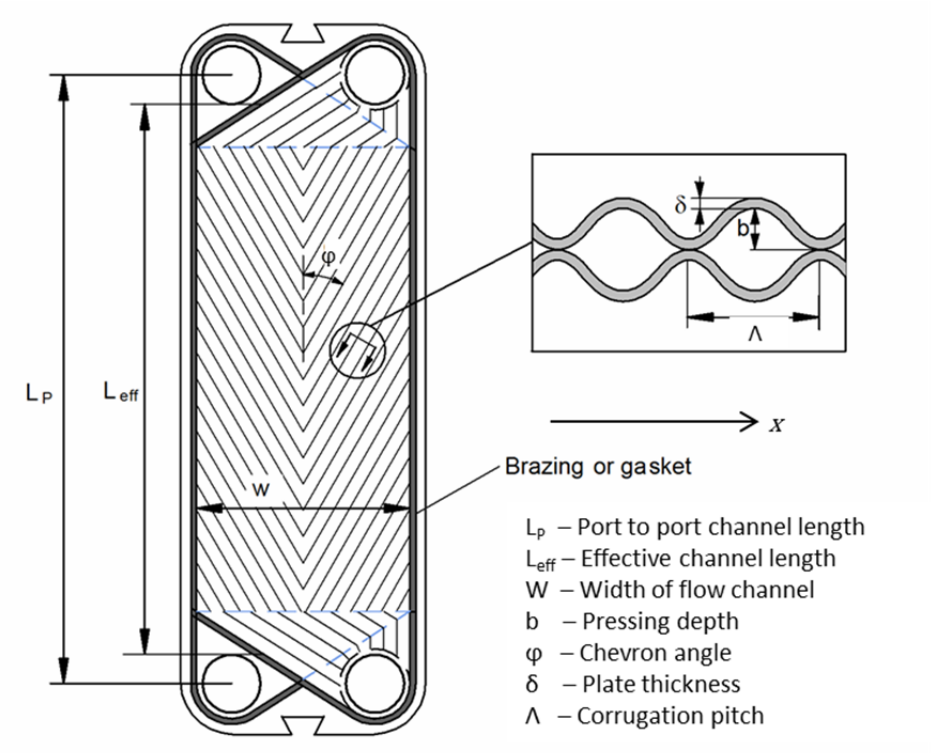

Figure 21: Geometry and features of a plate from a chevron-type PHE (Huang, 2010)

For PHE's, the hydraulic diameter may be expressed as a function of the pressing depth, b, and the surface enlargement factor, Φ

$$d_h = \frac{2 \cdot b}{\Phi} \quad (28)$$

The plates are considered to be made from titanium. Other materials such as copper or stainless steel may be utilized for this application; however corrosion phenomena may occur while having calcium chloride as the secondary fluid. Titanium has good mechanical and corrosion resistance which makes it an excellent material choice for PHE's applications; the main drawback being its high-cost (Ignatowicz, 2008). Therefore, the thermal conductivity of the plate is 21,9 $W.m^{-1}.K^{-1}$ at 27°C (Incropera, et al., 2007).

All evaporator features chosen for calculations are explained in Table 3. The heat transfer area for one plate is calculated as (Huang, 2010)

$$A_{ht} = W \cdot \Phi \cdot L_{eff} \quad (29)$$

where

- W is the plates' width in m.
- Φ is the surface enlargement factor, *dimensionless*.
- L_{eff} is the effective plate length in m.

4.1.2 Reynolds, Nusselt, and Prandtl number – Moody friction factor

This part is dedicated to the definition of all dimensionless number needed for calculations. Correlations used to calculate both the Nusselt number and the Moody friction factor are further presented in part 4.1.3, 4.1.4 and 4.1.5.

Table 3: PHE design features chosen for the theoretical comparison

PHE feature	Formula	Value	Unit
Pressing depth	b	0,003	m
Surface enlargement factor	Φ	1,18	-
Hydraulic diameter	d_h	5,08E-03	m
Number of plates	N_P	121	-
Number of channels	N_C	122	-
Chevron angle	ϕ	60	°
Reverse chevron angle	β	30	°
Corrugation pitch	Λ	0,012	m
Plate width	W_{plate}	0,4	m
Plate length (port to port)	L_{plate}	0,8	m
Heat transfer effective length	L_{eff}	0,64	m
Average heat transfer area (for one plate)	A_{ht}	0,30208	m^2
Plate thickness	δ	0,0005	m
Thermal conductivity of plate material	k_{plate}	21,9	$W.m^{-1}.K^{-1}$
Port diameter	D_{port}	0,1	m

In the literature, two different definitions of the hydraulic diameter may be found leading to two different definitions of the Reynolds (Re) and Nusselt (Nu) numbers, and the friction factor (f). Only the definition given in part 4.1.1 is used in this study. Hence the following definitions of those three dimensionless numbers (Huang, 2010)

$$Re = \frac{G \cdot d_h}{\mu} = 2 \cdot \frac{\dot{m_{tot}}}{W \cdot b \cdot N_C} \cdot \frac{d_h}{\mu} \quad (30)$$

where

- $\dot{m_{tot}}$ is the total mass flow of the fluid in $kg.s^{-1}$.
- G is the mass flux in $kg.m^{-2}.s^{-1}$.
- W is the plates' width in m.
- b is the pressing depth in m.
- N_C is the number of channels.
- d_h is the hydraulic diameter in m.
- μ is the dynamic viscosity in $Pa.s$.

and

$$Nu = \frac{h \cdot d_h}{k} \quad (31)$$

where

- h is the convection heat transfer coefficient in $W.m^{-2}.K^{-1}$.
- k is the thermal conductivity in $W.m^{-1}.K^{-1}$.
- d_h is as defined in eq.(30).

One can notice that the definition of G implies an even flow distribution in the PHE. This might not be true for a real PHE but in order to simplify the calculations it was assumed that the flow distribution is even.

The Prandtl number is simply defined as

$$Pr = \frac{C_p \cdot \mu}{k} \quad (32)$$

where

- C_p is the specific heat capacity in $J.kg^{-1}.K^{-1}$.
- k and μ are as defined in eq.(30)and (31)

As for the friction factor, also called Moody (Darcy) friction factor, its general equation when considering a channel is given as

$$f = 2 \cdot \frac{\Delta p \cdot d_h}{\rho \cdot u^2 \cdot L} \quad (33)$$

where

- Δp is the pressure drop in Pa.
- u is the fluid velocity in $m.s^{-1}$.
- $L\ (L_{eff})$ is the length of the channel in m.
- ρ is the density in $kg.m^{-3}$.
- d_h is the hydraulic diameter in m.

Care should be taken when using Moody and Fanning friction factor, c_f sinde those two factors are proportional but not equal (Huang, 2010). The Fanning friction factor may be expressed as

$$c_f = \frac{f}{4} \quad (34)$$

The Fanning friction factor is not used in any part of the study. When the term "friction factor" is employed it refers to the Moody friction factor.

4.1.3 Convective heat transfer phenomena on the secondary fluid side

The convective heat transfer on the secondary fluid side is characterized by the convection heat transfer coefficient. This coefficient can be determined if the Nusselt number is known. Several correlations exist to estimate the Nusselt number in PHE's. The one developed by Martin (1996) extending the Lévêque theory is a general correlation because it includes geometrical parameters of the plates. Nevertheless, a good agreement between the theoretical and experimental results was shown for commercial plates (Claesson, 2004). Therefore, this correlation is used and the expression of the Nusselt number is then given as

$$Nu = 0{,}122 \cdot Pr^{\frac{1}{3}} \cdot \left(\frac{\mu}{\mu_w}\right)^{\frac{1}{6}} \cdot (f \cdot Re^2 \cdot \sin(2 \cdot \varphi))^{0{,}374} \quad (35)$$

where

- μ and μ_w are respectively the bulk viscosity and the viscosity at the wall temperature in $Pa.s$.
- Pr is the Prandtl number as defined in eq.(32).
- f is the friction factor as defined in eq.(33).
- Re is the Reynolds number as defined in eq.(30).
- φ is the chevron angle in °.

The equation by Martin (1996) for the friction factor f used in eq.(35) is given in part 4.1.4 (eq.(39)).

The range of validity for this correlation was not specified in the original source; however other studies state that it can be used for Reynolds numbers between 400 and 10000 since it was the range in which it was varied originally (Claesson, 2004; Huang, 2010).

For Reynolds number smaller than 400, the correlation by Muley and Manglik (1999) is employed to compute the Nusselt number

$$Nu = 0{,}44 \cdot \left(\frac{\varphi}{30}\right)^{0{,}38} \cdot Re^{0{,}5} \cdot Pr^{\frac{1}{3}} \cdot \left(\frac{\mu}{\mu_w}\right)^{0{,}14} \quad (36)$$

Note that all parameters have been presented in eq.(35).

Other equations, such as the one by Wanniararchchi et al (1995), may be considered to calculate the convection heat transfer coefficient on the secondary fluid side.

4.1.4 Pressure drop on the secondary fluid side

The pressure drop in one channel may be directly found from eq.(33) writing the mass flux G as the product of the density ρ and the velocity u,

$$G = \rho \cdot u \quad (37)$$

and including geometrical definitions of the PHE, eq.(33) becomes

$$\Delta p = f \cdot \frac{G^2 \cdot L_{eff}}{2 \cdot \rho \cdot d_h} \quad (38)$$

The Moody friction factor is computed from the equation provided by Martin (1996). It depends on the chevron angle φ and the Reynolds number Re.

$$\frac{1}{\sqrt{f}} = \frac{\cos(\varphi)}{\sqrt{0{,}18 \cdot \tan(\varphi) + 0{,}36 \cdot \sin(\varphi) + \frac{f_0}{\cos(\varphi)}}} + \frac{1 - \cos(\varphi)}{\sqrt{3{,}8 \cdot f_{1,0}}} \quad (39)$$

where

$$f_0 = \begin{cases} {}^{64}/_{Re} & if\ Re < 2000 \\ (1{,}8 \cdot \log(Re) - 1{,}5)^{-2} & if\ Re \geq 2000 \end{cases}$$
$$f_{1,0} = \begin{cases} {}^{597}/_{Re} + 3{,}85 & if\ Re < 2000 \\ {}^{39}/_{Re^{0{,}289}} & if\ Re \geq 2000 \end{cases} \quad (40)$$

The pressure drop in the inlet and outlet ports of each plate must also be accounted. An extensively cited equation is the one provided by Shah and Focke (1988)

$$\Delta p_{ports} = 1{,}5 \cdot \left(\frac{G^2}{2 \cdot \rho}\right)_{inlet} \cdot N_{pass} \quad (41)$$

where

- N_{pass} is the number of pass (generally 1 in evaporators)
- G_{inlet} is the mass flux at the inlet port in $kg.m^{-2}.s^{-1}$.
- ρ is the density in $kg.m^{-3}$.

Nevertheless, it is stated that Martin's correlation for friction factor already accounts for the ports head losses (Palm & Claesson, 2006).

4.1.5 Boiling heat transfer phenomena on the ammonia side

Two different physical mechanisms contribute to boiling heat transfer. In the first one, called flow boiling, the heat is transferred to a fluid having a motion whereas, in the second one, called pool boiling, the fluid is stagnant. It should be noticed that the motion of the fluid is assessed with the heat source surface as a frame of reference. Since ammonia is circulating in the PHE, flow boiling is of interest in this study.

The flow boiling may be divided into two categories: nucleate boiling and convective evaporation. Nucleate boiling refers to the heat transfer caused by the formation of bubbles and their detaching from the heat source surface. This heat transfer phenomena is similar to the pool boiling, therefore the pool boiling correlations are often used. As for the convective evaporation process, it is similar to the convection phenomena happening with a single-phase fluid. As a consequence, known correlations for single-phase flow are most of the time used to quantify this part of the boiling heat transfer. The total heat

transfer is estimated by weighting and summing the contribution of each mechanism. It is often stated that bubble nucleation is suppressed by the forced convective evaporation. The interactions of those phenomena are however not yet well understood and most experimental studies conduct regression analysis to fit their experimental results (Claesson, 2004, Huang, 2010).

The correlation developed by Ayub (2003) is so far the most universal one, available for any type of commercial plates and any chevron angle. Huang (2010) claimed it was one of the most promising correlations although it is not dimensionally consistent. For those reasons, the heat transfer on the boiling side is characterized by this correlation. It was originally given in English units but it was converted by the latest cited author as

$$h = 0{,}025 \cdot C \cdot \left(\frac{k_l}{d_h}\right) \cdot \left(\frac{Re_l^2 \cdot h_{lg}}{L_{eff}}\right)^{0{,}4124} \cdot \left(\frac{P}{P_{crit}}\right)^{0{,}12} \cdot \left(\frac{65}{\beta}\right)^{0{,}35} \quad (42)$$

where

- $C = \begin{cases} 0{,}1121 & \text{for flooded evaporators} \\ 0{,}0675 & \text{for dry expansion (DX)} \end{cases}$
- The subscript l refers to liquid.
- k is the thermal conductivity in $W.m^{-1}.K^{-1}$.
- h_{lg} is the latent heat in $J.kg^{-1}$.
- P and P_{crit} are the evaporation pressure and the critical pressure in $bars$, respectively.
- β is the complementary angle to the chevron one in °.
- d_h is the hydraulic diameter in m.
- L_{eff} is the effective length of one plate in m.
- Re is the Reynolds number (calculated with the liquid-state viscosity).

4.1.6 Overall heat transfer coefficient *UA* and thermal resistance *R*

The heat transfer coefficient in PHE's UA is defined as

$$\dot{Q} = UA \cdot \Delta T_{LMTD} \quad (43)$$

where

- $\dot{Q}$ is the heat flow or the cooling capacity in W.
- ΔT_{LMTD} is the Log Mean Temperature Difference in K.

Since ammonia is an azeotropic mixture, the temperature on the primary refrigerant side is constant if the superheat process inside the evaporator is neglected. Thus, using temperatures definitions from Figure 22, the log mean temperature difference may be expressed as

$$\Delta T_{LMTD} = \frac{T_{sec.fl.-in} - T_{sec.fl.-out}}{\ln\left(\frac{T_{sec.fl.-in} - T_{evap}}{T_{sec.fl.-out} - T_{evap}}\right)} \quad (44)$$

As for the resistance, it may simply be defined as

$$R = \frac{1}{UA} \quad (45)$$

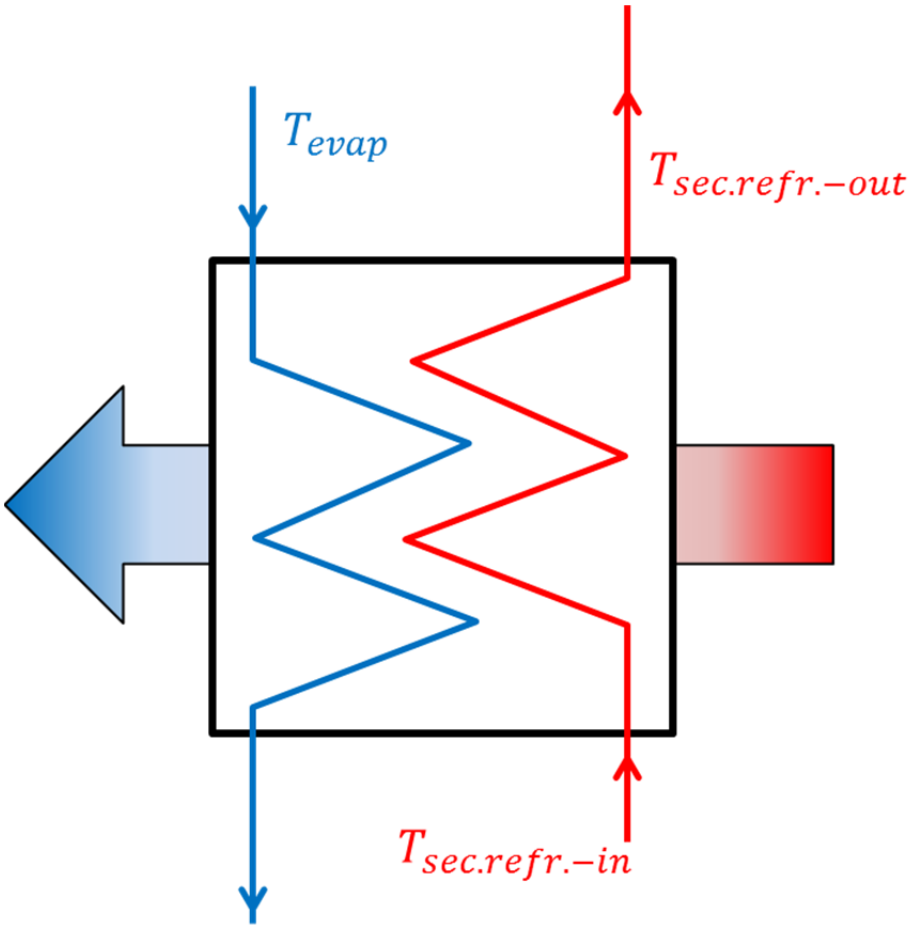

Figure 22: Heat transfer process inside the evaporator

To calculate the *UA* value, one-dimensional heat transfer process is considered within the PHE and the analysis is similar to one for a plane wall. A thermal resistance equivalent diagram is presented in Figure 23. The total heat transfer resistance for one plate can be calculated as the sum of all resistances. The resistance for each plate will be the same and plates are in parallel, hence the formula for *UA*

$$UA = A \cdot \frac{N_P}{\frac{1}{h_{boil}} + \frac{\delta}{k} + \frac{1}{h_{sec.fl.}}} \quad (46)$$

where

- A is the heat transfer area in m^2 (a single plate surface as defined in eq.(29)).
- h_{boil} and $h_{sec.fl.}$ refer to the boiling and secondary fluid convective heat transfer coefficients in $W.m^{-2}.K^{-1}$, respectively.
- N_P is the total number of plates in the PHE.
- δ is the plate's thickness in m.
- k is the plates thermal conductivity in $W.m^{-1}.K^{-1}$

In the literature as well as in industrial calculations, a fouling resistance for the secondary fluid is accounted. Nevertheless, the coefficients or correlations for the fouling resistance in PHE are still lacking (Huang, 2010). Henceforth no fouling is considered on either sides of the PHE for this study. Additionally, the evaporator is assumed to be insulated; meaning that all the heat from the secondary fluid is transmitted to the boiling primary refrigerant.

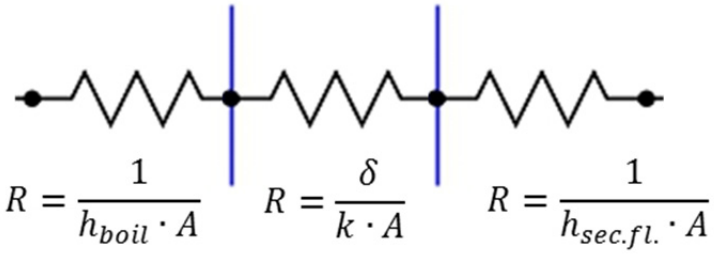

Figure 23: Thermal equivalent circuit for heat transfer through one plate of PHE

4.1.7 Results from ALFA LAVAL software

Alfa Laval is one of the biggest suppliers of evaporators for the ice rinks using ammonia as primary refrigerant in Sweden. The company has been involved in the design of several ice rink arenas such as the Moscow Ice Palace or the upcoming Bolshoi Ice Palace that will operate for 2014 Winter Olympics (Alfa Laval, 2012).

Alfa Laval has developed its own software to optimize the PHE design for given operational conditions. With the kind permission from Alfa Laval, this software was used to confirm the assumed design in this study of the heat transfer and pressure drop. Figure 24 shows the software interface as well as the calculation results for calcium chloride on the right side of the figure. The design results are slightly different from the fixed design in this comparative theoretical study. The number of plates is 142 whereas it is assumed in this study to be 123 (121 plus the two boundary plates). The total heat transfer area (34 m²) is also higher than assumed (31 m²). Several reasons may explain these slight differences. First of all, the aim of design software calculation is to find the best possible design for given conditions whereas it is not the aim in this study. A different heat transfer correlation (Boyko-Kruzhilin) is used; which may lead to different heat transfer rates. Finally, in this study no fouling was accounted whereas a fouling resistance is accounted in the Alfa Laval simulation software, leading to higher heat transfer resistance and, thus, to a larger heat transfer area needed.

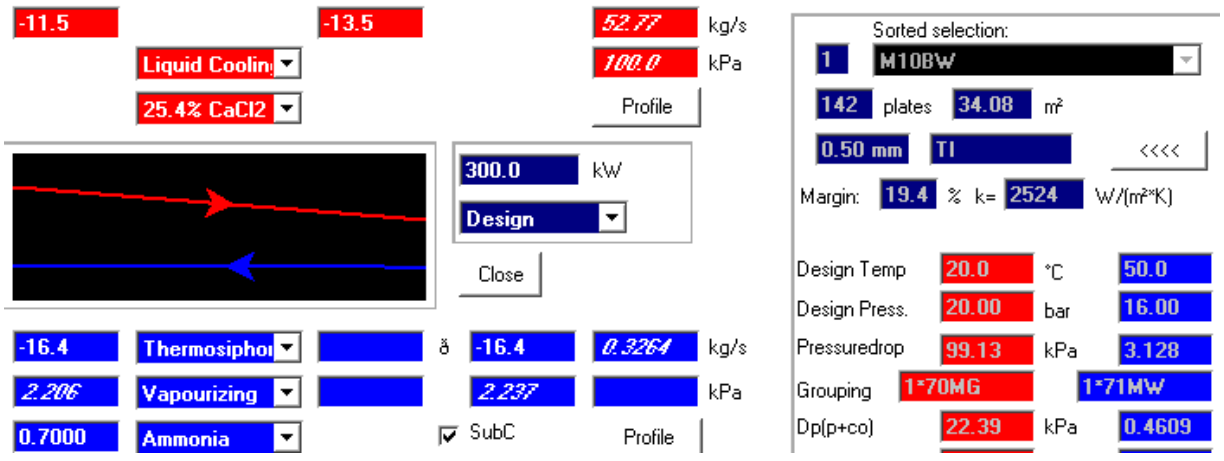

Figure 24: Alfa Laval software interface and PHE design results for calcium chloride

4.2 The ice rink design assumptions

As in most cases, the ice rink refrigeration system is an indirect refrigeration system. Some features of the ice rink design must be assumed in order to perform calculations.

4.2.1 Indirect loop and cooling loads

The indirect loop on the cooling side is considered to be as the one described in Figure 9. Regarding the heat transfer two components are of interest: the heat exchanger working as evaporator and the ice rink floor working as a huge heat exchanger itself. In this study, the heat gains from the ground are neglected since insulation below the ice rink is assumed. Numerical simulations have shown that the heat gains were negligible for the insulation thickness assumed in this study compared to the heat loads. The sum of ice floor heat loads, heat gains from the pumps, the headers and the distribution pipes represents then the total cooling capacity. According to values found in Karampour (2011), the heat loads and heat gains shares are taken as 90 % and 10 %, respectively. The cooling rate is a variable that can be changed in the simulation model.

The distribution pipes are linking the ice rink floor to the evaporator. Their length is assumed to be 20 m and their inner diameter as 150 mm. Those pipes are assumed to be made of steel with a roughness of 50 μm. The pump is also an important component to consider as well as the ice rink floor layout and the cooling machine. Further details on those elements are given in the following parts.

4.2.2 Pump control (ΔT)

When assessing the performance in terms of the heat transfer and pressure drop, the pump control method is a very important factor. Indeed, the flow rate has a direct influence on the total pumping power and impacts the convection heat transfer coefficients. Higher flow rates lead to higher heat transfer coefficients based on the Nusselt number correlations. Moreover, the flow regime strongly affects the heat transfer rate: laminar flow gives rather low convection heat transfer coefficient whereas those for turbulent flow are higher.

The secondary fluid flow in ice rink is controlled with regards to the given secondary fluid temperature difference since an even temperature distribution is required over the whole ice sheet. In this study as well as in many real ice rinks the pump is controlled in order to maintain a constant temperature difference; although it might not lead to the optimum power for the considered heat loads.

The optimum pump control is discussed in part 4.6. The results shown there highlight the fact that an optimum pump control, or ΔT, may be found for a given cooling capacity.

At a given cooling capacity $\dot{Q}$; temperature difference of the secondary fluid ΔT; density ρ and specific heat capacity C_p at average operational temperature, the total volumetric flow rate $\dot{V}_{tot}$ may be calculated as

$$\dot{V}_{tot} = \frac{\dot{Q}}{\Delta T \cdot \rho \cdot C_p} \quad (47)$$

The temperature over which the pump is controlled may be referred to as the pump control or the abbreviation ΔT.

Note that other ways of controlling the pump(s) in ice rinks exists but this type of pump control was assumed in this study.

Knowing the total flow rate; the distribution pipes diameters and pipe arrangement, the Reynolds number range inside the evaporator and inside the ice rink floor can be calculated. Eq.(30) gives the Reynolds number in the PHE and the ones in distribution pipes and ice rink floor are respectively given as

$$Re = 4\frac{\dot{V}_{tot} \cdot \rho}{\pi \cdot d_h \cdot \mu} \quad (48)$$

and

$$Re = 4\frac{\dot{V}_{tot} \cdot \rho}{N_{U-pipes} \cdot \pi \cdot d_h \cdot \mu} \quad (49)$$

where

- $N_{U-pipes}$ is the number of U-pipes in the ice rink floor.
- ρ is the density in $kg.m^{-3}$.
- $\dot{V}_{tot}$ is the total volumetric flow in $m^3.s^{-1}$.
- μ is the dynamic viscosity in $Pa.s$.
- d_h is the hydraulic diameter for the considered pipes.

The hydraulic diameter is different in the distribution and the ice rink floor pipes.

4.2.3 Refrigeration system and primary refrigerant

Since this study focuses on the secondary fluids less detailed analysis is performed for the cooling machine. Namely, calculations are based on a theoretical refrigeration cycle using key-values from ammonia pressure-enthalpy diagram ((P, h) diagram). Figure 25 presents such theoretical cycle on (R717) ammonia (P, h) diagram. Although the compressor isentropic efficiency depends significantly on the type of compressor used, system design and operational conditions, it is assumed as a constant value of 0,65. The expansion is isenthalpic and both evaporation and condensation pressures are taken constant. Since the evaporator is considered to be flooded type, rather small superheating of 1 K is chosen. As for subcooling, it is assumed to be 5 K. The system shall include the vapor/liquid separation process since the evaporator is flooded but the percentage of mass flow recirculating in the evaporator is not known. Eq. (42) was used to calculate the boiling heat transfer coefficient for the flooded evaporator (C=0,1121) with a slight superheat.

A constant condensation temperature of +20°C is assumed. Since the evaporation temperature depends on the type of secondary fluid used, its average temperature and the heat loads; the input data for every evaporation temperature need to be known in order to perform calculations. Thus, for each required data, it is necessary to have the function of input data value versus the temperature. In the literature, values are often only given for a discrete number of temperatures. But with help of the polynomial approximation tool in *Microsoft Excel*, such functions could be obtained. The variables needed for calculations are

- h_l and h_g: Enthalpies at the saturated liquid and vapor states in $J.kg^{-1}$.
- v_l: Specific volume at saturated liquid state in $m^3.kg^{-1}$.
- k_l: Thermal conductivity at saturated-liquid state in $W.m^{-1}.K^{-1}$.
- μ_l: Dynamic viscosity at saturated-liquid state in $Pa.s$.
- P: Evaporation pressure (absolute) in $bars$.
- COP_{is}: Isentropic coefficient of performance, *dimensionless.*
- $h_{superheat}$: Enthalpy of the superheated fluid after evaporation in $J.kg^{-1}$.
- $h_{subcool}$: Enthalpy of the subcooled (saturated) fluid after condensation in $J.kg^{-1}$.

Functions associated with the two latest variables were determined using *EES Property Calculator Software.* Other data were taken from Granryd et al. (2011) which uses data from *NIST* software *REFPROP 6.01.*

The critical pressure needed in eq. (42) was taken as 113,33 bars. The primary refrigerant mass flow is calculated with the cooling capacity $\dot{Q}$; enthalpies at the superheated state $h_{superheat}$ and at subcooled state $h_{subcool}$

$$\dot{m} = \frac{\dot{Q}}{h_{superheat} - h_{subcool}} \qquad (50)$$

Since the expansion is isenthalpic, the enthalpy at subcooled state is also the enthalpy of ammonia entering the evaporator.

The Reynolds number needed in eq. (42) is

$$Re_{lo} = \frac{G \cdot d_h}{\mu_l} = 2 \cdot \frac{\dot{m}}{W_{plate} \cdot b \cdot N_C} \cdot \frac{d_h}{\mu_l} \qquad (51)$$

All parameters are already explained in eq.(30). The mass flow $\dot{m}$ and the dynamic viscosity at liquid state μ_l refer to the primary refrigerant, ammonia.

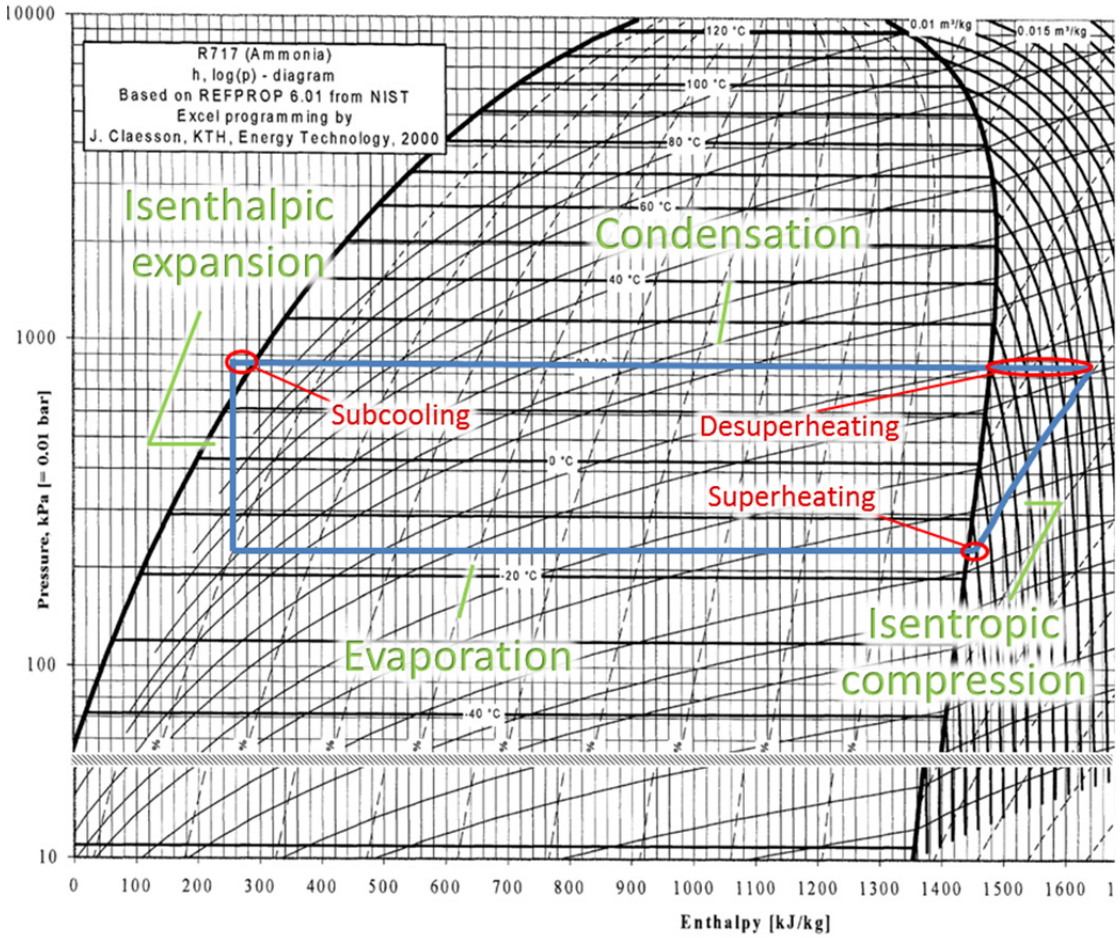

Figure 25: Pressure-enthalpy (P,h) diagram of ammonia – Example of theoretical refrigeration cycle with constant evaporation and condensation pressures, isenthalpic expansion and isentropic compression (Granryd, et al., 2011)

Tables used as reference and an example of polynomial approximation function are given in Appendix 2. Using interpolation function like cubic spline is scientifically more correct in this case. However, it is much less convenient to use in *Microsoft Excel* than the least square method for polynomial approximation suggested previously. Moreover, the least square method gives coefficients of determination (R^2) close to 1 and leads to sufficiently accurate results.

4.2.4 Ice rink floor layout

The ice rink is assumed to be used for the ice hockey purpose as the one shown in Figure 2. It is considered 60 m long and 30 m wide. From the supplying header to the return one, the cooling pipes have a U-shape as illustrated in Figure 26. The headers are located on one of the shorter sides of the ice rink so that the U-pipes are placed along the length. Moreover, the reverse-return header solution is recommended in order to have an evenly distributed flow. The spacing between two successive parallel straight pipes is 10 cm. The U-shaped pipes are embedded into a concrete layer of 15,5 cm as shown in Figure 27. Additionally, an ice layer of 3 cm and an insulation layer of 15 cm is assumed. Moreover, the pipe outer diameter is taken as 25 mm and its wall thickness as 2,3 mm.

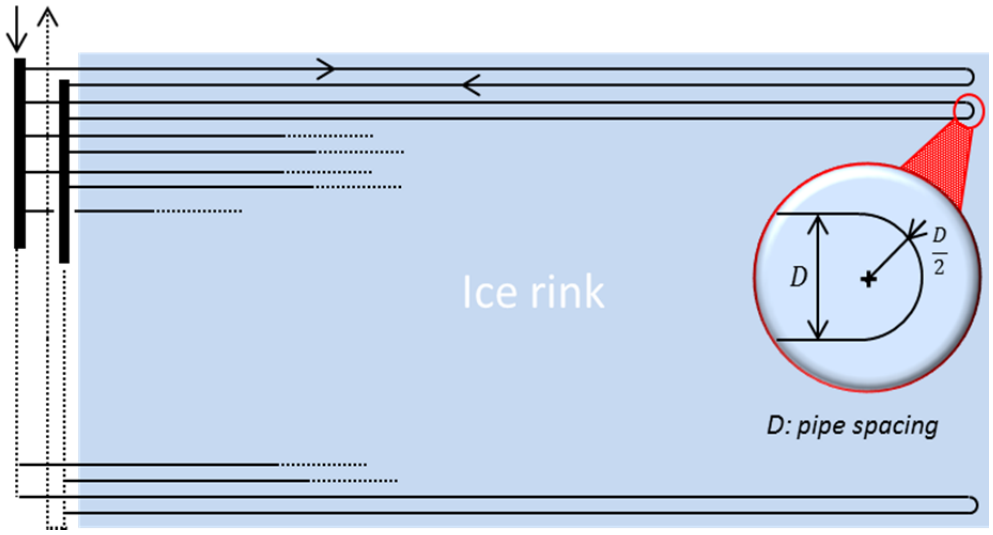

Figure 26: U-pipe arrangement in the ice rink floor with reverse return header

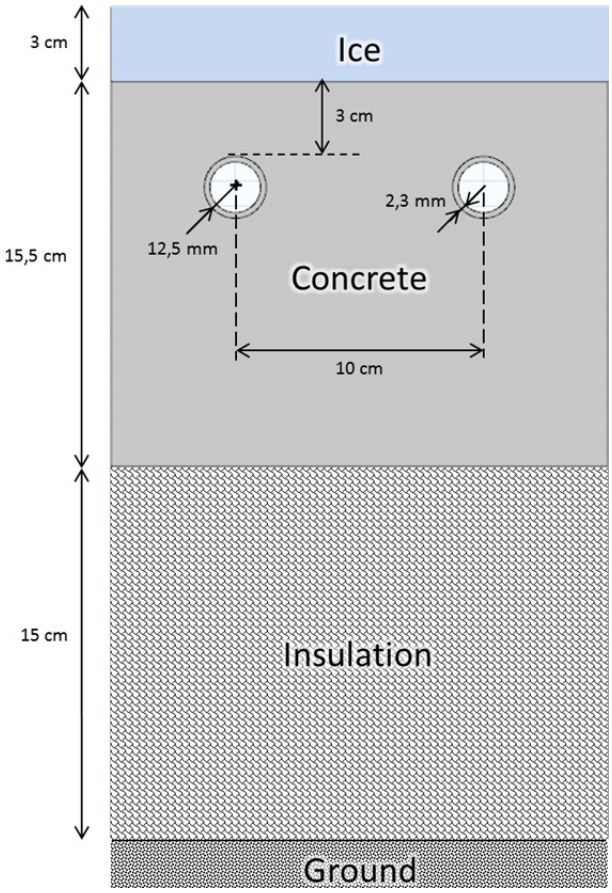

Figure 27: Ice pad cross section with U-pipe

The back-and-forth length of a U-pipe is approximately 120 m and the total number of U-pipes, $N_{U-pipes}$, is 150, calculated as

$$N_{U-pipes} = \frac{W_{ice}}{D_{spacing}} \quad (52)$$

where

- W_{ice} is the ice pad width in m.
- $D_{spacing}$ is the distance between two consecutive pipes in m.

4.2.5 Characterization of the heat transfer

The total heat transfer process occurring in the ice rink floor is based on convection and conduction mechanisms. The convection heat transfer coefficient strongly depends on the flow regime; hence two different equations are used. For Reynolds number Re greater than 2300, the widely used Gnielinski (1976) correlation is employed to calculate the Nusselt number Nu

$$Nu = \frac{\frac{f}{8} \cdot (Re - 1000) \cdot Pr}{1 + 12{,}7 \cdot \left(\frac{f}{8}\right)^{0{,}5} \cdot \left(Pr^{\frac{2}{3}} - 1\right)} \quad (53)$$

where

- f is the friction factor calculated as in eq.(61), *dimensionless*.
- Pr is the Prandtl number, *dimensionless*.

The Prandtl number range for using this correlation ($Pr > 0{,}5$) is always fulfilled. The upper limit for Reynolds number ($Re \leq 10^6$) is never exceeded. Seghouani and Galanis (2009) recommended using this equation to calculate the Nusselt number for the single-phase secondary fluids.

This equation is only valid for the fully-developed flow but the maximum entry length (thermal and hydraulic) for turbulent flow $x_{fd,max}$ is (Incropera, et al., 2007)

$$x_{fd,max} = 60 \cdot D_{in} \quad (54)$$

Considering an inner pipe diameter D_{in} of 0,0204 m, the equation stated above gives a value of 1,224 m, which is insignificant when comparing to the total 120 m pipes' length. Therefore, as long as the flow regime is turbulent, correlation (53) is used.

However, when laminar flow is occurring inside the ice floor pipes, the effect of the entry region needs to be considered. Indeed, due to high values of Prandtl numbers at low temperatures, the thermal entry length may be significant. The equation provided by Hausen (1943), incorporating Graetz number Gz is valid for all cases as long as the velocity profile is fully-developed.

$$Nu = 3{,}66 + \frac{0{,}0668 \cdot Gz}{1 + 0{,}04 \cdot Gz^{\frac{2}{3}}} \quad (55)$$

where the Graetz number Gz is calculated using the Reynolds and Prandtl numbers, Re and Pr, the inner diameter D_{in} and the pipes' length L, as

$$Gz = \left(\frac{D_{in}}{L}\right) \cdot Re \cdot Pr \quad (56)$$

This equation assumes a constant surface temperature of the pipe inner wall. As in the case of the turbulent flow, the hydraulic entry length $x_{fd,h}$ is negligible for laminar flow since it is given as

$$x_{fd,h} = Re \cdot D_{in} \cdot 0{,}05 \qquad (57)$$

The maximum possible hydraulic entry length is given for the highest laminar Reynolds number of 2300. Given the same pipe diameter D_{in} as previously mentioned, a maximum value of 2,346 m is found. Therefore, eq.(55) gives a good approximation for the total 120 m pipes' length.

To assess the equivalent heat transfer resistance from the pipe wall to the ice surface, a two-dimensional numerical model has been developed with *COMSOL Multiphysics* software. The choice of a two-dimensional simulation implies that the resistance is assumed constant along the pipe length and in the bends. A three-dimensional model has also been investigated and is quickly presented in part 8. The two models are also compared in this part. The results from the previously mentioned two-dimensional model are graphically presented in Figure 28 for the heat flow of 346 kW. The simulated streamline pattern shows that the heat gains from the ground have no significant effect on the overall heat transfer process. Without any insulation layer, the heat gains from the ground should be considered, but having a 15 cm insulation layer, makes the heat gains negligible. The boundary conditions are as following:

- constant heat outflow in the inner wall pipes (e.g. 14 W.m^{-1} per pipe)
- constant temperature at the ice top (e.g. -3°C)
- constant ground temperature of 5°C (Makhnatch, 2011)
- remaining boundaries as thermal insulation

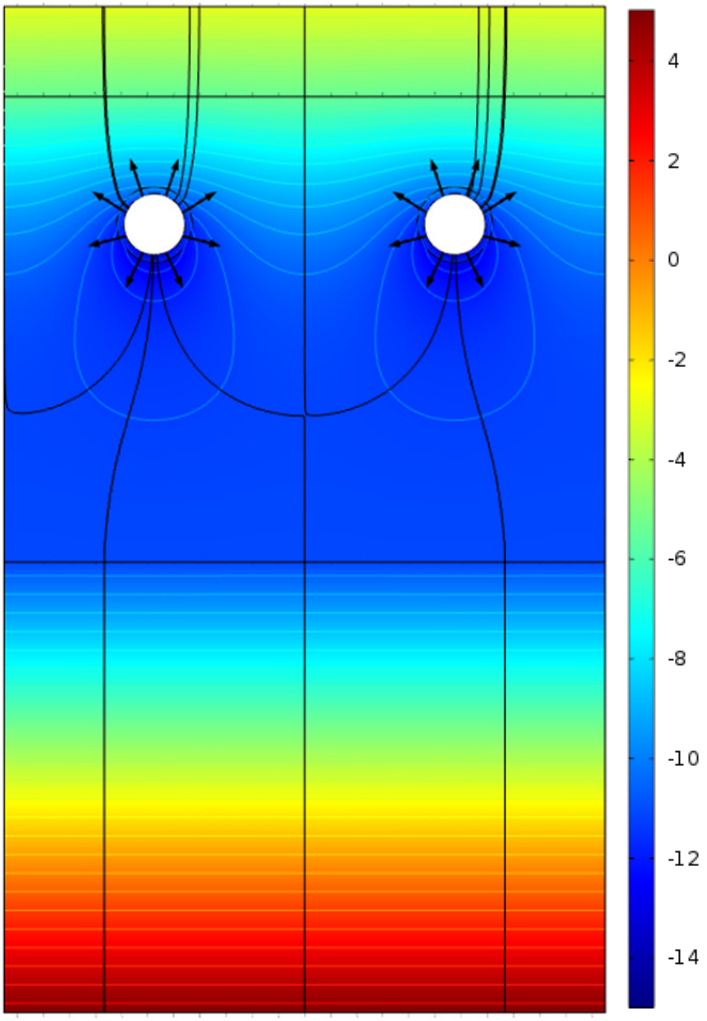

Figure 28: Temperature profile obtained from *COMSOL Multiphysics* simulation for a heat flow of 346 kW

Knowing the heat flow, Φ, and the ice top temperature, the conduction equivalent resistance is then calculated by taking the difference between the ice top temperature and the average temperature of the inner pipe wall, ΔT

$$R_{cond} = \frac{\Delta T}{\Phi} \quad (58)$$

Since a two-dimensional model is considered, the heat flow is provided in $W.m^{-1}$. Hence, the resistance unit is $m.K.W^{-1}$. The resistance was calculated for various heat outflows, and the average value from all simulation results was taken for further calculation. This value equals 0,5602 $m.K.W^{-1}$. All results are presented in a table in Appendix 5. The total heat transfer resistance is then calculated as a sum of the resistances

$$R_{ice-floor} = \frac{R_{cond} + \frac{1}{h \cdot \pi \cdot D_{in}}}{L \cdot N_{U-pipes}} \quad (59)$$

where $R_{cond}\ [m.K.W^{-1}]$ is the conduction resistance given in eq.(58), $h\ [W.m^{-2}.K^{-1}]$ is the convection heat transfer coefficient, $D_{in}\ [m]$ is the inner pipe diameter, $L\ [m]$ is a U-pipe's length, $N_{U-pipes}$ is the total number of U-pipes.

The total heat flow is then calculated using eq.(43) and (45). The LMTD equation is nonetheless slightly different from the one used for the PHE calculation since the heat loads are lower than the cooling capacity. Indeed, the heat gain heats up the secondary fluid outside the ice pad (pump work, heat gains through distribution pipes). Since the spatial distribution of the heat gains is not known, it is assumed that the ice floor inlet temperature equals the outlet temperature from the PHE. Additionally, the ice floor outlet temperature is lower than the inlet temperature of the PHE. Knowing the outlet temperature of the ice rink floor designated $T'_{sec.refr.-out}$

$$\Delta T'_{LMTD} = \frac{T_{sec.refr.-in} - T'_{sec.refr.-out}}{\ln\left(\frac{T_{sec.refr.-in} - T_{evap}}{T'_{sec.refr.-out} - T_{evap}}\right)} \quad (60)$$

4.2.6 Characterization of the pressure drop

The pressure drops are calculated according to eq.(33). Considering the hydraulic entry length negligible, Gnielinski equation may be used for turbulent flow ($Re > 2300$) to calculate the friction factor f

$$f = (0{,}79 \cdot \ln(Re) - 1{,}64)^{-2} \quad (61)$$

For fully-developed laminar flow, the friction factor is widely known as the Poiseuille's law

$$f = \frac{64}{Re} \quad (62)$$

The pressure drop in the distribution pipes is calculated assuming 20 m as the pipe total length and 150 mm as its diameter. Only major losses are considered since the system design differs from one case to another. In case of the U-pipes' total pressure drop, the minor losses created by U-shaped bend are accounted. The formula referred to as the Weisbach's formula (Saint-Gobain, 1989) is used. It gives the minor loss coefficient K of any bend as

$$K = \left(\left(0{,}131 + 1{,}847 \cdot \left(\frac{D_{in}}{2 \cdot r}\right)^{3{,}5}\right) \cdot \frac{\theta}{90}\right) \quad (63)$$

where

- r is the bend radius of curvature (taken as half the pipe spacing as shown in Figure 26) in m.
- θ is the bend angle in degrees (180° for this case).
- u is the secondary fluid velocity in $m.s^{-1}$.
- D_{in} is the inner pipe diameter in m.

Additionally, the pressure drop in both supply and return headers must be taken into account. The headers consist in a repetitive pattern as shown in Figure 29 for the supply header. Hence, the total pumping power associated with headers may be calculated as the sum of the pumping power for each motif. Three elements are to be considered for the pumping power calculation in each motif: the pumping power linked to the inlet $\left(\Delta p_f \cdot \dot{V}\right)_{in}$, the one linked to the outlet $\left(\Delta p_f \cdot \dot{V}\right)_{out}$ (calculated with the friction factor in eq.(61) or (62)) and eventually the one linked to the minor loss $\left(\Delta p_s \cdot \dot{V}_{in}\right)$ implied by the T-junction. Therefore, for the motif i the pumping power is

$$\left(E_{p,header}\right)_i = \frac{\left(\Delta p_{header} \cdot \dot{V}\right)_i}{e_{pump}} \qquad (64)$$

$$\left(\Delta p_{header} \cdot \dot{V}\right)_i = \left(\Delta p_f \cdot \dot{V}\right)_{in,i} + \left(\Delta p_f \cdot \dot{V}\right)_{out,i} + \left(\Delta p_s \cdot \dot{V}_{in}\right)_i$$

where $\Delta p_f [Pa]$ is the major head loss, $\Delta p_s\ [Pa]$ is the minor head loss, $\dot{V}\ [m^3.s^{-1}]$ is the secondary fluid flow, e_{pump} is the pump efficiency (constant and *dimensionless*).

One header presents as many motifs as the number of U-pipes that is 150 in this study. Considering an even flow distribution in the ice rink floor pipes; in other words a constant secondary fluid flow in each U-pipe; and applying the Vazsonyi's equation provided in Vasava (2007) to calculate the minor loss coefficient k_i for a zero angle (corresponding to a 90° junction) we obtain

$$K_i = \lambda_1 + (2 \cdot \lambda_2 - \lambda_1)\left(\frac{\dot{V}_{out,i}}{\dot{V}_{in,i}}\right)^2 - 2 \cdot \lambda_2 \cdot \left(\frac{\dot{V}_{out,i}}{\dot{V}_{in,i}}\right) \cdot \cos(\alpha') \qquad (65)$$

where

$$\lambda_1 = \begin{cases} 0{,}0712 \cdot \alpha^{0{,}7141} + 0{,}37 & for\ \alpha < 22{,}5° \\ 1 & for\ \alpha \geq 22{,}5° \end{cases}$$

$$\lambda_2 = \begin{cases} 0{,}0592 \cdot \alpha^{0{,}7029} + 0{,}37 & for\ \alpha < 22{,}5° \\ 0{,}9 & for\ \alpha \geq 22{,}5° \end{cases} \qquad (66)$$

$$\alpha' = 1{,}41\alpha - 0{,}00594\alpha^2$$

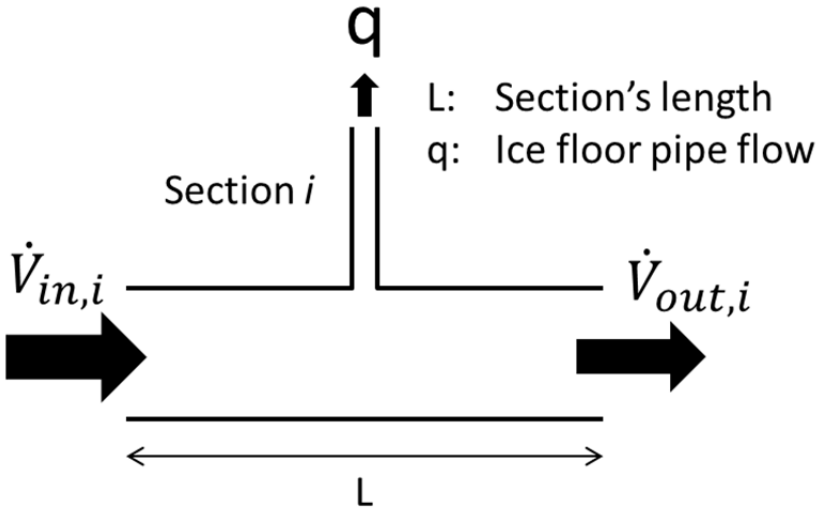

Figure 29: Repetitive flow motif in supply header

The total pumping power associated with one header can then be expressed as a function of the pressure drop – the secondary fluid flow product $(\Delta p \cdot \dot{V})_{tot}$ and the pump efficiency e_{pump}

$$\left(\dot{E}_{p,header}\right)_{tot} = \frac{\left(\Delta p \cdot \dot{V}\right)_{tot}}{e_{pump}}$$

$$\left(\Delta p \cdot \dot{V}\right)_{tot} = 8 \cdot \frac{\rho}{\pi^2} \cdot \frac{1}{d_h^4} \cdot \left(\frac{\dot{V}_{tot}}{150}\right)^3 \left\{ \frac{L}{d_h} \sum_{j=1}^{150} \left(f'_{in,j} \cdot j^3\right) + 0{,}37 \cdot \frac{150 \cdot 151}{2} \right\} \quad (67)$$

where

- ρ is the density in $kg.m^{-3}$.
- d_h is the hydraulic diameter of headers in m.
- $\dot{V}_{tot}$ is the total secondary fluid volumetric flow in $m^3.s^{-1}$.
- L is the length of one motif in m.
- $f'_{in,j}$ is the friction factor associated with the inlet of section *j*, *dimensionless*.

The demonstration of eq.(67) is provided in Appendix 6. The inner pipe diameter of headers is assumed to be slightly higher than the inner diameter of distribution pipe. The value taken is 0,2 m. The choice of correlations used in this study was based on the literature resources and Haglund Stignor et al. (2007), which focuses on the heat transfer and pressure drop in cooling coils using secondary fluids. The pressure drop associated with the evaporator is presented in details in part 4.1.4.

4.3 Secondary fluids assumptions

Two different freezing points of -30°C and -20°C are investigated in this study. After analyzing secondary fluid samples from the real installations, it was discovered that average secondary fluid's freezing point is around -30°C. Lower concentrations could nevertheless lead to better performance still preventing the secondary fluid from freezing if lower operating evaporation temperatures were maintained. The freezing point (or concentration) decrease is one of the energy saving options to consider. Both theoretical pure secondary fluids and commercial secondary fluids are included in this study. In case of the pure secondary fluids, the data were retrieved from Melinder (2010). Table 4 gives an example of thermo-physical properties for ammonia-water mixture having a freezing point of -30°C. As for commercial secondary fluids used in the ice rink refrigeration systems, dynamic viscosity, density and thermal conductivity are measured in the laboratory with different measuring equipment. For the time being, no equipment was available to measure the specific heat capacity, therefore, data for pure secondary fluids were used. Additionally, the thermo-physical properties may differ for pure and real secondary fluids due to additives used. The real secondary fluids included in this study were sampled from Järfälla and Nacka ice rinks, which operating data are further analyzed in part 6. The freezing points of those secondary fluids were also experimentally measured in the laboratory to define the approximated concentrations. All procedures regarding thermo-physical properties tests are presented in part 5.

Table 4: Thermo-physical properties of ammonia-water mixture with a freezing point of -30°C

T_f (°C)	[C] (wt-%)	T (°C)	ϱ (kg.m^{-3})	C_p (J.kg^{-1}.K^{-1})	k (W.m^{-1}.K^{-1})	μ (mPa.s)
-30	17,75	30	925,7	4205	0,507	0,96
		20	930,3	4208	0,49	1,24
		10	934,4	4216	0,472	1,61
		0	938,2	4228	0,455	2,16
		-10	941,3	4245	0,437	3,01
		-20	943,9	4265	0,42	4,43
		-30	945,8	4287	0,402	6,98

4.4 Calculation process

To perform faster all calculations a special program including several sub-functions was developed using the *VBA* compiler associated to *Microsoft Excel*. Moreover, eq.(33) (34) (40) (42) and (58) require iterative solving which was done using sub-routines including the *Solver* tool of Excel. An example of sub-routine and program interface is shown in Appendix 4.The total pumping power is calculated by summing the pumping powers associated with the ice rink floor, the headers, the distribution pipes and the PHE. A constant efficiency of 0,5 is assumed for the pumps.

The compressor power is calculated with data from Granryd et al. (2011) that give the isentropic compressor power versus the evaporation temperature for a given condensation temperature. In this study, the condensation temperature is assumed to be 20°C. The larger the evaporation and condensation temperature difference, the lower the efficiency. Therefore, having higher temperature differences in the refrigeration system lead to poorer energy efficiency.

The abbreviations previously-mentioned are used to designate the different secondary fluids: $CaCl_2$ for calcium chloride; *PG* for propylene glycol, *EG* for ethylene glycol; *EA* for ethyl alcohol (ethanol); NH_3 for ammonia; *K-acetate* for potassium acetate and *K-formate* for potassium formate. Other abbreviations are used for the cooling capacity (*CC*); the ice temperature (T_{ice}); the secondary fluid average temperature (T_{av}); the freezing point (*Fp*) and the pump control which is the secondary fluid temperature difference (ΔT). The assumptions are reminded in the caption of each presented figure.

4.5 Secondary fluids performance comparison

This part is devoted to the comparison between the different types of secondary fluid. They are assessed in terms of the heat transfer, pressure drop and efficiency. The refrigeration system efficiency is defined as the COP for a regular system but it also includes the pumping power. Hence it is the ratio between the useful power (cooling capacity) and the power provided to the refrigeration system (compressor and secondary fluid pumping power)

$$COP_{refr} = \frac{Cooling\ capacity}{Compressor + Pumping\ power} \quad (68)$$

This definition of the COP will be used throughout this study.

4.5.1 Heat transfer comparison

Figure 30 and Figure 31 show the convection heat transfer coefficients in one U-pipe of the ice floor and one plate of the PHE, respectively. It is possible to see that K-formate gives the best heat transfer features while PG has the poorest heat transfer properties. $CaCl_2$ and NH_3 have good heat transfer features in both the U-pipe and the PHE. Both convection heat transfer coefficients decrease with the decreasing temperature. Hence, it is preferable to keep the secondary fluid average temperature as high as possible in terms of the heat transfer. Moreover, lower secondary fluid temperatures lead to lower evaporation temperature reducing the performance. The chosen cooling capacity is close to the common operational cooling capacity for the ice rink.

In Figure 30, a discontinuity may be observed in the $CaCl_2$ and K-acetate curve. This is due to the change in the flow regime. Lower secondary fluid temperatures give a higher viscosity and laminar flow may then occur. Similarly in Figure 31, a discontinuity may be observed for $CaCl_2$ and NH_3. This is due to the change in correlation used, similar to the correlation change from the laminar to turbulent flow. The laminar flow gives rather low convection heat transfer coefficients ($\approx$ 100 $W.m^{-2}.K^{-1}$) as shown in Figure 30 and it should be avoided. For the same given conditions, PG, EG and EA stays in the laminar flow regime whatever the operating temperature is. The $CaCl_2$ case shows a flow regime shift at -13 °C, a temperature that will only be reached for high heat loads. K-acetate has a flow regime shift at -5,5 °C that is close to the common operational temperatures. NH_3 and K-formate also remain in the turbulent regime.

For higher heat loads and the same pump control, the flow would be higher leading to the turbulent flow. Decreasing the temperature difference over which the pump is controlled allows having higher flow that may lead to turbulent flow regime and higher evaporation temperature. On the other hand, decreasing the temperature difference leads to higher pumping power.

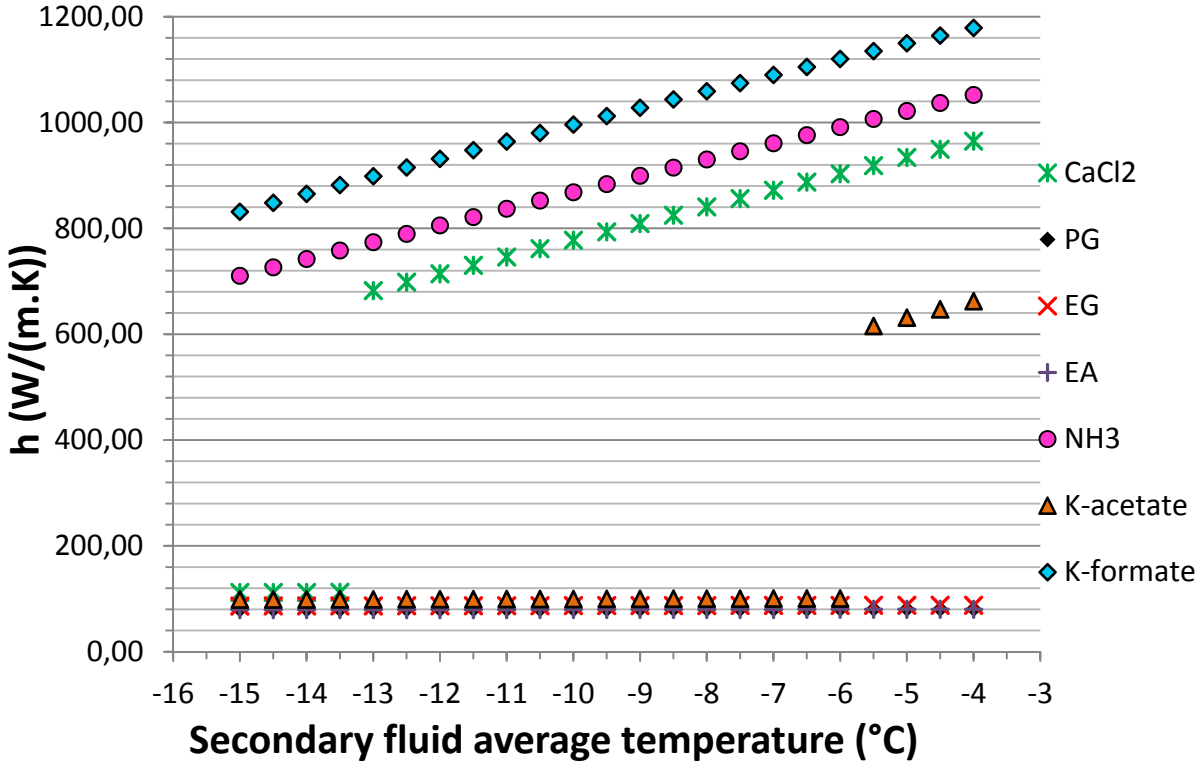

Figure 30: Convection heat transfer coefficient in one U-pipe VS T_{av} (CC = 200 kW; F_p = -30 °C; ΔT = 2 K)

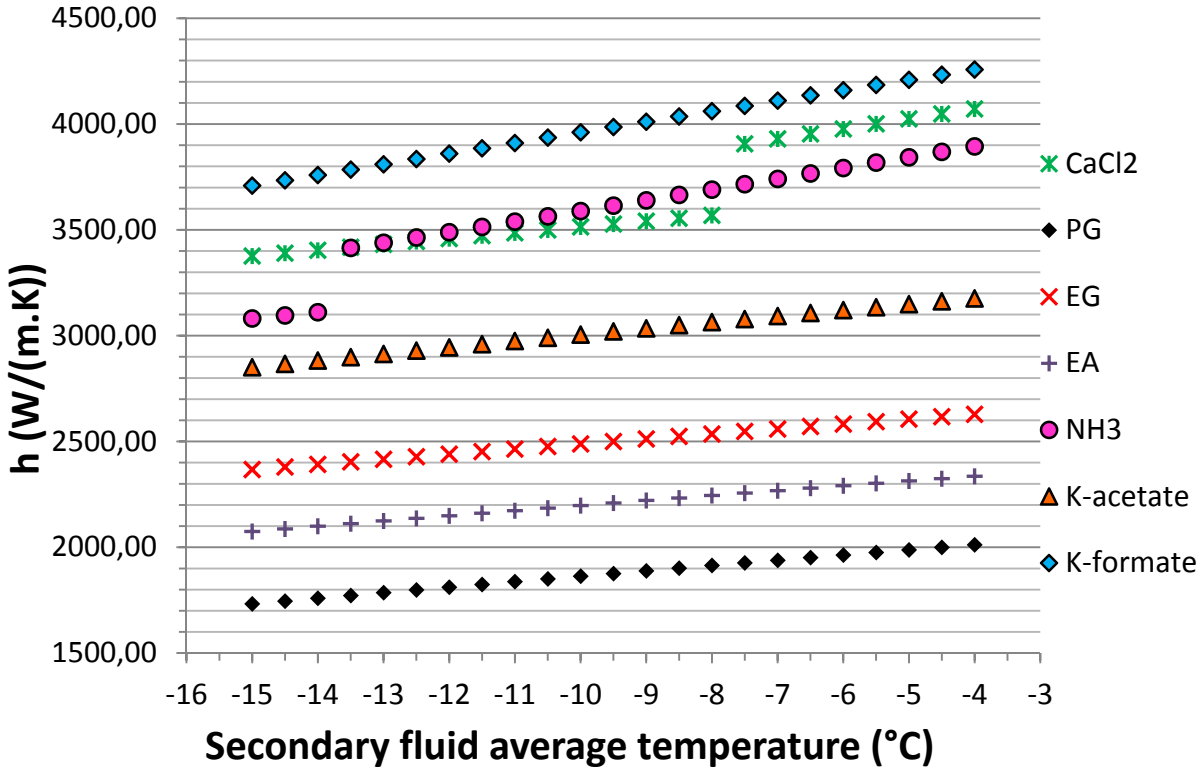

Figure 31: Convection heat transfer coefficient in one plate of the PHE VS T_{av} (CC = 200 kW; F_p = -30 °C; ΔT = 2 K)

It is shown in Figure 30 that PG, EG and EA almost always remain in the laminar flow regime, even for higher heat loads (300 kW) and lower temperature difference (1,5 K).

Figure 32and Figure 33 show the temperature differences – proportional to the heat transfer resistances – in the ice rink floor and the evaporator, respectively. The temperature differences are: T_{ice}-T_{av} for the ice rink floor and T_{av}-T_{evap} for the PHE. These figures also show the resistance shares of the different components of the ice rink floor and the PHE. The values are calculated for the cooling capacity of 150 kW, the ice temperature of -3,5 °C and the pump control of 1,5 K.

Figure 32 also highlights the poor heat transfer properties associated with the laminar flow. Indeed, all secondary fluids presenting a large convection share are in the laminar flow regime, for these conditions. As shown, PG, EG, EA and K-acetate have a much higher ice/secondary fluid temperature difference than $CaCl_2$, NH_3 and K-formate which are in turbulent flow range.

Figure 33 shows that secondary fluid convection may account for a large share in the total temperature difference, depending on the thermo-physical properties of the secondary fluid. The boiling process always accounts for a large share in the thermal resistance of the PHE. The titanium plate does not have a large share in the overall heat transfer resistance.

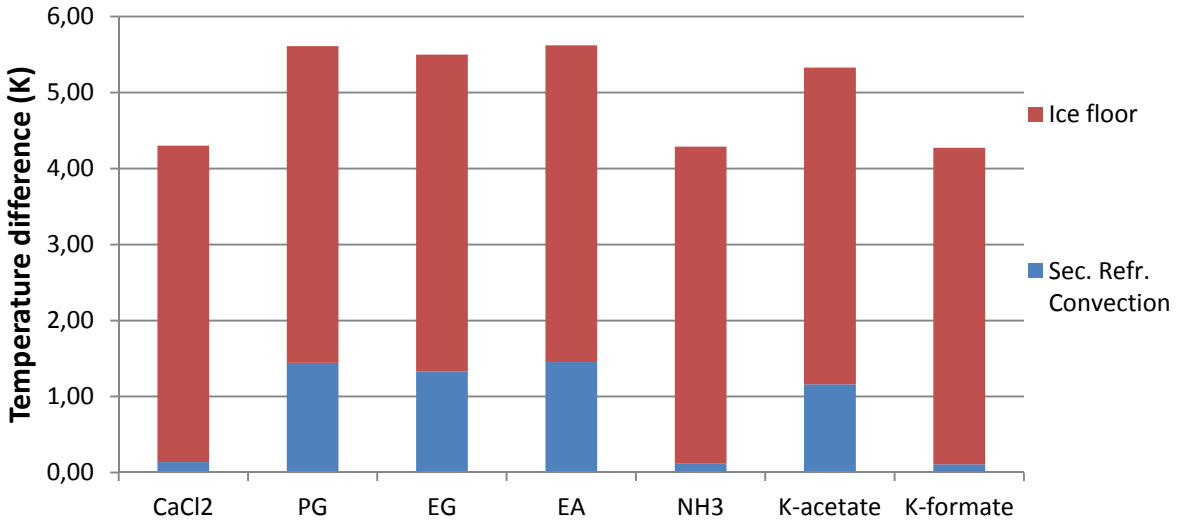

Figure 32: Ice / secondary fluid temperature differences (CC = 150 kW; F_p = -30 °C; ΔT = 1,5 K; T_{ice} = -3,5 °C)

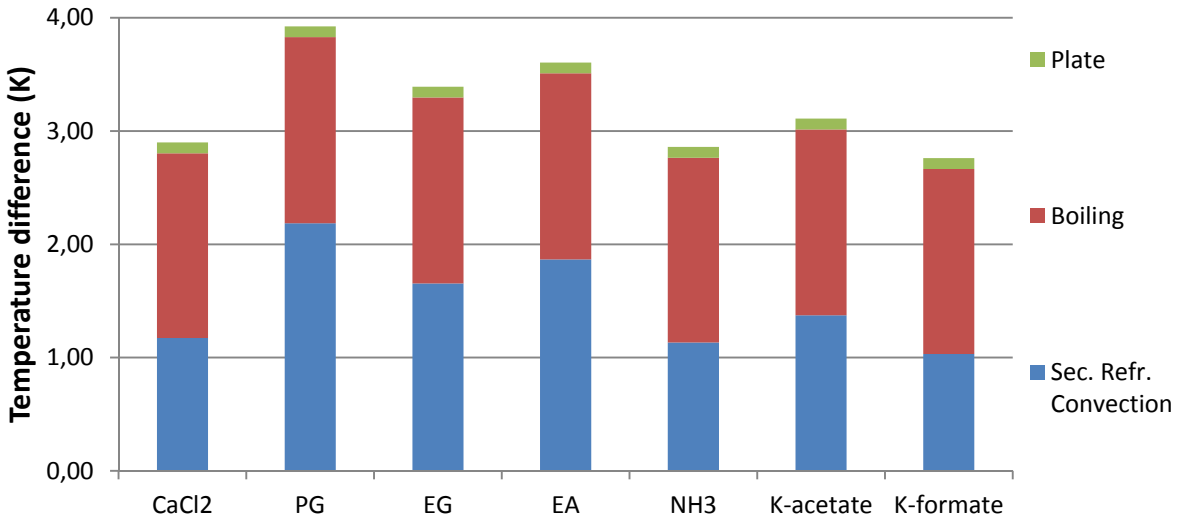

Figure 33: Secondary fluid / evaporation temperature differences (CC = 150 kW; F_p = -30 °C; ΔT = 1,5 K; T_{ice} = -3,5 °C)

Figure 34 shows the heat transfer coefficient of the evaporator, UA, versus the secondary fluid average temperature. This coefficient is the product of the overall heat transfer coefficient U ($W.m^{-1}.K^{-1}$) and the heat transfer area A (m^2). Lower UA values lead to higher temperature difference for a given cooling capacity, and lower refrigeration system efficiency. In reality, PHE are designed for a given UA value or a given temperature difference. Therefore, facilities using PG for example would not use a PHE with same design but a PHE with a larger heat transfer area, implying higher investment cost. Stainless steel may also be used as the plate material, depending on the secondary fluid type. The aim of this study is to compare the different secondary fluids on the same basis and the same PHE design is chosen. It is possible to compare the UA-value of $CaCl_2$ at an average temperature of -12,5 °C with the value from *Alfa Laval Software*. Taking the U-value (designated as k) of 2524 $W.m^{-2}.K^{-1}$ and the heat transfer area of 34,08 m^2 given in Figure 24, we found a UA heat transfer coefficient of roughly 86000 $W.K^{-1}$. The Microsoft Excel simulation gives a value of roughly 78900 $W.K^{-1}$. The difference may be caused by the different correlations used, and the fouling resistance consideration.

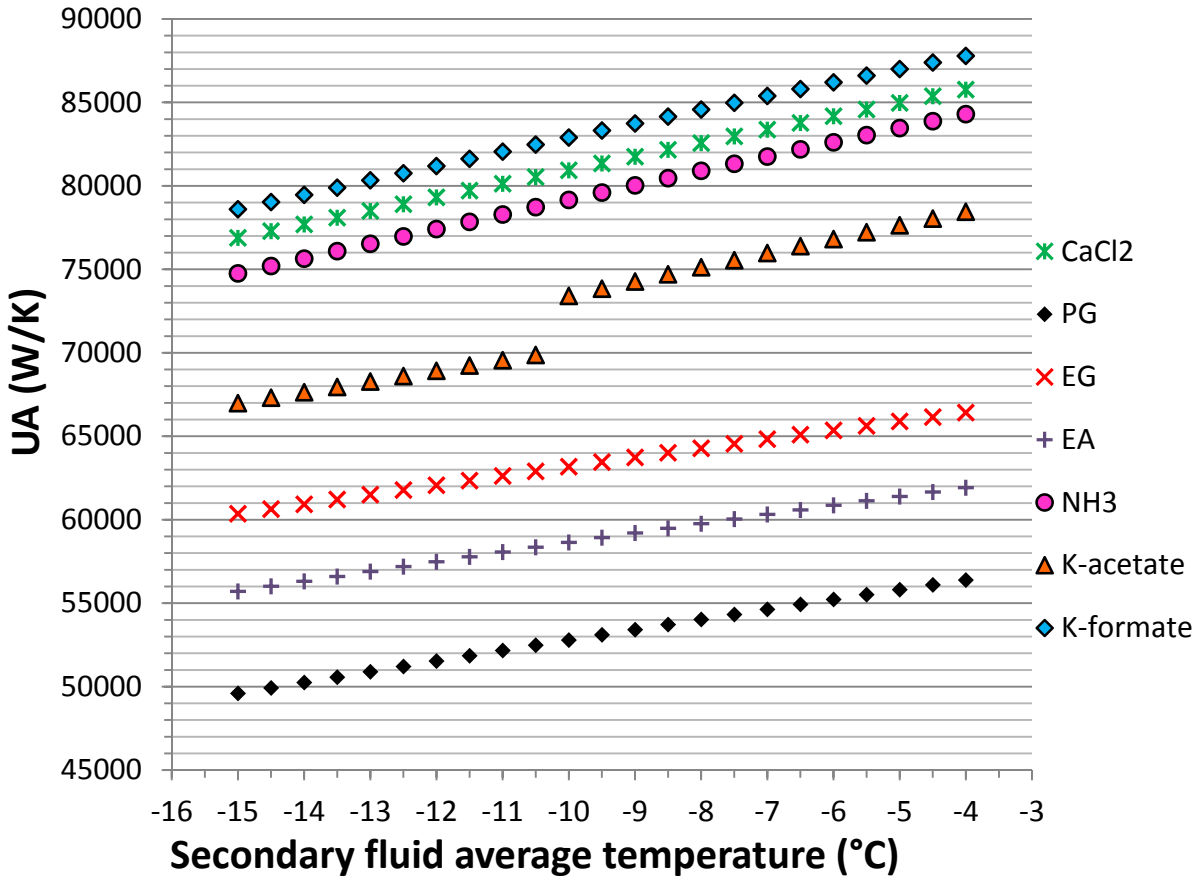

Figure 34: Evaporator UA values versus T_{av} (CC = 300 kW; F_p = -30 °C; ΔT= 2 K)

4.5.2 Pumping power comparison

Figure 35 shows the pumping power for all the secondary fluids versus their average operational temperature. PG is the secondary fluid leading to the largest pumping power, due to its high viscosity at low temperatures. Ammonia leads to low pressure drop and the lowest pumping power. Except for PG, the pumping power is varying between 2 and 7 kW which is rather low due to the fact that the assumption of variable speed pump was made. Once again, the discontinuities that may be observed in the curves are due to the flow regime change. The laminar flow may lead to lower pumping power than turbulent flow but on the other hand the heat transfer coefficients decrease. The higher the temperature difference over which the pump is controlled, the lower the pumping power and lower the evaporation temperature.

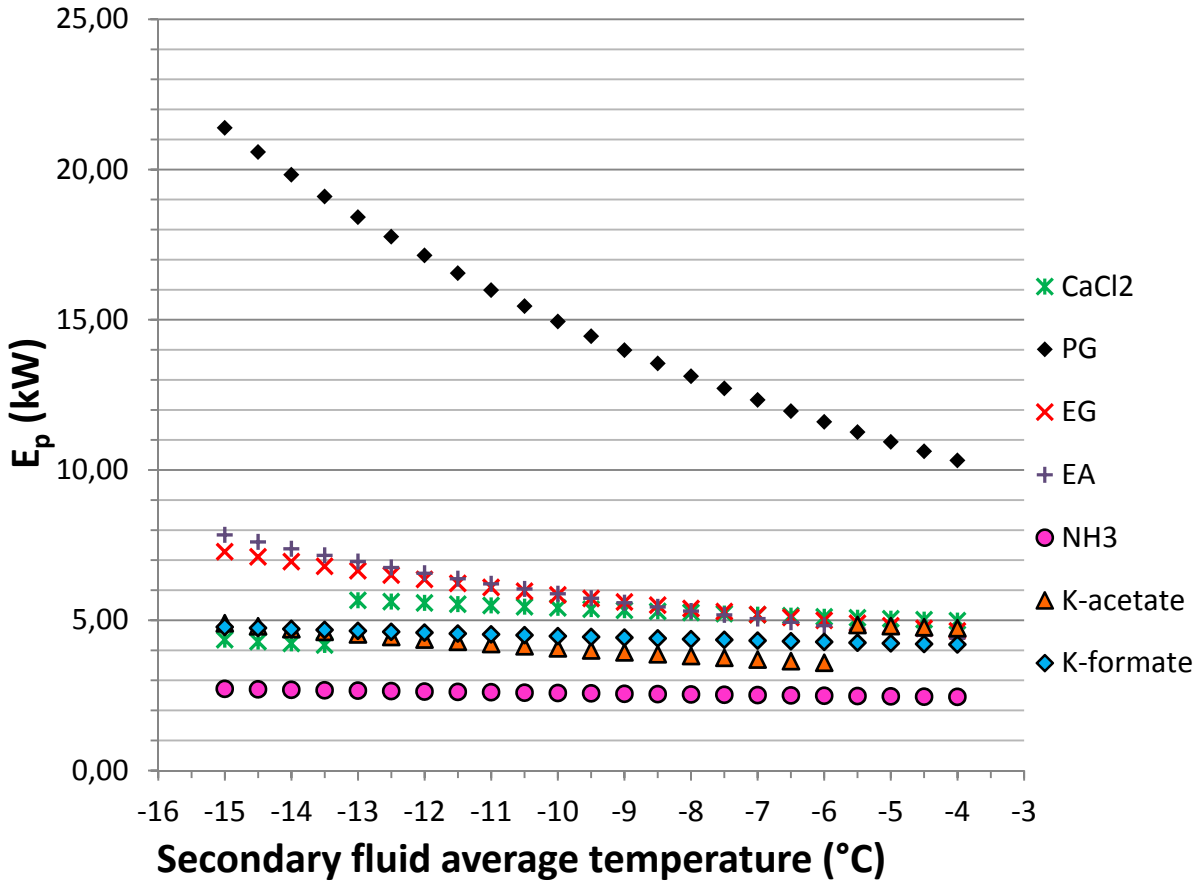

Figure 35: Pumping power versus T_{av} (CC = 200 kW; F_p = -30 °C; ΔT = 2 K)

The pumping shares in the secondary loop are displayed in Figure 36 for calcium chloride. As seen, the pressure drop is the biggest in the ice rink floor and the PHE. On the contrary, the pressure drops in headers and distribution pipes only account for a small share in the total pressure drop (or pumping power). In reality, the pressure drops in the PHE may not be as high as in this study because PHE manufacturers are more restricted by the pressure drop limit when defining the PHE design. $CaCl_2$ was chosen to be displayed in this graph since it is the most common secondary fluid in the Swedish facilities.

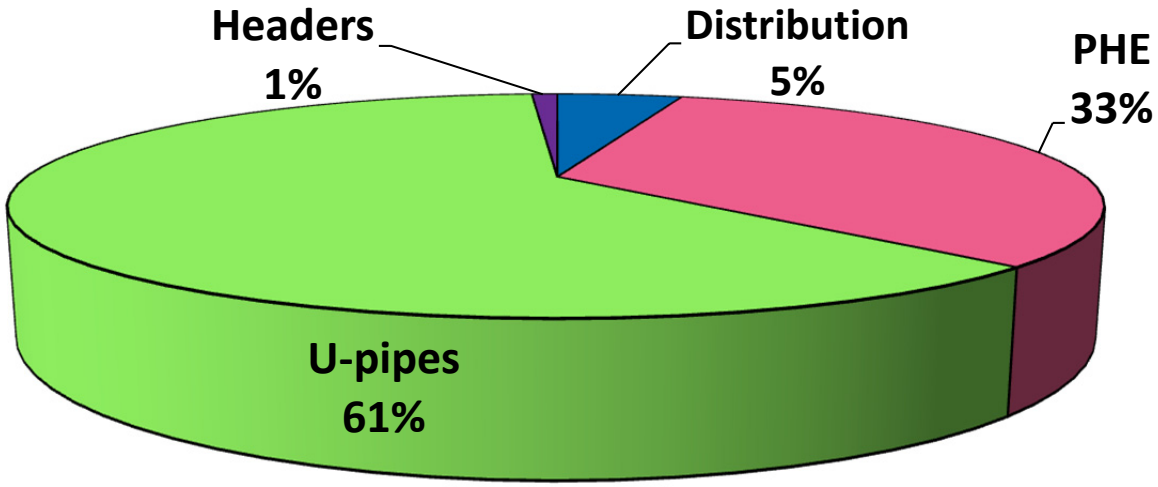

Figure 36: Pumping power shares for $CaCl_2$ (CC = 200 kW; F_p = -30 °C; ΔT = 2 K; T_{av} = -6,5 °C)

4.5.3 Comparison of the refrigeration system efficiency (COP)

The term efficiency refers to the COP definition as presented in eq.(68). Figure 37 shows the COP variation with the ice temperature for each secondary fluid and operational cooling capacity. This graph is particularly important since it sums up the secondary fluid overall performance. Hence, it allows ranking the secondary fluids in terms of the refrigeration efficiency. Calcium chloride, potassium formate and ammonia are the best secondary fluids in terms of the performance COP and show really close values. Potassium acetate also gives rather high COP values while PG, EG and EA show lower COP values. The worst secondary fluid in terms of refrigeration performance according to this analysis is PG. The performance of other secondary fluids are rather close in this case since the pump control (ΔT) is high and the cooling capacity low, leading to low volume flow values and the laminar flow regime.

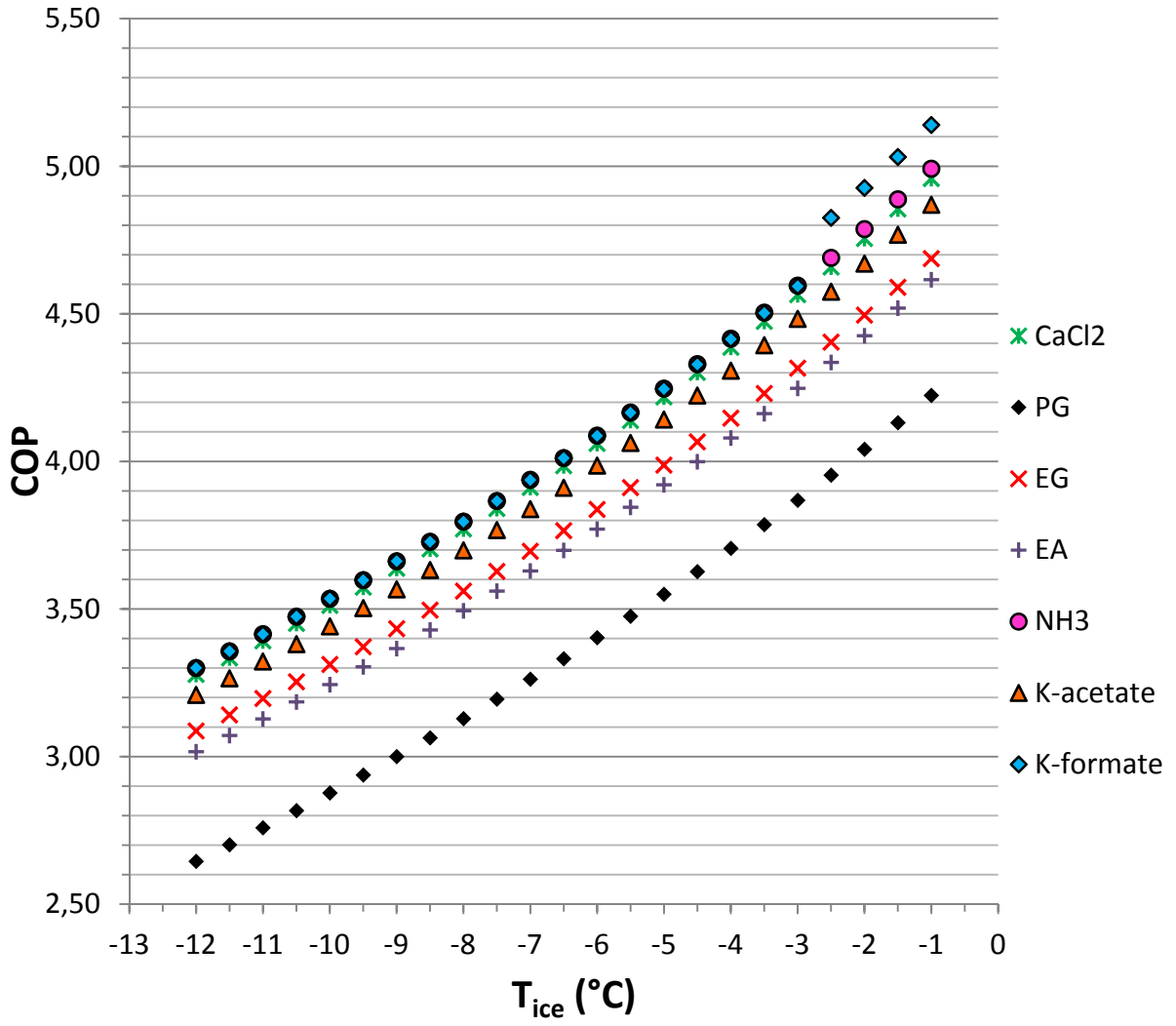

Figure 37: COP versus T_{ice} (CC = 150 kW; F_p = -30 °C; ΔT = 2,5 K)

For a lower pump control and higher heat loads, differences start to appear between the various secondary fluids as shown in Figure 38. Thus, it is possible to define a rank for each secondary fluid in terms of the refrigeration system performance. From the best to the worst secondary fluids ranking is: NH_3; K-formate; $CaCl_2$; K-acetate; EG; EA; and finally PG. It is interesting to notice the similarity between this ranking and the "viscosity ranking" that may be established from Figure 17: This qualitative correlation shows the influence of viscosity on the coefficient of performance. It may be noticed that high cooling capacities lead to lower evaporation temperature and hence to lower COP.

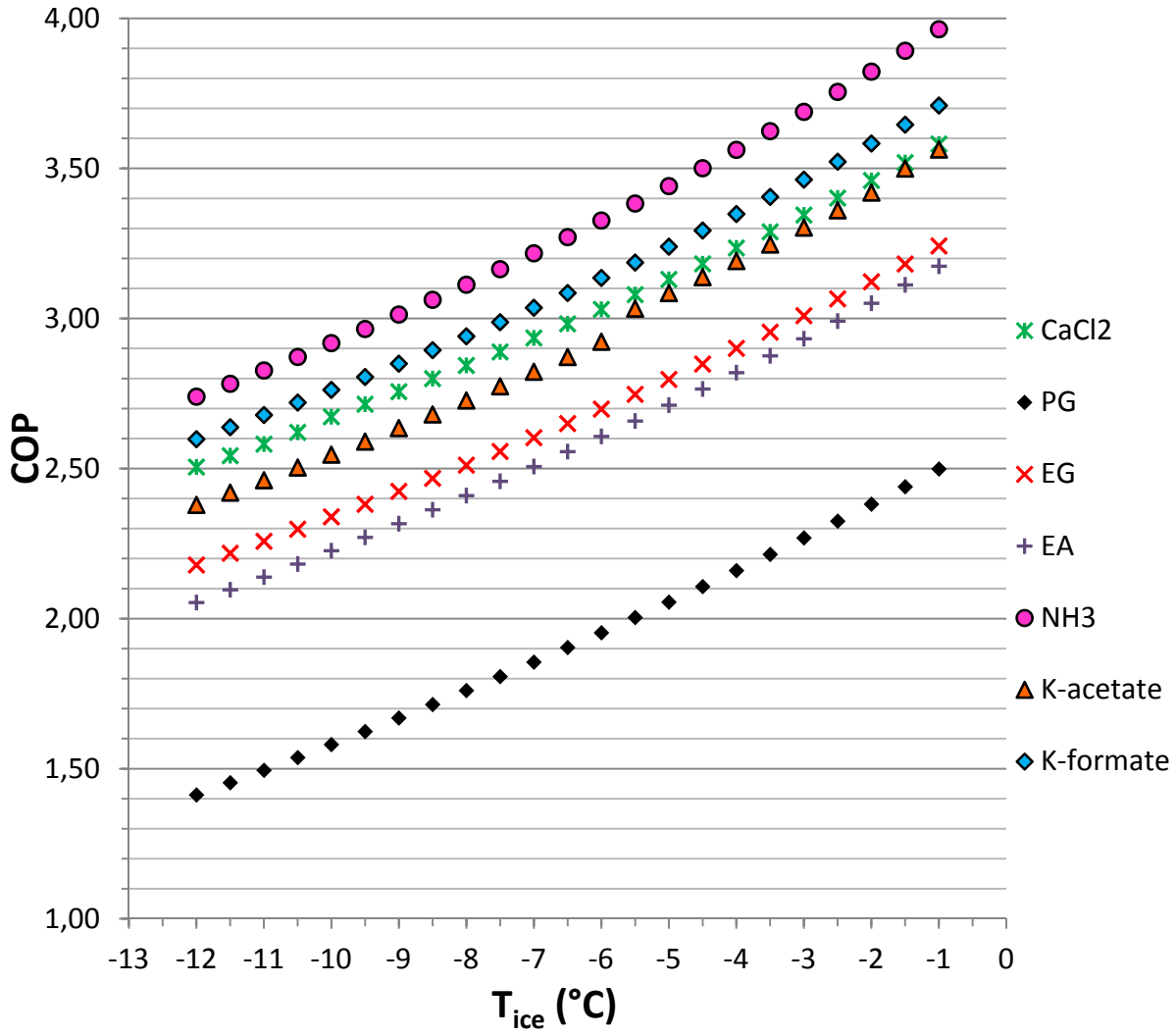

Figure 38: COP versus Tice (CC = 300 kW; F_p = -30 °C; ΔT = 2 K)

4.6 Optimum pump control

For each secondary fluid, an optimum pump control, or secondary fluid temperature difference (ΔT), exists for a given heat load. Indeed, low ΔT lead to high pumping power but also lower compressor power. On the contrary, high ΔT's imply low pumping power but higher compressor powers. A lower ΔT is in general preferable since it gives more uniform temperatures over the ice surface.

Figure 39 and Figure 40 show the COP variations due to the pump control change for the cooling capacities of 150 and 400 kW, respectively. Once again the discontinuities are due to the flow regime shift that may happen in the secondary loop. The negative effects of the laminar flow are thereby highlighted. NH_3 and K-formate show the best COP for the lowest optimum pump control ΔT; that is an important aspect for the COP and homogeneity of the ice temperature that is one of the factors leading to a good ice quality. PG is the secondary fluid showing the largest optimum pump controls ΔT for the lowest COP. It is possible to see more or less the same ranking as the one made in part 4.5.3. It can be noticed as well that the optimum pump control ΔT increases with increasing cooling capacity, regardless of the secondary fluid type.

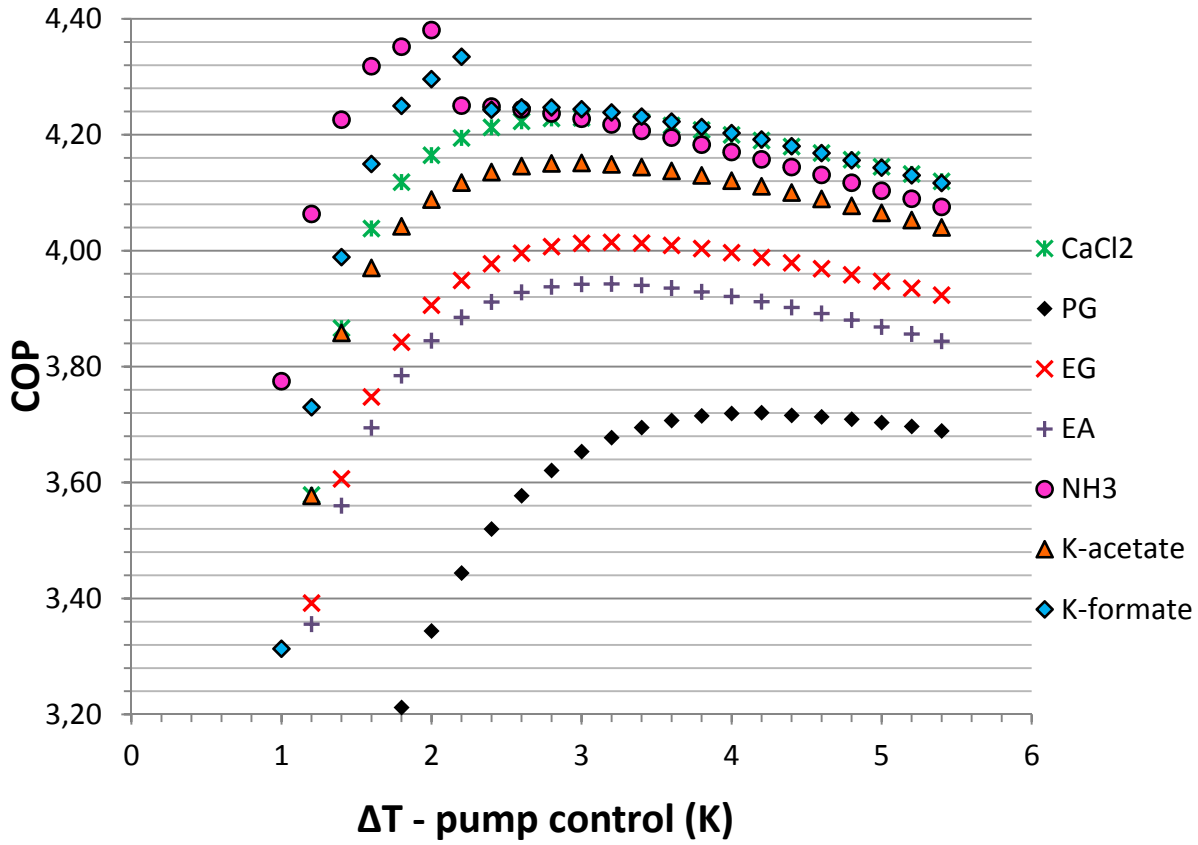

Figure 39: COP versus ΔT (CC = 150 kW; F_p = -30 °C; T_{ice} = -5 °C)

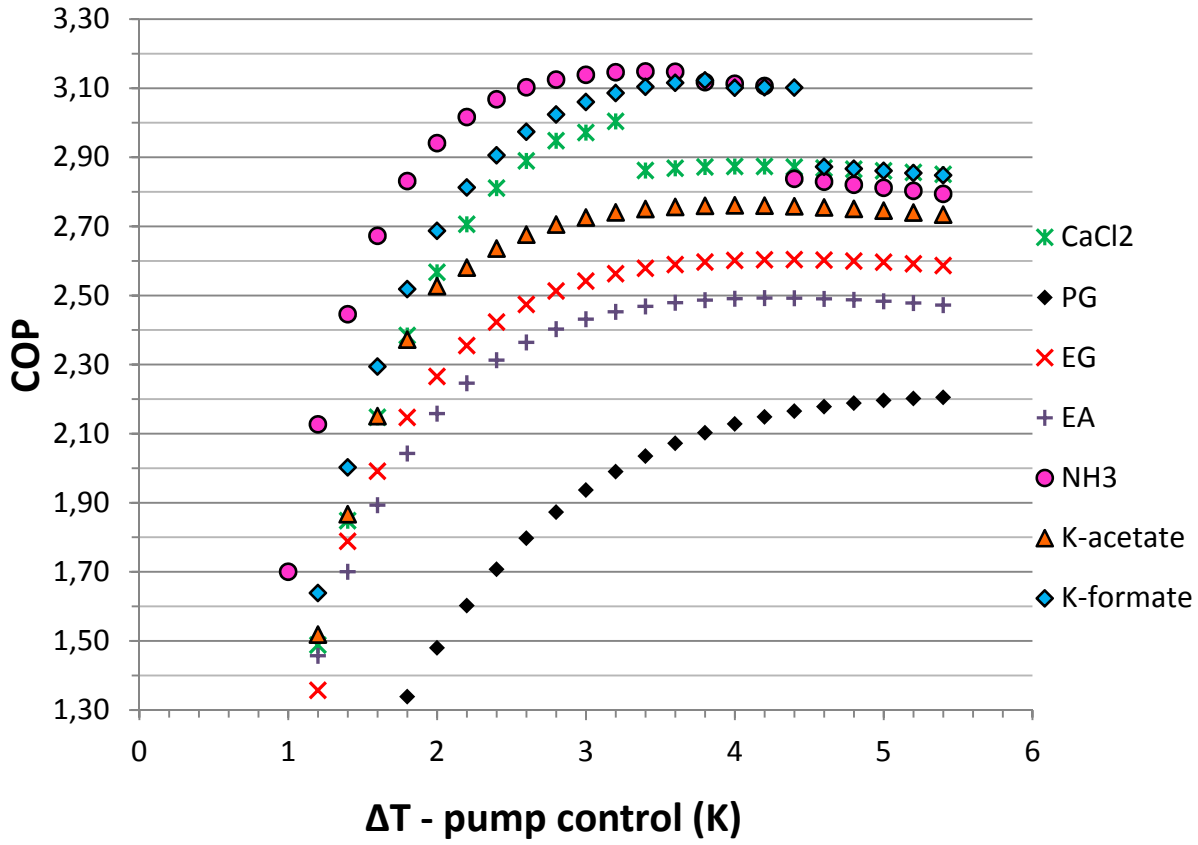

Figure 40: COP versus ΔT (CC = 400 kW; F_p = -30 °C; T_{ice} = -5 °C)

The best solution to control the pump would be to define the optimum temperature difference value for the different cooling capacities. It is not always possible to do so, thus a constant temperature difference is often chosen as the main control parameter. For instance, North American ice rinks have more commonly controls closer to 1K although it does not lead to the best efficiency according to this study. In Sweden, the pump control ΔT is often close to 2K. One of the advantages with the constant temperature method is that a better uniformity of the ice surface temperature is obtained. However, it is worth looking at what could the optimum pump control ΔT for operational cooling capacities (100-150-200 kW) so a relevant temperature difference can be setup as the main control parameter

4.7 Performance comparison with calcium chloride

Since calcium chloride is used in more than 97% of the Swedish ice rinks, it is interesting to compare the performance of other secondary fluids to this specific one. Figure 41 displays the COP ratios versus ice temperatures, with $CaCl_2$ as a comparison basis. It is possible to see that for all ice temperatures, NH_3 and K-formate show better COP than $CaCl_2$. All other secondary fluids have lower COP than $CaCl_2$. For an ice temperature of -5°C NH_3 leads to 5% higher COP while K-formate leads to 3 % higher COP.

Measurements performed in the real facilities using calcium chloride as the secondary fluid give energy consumption associated with the refrigeration system around 300 MWh per year. Considering that 150 kW is the average cooling capacity over a year and that the ice temperature is controlled to be constantly -5°C, using ammonia or potassium formate instead of calcium chloride in the same system would lead to energy savings of 15 MWh or 10,5 MWh per year, respectively.

Nevertheless, other parameters such as corrosion, application and environmental impact should be taken into account when choosing the secondary fluid type. The best way of assessing the real impact of the secondary fluid on the system would be to perform a Life-Cycle Cost (LCC) study including all parameters that influence either: the investment cost, the operating cost or the lifetime of the system.

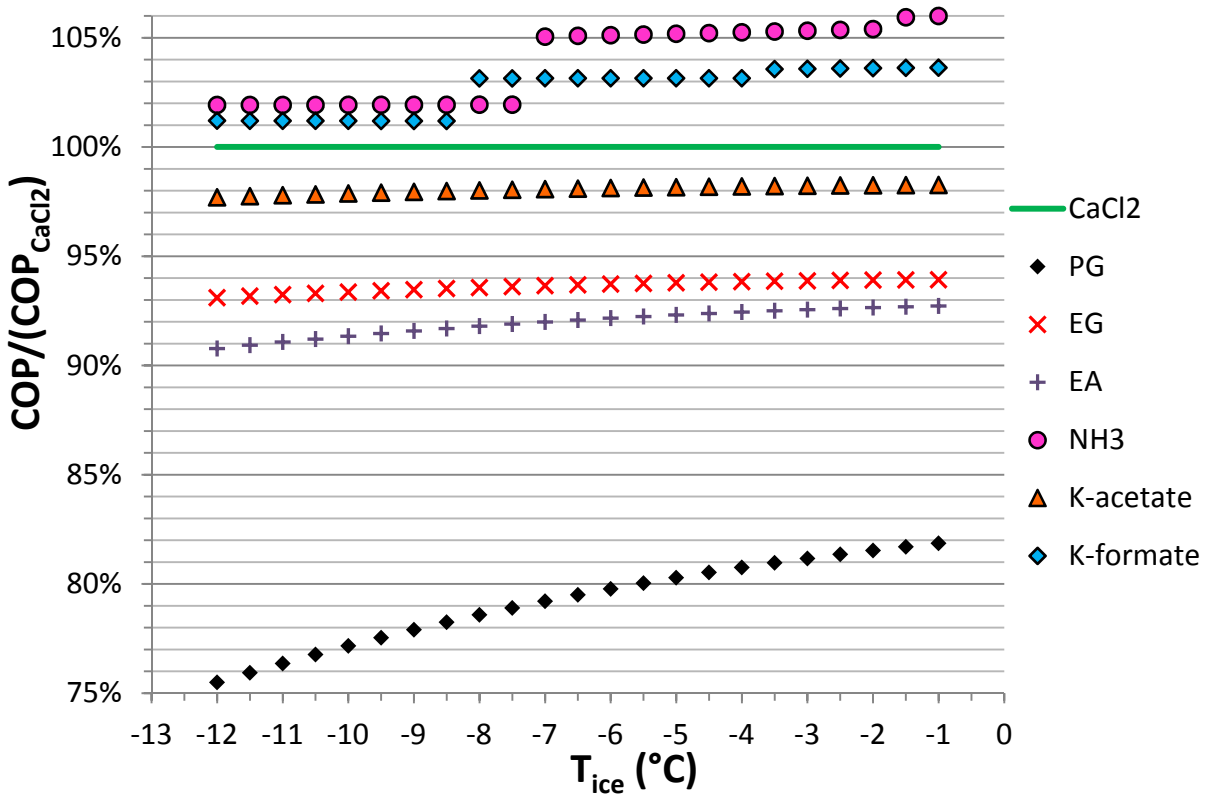

Figure 41: Efficiency ratios with $CaCl_2$ as comparison basis (CC = 150 kW; F_p = -30 °C; ΔT = 2 K)

4.8 Freezing point comparison

The freezing point, or concentration, directly influences the thermo-physical properties of the secondary fluid and, thus, the heat transfer and pressure drop features. The recommended concentration in ice rinks is 24 wt-% for calcium chloride; that corresponds to a freezing point of around -26,5 °C. However, measurements performed on several samples from Swedish ice rinks showed freezing points closer to -30 °C rather than the recommended -26,5 °C. Additionally, the freezing point could be even higher since the normal operating temperatures rarely exceed -10 °C in ice rinks. Melinder (2007) recommends having a concentration giving a freezing point 10 K lower than normal operating temperatures. Two different freezing points are compared in this part: - 20 °C and -30 °C. As long as the lowest temperature in the system (that is in the evaporator) is not too close to the freezing point, damages are likely to be avoided. In the two ice rinks where data were analyzed, the minimum measured temperature of the secondary fluid was -9,1°C while the minimum measured evaporation temperature was -17 °C. Hence a freezing point of -20 °C would be sufficient to protect the systems from freezing, at least for those two ice rinks. Figure 42 show the gains that would be obtained if using the same secondary fluid having a freezing point of -20 ° C instead of -30 °C. The COP gain, expressed in percentage, is calculated as

$$COP\ gain = \frac{COP_{F_p=-20} - COP_{F_p=-30}}{COP_{F_p=-30}} \quad (69)$$

The highest gains can be seen for the secondary fluids which thermo-physical properties are poor in comparison to water; those are PG, EG and EA. While $CaCl_2$, K-acetate and K-formate show gains equal or slightly higher than 3 % for high cooling capacities, the COP gains for NH_3 never exceed 1 %. For common refrigeration loads around 150 kW the gains are: 1,3 % for $CaCl_2$; 10,5 % for PG; 3,6 % for EG; 2,8 % for EA; 0,4 % for NH_3; 1,7 % for K-acetate and 1,4 % for K-formate. For all secondary fluids, the COP gain increases with increasing cooling capacity.

Considering the same refrigeration system's yearly consumption (300 MWh) and the average cooling capacity (150 kW) as in part 4.7,calcium chloride with the freezing point of -20°C instead of -30°C would lead to 3,9 MWh of energy savings according to the results from model.

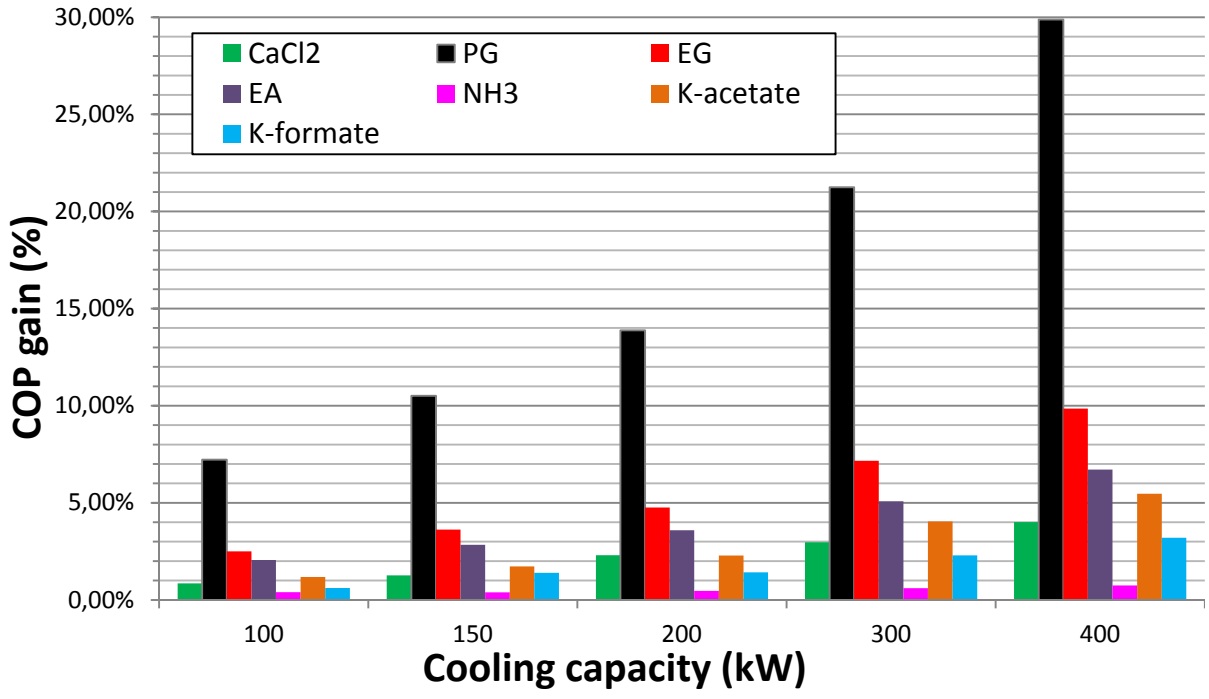

Figure 42: COP gain for a freezing point of -20 °C expressed as percentage gain in comparison to the COP obtained with a freezing point of -30 °C (T_{ice} = -5 °C; ΔT = 2 K)

4.9 Performance comparison between pure and commercial secondary fluids

Commercial secondary fluids may have different thermo-physical properties than those given for pure secondary fluid mixtures. Indeed, various additives may be added like corrosion inhibitors that may modify the thermo-physical properties. The commercial secondary fluids may also be mixtures of water and several freezing point depressants (Ignatowicz, 2008).

With a kind assistance from the company QTF, samples from 8 different ice rinks were collected. Those samples were analyzed with appropriate measurement equipment. The experimental procedures and devices used to measure the thermo-physical properties are explained in part 5. Nevertheless, only the samples from the two studied ice rinks (situated in Nacka and Järfälla municipalities in Sweden) are investigated in this study. The freezing point of those secondary fluids were measured and appear to be -24 °C for Nacka ice rink and -31 °C for Järfälla ice rink.

Viscosity, thermal conductivity and density were also measured but specific heat capacity could not be measured since the required measuring instrument has been purchased later. Therefore, values given for the pure secondary fluids were taken for the specific heat capacity. In order to perform the comparison with pure secondary fluids, the thermo-physical properties are taken at the same freezing points as the commercial secondary fluids used in those two real facilities.

The secondary fluid performance are compared for several cooling capacities but the percentage error between the performance of pure and real secondary fluids obtained by

$$\%\ Error = \frac{\left|COP_{pure} - COP_{real}\right|}{COP_{real}} \qquad (70)$$

never exceeds 1,3 %. Figure 43 show the COP for the commercial secondary fluids and the associated pure ones.

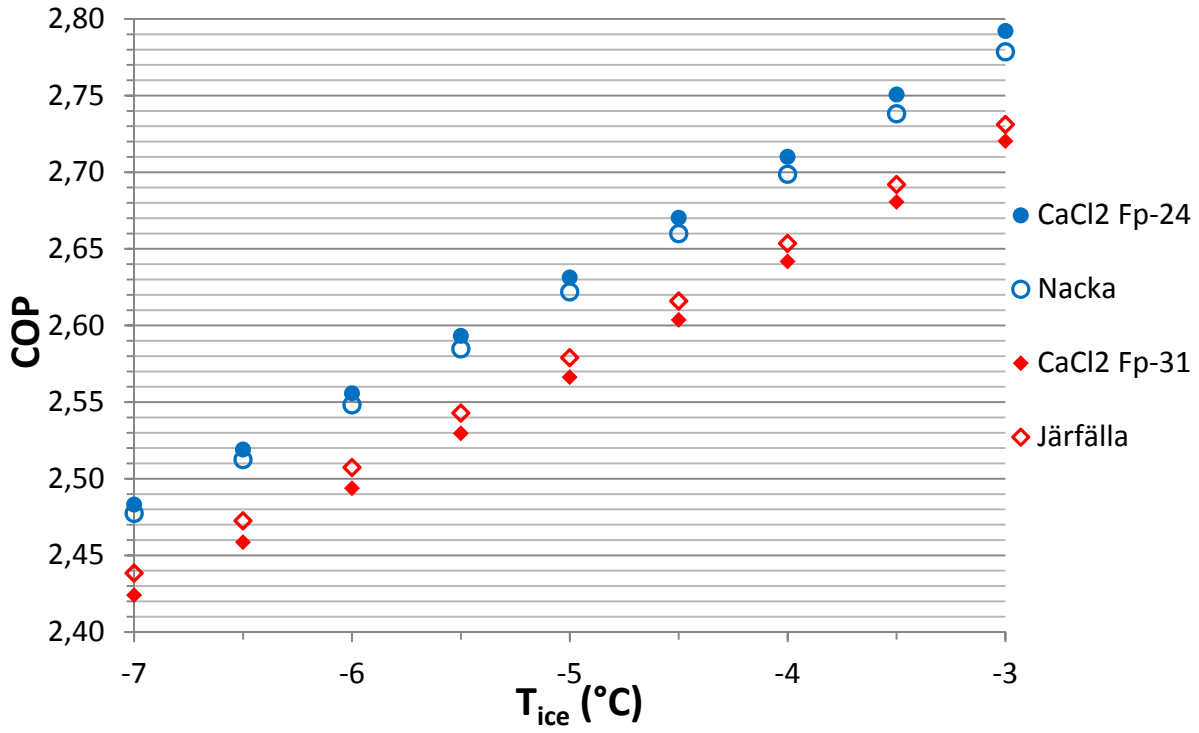

Figure 43: Comparison between commercial and pure secondary fluids in terms of performance (CC = 400 kW; ΔT= 2 K)

Using the thermo-physical properties for performance calculations when designing the refrigeration system is acceptable since the difference is rather small. Nevertheless, the results shown in this comparison should be analyzed with care since the specific heat capacity was taken the same for both commercial and pure secondary fluids. The differences between performance obtained for the pure and real secondary fluids may be larger if the specific heat capacity was measured and used for calculation Moreover, density values were partly based one theoretical values as explained in part 5.

In Figure 43, the real calcium chloride aqueous solution used as secondary fluid in Järfälla ice rink shows better COPs than pure calcium chloride aqueous solution with the same concentration (same freezing point). This result was not expected since real secondary fluids usually have worse thermo-physical properties than pure ones due to the additives (e.g. corrosion inhibitors) that may be found in the solution. This unexpected result may be a consequence of the specific heat capacity assumption. Further tests should be performed to check this result.

Finally, the thermo-physical properties are measured with uncertainties due to measuring instrument precisions. Moreover, measurement errors could be not assessed since no information was known about the samples properties.

4.10 Scope and limitations of this study

The Microsoft Excel program developed for this heat transfer and pressure drop study includes several devices or processes which modeling would deserve further investigation. In particular the compressors and the associated efficiency, the pumps and their efficiency, the various control strategies and the modeling of superheat in the PHE.

The two-dimensional model developed with *COMSOL Multiphysics* may be turned into a three dimensional model including the secondary fluid flow and temperature profile along the U-pipes. The ice rink floor conduction resistance would then be more accurate.

The properties of secondary fluids may be changed along the secondary loop considering a finite number of isothermal volumes influencing one another.

This partial model could be further developed in a more global one; simulating all energy devices in the ice rink buildings as in Seghouani et al. (2011). Moreover, this steady-state simulation should be turned into an unsteady-state one in further studies, in an evaluation of yearly energy consumptions perspective.

As it was previously evoked, no other features than the heat transfer, pumping power and the resulting refrigeration capacity were investigated. The long-time effects such as: corrosion, environmental aspects or maintenance and operation should also be accounted if the secondary fluids are to be assessed from a LCC point-of-view.

All the statements in this part should be kept in mind when looking at the presented results.

5 THERMO-PHYSICAL PROPERTIES MEASUREMENTS

In total, 11 samples from different ice rinks have been collected. 8 of those samples are calcium chloride solutions used on the cooling side while the remaining 4 are glycol solutions used on the condenser side. The freezing point, viscosities, thermal conductivities and density were measured for all those samples. All the procedures are presented in the following parts. The results are given only for the calcium chloride samples from Järfälla and Nacka which energy savings are evaluated in part 6. At that time no device was available to determine the specific heat capacity.

5.1 Freezing point test

The freezing point is indicative of the freezing point depressant concentration for a given solution. The concentration influences directly all other thermo-physical properties and is henceforth of a particular importance. To measure the freezing point, 9 identical plastic beakers are filled with 90 ml of the tested secondary fluid. Those 9 containers, kept together by a specially designed sample holder, are placed into an ultra-low temperature freezer (operating down to -90 °C) until they are frozen while their temperature is measured over time by 9 thermocouples (one per beaker) associated with a data acquisition unit. The thermocouples are placed in the center of each beaker and are calibrated with an accuracy of +/- 0,1 °C. The test rig is presented in Figure 44.

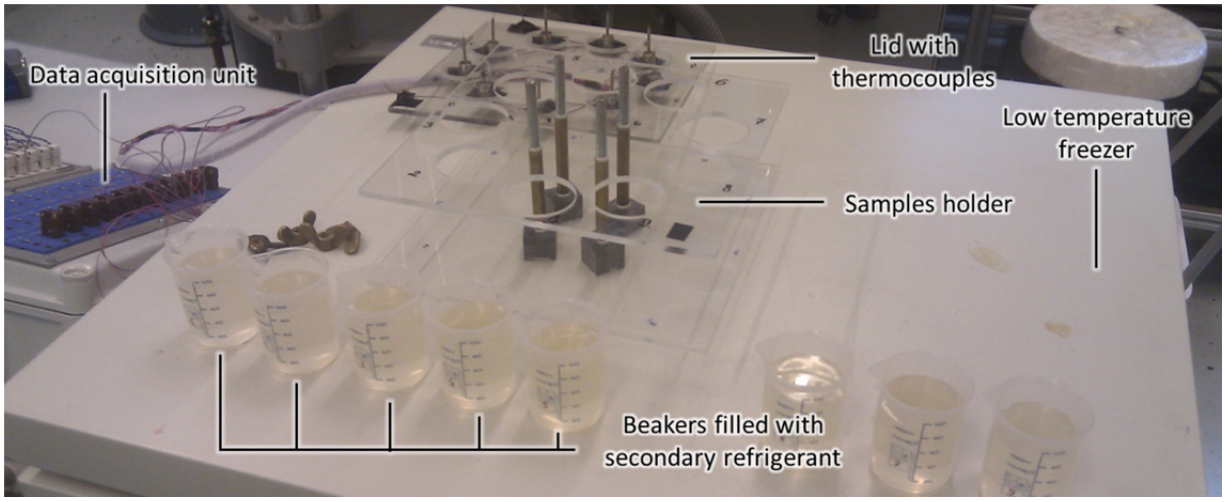

Figure 44: The freezing point test components

The temperatures at which the samples freeze may be detected by looking at the temperature change profile over time. Indeed, as long as a sample is not frozen, its temperature decreases over time, but the following phenomenon illustrated in Figure 45 happens once it starts freezing:

- The sample starts freezing from the interior perimeter of the beaker to the center
- The subcooling process is measured by thermocouples as a slight temperature increase
- Each secondary fluid has its own specific freezing pattern with different range of subcooling ΔT

This phenomenon is called the subcooling effect. This slight increase can be seen in Figure 45 where the subcooling effect is also outlined. The temperatures denoted T1, T2, T3,…, T9, represent the temperatures measured in each beaker. The sample may show different freezing points because of the thermocouples accuracy and calibration. Therefore, correction coefficients are applied to the measurements so that the uncertainties are minimized. Moreover, some samples may be slightly contaminated with particles (e.g. dust) that may change the freezing point as seen in Figure 45. Thus, the average of freezing points is taken as the secondary fluid freezing temperature.

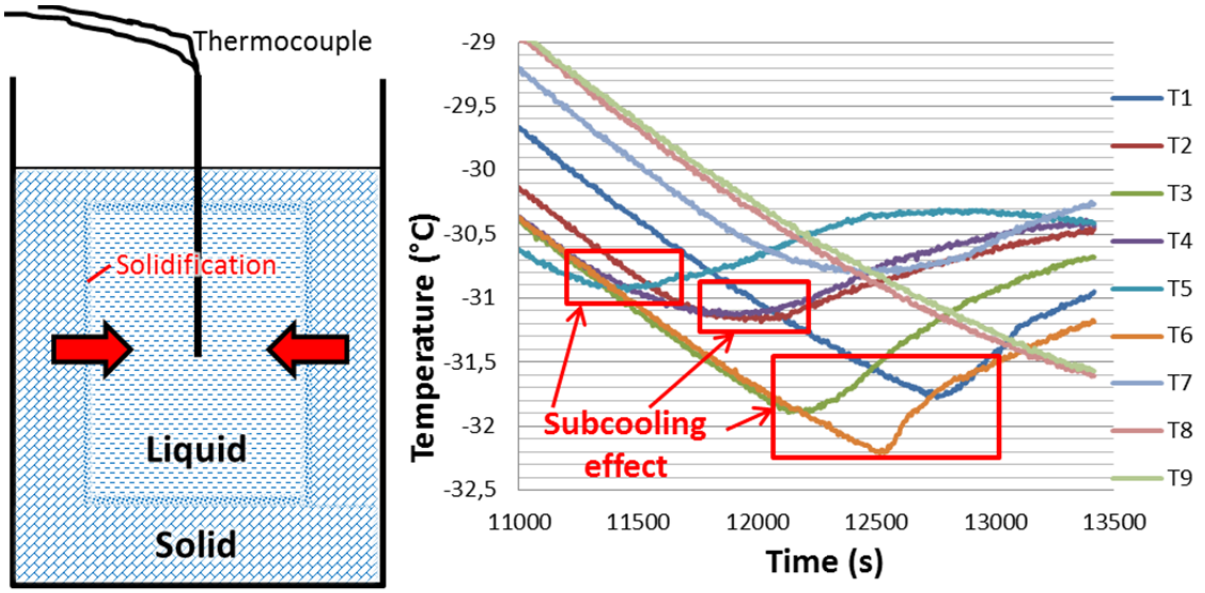

Figure 45: Solid subcooling effect and temperature profile measurements during freezing point test

The exact measures of freezing point temperatures for Järfälla and Nacka are -31,2 °C and -24,0 °C, respectively.

5.2 Viscosity test

The viscosity is measured with a *Brookfield Rotational Viscometer PRO-II* and UL adapter connected to a temperature-controlled water-ethylene glycol jacket cooled down by a refrigeration unit as shown in Figure 46. The viscosity may be measured between -20 and +100 °C with a viscometer temperature accuracy of +/- 0,2 °C and cooling bath +/- 1,0 °C. The principle of the rotational viscometer is to spin a cylinder (spindle) that is immersed into the secondary fluid; and measure the resulting viscous drag of the fluid against the spindle expressed as the spring deflection measured with a rotary transducer at a given temperature. Thus, the dynamic viscosity may be calculated from eq.(22).

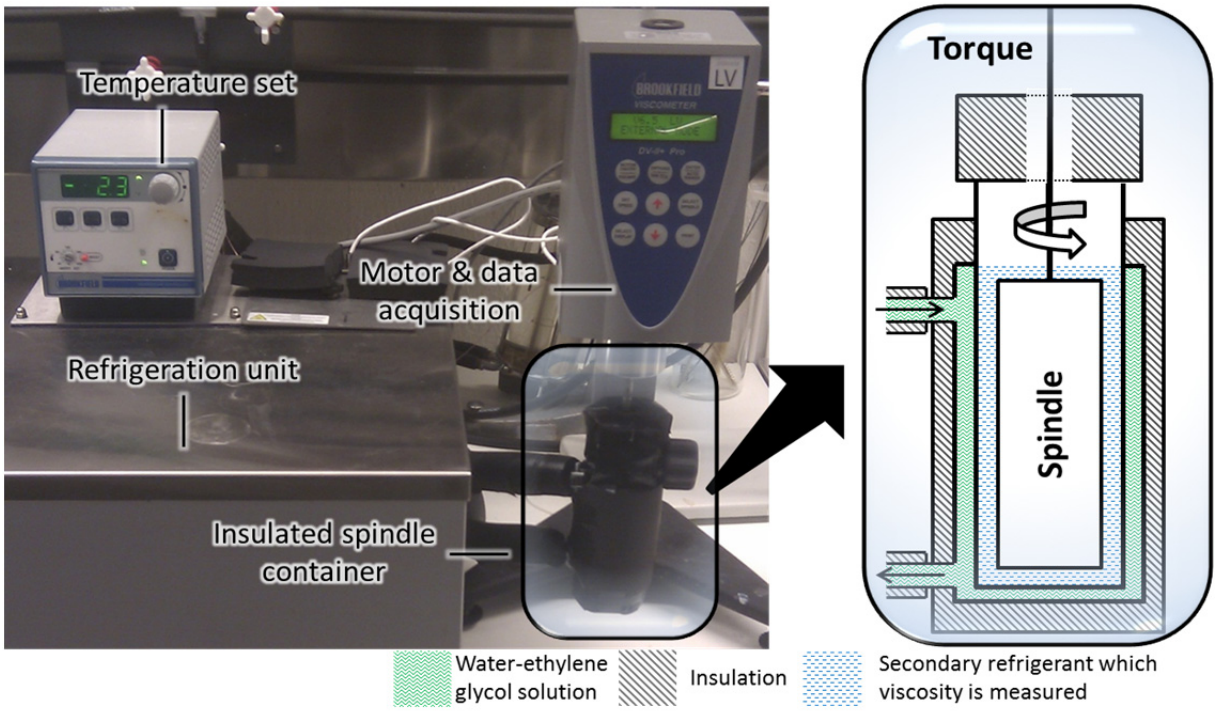

Figure 46: Brookfield Rotational Viscometer PRO-II and cross-sectional view of UL adapter

In case of low viscosity, too high spindle rotational speed may imply an important centrifugation effect that may disturb the measurement. In this case, data regression analysis may be conducted to keep only undisturbed measurements or a smaller spindle may be used for the test. A program associated with the test allows choosing the starting speed and the speed increment step for each test at a given temperature. In total the shear stress is measured for 12 different loops at each temperature.

In this study, tests have been conducted for temperatures between -15 and +40 °C. The test results for Järfälla and Nacka are presented in Figure 47. Theoretical values for the same freezing point were also included in order to compare the theory to the real values.

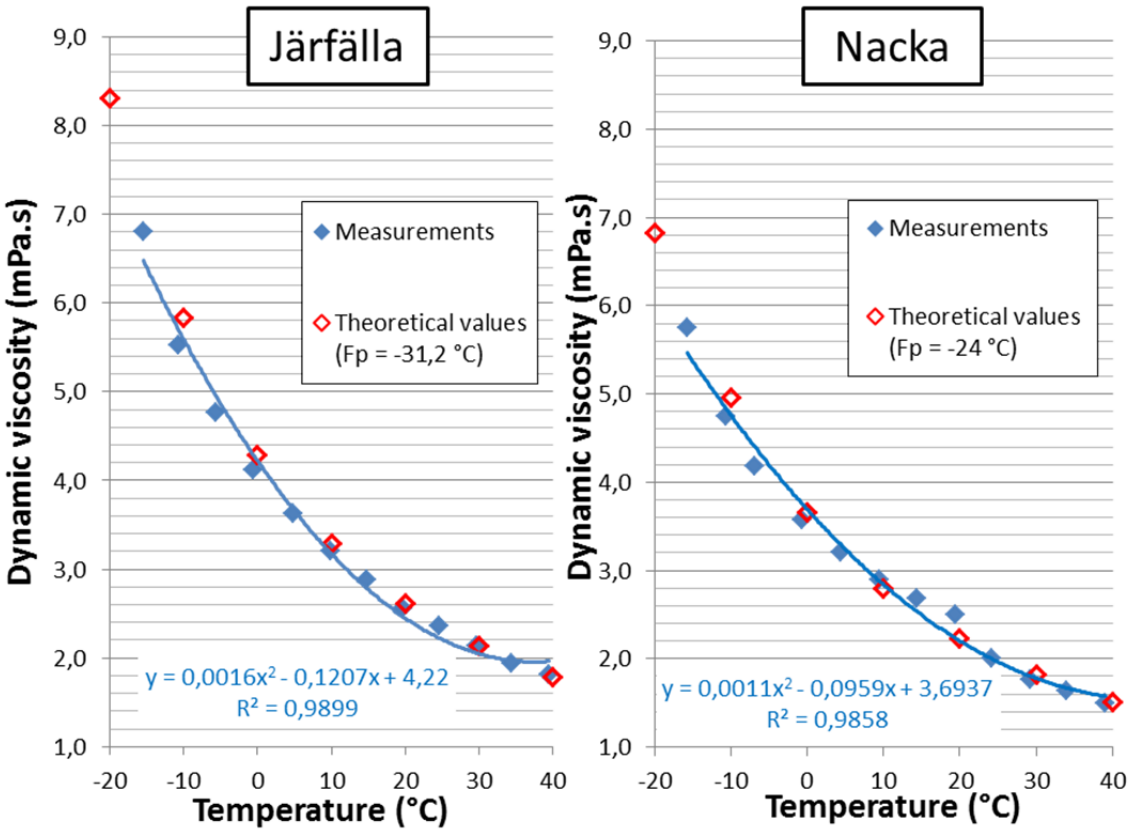

Figure 47: Dynamic viscosity measurements and comparison with theoretical values

5.3 Thermal conductivity test

The thermal conductivity at a given temperature is measured by a Transient Plane Source (TPS) method. The method is based on passing an electrical current, high enough to increase the temperature of the sample between a fraction of a degree up to several degrees, and at the same time recording the resistance (temperature) increase as a function of time. The sensor is used both as a heat source and as a dynamic resistance temperature detector (RTD) sensor. The main component of this test is the Hot Disk Thermal Constants Analyser TPS-2500, described in Figure 48 which ensures both the sensor and plane heat source functions.

Figure 48: The Hot Disk ® Kapton sensor (left) and the sample holder with the sandwiched sensor (right)

The Hot Disk ® Kapton sensor consists of an electrically conducting pattern in the shape of a double spiral, which has been etched out of a thin metal (Nickel) foil. This spiral is sandwiched between two thin sheets of an insulating material (Kapton).

To measure the thermal conductivity of a liquid, the sensor's spiral must be placed in the center of a sample so that the TPS calculation assumption is accurate. In order to do so, the sample holder shown in Figure 48 is used to keep the liquid sample around the sensor. The sample holder consists of two stainless steel blocks that have a circular cavity in their center, meant to receive the sample. The sample holder is filled through three channels which extremities are on its top. The filling is done with a syringe, to be sure that all air bubbles that may be in the cavity are expelled out.

The sample holder is immersed in an ethylene glycol/water bath which temperature is controlled by a reversible heat pump. When measuring the thermal conductivity of liquids, natural convection should be avoided. Therefore, short period of times are chosen so that any particular movement in the sample is impossible to occur.

The tests are conducted 6 times for each temperature with two different powers and the suitable measurement time. In general, the two powers used were 0,020 and 0,025 W with a measurement time of 3 seconds. The precision of the instrument is said to be +/- 2% (Ignatowicz, 2012). Figure 49 shows the results from the measurements as well as the theoretical values from Melinder (2010).

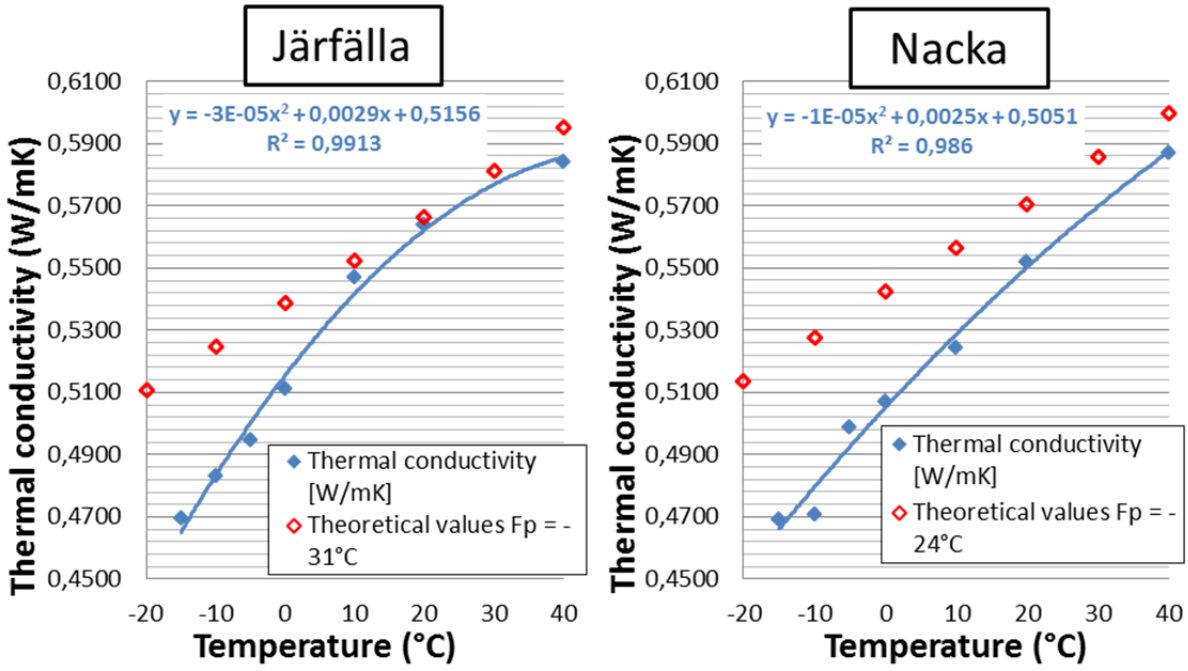

Figure 49: Thermal conductivity measurements and comparison with theoretical values

5.4 Density test

The density is measured at 15 and 20 °C with aerometer (hydrometer) and pycnometer, respectively. The aerometer is a hollow instrument using Archimedes forces to measure density. The integrated scale on the instrument is calibrated at a given temperature and it gives the specific density at this temperature.

The pycnometer is a simple vial which volume is accurately calibrated with a capillary tube integrated in the container's stopper. A pycnometer with its stopper is shown in Figure 50. The principle of the pycnometer is rather simple: the density is determined by measuring the mass of a well-defined volume of solution. First the dry vial is weighed and then the vial filled with the secondary fluid.

If the volume of the pycnometer was not calibrated by the manufacturer, distilled water – which density is well known – is used to calibrate it. The pycnometer used for the tests was already calibrated.

The volume of the vial without the stopper is 25 ml while it becomes 25,131 ml with the stopper, due to the capillary tube in it. If a highly-accurate weighing scale is used, the density is measured with high precision since the volume is also accurately defined. Matter Toledo High Accuracy Analytical Scale instrument used in this study has a precision of +/- 0,0001 g. After filling up the vial, the excess liquid that leaks from the capillary tube should be dried so that only the volume in the container is weighed.

Figure 50: The pycnometer (left) and the Mattler Toledo weighing scale (right)

Since the density was measured at only two temperatures, the data from Melinder (2007) were used to define the density variations with temperature. Due to the lack of accuracy of the measurement at 15 °C, only the pycnometer measurement at 20°C was kept. In order to determine the density function versus temperature, the function's slope was considered the same as the one given in Melinder (2007) and the created curve crosses through the measurement point at 20 °C. Figure 51 shows the theoretical and determined functions for Järfälla's secondary fluid.

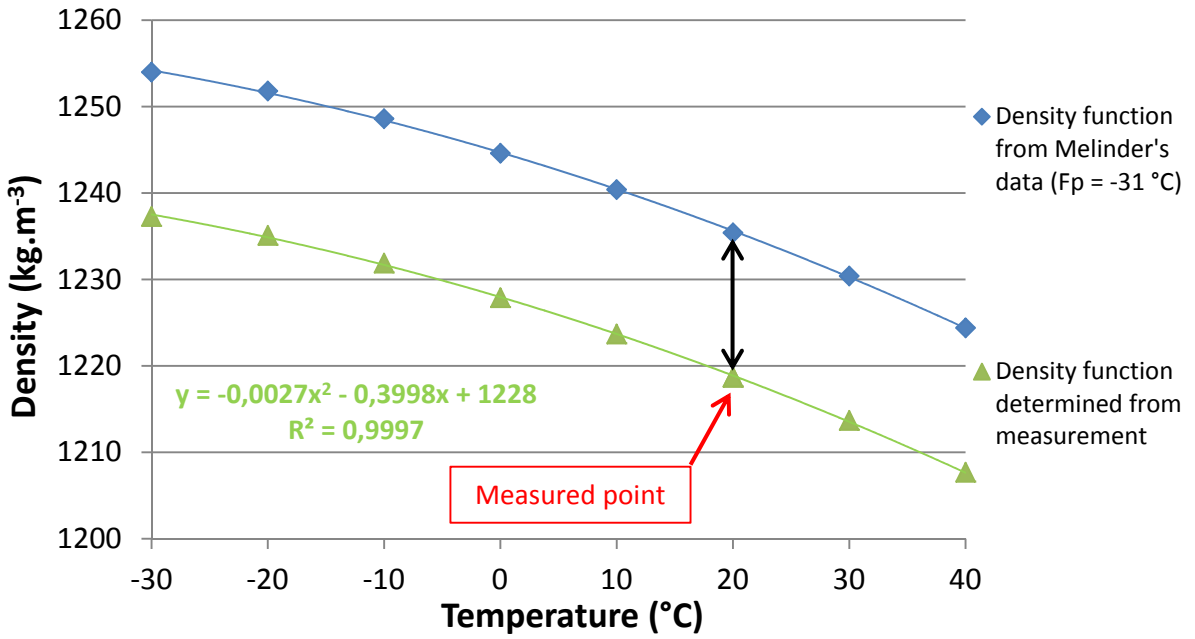

Figure 51: Järfälla density functions from theoretical data and measurements

6 CASE STUDIES

This chapter focuses on the performance of real refrigeration systems. The performance of two ice rinks was investigated. The first one is situated in the Järfälla municipality whereas the other one is situated in the Nacka municipality. Those two facilities will be simply referred to as Järfälla and Nacka.

6.1 ClimaCheck performance analyzer

6.1.1 Presentation of the ClimaCheck tool

ClimaCheck is a tool to analyze the performance of refrigeration, air conditioning or heat pump systems (Karampour, 2011). EU has introduced regulation requirements for all air conditioning systems above 12 kW to be "performance inspected" (Berglöf, 2010). Table 5 gives a non-exhaustive list of measurements or calculated values that can be performed with the ClimaCheck instrumentation. Although the ClimaCheck instrumentation is meant for refrigeration systems, energy and power measurements can be performed on other devices such as Domestic Hot Water (DHW) auxiliary heater, HVAC system or lightings. The ClimaCheck analyzer may be used for a large range of refrigeration applications: from 1 kW air-conditioner to district heat pump system with 20 MW cooling capacity.

The measures are stored on the ClimaCheck web interface and it is possible to download any required measurement period and analyze. The measures are performed each minute when the system is in operation and each five minutes when the system is shut off. Examples of ClimaCheck processed data are shown in Appendix 7. The basic flowchart and sensors of the ClimaCheck equipment can be seen in Figure 52.

Measures / Location	Temperature	Pressure	Power / Energy	Relative humidity
Refrigeration unit	After / Before comp.	After comp.	Compressors	
	Before expansion valve	Before comp.		
	Evaporation		Cooling capacity	
	Condensation		Heating capacity	
	Oil cooling after/before comp.		Oil cooling	
			Auxiliary devices	
	Superheating / Subcooling			
Secondary loop(s)	After / Before evap.		Cooling capacity	
	After / Before cond.		Heating capacity	
			Pumps	
	Return temp. ice rink(s)			
Ice hall(s)	Ice		Dehumidifier	
	Indoor (ambient)		Air handling	Indoor
	Over ice			Over ice
			Lighting	
	Outdoor			
Lockers room			DHW	

Table 5: Non exhaustive list of measurements possible to perform with the ClimaCheck instrumentation

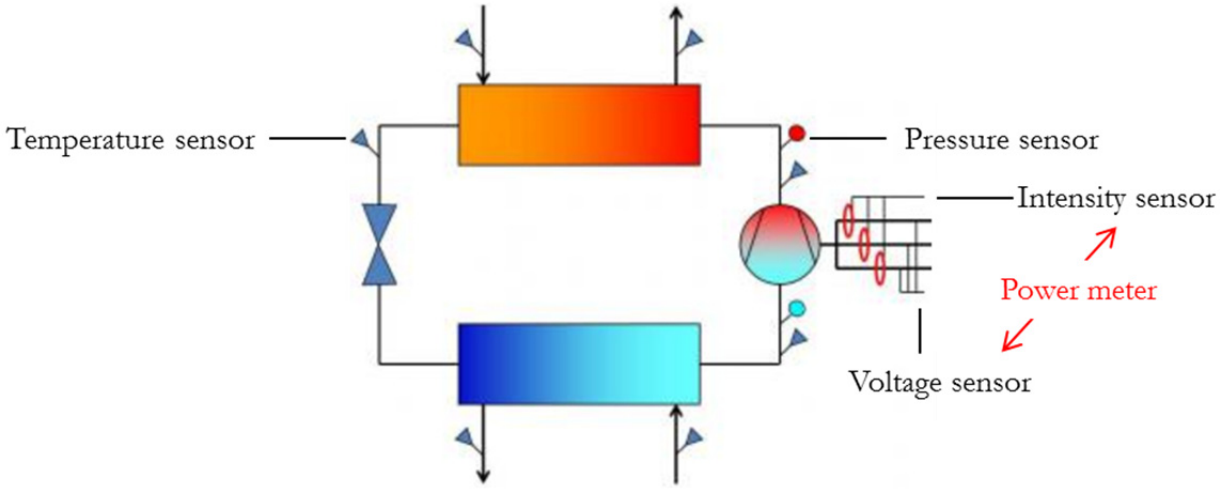

Figure 52: ClimaCheck basic instrumentation configuration

6.1.2 Mass flow calculation – Energy balance method

The ClimaCheck method to establish the refrigeration process is based on an energy balance over the compressor. This method is also called the "internal method". The different losses can be seen in Figure 53. Most of the time, the reciprocating compressors are associated with asynchronous motor but the frequency converter is optional (Destoop, 1989). The different losses L are (W): the frequency converter losses, L_{fc} ; the stator and rotor Joule losses, L_{Js} and L_{Jr} respectively ; the stator and rotor core or iron losses, L_{Cs} and L_{Cr} respectively ;and the compressor body losses, L_{comp}. The terms P refer to power (W).

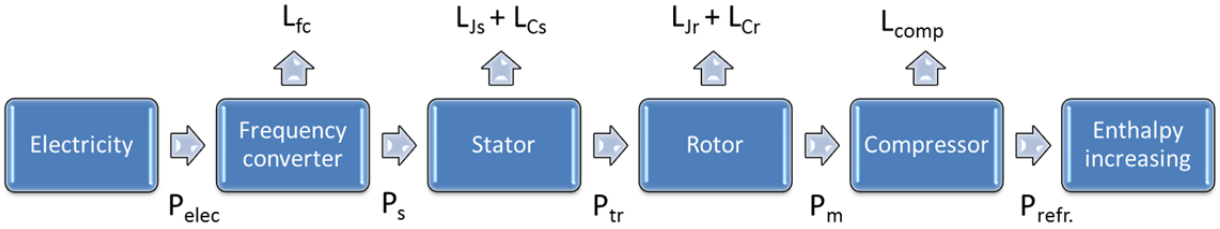

Figure 53: Energy losses from electrical power to refrigerant

The electrical efficiency may be defined as

$$\eta_{el} = \frac{P_m}{P_{elec}} \quad (71)$$

where P_{elec} is the electrical power provided to the motor and P_m is the mechanical power provided to the pistons. In general, the frequency converters efficiency ranges 97-99 % while the motor efficiency (from stator to the propeller shaft) is around 90 %, giving a global electrical efficiency of about 90 % (Karampour, 2011).

Since the effective power received by the primary refrigerant $P_{refr.}$ can be expressed as

$$P_{refr.} = \dot{m}(h_{comp,out} - h_{comp,in}) \quad (72)$$

where

- $\dot{m}$ is the mass flow, in $kg.s^{-1}$.
- $h_{comp,out}$ is the enthalpy of the primary refrigerant leaving the compressor, in $J.kg^{-1}$.
- $h_{comp,in}$ is the enthalpy of the primary refrigerant entering the compressor, in $J.kg^{-1}$.

The mass flow may then be expressed as

$$\dot{m} = \frac{\eta_{el} P_{elec} - L_{comp}}{h_{comp,out} - h_{comp,in}} \quad (73)$$

In the ClimaCheck method, it is assumed that the compressor losses are only heat losses which represent 7% of the mechanical input power (P_m). Since the primary refrigerant type is known as well the temperatures and pressures after and before the compressors, the enthalpy difference can be calculated. Hence, the mass flow is known and all features of the refrigeration cycle can be found with all the other sensors of the ClimaCheck equipment.

6.2 Järfälla ice rink

6.2.1 Presentation of the refrigeration system

Järfälla is rather an old ice rink having a partially indirect refrigeration system. The condenser is air-cooled while the evaporator cools down the secondary fluid as shown in Figure 54. Hence, the heat from the condenser is not recovered in this plant.

Initially the refrigeration plant was meant to cool down an indoor and an outdoor ice rink. However, the outdoor ice rink is not in operation anymore. The refrigeration unit uses ammonia as the primary refrigerant, has three reciprocating compressors and a shell-and-tube heat exchanger working as the evaporator. The pumps only work in full-speed mode and consume around 18 kW. The secondary fluid used is calcium chloride (F_p = -31 °C). The thermo-physical properties data were determined by analyzing the sample of the secondary fluid used in the facility. Those results are listed in part 5. The refrigeration plant is in operation from the 25/07 to the 03/04, which is 36 weeks in total.

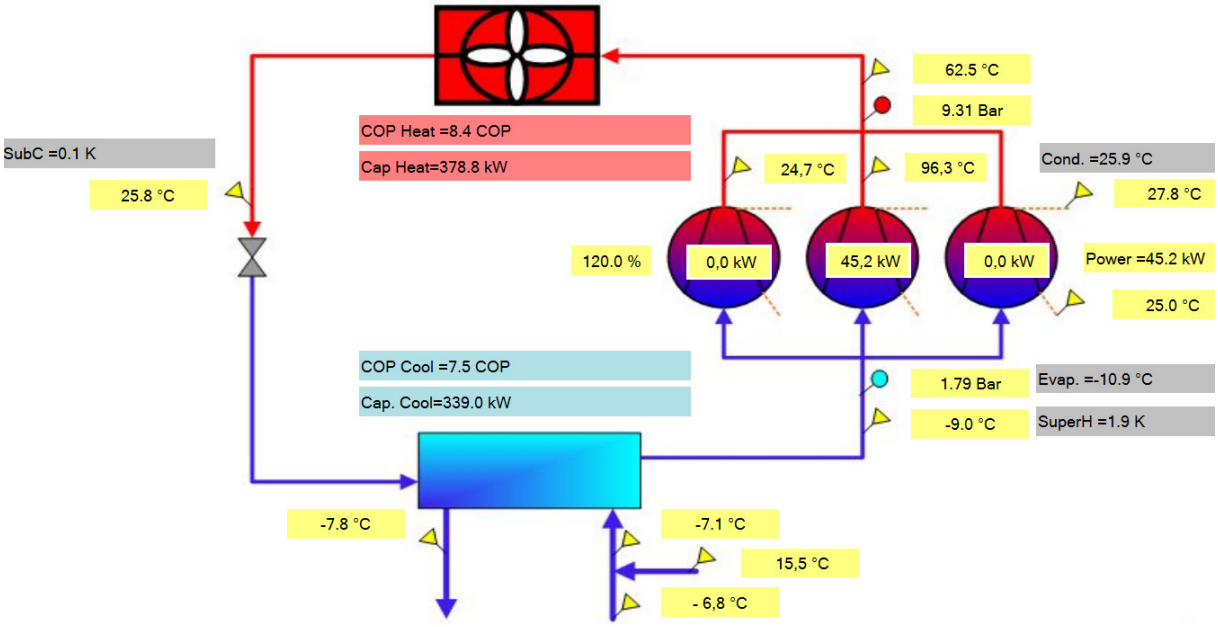

Figure 54: ClimaCheck flowchart of Järfälla ice rink

6.2.2 Data processing – Results

The data were analyzed for one significant week in November (19/11/12 to 25/11/12). Figure 55 shows the different temperatures measured in the refrigeration system during one day. It highlights the additional temperatures differences implied by the indirect systems. The sensor measuring the ice temperature is embedded in the ice and the readings may be lower than the real ice surface temperature.

The system is shut down at 23h every night and starts again at 7h every morning implying very high cooling demand in the morning. This control strategy is used to try to save energy since the condensing

heat is not recovered, although it has not been proven that energy is saved by shutting down the refrigeration system at night. The high cooling capacity needed in the morning may lead to higher energy consumption than if the refrigeration system was still running at reduced power for instance. That is why low evaporation temperatures may be seen from 7h to 10h. It shall be notice that the pumps are not shut down at night and work 24h a day. The discontinuities that may be observed in the ice temperature curve are due to ice resurfacings done after each activity session.

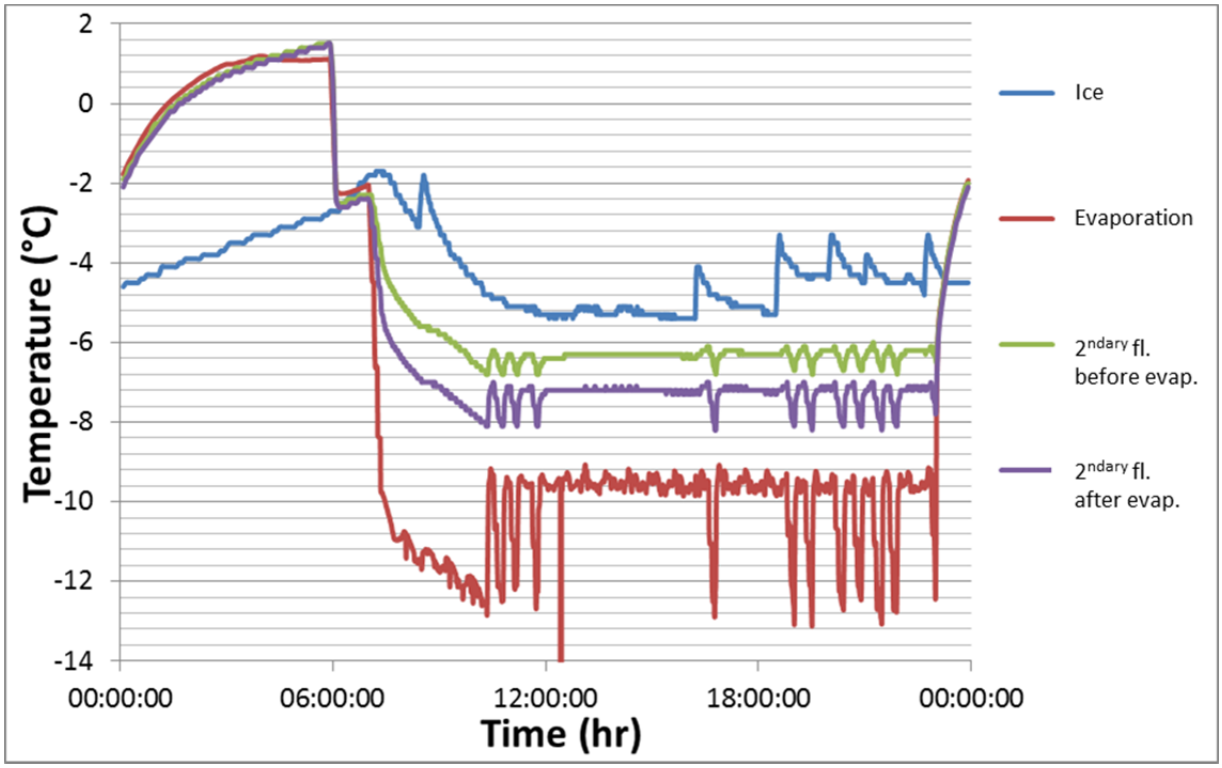

Figure 55: Refrigeration system in Järfälla (19/11/2012)

The secondary fluid temperature seems to be maintained constant throughout the day. Since the pumps only work in full-speed mode, the compressors' work must be regulated to keep this temperature difference constant. Investigating the compressors' control, it appears that they are indeed stage-regulated according the secondary fluid temperature difference (ΔT). During this whole week, only one of the three compressors was used. The other ones are only turned on when the cooling demand is high. After processing the data, the power consumed by compressors was modeled as shown in Figure 56 (during the operational period): 27,1 kW when the ΔT is below 0,7; 41,3 kW when the ΔT is between 0,7 and 1; 59,7 kW when the ΔT is between 1 and 1,2; 77,1 kW when the ΔT is above 1,2. Figure 56 shows the different temperatures and the compressor powers (real and modeled) of the refrigeration system during 6 hours.

This model was investigated in order to assess the potential energy savings if the secondary fluid with a lower freezing point was used. As a comparison baseline, the recommended calcium chloride 24 wt-% with a freezing point of -26,5 °C was taken. The ice temperature profile, as well as the heat loads profile was kept constant.

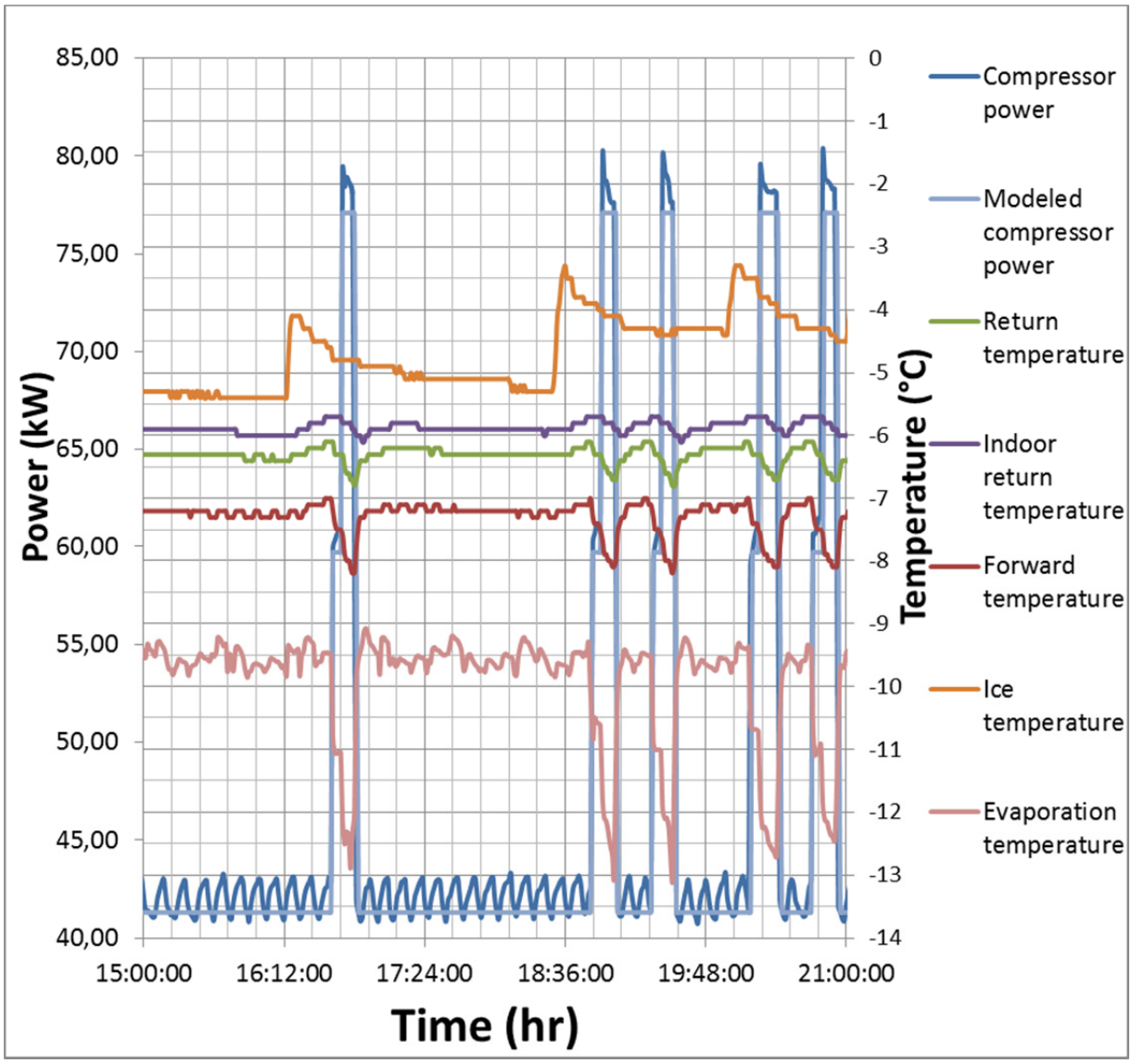

Figure 56: Temperatures and compressor powers (real and modeled) for Järfälla ice rink during 6h

Although the pumps were considered to work in full-speed mode, the volumetric flow was slightly different for the two different secondary fluids due to the change in thermo-physical properties. The flow of the real secondary fluid $\dot{V}_{tot}$ is calculated in $m^3.h^{-1}$ according to the average secondary fluid temperature T_{av} as

$$\dot{V}_{tot} = 0{,}0084 \cdot T_{av}^2 + 0{,}5429 \cdot T_{av} + 200{,}57 \quad (74)$$

while the flow associated with the recommended calcium chloride (F_p = -26,5 °C) is

$$\dot{V}_{tot} = -0{,}0035 \cdot T_{av}^2 + 0{,}6855 \cdot T_{av} + 203{,}01 \quad (75)$$

To check the accuracy of the algorithm calculating the compressor energy, the real secondary fluid properties were accounted, so it would be possible to perform the comparison with the measured energy. The real energy consumption for the week was 6,177 MWh while the algorithm gave 6,191 MWh. This represents a percentage error of 0,24%, henceforth, it was concluded that the algorithm gave sufficiently accurate results.

Additionally, the possibility of extrapolating the weekly energy consumption of compressors with good accuracy was checked. The yearly measured energy consumption for compressors is 228,8 MWh. When extrapolating both the real and calculated weekly compressor energy consumption, we obtain 222,4 and

222,9 MWh, respectively. That is less than 3 % error in both cases. Thus, it was considered correct to extrapolate the compressor energy consumption over the 36 operational weeks in a year.

Then, using the thermo-physical properties of calcium chloride with recommended concentration 24 wt-%, the algorithm gave an energy consumption of 176,0 MWh for the compressors. This represents a potential energy saving of roughly 46,8 MWh per year. Considering the freezing point difference, the potential energy saving is of 10,8 MWh when increasing the freezing point of 1 K (or 26,9 MWh per each 1 wt-% concentration).

This potential energy saving represents 12 % of the total energy consumption associated with the refrigeration (compressors and pumps). Hence, it seems important not to have too high freezing point depressant concentration in the system. Moreover, these values show that the energy saving potential regarding the freezing point may be significant in some of the ice rinks. All results are summed up in Figure 57 and Table 6.

The results found in this case study are different from the general figures given in the theoretical comparison but there are many differences between these two studies: the refrigeration system, the control strategy, the steady-state approximation, etc. Another interesting feature for Järfälla ice rink that should be noticed is that energy consumed by the pumps, 178 MWh per year, is particularly high since they are running full-time and full-speed. The pumping energy consumption accounts for 44 % of the total refrigeration consumption.

Finally, the Seasonal Performance Factor (SPF), or seasonal COP was calculated resulting in 1,62, in which the pumping energy was included. The main results of the Järfälla case study are graphically presented in Figure 57. Table 6 sums up all the results associated with Järfälla ice rink. Note that CP stands for compressor.

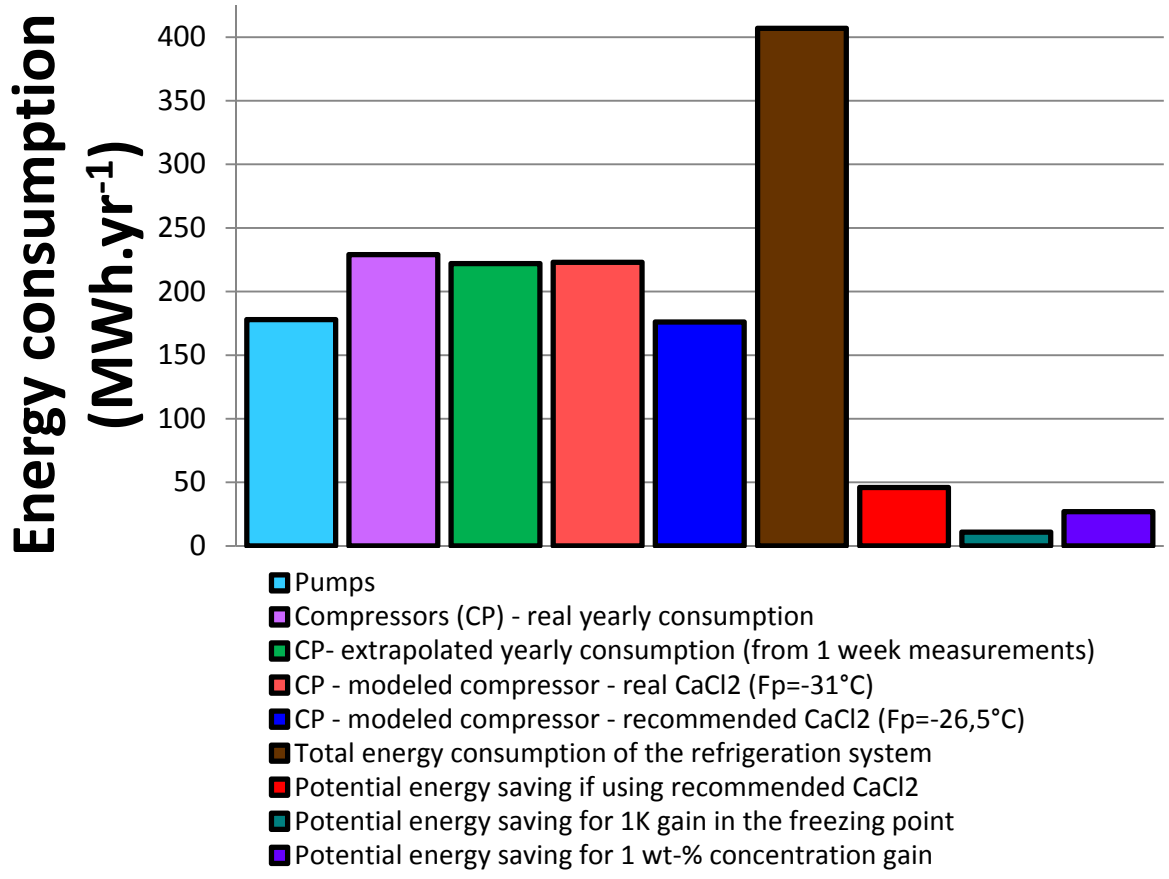

Figure 57: Main results from Järfälla case study

Table 6: Results summary table for Järfälla ice rink

Energy feature related to the refrigeration system	Value
Pumping power - pump 1	18 kW
Pumping power - pump 2	11 kW
Pumping energy consumption	178 MWh.yr^{-1}
Compressors (CP) – real yearly energy consumption	229 MWh.yr^{-1}
CP - extrapolated yearly consumption from 1 week measurements	222 MWh.yr^{-1}
CP - modeled compressor - real $CaCl_2$ (Fp=-31°C)	223 MWh.yr^{-1}
Compressors - modeled compressor - recommended $CaCl_2$ (Fp=-26,5°C)	176 MWh.yr^{-1}
Potential energy saving (if recommended 24 wt-% $CaCl_2$ was used)	46 MWh.yr^{-1}
Potential energy saving for 1K gain in the freezing point	10,8 MWh.yr^{-1}
Potential energy saving for 1% gain in the weight concentration	26,9 MWh.yr^{-1}
Potential energy saving percentage per year	12%
Seasonal Performance factor (SPF)	1,62
Total refrigeration energy consumption (compressor and pump)	407 MWh.yr^{-1}

6.3 Nacka ice rink

6.3.1 Presentation of the refrigeration system

The refrigeration system is fully-indirect and the heat is recovered from the condenser and the desuperheater, as it can be seen in Figure 58.

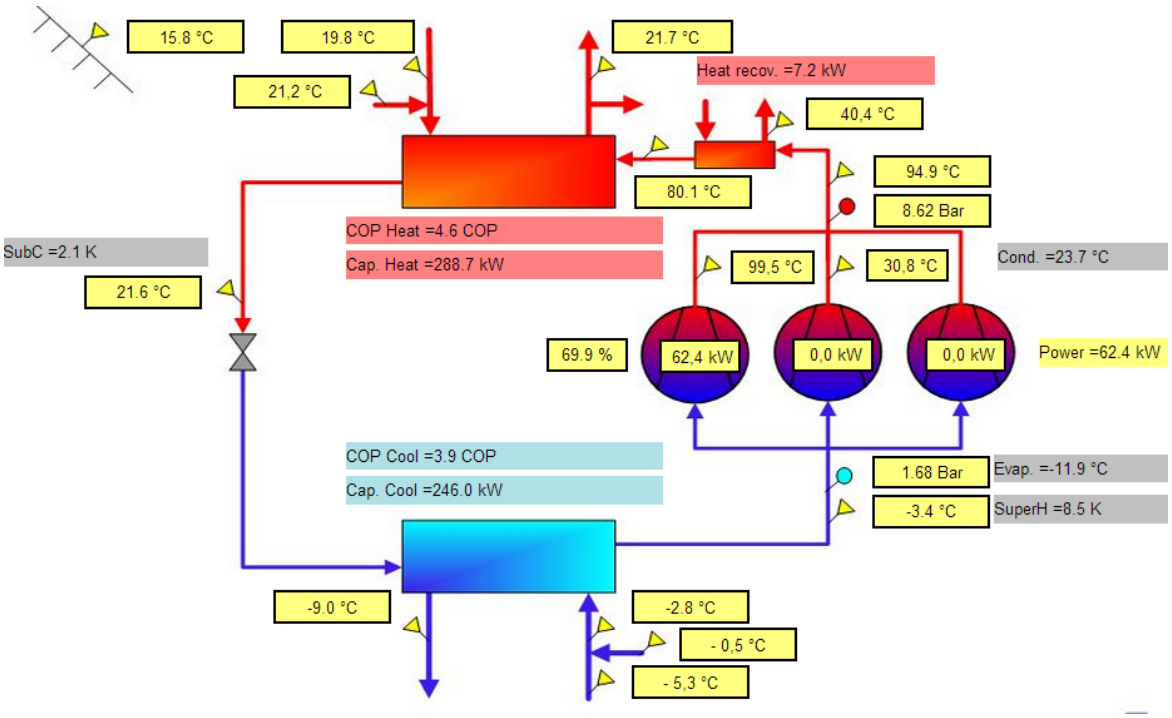

Figure 58: ClimaCheck flowchart of Nacka ice rink

The refrigeration system is used to cool down two rinks: one indoor and another outdoor. The refrigeration unit uses the reciprocating compressors and ammonia as the primary refrigerant. As for the secondary fluid, an aqueous solution of calcium chloride with a freezing point of -24°C is used. Since this freezing point is already below the recommended one (24 wt-%), energy savings obtained by lowering the secondary fluid's concentration are not assessed as it was in the Järfälla case. Moreover, the plate heat exchanger is used as the flooded evaporator.

Unfortunately, the pumping power is not measured and no information was found on the pump control, except the fact that variable speed pumps were used. Additionally, the sensor measuring the ice temperature was disabled and no information could be retrieved on the ice temperature profile. The facility is in operation from the 30/07 to the 05/05 so nearly 40 weeks.

6.3.2 Data processing – Results

The data were analyzed for the same week as Järfälla (19/11/12 to 25/11/12). Figure 59 shows the different temperatures measured in the refrigeration system during one day. The Nacka refrigeration system is not shut down at night as it was in Järfälla. The operation cycles are shorter than in Järfälla because the control strategy used for compressors is an ON-OFF strategy as shown in Figure 60. The compressors seem to be controlled with the secondary fluid return temperature; however no clear pattern was found. When the compressors stop, the secondary fluid outlet temperature from the evaporator keeps decreasing. Henceforth, the pumps must be running during this time since the secondary fluid is still being cooled down by the evaporator.

The measured energy consumption of compressors over a year is 250 MWh. This value is slightly higher than the one measured in Järfälla; however the heat is recovered in this plant which may lead to higher condensation temperature and higher compressor power but higher overall efficiency. Moreover, the ice rink runs four more weeks during a year.

In order to compare the pumping power with Järfälla, the flow was calculated with the temperature difference, the cooling capacity and the specific heat capacity of the secondary fluid. The pumping power share associated with the rink floor piping was calculated taking a pump efficiency of 0,5. This share was supposed to be around 60 % of the total pumping power as in Figure 36. All these assumptions lead to a pumping energy of 41 MWh per year. If this figure proves to be accurate, the pumping energy would account for 16 % of the total refrigeration energy consumption, contrasting with the 44 % share in Järfälla and showing the beneficial effect of using variable speed pumps.

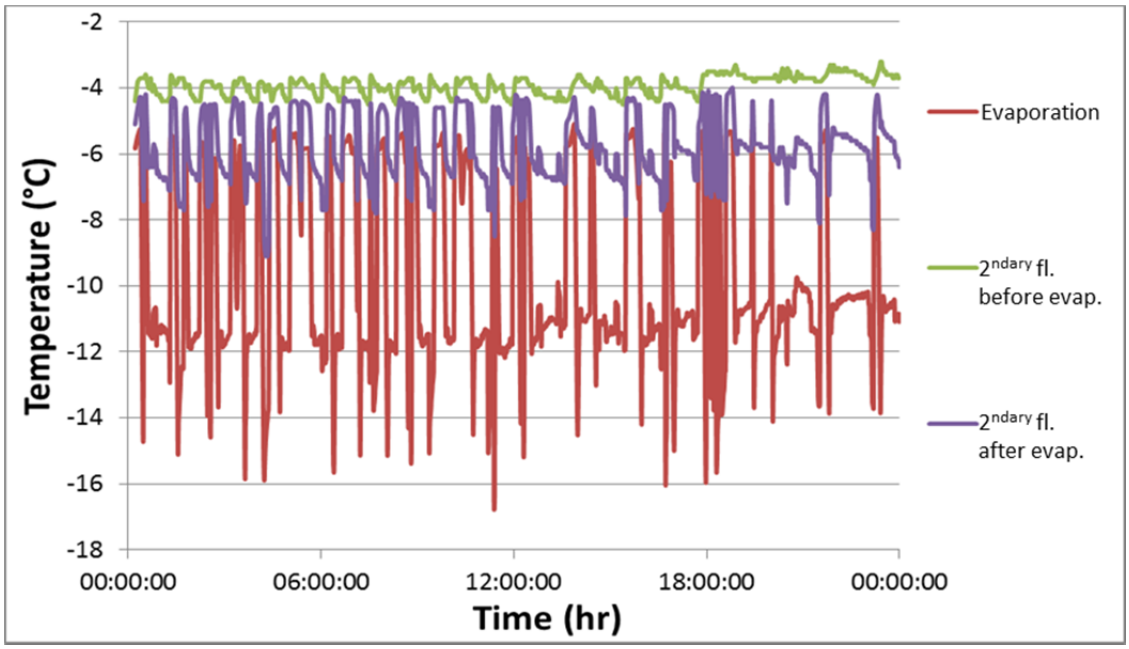

Figure 59: Refrigeration system in Nacka (19/11/2012)

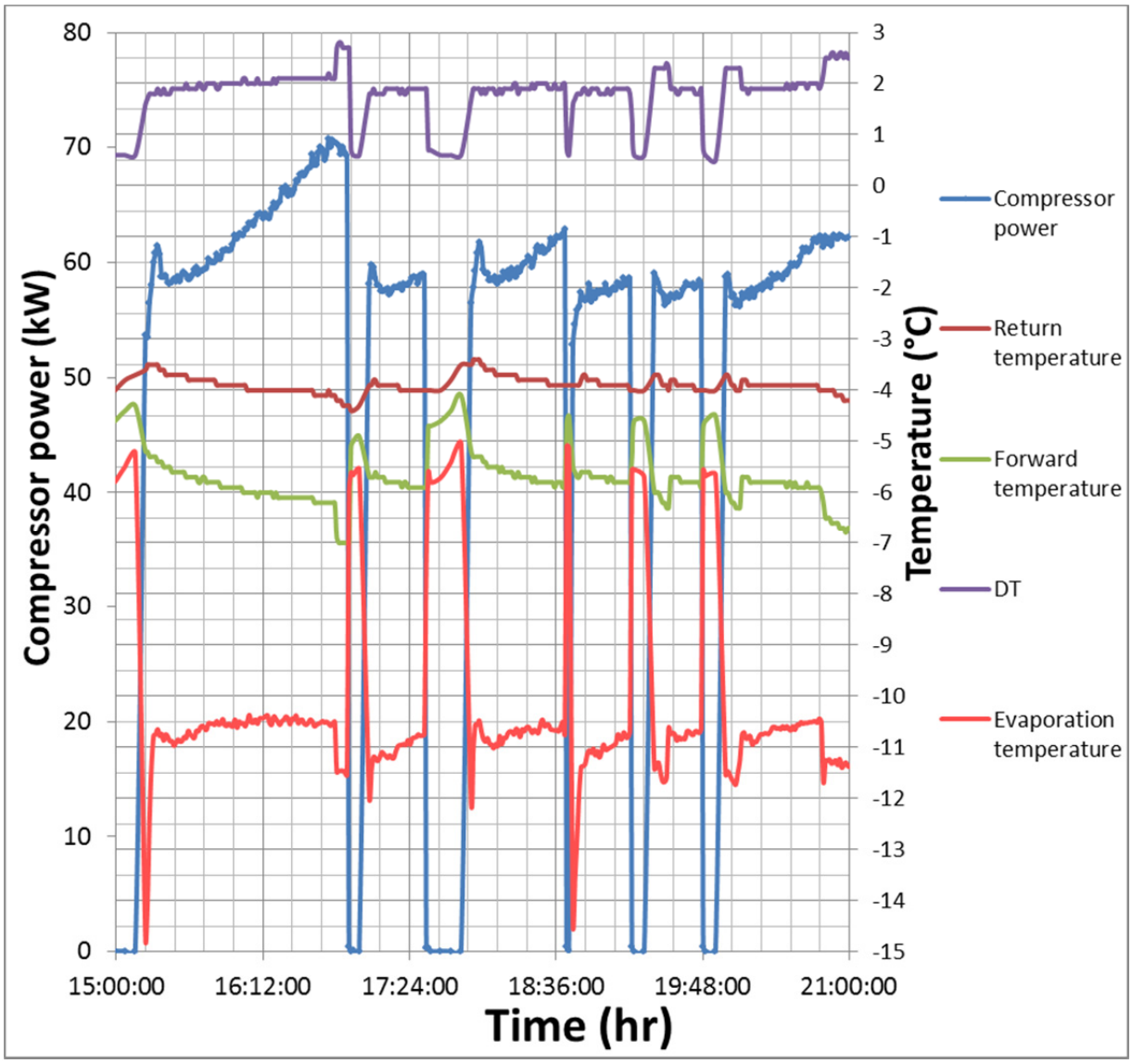

Figure 60: Temperatures and compressor powers (real and modeled) for Nacka ice rink during 6h

In contrary to Järfälla's ice rink, other energy consumptions are measured in Nacka such as lighting, DHW, dehumidification, etc. Thus, the energy consumption distribution could be evaluated and is presented in Figure 61. Note that some energy consumptions such as lighting in the locker rooms and domestic electrical devices were not measured and are therefore not included. The total measured energy consumption for a year is 952 MWh. If 10 % is assumed to be the share of the non-measured energy consumptions in the total energy consumption, this total would reach around 1060 MWh per year.

Since many data were missing, no significant outcomes have been found for this ice rink regarding the secondary fluid. The measured SPF over a year is 2,90 that is significantly higher than Järfälla even though the recovered heat is not accounted in the SPF calculation. This difference between SPF may be due to the use of variable speed pumps and the differences in the system design.

SPF:
2,90

Total energy consumption:
952 MWh

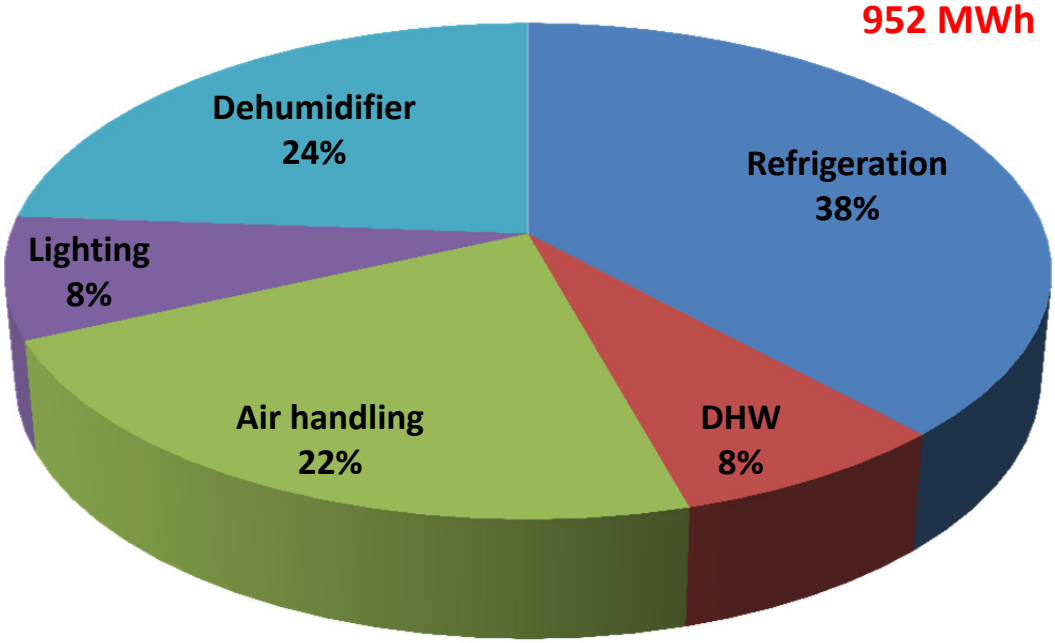

Figure 61: Energy consumption distribution in Nacka's ice rink

7 CONCLUSION

In this study, the influence of secondary fluids' thermo-physical properties has been investigated in a qualitative and quantitative way. A model was developed in order to assess the performance of secondary fluids used in ice rinks in terms of the heat transfer, pressure drops and refrigeration efficiency. The calculations for the theoretical model were performed assuming the steady-state conditions and considering a fixed ice rink design independently of the secondary fluid type.

It was shown that potassium formate has the best heat transfer properties while ammonia leads to the lowest pressure drops and pumping power. Propylene glycol shows the worst features in both cases. A relation was made between the secondary fluids efficiency and viscosity. Indeed, the secondary fluids showing the lowest viscosity at low temperatures are the ones leading to the best refrigeration efficiency. In decreasing order, the refrigeration efficiency is the highest for: ammonia (NH_3), potassium formate (K-formate), calcium chloride ($CaCl_2$), potassium acetate (K-acetate), ethylene glycol (EG), ethyl alcohol (EA) and propylene glycol (PG). Particularly, NH_3 and K-formate show respectively 5 % and 3 % higher COP than calcium chloride for typical heat loads of 150 kW. In this study, no long-term effects such as corrosion were considered.

The poor heat transfer properties of all secondary fluids were shown for laminar flow regime. The turbulent flows lead to significantly higher efficiency although the pumping power may be slightly higher than for laminar flows. The temperature differences between: the ice top and the average secondary fluid temperature; the secondary fluid average temperature and the evaporation temperature were calculated. The heat transfer resistance shares associated with the different heat transfer mechanisms in the ice rink floor (conduction/convection) and the evaporator (convection/conduction/boiling) were also investigated. For the heat loads of 150 kW and the ice temperature of -3,5°C, the temperature differences found for the ice rink floor are: 4,30 K for $CaCl_2$; 5,61 K for PG; 5,50 K for EG; 5,62 K for EA; 4,29 K for NH_3; 5,33 K for K-acetate and 4,27 K for K-formate. The convection share in the ice rink floor heat transfer resistance is larger for the secondary fluids which thermo-physical properties lead to the laminar flow in the ice rink floor piping rather than for the secondary fluids for which the turbulent flow occurs. For PG, EG, EA and K-acetate which obtain laminar flow in the ice rink floor pipes, the convection share is 25,7 %, 24,2 %, 25,9 % and 21,8 %, respectively, while it is 3,2 %, 2,9 % and 2,5 % for $CaCl_2$, NH_3 and K-formate, respectively.

When controlling the pump over a temperature difference ΔT, the existence of the optimum pump control or optimum flow was highlighted. This optimum pump control ΔT depends on the secondary fluid considered as well as on the heat loads. For typical heat loads of 150 kW this optimum pump control ΔT is around: 2,8 K for $CaCl_2$; 4,2 K for PG; 3,2 K for EG; 3,0 K for EA; 2,0 K for NH_3; 3,0 K for K-acetate and 2,2 K for K-formate. The optimum pump control ΔT is increasing with increasing cooling capacity independently of the secondary fluid type.

The theoretical model was also used to assess how the reduction of the freezing point depressant concentration would affect the system performance. It was found that increasing the freezing point by 10 K allows COP improvements of: 1,3 % for $CaCl_2$; 10,5 % for PG; 3,6 % for EG; 2,8 % for EA; 0,4 % for NH_3; 1,7 % for K-acetate and 1,4 % for K-formate; for heat loads of 150 kW. Nevertheless, the Järfälla case study showed even higher energy saving potential with regard to concentration decrease for calcium chloride.

Two study cases (Järfälla and Nacka ice rinks) were performed with the performance analyzer ClimaCheck. The main difficulty was to understand how the refrigeration systems are handled and controlled. The two ice rinks showed energy consumption linked to the refrigeration system of 407 MWh and 320 MWh per year, respectively. The SPFs were calculated as 1,62 for Järfälla and 2,90 for Nacka. A performance comparison between two secondary fluids with different freezing point was performed for the Järfälla case. The results showed a potential energy saving of 12 %, corresponding to 46 MWh per year. Potentially, an increase by 1 K of the secondary fluid freezing point may lead to 10,8 MWh savings

per year. Due to the lack of the ice temperature measurement, it was not possible to conduct the same type of comparison for Nacka. However, the yearly energy consumption shares could be measured showing that refrigeration accounts for 38 % of the total energy consumption. This result is similar to the 43 % obtained from the STOPPSLADD project. On the contrary, the share for dehumidification is 24 % which is higher than the expected 6 %. This may indicate that the energy consumption of dehumidification systems is underestimated.

The benefits of variable speed pumps were also emphasized although no significant features could be drawn from the measurements.

8 FUTURE WORK

The theoretical model developed could be enhanced in several ways: by integrating it to a more global simulation of the ice rink building, by including different control strategies, by developing further the numerical *COMSOL* simulation and accounting for unsteady-state phenomena. A three dimensional model has started to be investigated but only the conduction part could be modeled as shown in Figure 62

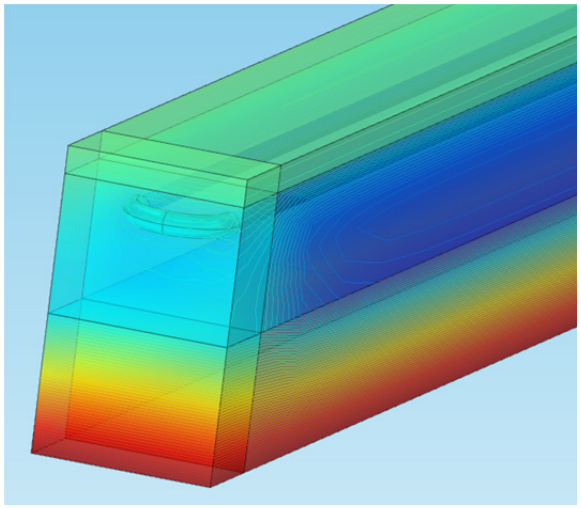

Figure 62: COMSOL 3D model of ice rink floor - Conduction part

The influence of the heat recovery on the overall performance should be further investigated. It may be relevant to investigate the existence of an optimum indoor air temperature leading to the lowest possible heat loads while providing comfortable conditions. The model may be turned into a calculation program enabling choosing different designs and parameters to find the best system design for a given ice rink building.

Another performance study could be led considering the highest possible cooling capacity instead of the COP for given conditions.

An analytical expression based on the theoretical model's calculations giving the optimum pump control could be developed and tested in the reality to validate the model.

The density of the secondary fluid samples should be further tested to define the density gradients and obtain the density function versus the temperature. As for the specific heat capacity, it should be tested with the suitable measuring instrument.

Finally, more case studies should be conducted to strengthen the results found in this study.

REFERENCES

Acuña, J., 2013. *Distributed thermal response tests: New insights on U-pipe and Coaxial heat exchangers in groundwater-filled boreholes,* Stockholm: KTH, Royal Institute of Technology.

Alfa Laval, 2012. *Newsletter for Refrigeration Industry.* [Online]. Available at: www.alfalaval.com/newsletter/refrigeration/en/issue-1-2012
[Accessed 01 08 2013].

ASHRAE, 2010. Chapter 44, Ice Rinks. In: *ASHRAE handbook.* ASHRAE, Inc., pp. 44.1-44.11.

Ayub, Z. H., 2003. Plate Heat Exchanger Literature Survey and New Heat Transfer and Pressure Drop Correlations for Refrigerant Evaporators. *Heat Transfer Engineering,* 24(5), pp. 3-16.

Berglöf, K., 2010. *Optimization through performance inspections.* Stockholm, IIF / IIR.

Blades, R. W., 1992. Modernizing and retrofiting ice skating rinks. *ASHRAE Journal,* 34(4), pp. 34-43.

Briley, G. C., 2004. Secondary Coolants. *ASHRAE Journal,* p. 36.

Caliskan, H. & Hepbasli, A., 2010. Energy and exergy analyses of ice rink buildings at varying reference temperatures. *Energy and Buildings,* Issue 42, p. 1418–1425.

Calm, J. M., 2008. The next generation of refrigerants – Historical review, considerations, and outlook. *International Journal of Refrigeration,* Volume 31, pp. 1123-1133.

CETC, 2007. Heat recovery and fincancial assistance. In: *The Energy Management Manual for Arena and Rink Operators.* Varennes: Canadian Energy Technology Center, pp. 162-167.

Claesson, J., 2004. *Thermal and Hydraulic Performance of Compact Brazed Plate Heat Exchangers Operating as Evaporators in Domestic Heat Pumps,* Stockholm: KTH.

CSST, 2009. *Systèmes de réfrigération fonctionnant à l'ammoniac - Mesures de préventions.* 2e ed. Montréal: Bibliothèque Nationale du Québec.

Daoud, A., Galanis, N. & Bellache, O., 2008. Calculation of refrigeration loads by convection, radiation and condensation in ice rinks using a transient 3D zonal model. *Applied Thermal Engineering,* 28(14), pp. 1782-1790.

Destoop, T., 1989. Compresseurs volumétriques. In: *traité Génie mécanique.* Paris: Techniques de l'Ingénieur, pp. 1-25.

Egolf, P. W., Frei, B. & Furter, R., 2000. Thermodynamics of moist air: contribution to error estimates. *Applied Thermal Engineering,* Volume 20, pp. 1-19.

Gnielinski, V., 1976. New equations for heat and mass transfer in turbulent pipe and channel flows. *Int. Chem. Eng.,* Volume 16, pp. 359-368.

Granryd, E. et al., 2011. *Refrigeration Engineering.* Stockholm: Royal Institute of Technology, KTH.

Haglund Stignor, C., Sundén, B. & Fahlén, P., 2007. Liquid side heat transfer and pressure drop in finned-tube cooling-coils operated with secondary fluids. *International Journal of Refrigeration,* Volume 30, pp. 1278-1289.

Hausen, H., 1943. Darstellung des Wärmeüberganges in Rohren durch verallgemeinerte. *VDI Verfahrenstechnik,* Volume 4, pp. 91-98.

Hillerns, F., 2001. *Thermophysical Properties and Corrosion Behavior of Secondary Coolants.* Atlanta, ASHRAE Winter Meeting.

Huang, J., 2010. *Performance Analysis of Plate Heat Exchangers Used as Refrigerant Evaporators,* Johannesburg: University of the Witwatersrand.

Ignatowicz, M., 2008. *Corrosion aspects in indirect systems with secondary fluids,* Stockholm: KTH.

Ignatowicz, M., 2012. *Status report 2012-12-05: The influence of adsorption corrosion inhibitors and additives on the heat transfer and other thermo-physical properties of secondary fluids,* Stockholm: KTH, Royal Institute of Technology.

IIHF, 2010. *Ice Rink Manual of the International Ice Hockey Federation.* 1st ed. Zürich: IIHF.

Incropera, F. P., DeWitt, D. P., Bergman, T. L. & Lavine, A. S., 2007. *Fundamentals of Heat and Mass Transfer.* 6th ed. New York: John Wiley & Sons Inc..

Ingvar, 2007. *Ice Skating Rink - Movable.* [Online]. Available at: http://www.ingvar.is/Plants/IceSkatingRink/IceSkatingRink.html
[Accessed 22 06 2013].

International Energy Agency, 2008. *Energy Policies of IEA Countries, Sweden 2008 Review,* Paris: OECD/IEA.

Karampour, M., 2011. *Measurement and Modelling of Ice Rink Heat Loads,* Stockholm: KTH, Royal Institute of Technology.

Makhnatch, P., 2011. *Technology and Energy Inventory of Ice Rinks,* Stockholm: Royal Institute of Technology, KTH.

Martin, H., 1996. A theoretical approach to predict the performance of chevron-type plate heat exchangers. *Chemical Engineering and Processing,* 35(4), pp. 301-310.

Marvillet, C., 2003. Fluides frigoporteurs. In: É. T.I., ed. *Échanges de chaleur et isolation.* Paris: Techniques de l'Ingénieur, pp. 55-57.

Masters, G. M. & Ela, W., 2008. *Introduction to Environmental Engineering and Science.* 3rd ed.:Prentice Hall.

Melinder, Å., 2007. *Thermophysical Properties of Aqueous Solutions Used as Secondary Working Fluids,* Stockholm: Royal Institute of Technology, KTH.

Melinder, Å., 2009. *Handbook on indirect refrigeration and heat pump systems.* Stockholm: KTH, Royal Institute of Technology.

Melinder, Å., 2010. *Properties of Secondary Working Fluids for Indirect Systems.* Paris: International Institute of Refrigeration, IIR.

Muley, A. & Manglik, R. M., 1999. Experimental Study of Turbulent Flow Heat Transfer and Pressure Drop in a Plate Heat Exchanger with Chevron Plates. *ASME Journal of Heat Transfer,* Volume 121, pp. 110-117.

Mun, J. & Krarti, M., 2011. An ice rink floor thermal model suitable for whole-building energy simulation analysis. *Building an Environment,* Volume 46, pp. 1087-1093.

Munters, 2011. *Engineering Catalog, DryCool Dehumidification System.* Munters.

Nguyen, T., 2012. *Carbon Dioxide in Ice Rink Refrigeration,* Stockholm: KTH, Royal Institute of Technology.

Nichols, L., 2009. Improving Efficiency In Ice Hockey Arenas. *ASHRAE Journal,* 51(6), pp. 16-20.

Nishimori, H., 1981. Internal Energy, Specific Heat and Correlation Function of the Bond-Random Ising model. *Progress of Theoretical Physics,* 66(4), pp. 1169-1181.

Norton, B. & Edmonds, J. E., 1991. Aqueous Propylene-Glycol concentrations for the Freeze Protection of Thermosyphon Solar Energy Water Heaters. *Solar Energy,* 47(5), pp. 375-382.

Palm, B. & Claesson, J., 2006. Plate Heat Exchangers: Calculation Methods for Single and Two-Phase Flow. *Heat Transfer Engineering,* 27(4), pp. 88-98.

Piché, O. & Galanis, N., 2010. Thermal and economic evaluation of heat recovery measures for indoor ice rinks. *Applied Thermal Engineering,* Volume 30, pp. 2103-2108.

QTF, 2012. *The QTF method makes heating and cooling systems more effective.* [Online]. Available at: http://www.qtf.se/filer/QTF-Presentation_20120426_en.pdf
[Accessed 05 06 2013].

RETscreen, 2005. *Energy Efficiency Project Analysis for Supermarkets and Arenas,* Canada: Canmet Energy.

Rogstam, J., 2010. *Energy usage statistics and saving potential in ice rinks.* Stockholm, IIF/IIR.

Rogstam, J., 2013. *Project kickoff meeting* [Interview] (18 03 2013).

Saint-Gobain, 1989. Formulaire. In: L. &. DOC, ed. *Pont-à-Mousson.* Paris: pp. 1-40.

Sawalha, S. & Chen, Y., 2010. *Investigations of Heat Recovery in Different Refrigeration System Solutions in Supermarkets, Effsys2 Project final report,* Stockholm: KTH, Royal Institute of Technology.

Seghouani, L., Daoud, A. & Galanis, N., 2011. Yearly simulation of the interaction between an ice rink and its refrigeration system: A case study. *International Journal of Refrigeration,* Volume 34, pp. 383-389.

Seghouani, L. & Galanis, N., 2009. Quasi-steady state model of an ice rink refrigeration system. *Building simulation,* 2(2), pp. 119-132.

Shah, R. & Focke, W., 1988. Plate heat exchanger and their design theory. In: *Heat Transfer Equipment Design.* Washington: Hemisphere Publishing Corporation, pp. 227-254.

Somrani, R., Mun, J. & Krarti, M., 2008. Heat transfer beneath ice-rink floor. *Building and Environment,* Volume 43, pp. 1687-1698.

Stegmann, R., 2005. *Using Ammonia as a Refrigerant.* [Online]. Available at: http://www.process-cooling.com/
[Accessed 6 June 2013].

Sterner, D. & Sunden, B., 2006. Performance of Plate Heat Exchangers for Evaporation of Ammonia. *Heat Transfer Engineering,* 27(5), pp. 45-55.

van der Ham, F., Witkamp, G. J., de Graauw, J. & van Rosmalen, G. M., 1998. Eutectic freeze crystallization: Application to process streams and waste water purification. *Chemical Engineering and Processing,* 37(2), pp. 207-213.

Wang, K., Eisele, M., Hwang, Y. & Radermarcher, R., 2010. Review of secondary loop refrigeration systems. *International Journal of Refrigeration,* Volume 33, pp. 212-234.

Wanniararchchi, A., Ratman, U., Tilton, B. & Dutta-Roy, K., 1995. Approximate correlations for chevron-type plate heat exchangers. *ASME HTD-Vol. 314, 1995 National Heat Transfer Conference,* Volume 12, pp. 145-151.

Vasava, P. R., 2007. *Fluid Flow in T-junction,* Lappeenranta: Lappeenranta University of Technology.

KTH Industrial Engineering and Management

Appendix

APPENDIX

Appendix 1: Thermo-physical properties of secondary fluids commonly used in ice rink for a freezing point of -30°C

The data presented in this Appendix were retrieved from Melinder (2010).

$CaCl_2$

T_f (°C)	[C] (wt-%)	T (°C)	ϱ (kg.m^{-3})	C_p (J.kg^{-1}.K^{-1})	k (W.m^{-1}.K^{-1})	μ (mPa.s)
-30	25,4	40	1221	2944	0,596	1,74
		30	1227	2926	0,582	2,09
		20	1232	2904	0,567	2,56
		10	1237	2879	0,553	3,22
		0	1241	2851	0,539	4,19
		-10	1245	2820	0,525	5,7
		-20	1248	2788	0,511	8,1
		-25	1250	2772	0,504	9,9
		-30	1251	2755	0,496	12,3

PG

T_f (°C)	[C] (wt-%)	T (°C)	ϱ (kg.m^{-3})	C_p (J.kg^{-1}.K^{-1})	k (W.m^{-1}.K^{-1})	μ (mPa.s)
-30	48,82	40	1024,4	3630	0,374	2,84
		20	1037,9	3555	0,363	6,14
		10	1044	3518	0,358	10,08
		0	1049,6	3481	0,353	18,06
		-10	1054,6	3443	0,348	35,7
		-20	1059	3406	0,344	78,8
		-30	1062,6	3368	0,339	196,3

EG

T_f (°C)	[C] (wt-%)	T (°C)	ϱ (kg.m^{-3})	C_p (J.kg^{-1}.K^{-1})	k (W.m^{-1}.K^{-1})	μ (mPa.s)
-30	45,5	40	1048,7	3492	0,418	1,84
		20	1059,7	3398	0,404	3,22
		10	1064,6	3348	0,398	4,55
		0	1068,9	3298	0,391	6,78
		-10	1072,7	3247	0,384	10,7
		-20	1076	3196	0,378	18,2
		-30	1078,7	3145	0,371	33,2

Appendix 1: Thermo-physical properties of secondary fluids commonly used in ice rink for a freezing point of -30°C

EA

T_f (°C)	[C] (wt-%)	T (°C)	ϱ (kg.m^{-3})	C_p (J.kg^{-1}.K^{-1})	k (W.m^{-1}.K^{-1})	μ (mPa.s)
		40	918,4	4119	0,366	1,47
		30	926	4078	0,362	2,02
		20	933,5	4024	0,358	2,88
		10	940,8	3957	0,354	4,35
-30	40,7	0	947,8	3877	0,349	7,03
		-10	954,6	3783	0,345	12,4
		-20	961,1	3675	0,341	24
		-25	964,1	3616	0,339	34,9
		-30	967,1	3553	0,337	52,2

NH_3

T_f (°C)	[C] (wt-%)	T (°C)	ϱ (kg.m^{-3})	C_p (J.kg^{-1}.K^{-1})	k (W.m^{-1}.K^{-1})	μ (mPa.s)
		30	925,7	4205	0,507	0,96
		20	930,3	4208	0,49	1,24
		10	934,4	4216	0,472	1,61
-30	17,75	0	938,2	4228	0,455	2,16
		-10	941,3	4245	0,437	3,01
		-20	943,9	4265	0,42	4,43
		-30	945,8	4287	0,402	6,98

K-acetate

T_f (°C)	[C] (wt-%)	T (°C)	ϱ (kg.m^{-3})	C_p (J.kg^{-1}.K^{-1})	k (W.m^{-1}.K^{-1})	μ (mPa.s)
		40	1170	3167	0,513	1,66
		30	1175	3137	0,501	2,07
		20	1180	3115	0,488	2,64
		10	1184	3093	0,476	3,5
-30	34	0	1188	3072	0,464	4,9
		-10	1192	3051	0,452	7,04
		-20	1195	3029	0,44	12,1
		-25	1197	3017	0,434	16
		-30	1198	3006	0,428	21,9

Appendix 1: Thermo-physical properties of secondary fluids commonly used in ice rink for a freezing point of -30°C

K-formate

T_f (°C)	[C] (wt-%)	T (°C)	ϱ (kg.m^{-3})	C_p (J.kg^{-1}.K^{-1})	k (W.m^{-1}.K^{-1})	μ (mPa.s)
-30	36,8	40	1229	2995	0,55	1,32
		30	1233	2977	0,538	1,57
		20	1237	2959	0,526	1,89
		10	1242	2941	0,514	2,34
		0	1246	2923	0,502	3,01
		-10	1249	2905	0,49	4,11
		-20	1252	2886	0,478	6
		-30	1255	2868	0,466	9,5

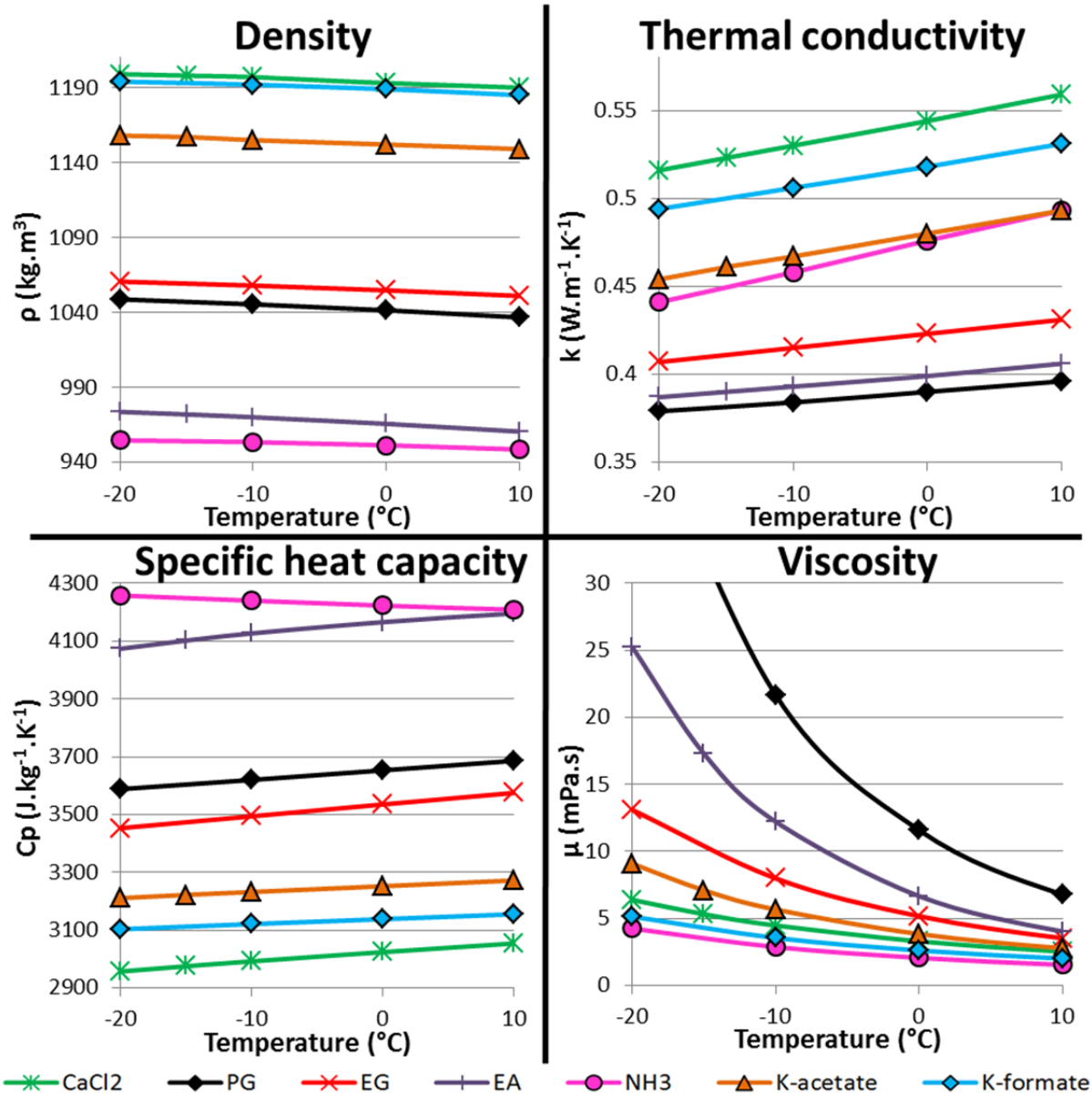

Appendix 2: Properties of ammonia as a refrigerant – Example of developed functions

Data were retrieved from Granryd et al. (2011) and EES property calculator software. The first authors based their values on REFPROP 6.01 by NIST.

R717	P_{crit}	113,33	bar		T_{cond}:	20	°C			
Evap. temp.	h_l	h_g	v_l	$q_{v,data}$	$e_{v,is,data}$	k_l	μ_l	P_{abs}	P_{abs}/P_{crit}	total mass flow
(°C)	kJ.kg^{-1}	kJ.kg^{-1}	dm^3.kg^{-1}	kJ.m^{-3}	kJ.m^{-3}	W.m^{-1}.K^{-1}	µPa.s	bar	-	kg.s^{-1}
-4,0	181,5	1457,8	1,553	3494,4	342,6	0,5715	177,7	3,70	0,0327	156,7
-5,0	176,9	1456,7	1,550	3366,2	346,4	0,5746	179,7	3,56	0,0314	156,3
-6,0	172,3	1455,5	1,546	3240,8	349,5	0,5777	181,7	3,43	0,0302	155,9
-7,0	167,7	1454,3	1,543	3118,0	352,1	0,5808	183,8	3,29	0,0291	155,4
-8,0	163,2	1453,1	1,540	2997,8	354,1	0,5839	185,9	3,17	0,0279	155,1
-9,0	158,6	1451,9	1,537	2880,0	355,6	0,5870	188,0	3,04	0,0268	154,6
-10,0	154,0	1450,7	1,534	2764,6	356,5	0,5901	190,2	2,92	0,0258	154,2
-11,0	149,4	1449,5	1,530	2651,6	357,0	0,5933	192,4	2,80	0,0247	153,8
-12,0	144,9	1448,2	1,527	2540,9	357,0	0,5964	194,7	2,69	0,0237	153,5
-13,0	140,3	1446,9	1,524	2432,3	356,5	0,5996	197,0	2,57	0,0227	153,1
-14,0	135,8	1445,7	1,521	2325,9	355,6	0,6028	199,3	2,47	0,0218	152,7
-15,0	131,2	1444,4	1,518	2221,5	354,3	0,6059	201,7	2,36	0,0208	152,3
-16,0	126,7	1443,1	1,515	2119,1	352,6	0,6091	204,2	2,26	0,0199	151,9
-17,0	122,1	1441,7	1,512	2018,7	350,5	0,6123	206,7	2,16	0,0191	151,6
-18,0	117,6	1440,4	1,509	1920,0	348,1	0,6155	209,2	2,07	0,0182	151,2
-19,0	113,1	1439,0	1,506	1823,2	345,3	0,6187	211,8	1,98	0,0174	150,8
-20,0	108,6	1437,7	1,503	1728,0	342,3	0,6220	214,4	1,89	0,0167	150,5
-21,0	104,0	1436,3	1,501	1634,5	338,9	0,6252	217,1	1,80	0,0159	150,1
-22,0	99,5	1434,9	1,498	1542,5	335,3	0,6284	219,8	1,72	0,0152	149,8
-23,0	95,0	1433,5	1,495	1452,0	331,4	0,6317	222,7	1,64	0,0145	149,4
-24,0	90,5	1432,1	1,492	1362,9	327,3	0,6349	225,5	1,57	0,0139	149,1
-25,0	86,0	1430,7	1,489	1275,2	322,9	0,6382	228,4	1,50	0,0132	148,7

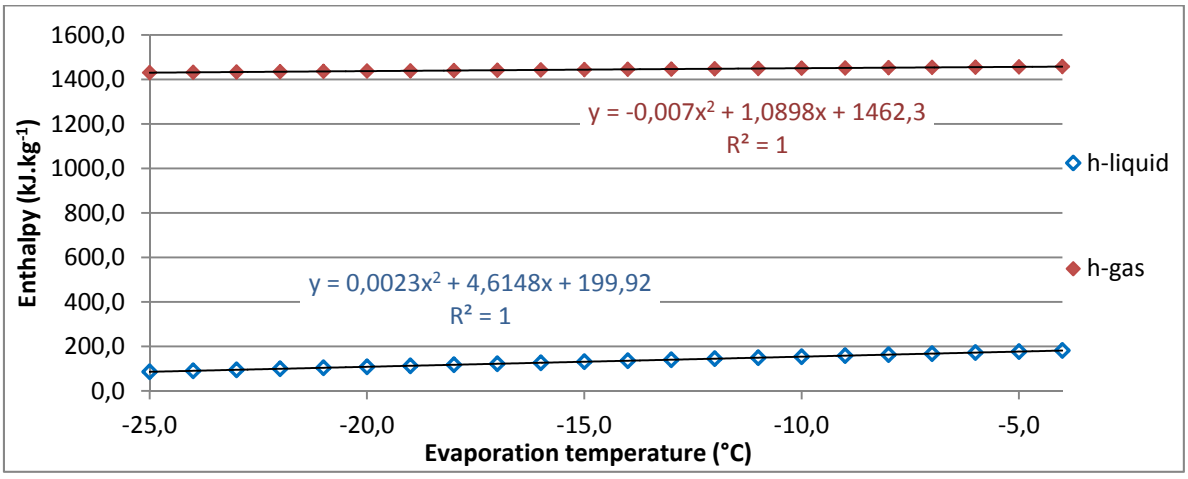

T_{cond}	T_{evap}	HP	LP	q_v	$e_{v,is}$	COP_{is}
°C	°C	bar	bar	kJ.m^{-3}	kJ.m^{-3}	-
10	-30	6,15	1,194	1220,7	238,1	5,13
	-20	6,15	1,901	1909,7	256,3	7,45
	-10	6,15	2,907	2878,6	237,6	12,12
	0	6,15	4,294	4202,2	160,7	26,15
20	-30	8,57	1,194	1171,8	298,0	3,93
	-20	8,57	1,901	1834,0	342,0	5,36
	-10	8,57	2,907	2765,8	356,5	7,76
	0	8,57	4,294	4038,9	321,3	12,57
30	-30	11,67	1,194	1122,0	357,5	3,14
	-20	11,67	1,901	1757,0	427,3	4,11
	-10	11,67	2,907	2651,1	474,8	5,58
	0	11,67	4,294	3873,1	481,2	8,05
40	-30	15,55	1,194	1071,3	416,6	2,57
	-20	15,55	1,901	1678,7	511,9	3,28
	-10	15,55	2,907	2534,2	592,3	4,28
	0	15,55	4,294	3704,2	640,1	5,79
50	-30	20,34	1,194	1019,4	475,0	2,15
	-20	20,34	1,901	1598,5	595,7	2,68
	-10	20,34	2,907	2414,7	708,7	3,41
	0	20,34	4,294	3531,4	797,5	4,43

		Enthalpy (kJ.kg^{-1})									
P_{evap}	T_{evap}	Superheat									
bar	(°C)	1 K	2 K	3 K	4 K	5 K	6 K	7 K	8 K	9 K	10 K
3,70	-4,0	1460,3	1462,9	1465,5	1468,1	1470,7	1473,2	1475,8	1478,3	1480,8	1483,3
3,56	-5,0	1459,2	1461,7	1464,3	1466,9	1469,4	1472,0	1474,5	1477,0	1479,6	1482,1
3,43	-6,0	1457,9	1460,5	1463,1	1465,6	1468,2	1470,7	1473,2	1475,7	1478,2	1480,7
3,29	-7,0	1456,8	1459,4	1461,9	1464,5	1467,0	1469,5	1472,0	1474,5	1477,0	1479,5
3,17	-8,0	1455,5	1458,1	1460,6	1463,1	1465,7	1468,2	1470,7	1473,1	1475,6	1478,1
3,04	-9,0	1454,3	1456,9	1459,4	1461,9	1464,4	1466,9	1469,4	1471,9	1474,4	1476,8
2,92	-10,0	1453,1	1455,6	1458,2	1460,7	1463,2	1465,6	1468,1	1470,6	1473,0	1475,5
2,69	-12,0	1450,6	1453,1	1455,6	1458,1	1460,6	1463,0	1465,5	1467,9	1470,3	1472,8
2,47	-14,0	1448,1	1450,6	1453,0	1455,5	1457,9	1460,4	1462,8	1465,2	1467,7	1470,1
2,26	-16,0	1445,6	1448,0	1450,5	1452,9	1455,3	1457,7	1460,2	1462,6	1464,9	1467,3
2,07	-18,0	1442,9	1445,3	1447,8	1450,2	1452,8	1455,0	1457,4	1459,8	1462,1	1464,5
1,89	-20,0	1440,2	1442,8	1445,0	1447,4	1449,8	1452,2	1454,6	1456,9	1459,3	1461,6
1,72	-22,0	1437,5	1439,9	1442,3	1444,7	1447,0	1449,4	1451,7	1454,1	1456,4	1458,7
1,57	-24,0	1434,7	1437,0	1439,4	1441,8	1444,1	1446,4	1448,8	1451,1	1453,4	1455,7

Appendix 3: Specification example of Alfa Laval PHE

Alfa Laval Plate Heat Exchanger Technical Specification

1*M10-BW Cocurrent SA Titanium 120/124pl 28.8/29.8 m²

p_{des}=16.0 barg **T_{des}**=0.0/-5.0 °C **k**=3195/2660 W/(m²*K)
Osurf=9 % **Foul.**=0.35(0.63)*10^{-4} m²*K/W **Load**=301.0 kW **MTD**=3.9 K

Hot Side 22.0% CaCl2		**Cold Side**	**Ammonia**		
Liquid Cooling			Vapourizing		
1*61 MG Dp=85.6< kPa			1*62 MW Dp=2.68< kPa		
Dp(ch) 79.376 Dp(p) 2.704/3.562			Dp(ch) 2.514 Dp(p) -0.001/0.125		
Dp(c) 1/2 0.000/0.000			Dp(c) 1/2 0.000/0.000		
v(c/neck/ch)=4.95/2.42/0.796			v(c/neck/ch)=0.0748/0.0371/0.0122		
v(ch/neck/c)=0.795/2.41/2.47			v(ch/neck/c)=2.43/7.37/7.43		
T (v/l)	**P**	**Q**	**T (v/l)**	**P**	**Q**
-8.9		Subcooled	-14.0	2.47	Subcooled
-11.0		Subcooled	-14.0	2.44	0.600
Twall min/max	-12.3/-9.8		Twall min/max	-12.9/-10.2	
22.0% CaCl2	**= 47.15 kg/s**		**Ammonia**	**= 0.3845 kg/s**	
In v/l	0.000/47.15		In v/l	0.000/0.3845	
Out v/l	0.000/47.15		Out v/l	0.2307/0.1538	

	Hot side Liquid In/Out	**Cold side Liquid In/Out**	**Vapour In/Out**
Dens	1212/1213	654.1/654.1	2.002/1.980
Sp.Heat	2.977/2.971	4.534/4.534	2.487/2.487
Visc	5.02/5.49	0.198/0.198	0.0087/0.0087
Th.Cond	0.527/0.524	0.548/0.548	0.0206/0.0206
Bub. p.			-14.0
Dew p.			-14.0
Mol.W.			17.03/17.03
Cr.pr.			112.60/112.60
Cr.temp.			132.3/132.3
Lat.heat			1304.8/1304.8

Note : Small channel pressure drop for Ammonia (<3.60)
Note : Outer welded channels are blinded!

Appendix 4: Example of VBA program and interface

```
Sub UpDatingAllFile(FilePath1 As String, FilePath2NewC As String)
    Dim i, j, k, h(2), g, f As Integer
    Dim interM(23, 7) As Double
    Dim FirstColumn(23) As Double
    Dim CCString(5) As String
    Dim FilePathOk() As String
    Dim wb_B As Workbook
    i = Sheets("COP data").Index
    f = Sheets("COP data - NewC").Index
    While i < f
        FilePathOk = TroncString(FilePath1)
        Sheets(i).Activate
        h(0) = 0
        h(1) = 40
        If i = Sheets("COP data").Index Then
            h(0) = 80
        ElseIf i = Sheets("COP data").Index + 1 Then
            h(0) = 78
            h(1) = 2
        ElseIf i = Sheets("COP data").Index + 2 Then
            h(0) = 113
        ElseIf i = Sheets("COP data").Index + 3 Then
            h(0) = 52
        End If
        For k = 3 To 7
            CCString(k - 3) = Cells(4, k).Value
            Set wb_B = Workbooks.Open(FilePathOk(0) & "CC " & CCString(k - 3) & " -" & FilePathOk(1),
, False)
            wb_B.Windows(1).Visible = False
            For j = 0 To 22
                FirstColumn(j) = wb_B.Sheets("Graphs data").Cells(j + 25, 1)
                For g = 0 To 6
                    interM(j, g) = wb_B.Sheets("Graphs data").Cells(j + h(0), h(1) + g)
                    Next g
                Next j
            wb_B.Windows(1).Visible = True
            wb_B.Save
            wb_B.Close
            ThisWorkbook.Activate
            For j = 0 To 22
                For g = 0 To 6
                    ThisWorkbook.Sheets(i).Cells(j + 5, 2) = FirstColumn(j)
                    ThisWorkbook.Sheets(i).Cells(j + 5, k + g * 5).Value = interM(j, g)
                    Next g
                Next j
            Next k
        i = i + 1
    Wend
```

```
    While f <= Sheets.Count
        FilePathOk = TroncString(FilePath2NewC)
        Sheets(f).Activate
        h(0) = 0
        h(1) = 40
        If f = Sheets("COP data - NewC").Index Then
            h(0) = 80
        ElseIf f = Sheets("COP data - NewC").Index + 1 Then
            h(0) = 78
            h(1) = 2
        ElseIf f = Sheets("COP data - NewC").Index + 2 Then
            h(0) = 113
        ElseIf f = Sheets("COP data - NewC").Index + 3 Then
            h(0) = 52
        End If
        For k = 3 To 7
            CCString(k - 3) = Cells(4, k).Value
            Set wb_B = Workbooks.Open(FilePathOk(0) & "CC " & CCString(k - 3) & " -" & FilePathOk(1),
, False)
            wb_B.Windows(1).Visible = True
            For j = 0 To 22
                FirstColumn(j) = wb_B.Sheets("Graphs data").Cells(j + 25, 1)
                For g = 0 To 6
                    interM(j, g) = wb_B.Sheets("Graphs data").Cells(j + h(0), h(1) + g)
                    Next g
                Next j
            wb_B.Save
            wb_B.Close
            ThisWorkbook.Activate
            For j = 0 To 22
                For g = 0 To 6
                    ThisWorkbook.Sheets(f).Cells(j + 5, 2) = FirstColumn(j)
                    ThisWorkbook.Sheets(f).Cells(j + 5, k + g * 5).Value = interM(j, g)
                    Next g
                Next j
            Next k
        f = f + 1
    Wend
End Sub
```

```
Sub UpdateDTAndSecRefr()
    Dim C As Double
    Dim err(2) As Double
    Range("B38").Select
    C = ActiveCell.Value
    Dim i, j, k, l As Integer
    Dim pos As Integer
    err(1) = 1#
    For i = 5 To 27
        Range("B" & i).Select
        err(2) = Abs(C - ActiveCell.Value)
        If err(2) < err(1) Then
            pos = i
            err(1) = err(2)
        End If
        Next i
    Range("F32").Activate
    l = (ActiveCell.Value - 1) * 5 + 3
    i = Sheets("COP data").Index
    While i <= Sheets.Count
        Sheets(i).Activate
        j = l
        For k = 3 To 7
            Cells(38, k) = Cells(pos, j)
            j = j + 1
            Next k
        i = i + 1
    Wend
    Sheets("COP data").Select
End Sub

Sub ChooseDT()
    Sheets("COP data").Select
End Sub
```

```
Function TroncString(FilePath1 As String)
   Dim Tableau() As String
   Dim Tableau2() As String
   Dim i As Integer
   Tableau = Split(FilePath1, "CC")
   Tableau2 = Split(Tableau(1), "-")
   Tableau(1) = ""
   For i = 1 To UBound(Tableau2) - 1
      Tableau(1) = Tableau(1) & Tableau2(i) & "-"
      Next i
      Tableau(1) = Tableau(1) & Tableau2(UBound(Tableau2))
   TroncString = Tableau
End Function
```

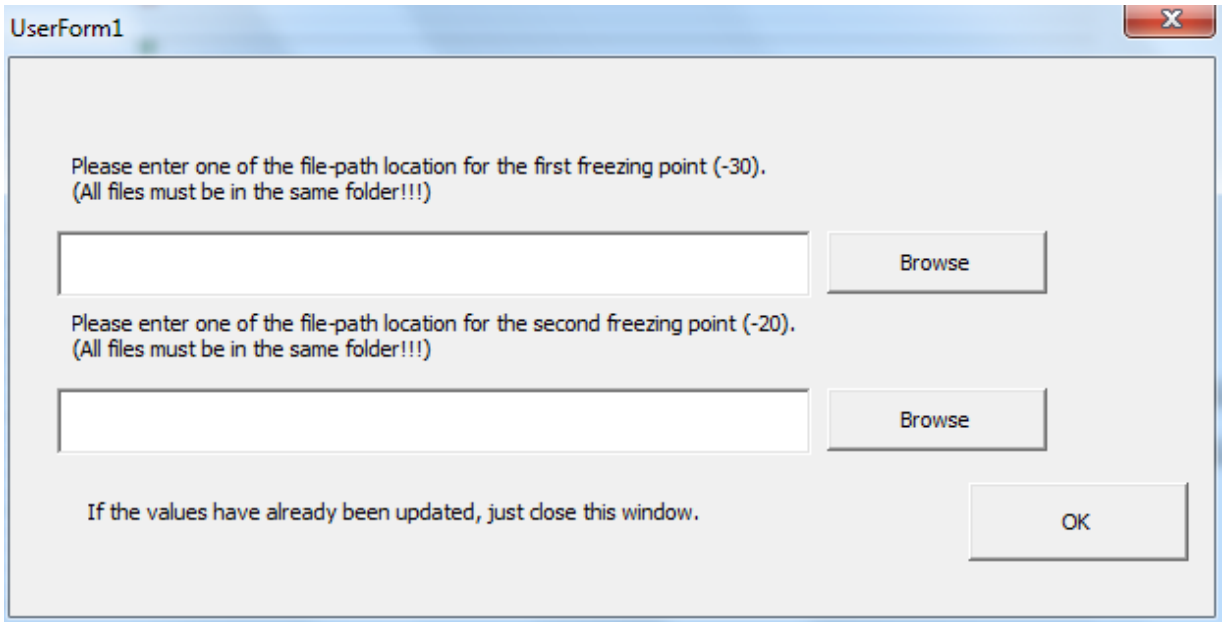

Choose ΔT, T_{ice} or $T_{sec.refr.}$ to display	-3,5	Choose ΔT, T_{ice} or $T_{sec.refr.}$ to display	-2,0
Choose sec.refr. to display	EG	Choose sec.refr. to display	CaCl2

	COP					
		EG - Fp -30°C				
	CC	100	150	200	300	400
ΔT	-3,5	4,69	4,14	3,69	2,95	2,39

	COP					
		CaCl2 - Fp -30°C				
	CC	100	150	200	300	400
ΔT	-2,0	5,24	4,69	4,27	3,46	2,81

```
Sub SolvingViscosity()
   Dim A As Double
   Dim i As Integer
   Dim C As Double
   Dim fErr As Boolean
   A = 1#
   i = 4
   fErr = True
         While i < 27
            While fErr
               Range("AZ" & i).Select
               ActiveCell.FormulaR1C1 = A
               SolverOk SetCell:="$AY$" & i, MaxMinVal:=3, ValueOf:=0, ByChange:="$AZ$" & i,
Engine :=1, EngineDesc:="GRG Nonlinear"
               SolverSolve UserFinish:=True
               Range("AY" & i).Select
               If IsError(ActiveCell.Value) Then
                  fErr = True
                  C = 0#
                  A = A - 0.1
               Else
                  C = ActiveCell.Value
                  If C > 0.001 Then
                     fErr = True
                     A = A - 0.1
                  Else
                     fErr = False
                  End If
               End If
            Wend
            i = i + 1
            fErr = True
         Wend
End Sub
```

The calculations are shown for:

- calcium chloride having a freezing point of -30 °C
- a cooling capacity of 200 kW
- a pump control of 2 K
- a range of ice temperature from -1 to -12 °C

Ice temp.	G	Re_{dh}	j_{Nu}	Nu_{dh}	f_0	$f_{1,0}$	f	$\Delta\mu/\mu_{wall}$	$(\mu/\mu_{wall})_0$	Nu
°C	$kg.m^{-2}.s^{-1}$	-	-	Wanniarachchi	-	-	-	-	Variable1	Martin
-1	482,5	412	15	46,03	0,16	5,30	2,53	3E-08	0,95	37,85
-1,5	482,8	405	15	45,77	0,16	5,33	2,54	6E-08	0,95	37,67
-2	483,0	398	15	45,48	0,16	5,35	2,56	8E-08	0,95	-
-2,5	483,3	391	15	45,23	0,16	5,38	2,57	4E-08	0,95	-
-3	483,6	384	15	44,97	0,17	5,40	2,59	4E-08	0,95	-
-3,5	483,8	377	15	44,71	0,17	5,43	2,60	8E-10	0,95	-
-4	484,1	371	14	44,46	0,17	5,46	2,62	2E-07	0,94	-
-4,5	484,4	364	14	44,20	0,18	5,49	2,64	2E-07	0,94	-
-5	484,6	358	14	43,94	0,18	5,52	2,65	4E-08	0,94	-
-5,5	484,9	351	14	43,68	0,18	5,55	2,67	8E-07	0,94	-
-6	485,2	345	14	43,43	0,19	5,58	2,69	4E-09	0,94	-
-6,5	485,4	339	14	43,17	0,19	5,61	2,71	6E-07	0,94	-
-7	486,4	319	13	42,32	0,20	5,72	2,77	7E-07	0,94	-
-7,5	486,6	313	13	42,07	0,20	5,76	2,79	2E-08	0,94	-
-8	486,9	307	13	41,82	0,21	5,79	2,81	9E-08	0,94	-
-8,5	487,2	302	13	41,57	0,21	5,83	2,83	8E-08	0,94	-
-9	487,5	296	12	41,32	0,22	5,87	2,85	2E-07	0,94	-
-9,5	487,8	291	12	41,07	0,22	5,90	2,87	4E-07	0,94	-
-10	488,1	285	12	40,82	0,22	5,94	2,89	4E-07	0,94	-
-10,5	488,4	280	12	40,57	0,23	5,98	2,91	3E-07	0,94	-
-11	488,6	275	12	40,32	0,23	6,02	2,94	3E-07	0,94	-
-11,5	488,9	270	12	40,08	0,24	6,06	2,96	2E-07	0,94	-
-12	489,2	265	11	39,83	0,24	6,11	2,98	2E-10	0,94	-

Solve viscosity ratio

Ice temp.	h	T_{wall}	μ_{wall}	μ/μ_{wall}	hA	Δp_f (Martin)	Total pumping power in PHE
°C	$W.m^{-2}.K^{-1}$	°C	mPa.s	Variable2	$W.K^{-1}$	Pa	W
-1	3942,95	-8,12	5,30	0,95	1191,09	29810,79	1693
-1,5	3919,36	-8,63	5,40	0,95	1183,96	30003,78	1705
-2	3575,87	-9,26	5,53	0,95	1080,20	30201,56	1717
-2,5	3562,09	-9,77	5,63	0,95	1076,04	30404,19	1729
-3	3548,29	-10,28	5,74	0,95	1071,87	30611,77	1741
-3,5	3534,47	-10,79	5,84	0,95	1067,69	30824,40	1754
-4	3520,64	-11,30	5,95	0,94	1063,51	31042,14	1767
-4,5	3506,79	-11,81	6,07	0,94	1059,33	31265,11	1781
-5	3492,93	-12,32	6,19	0,94	1055,14	31493,38	1794
-5,5	3479,07	-12,83	6,30	0,94	1050,96	31727,05	1809
-6	3465,20	-13,35	6,43	0,94	1046,77	31966,22	1823
-6,5	3451,33	-13,86	6,55	0,94	1042,58	32210,98	1838
-7	3405,73	-15,54	6,99	0,94	1028,80	33057,37	1889
-7,5	3392,01	-16,05	7,12	0,94	1024,66	33324,89	1905
-8	3378,32	-16,56	7,26	0,94	1020,52	33598,27	1921
-8,5	3364,66	-17,07	7,41	0,94	1016,40	33877,59	1938
-9	3351,02	-17,57	7,55	0,94	1012,28	34162,93	1955
-9,5	3337,42	-18,08	7,70	0,94	1008,17	34454,38	1973
-10	3323,84	-18,59	7,85	0,94	1004,07	34752,02	1991
-10,5	3310,31	-19,10	8,01	0,94	999,98	35055,94	2009
-11	3296,81	-19,61	8,17	0,94	995,90	35366,21	2028
-11,5	3283,35	-20,12	8,33	0,94	991,83	35682,93	2047
-12	3269,93	-20,62	8,50	0,94	987,78	36006,16	2067

```
Sub SolvingTevap()
   Dim A As Double
   Dim i, j As Integer
   Dim C As Double
   Dim fErr As Boolean
   A = -13#
   i = 4
   fErr = True
         While i < 27
            j = 0
            While fErr
               Range("BK" & i).Select
               ActiveCell.FormulaR1C1 = A
               SolverOk SetCell:="$BL$" & i, MaxMinVal:=3, ValueOf:=0, ByChange:="$BK$" & i,
Engine :=1, EngineDesc:="GRG Nonlinear"
               SolverSolve UserFinish:=True
               Range("BL" & i).Select
               If IsError(ActiveCell.Value) Then
                  fErr = True
                  C = 0#
                  If i > 4 Then
                     Range("BK" & i - 1).Select
                     A = ActiveCell.Value + j
                  Else
                     A = A - 3
                  End If
               Else
                  C = ActiveCell.Value
                  If C > 0.001 Then
                     fErr = True
                     A = A - 1
                  Else
                     fErr = False
                  End If
               End If
               j = j + 3
            Wend
            i = i + 1
            fErr = True
         Wend
End Sub
```

The calculations are shown for:

- calcium chloride having a freezing point of -30 °C
- a cooling capacity of 200 kW
- a pump control of 2 K
- a range of ice temperature from -1 to -12 °C

Ice temp.	$(T_{evap})_0$	Q_0-Q_{tot}	μ_l	k_l	ϱ_l	P_{abs}	x_{in}	h_{lg} (latent heat)	h_{out}-h_{in}
°C	°C	kW	µPa.s	$W.m^{-1}.K^{-1}$	$kg.m^{-3}$	bar	-	$kJ.kg^{-1}$	$kJ.kg^{-1}$
-1	-10,01	3,35E-04	190,2	0,5898	652,03	2,92	0,09	1296,46	1184,80
-1,5	-10,53	1,80E-06	191,3	0,5914	652,71	2,86	0,09	1298,15	1184,16
-2	-11,17	3,44E-05	192,8	0,5934	653,55	2,78	0,09	1300,24	1183,37
-2,5	-11,69	2,78E-05	193,9	0,5950	654,22	2,72	0,09	1301,91	1182,72
-3	-12,20	1,25E-04	195,1	0,5967	654,89	2,66	0,10	1303,58	1182,08
-3,5	-12,72	1,24E-04	196,3	0,5983	655,56	2,60	0,10	1305,25	1181,43
-4	-13,24	3,10E-04	197,5	0,5999	656,22	2,55	0,10	1306,91	1180,77
-4,5	-13,75	4,47E-05	198,7	0,6015	656,88	2,49	0,10	1308,57	1180,11
-5	-14,27	3,07E-05	200,0	0,6031	657,54	2,44	0,10	1310,22	1179,45
-5,5	-14,79	2,38E-05	201,2	0,6048	658,19	2,38	0,10	1311,87	1178,78
-6	-15,30	7,21E-05	202,5	0,6064	658,84	2,33	0,10	1313,51	1178,12
-6,5	-15,82	2,43E-05	203,8	0,6080	659,49	2,28	0,11	1315,16	1177,44
-7	-17,53	6,38E-05	208,0	0,6134	661,60	2,11	0,11	1320,53	1175,20
-7,5	-18,05	8,69E-06	209,4	0,6151	662,23	2,06	0,11	1322,14	1174,52
-8	-18,56	1,18E-05	210,7	0,6167	662,86	2,02	0,12	1323,75	1173,83
-8,5	-19,08	5,61E-05	212,0	0,6184	663,48	1,97	0,12	1325,35	1173,15
-9	-19,59	1,02E-05	213,4	0,6200	664,10	1,92	0,12	1326,95	1172,45
-9,5	-20,11	9,18E-05	214,8	0,6216	664,71	1,88	0,12	1328,55	1171,76
-10	-20,63	9,38E-04	216,1	0,6233	665,33	1,83	0,12	1330,13	1171,06
-10,5	-21,14	7,04E-04	217,5	0,6250	665,94	1,79	0,12	1331,72	1170,36
-11	-21,66	7,86E-04	218,9	0,6266	666,54	1,75	0,12	1333,30	1169,65
-11,5	-22,17	8,22E-05	220,3	0,6283	667,15	1,71	0,13	1334,87	1168,94
-12	-22,69	1,11E-04	221,8	0,6299	667,74	1,67	0,13	1336,44	1168,23

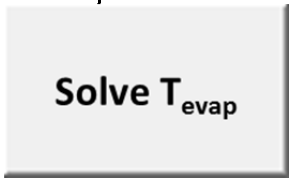

Ice temp. °C	Total mass flow kg.s^{-1}	G kg.m^{-2}.s^{-1}	Re_{lo} -	h_{boil} (Ayub) W.m^{-2}.K^{-1}	$R_{1\text{-plate}}$ K.W^{-1}	LMTD K	$h_{superheat}$ kJ.kg^{-1}	Q_{tot} kW
-1	0,17	2,3	62	3281,01	0,001924	3,18	1453,05	200,00
-1,5	0,17	2,3	61	3268,52	0,001933	3,20	1452,41	200,00
-2	0,17	2,3	61	3252,91	0,002019	3,34	1451,61	200,00
-2,5	0,17	2,3	61	3240,27	0,002027	3,35	1450,97	200,00
-3	0,17	2,3	60	3227,53	0,002034	3,36	1450,32	200,00
-3,5	0,17	2,3	60	3214,71	0,002042	3,38	1449,67	200,00
-4	0,17	2,3	60	3201,81	0,002050	3,39	1449,02	200,00
-4,5	0,17	2,3	59	3188,82	0,002058	3,40	1448,36	200,00
-5	0,17	2,3	59	3175,77	0,002066	3,41	1447,70	200,00
-5,5	0,17	2,3	59	3162,64	0,002074	3,43	1447,03	200,00
-6	0,17	2,3	58	3149,44	0,002082	3,44	1446,36	200,00
-6,5	0,17	2,3	58	3136,18	0,002090	3,46	1445,69	200,00
-7	0,17	2,3	57	3092,11	0,002118	3,50	1443,45	200,00
-7,5	0,17	2,3	57	3078,73	0,002127	3,52	1442,77	200,00
-8	0,17	2,3	56	3065,32	0,002135	3,53	1442,08	200,00
-8,5	0,17	2,3	56	3051,87	0,002144	3,54	1441,39	200,00
-9	0,17	2,3	56	3038,40	0,002153	3,56	1440,70	200,00
-9,5	0,17	2,3	55	3024,91	0,002162	3,57	1440,00	200,00
-10	0,17	2,3	55	3011,40	0,002171	3,59	1439,30	200,00
-10,5	0,17	2,3	55	2997,88	0,002180	3,60	1438,60	200,00
-11	0,17	2,3	54	2984,35	0,002189	3,62	1437,89	200,00
-11,5	0,17	2,3	54	2970,83	0,002198	3,63	1437,19	200,00
-12	0,17	2,3	54	2957,31	0,002207	3,65	1436,47	200,00

```
Sub SolvingTice()
  Dim A As Double
   Dim i, j As Integer
   Dim C As Double
   Dim fErr As Boolean
   A = -13#
   i = 4
   fErr = True
        While i < 27
          j = 0
          While fErr
            Range("CJ" & i).Select
            ActiveCell.FormulaR1C1 = A
            SolverOk SetCell:="$CK$" & i, MaxMinVal:=3, ValueOf:=0, ByChange:="$CJ$" & i,
Engine :=1, EngineDesc:="GRG Nonlinear"
            SolverSolve UserFinish:=True
            Range("CK" & i).Select
            If IsError(ActiveCell.Value) Then
              fErr = True
              C = 0#
              If i > 4 Then
                Range("CJ" & i - 1).Select
                A = ActiveCell.Value + j
              Else
                A = A - 3
              End If
            Else
              C = ActiveCell.Value
              If C > 0.001 Then
                fErr = True
                A = A - 1
              Else
                fErr = False
              End If
            End If
            j = j + 3
          Wend
          i = i + 1
          fErr = True
        Wend
End Sub
```

The calculations are shown for:

- calcium chloride having a freezing point of -30 °C
- a cooling capacity of 200 kW
- a pump control of 2 K
- a range of ice temperature from -1 to -12 °C

Ice temp. °C	$T_{sec.fl., average}$ °C	HL_0-HL_{tot}	LMTD K	R' m.K.W^{-1}	UA_{tot} W.K^{-1}	HL_{tot} kW	$R_{sec.fl.}/R_{tot}$ %	R_{cond}/R_{tot} %
-1	-6,7	0,0	5,78	0,58	31135	180,00	3,07%	96,93%
-1,5	-7,2	0,0	5,78	0,58	31118	180,00	3,12%	96,88%
-2	-7,7	0,0	5,79	0,58	31099	180,00	3,18%	96,82%
-2,5	-8,2	0,0	5,79	0,58	31081	180,00	3,24%	96,76%
-3	-8,7	0,0	5,80	0,58	31061	180,00	3,30%	96,70%
-3,5	-9,2	0,0	5,80	0,58	31041	180,00	3,36%	96,64%
-4	-9,7	0,0	5,80	0,58	31020	180,00	3,42%	96,58%
-4,5	-10,3	0,0	5,81	0,58	30998	180,00	3,49%	96,51%
-5	-10,8	0,0	5,81	0,58	30975	180,00	3,56%	96,44%
-5,5	-11,3	0,0	5,82	0,58	30951	180,00	3,64%	96,36%
-6	-11,8	0,0	5,82	0,58	30926	180,00	3,72%	96,28%
-6,5	-12,3	0,0	5,83	0,58	30900	180,00	3,80%	96,20%
-7	-13,9	0,0	7,00	0,70	25727	180,00	19,90%	80,10%
-7,5	-14,4	0,0	7,00	0,70	25721	180,00	19,92%	80,08%
-8	-14,9	0,0	7,00	0,70	25715	180,00	19,94%	80,06%
-8,5	-15,4	0,0	7,00	0,70	25709	180,00	19,96%	80,04%
-9	-15,9	0,0	7,00	0,70	25703	180,00	19,98%	80,02%
-9,5	-16,4	0,0	7,00	0,70	25697	180,00	20,00%	80,00%
-10	-16,9	0,0	7,01	0,70	25691	180,00	20,01%	79,99%
-10,5	-17,4	0,0	7,01	0,70	25685	180,00	20,03%	79,97%
-11	-17,9	0,0	7,01	0,70	25679	180,00	20,05%	79,95%
-11,5	-18,4	0,0	7,01	0,70	25673	180,00	20,07%	79,93%
-12	-19,0	0,0	7,01	0,70	25667	180,00	20,09%	79,91%

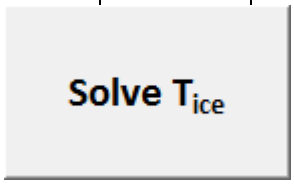

```
Sub SolvingHeader()
    Dim i As Integer
    Dim j As Integer
    Dim rho As Double
    Dim visc As Double
    Dim Q As Double
    Dim Qtot As Double
    Dim K As Double
    Dim f As Double
    Dim Re As Double
    Dim Re_tot As Double
    Dim Sum As Double
    Dim diam As Double
    Dim Pi As Double
    Dim ePump As Double
    Dim N_u As Integer
'
    Range("CW34").Select
    ePump = ActiveCell.Value
    Range("CW1").Select
    diam = ActiveCell.Value
    Range("CW37").Select
    N_u = ActiveCell.Value
    i = 4
    Pi = WorksheetFunction.Pi
        While i < 27
            Range("D" & i).Select
            rho = ActiveCell.Value
            Range("F" & i).Select
            Qtot = ActiveCell.Value / 3600
            Range("C" & i).Select
            visc = ActiveCell.Value * 0.001
            Re_tot = 4 * Qtot * rho / (visc * Pi * diam)
            Sum = 0
            For j = 1 To N_u
                Q = Qtot / N_u * j
                Re = Re_tot / N_u * j
                f = (0.79 * Log(Re) - 1.62) ^ (-2)
                Sum = Sum + f * j ^ 3
            Next j
            Sum = ((0.2 / diam * Sum + 0.37 * N_u * (N_u + 1) / 2) * rho * 8 / (Pi ^ 2 * diam ^ 4) *
(Qtot / N_u) ^ 3) / ePump
            Range("CW" & i).Select
            ActiveCell.FormulaR1C1 = ""
            ActiveCell.Value = Sum
            i = i + 1
        Wend
    Range("CX31").Select
    ActiveCell.FormulaR1C1 = "=R[-1]C"
End Sub
```

	0,2	Header diameter
Ice temp. °C	Pumping power in the supply header W	Pumping power in both headers W
-1	24,98	49,95
-1,5	25,11	50,22
-2	25,25	50,50
-2,5	25,39	50,77
-3	25,53	51,06
-3,5	25,67	51,34
-4	25,82	51,63
-4,5	25,96	51,93
-5	26,11	52,23
-5,5	26,26	52,53
-6	26,42	52,83
-6,5	26,57	53,14
-7	27,10	54,20
-7,5	27,26	54,52
-8	27,43	54,85
-8,5	27,59	55,19
-9	27,76	55,52
-9,5	27,93	55,86
-10	28,10	56,21
-10,5	28,28	56,56
-11	28,45	56,91
-11,5	28,63	57,27
-12	28,81	57,63

```
Sub SolvingAllRefr()
    Load UserForm1
    UserForm1.Show vbModeless
    UserForm1.Repaint
    Application.Cursor = xlWait
    Dim AllSheet(7) As String
    AllSheet(1) = "CaCl2"
    AllSheet(2) = "PG"
    AllSheet(3) = "EG"
    AllSheet(4) = "EA"
    AllSheet(5) = "NH3"
    AllSheet(6) = "K-acetate"
    AllSheet(7) = "K-formate"
    Dim i As Integer
    For i = 1 To UBound(AllSheet)
        Sheets(AllSheet(i) & " - calcul").Select
        Call SolvingTice
        Call SolvingViscosity
        Call SolvingTevap
        Call SolvingHeader
        Next i
    Unload UserForm1
    Application.Cursor = xlDefault
    Sheets("h - Upipe").Select
    MsgBox ("The calculation is over." & vbCr & vbCr & "Nacka & Järfälla were not included")
End Sub
```

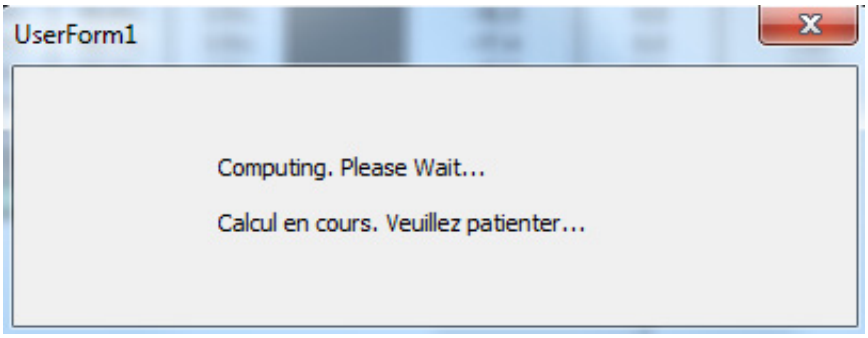

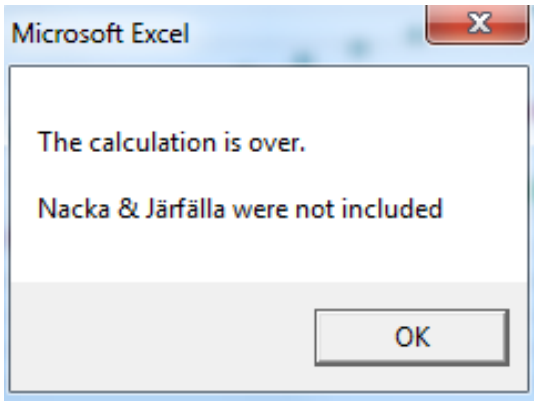

Results / Charts (CC = 200 kW; F_p = -30 °C; ΔT = 2 K)

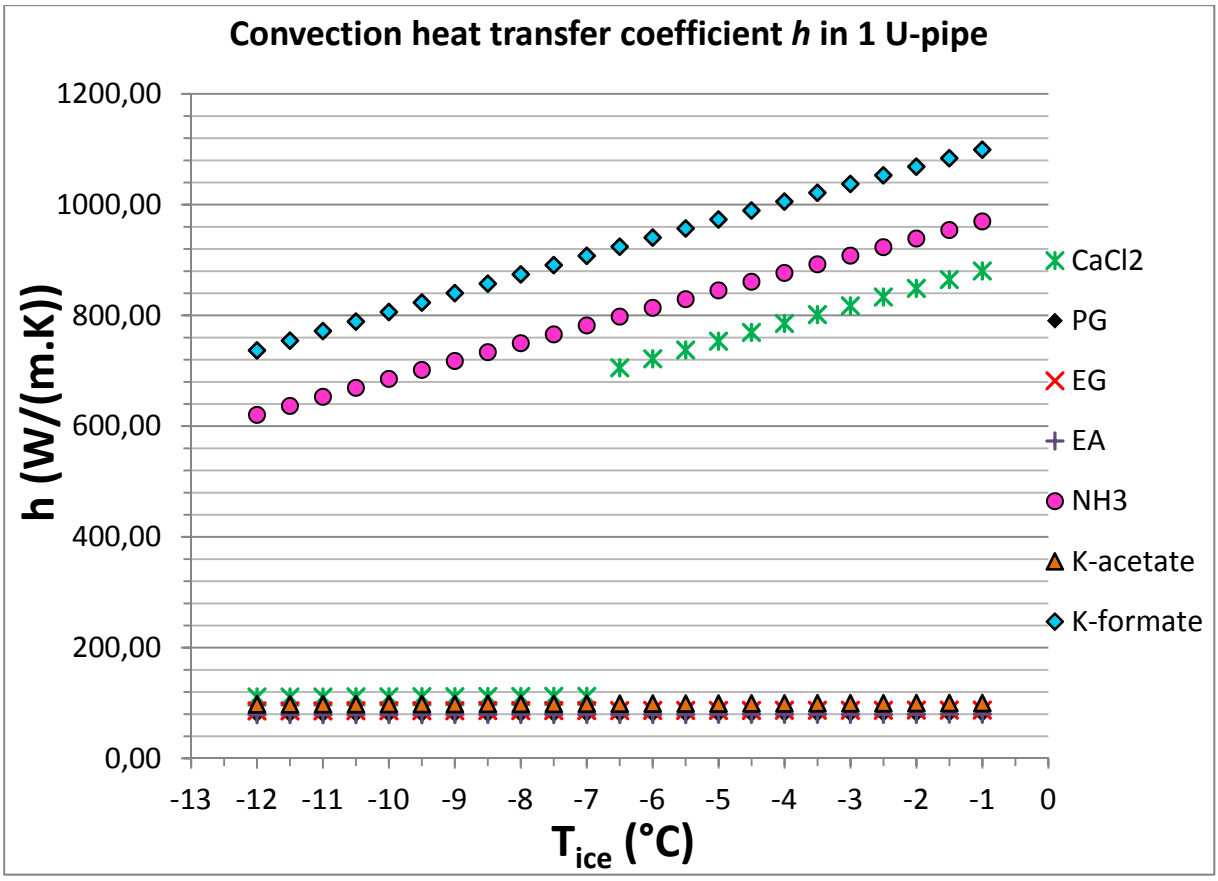

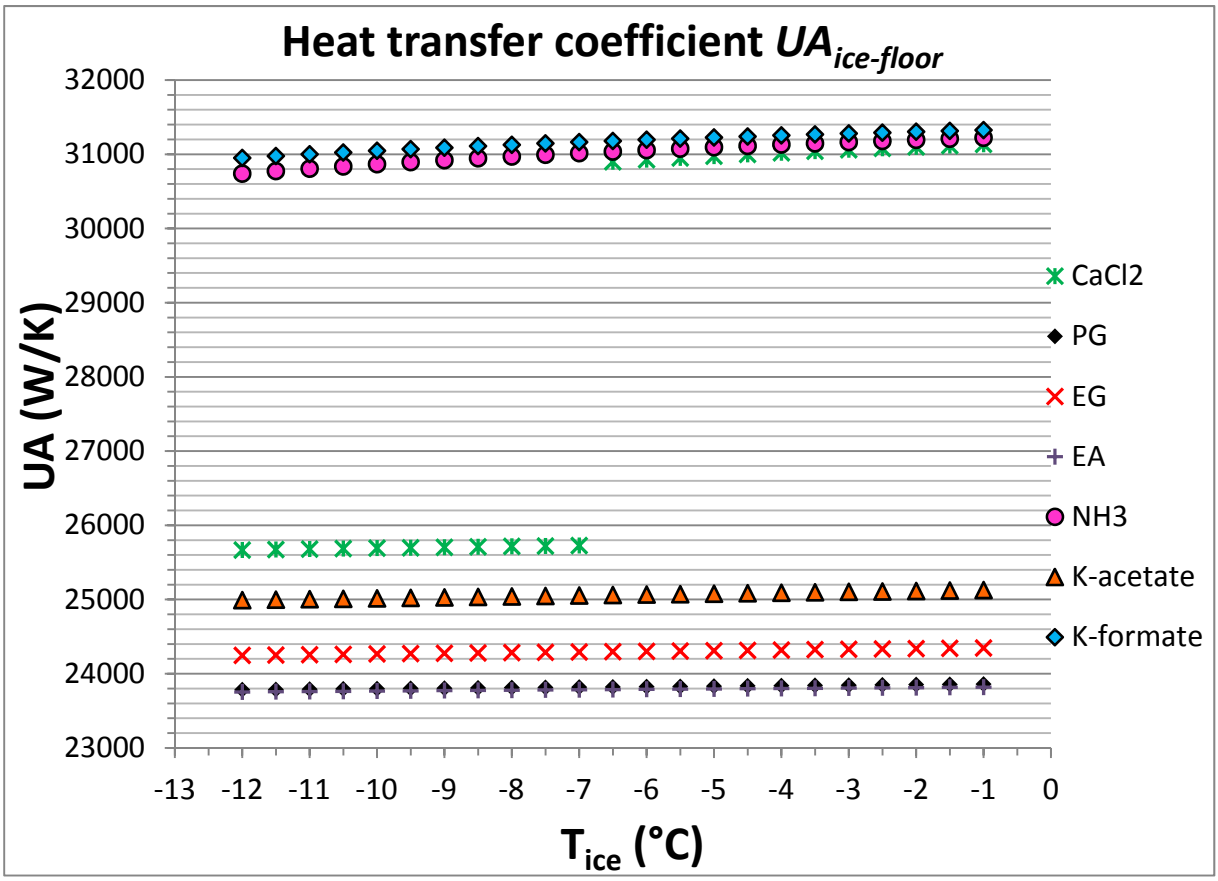

Results / Charts (CC = 200 kW; F_p = -30 °C; ΔT = 2 K)

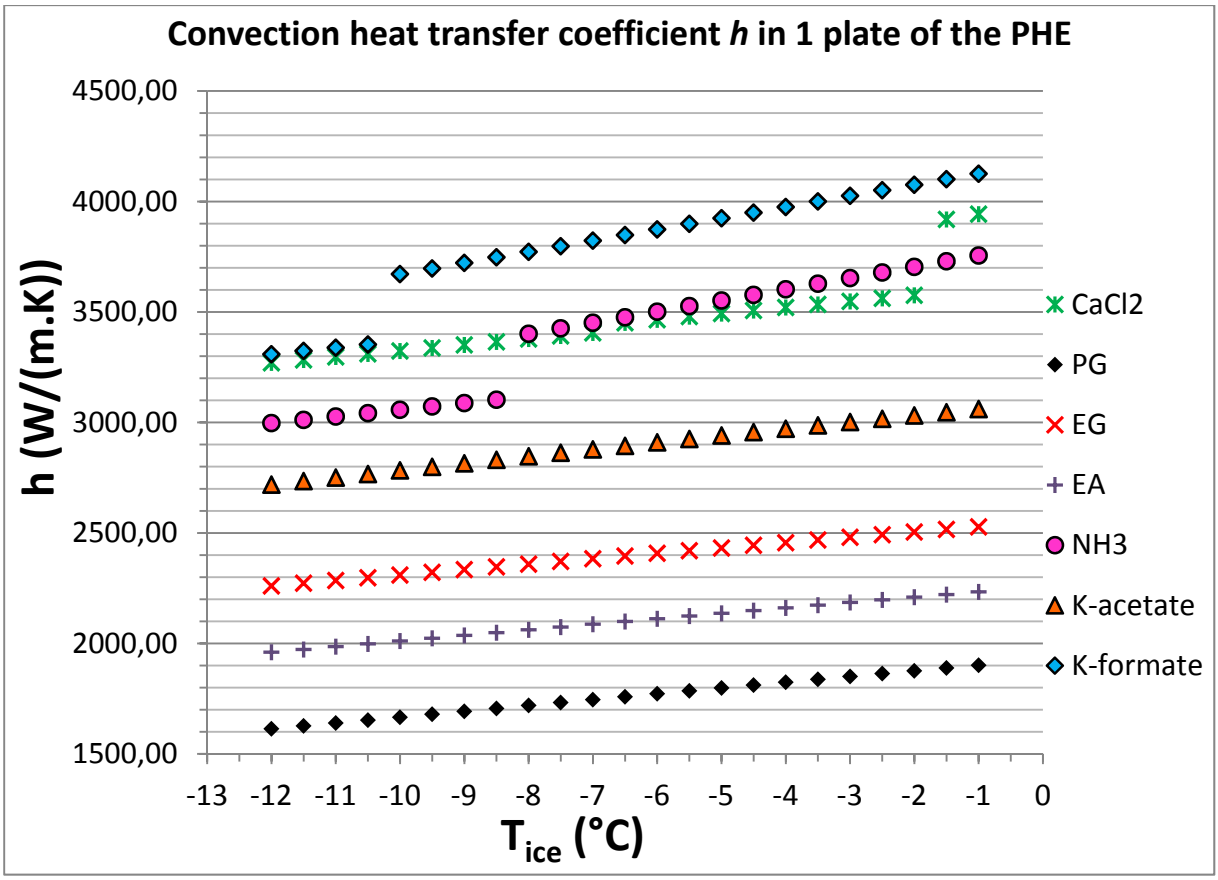

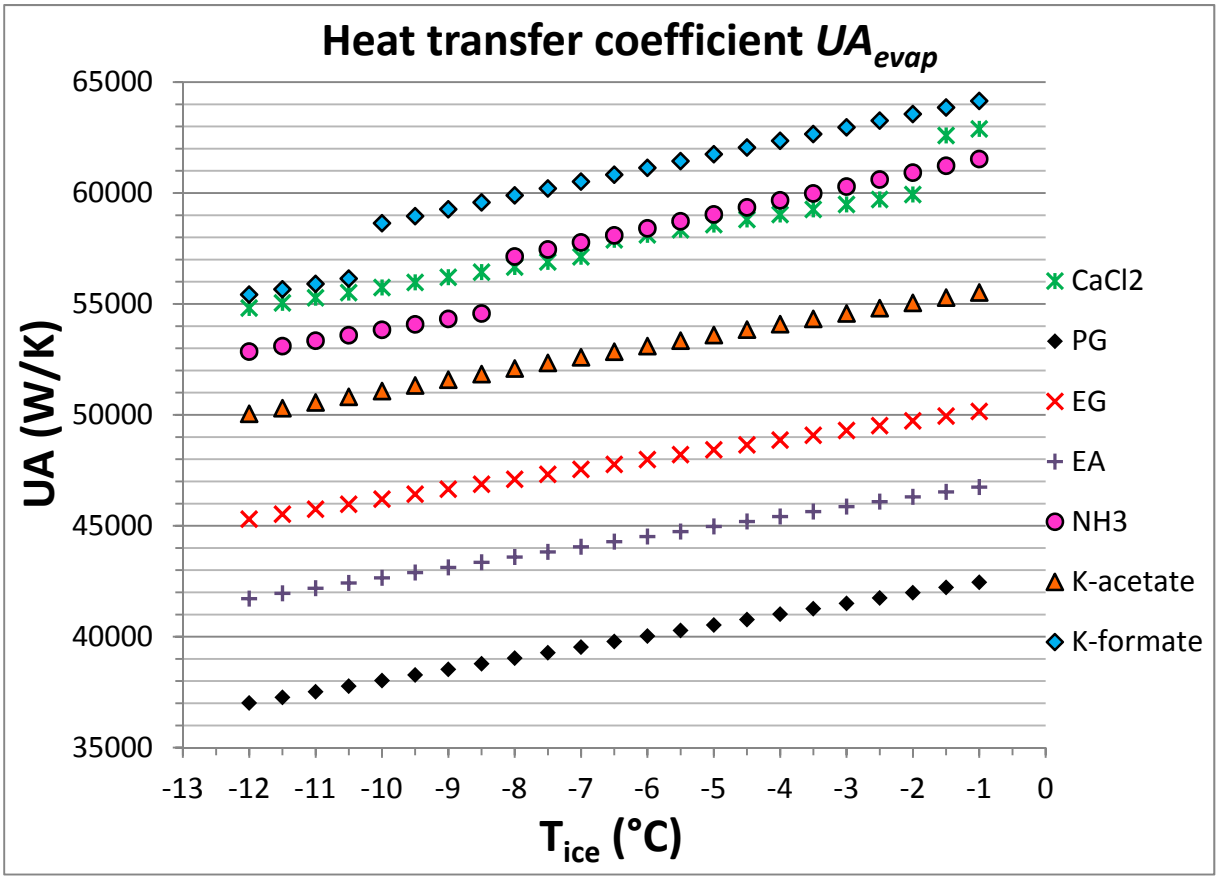

Results / Charts (CC = 200 kW; F_p = -30 °C; ΔT = 2 K)

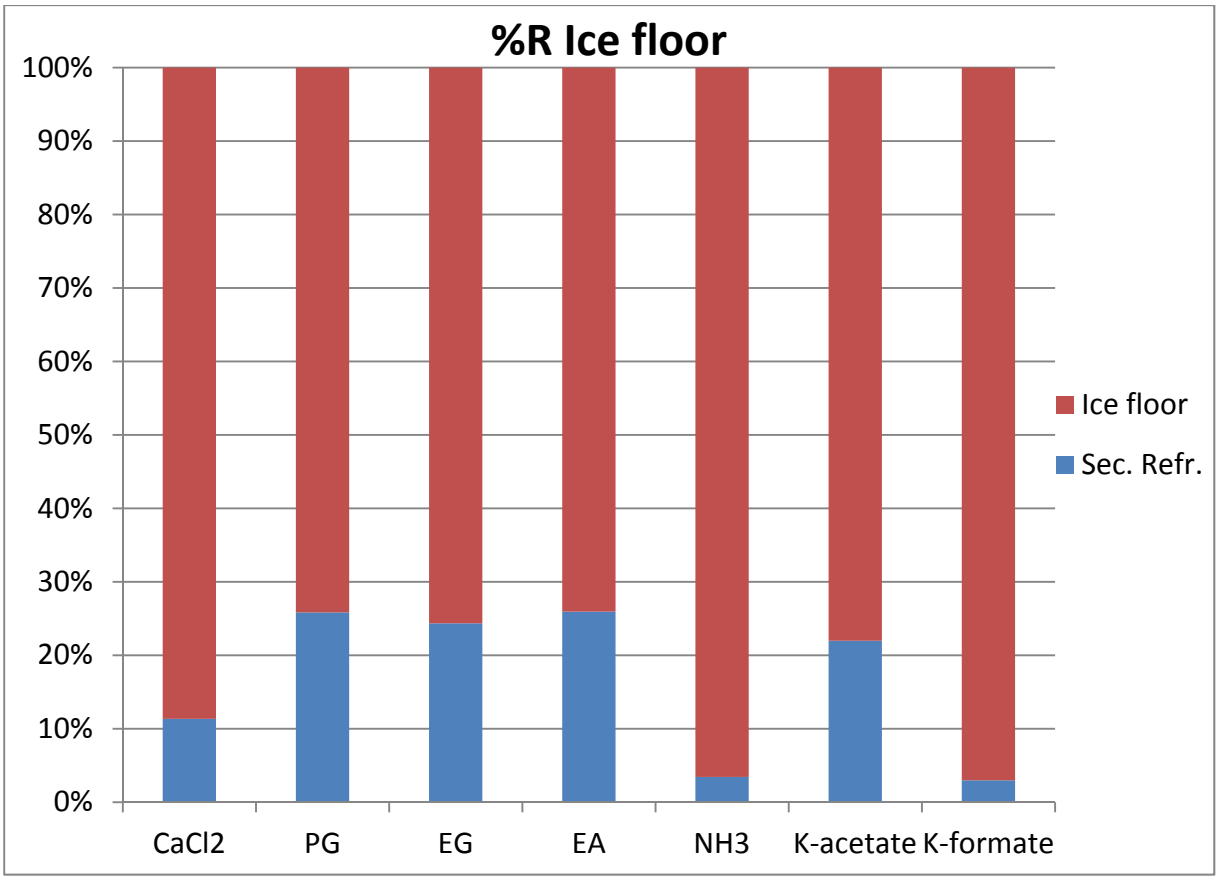

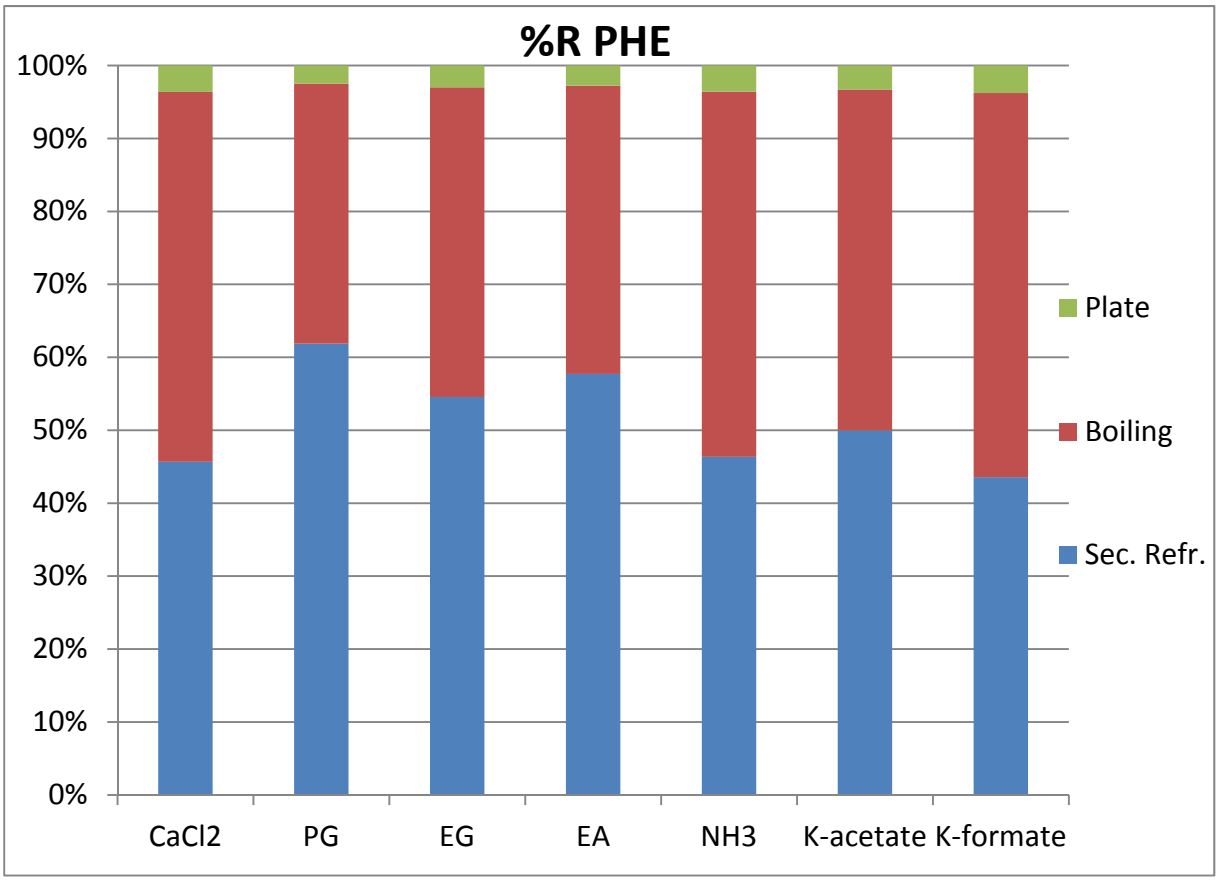

Results / Charts (CC = 200 kW; F_p = -30 °C; ΔT = 2 K)

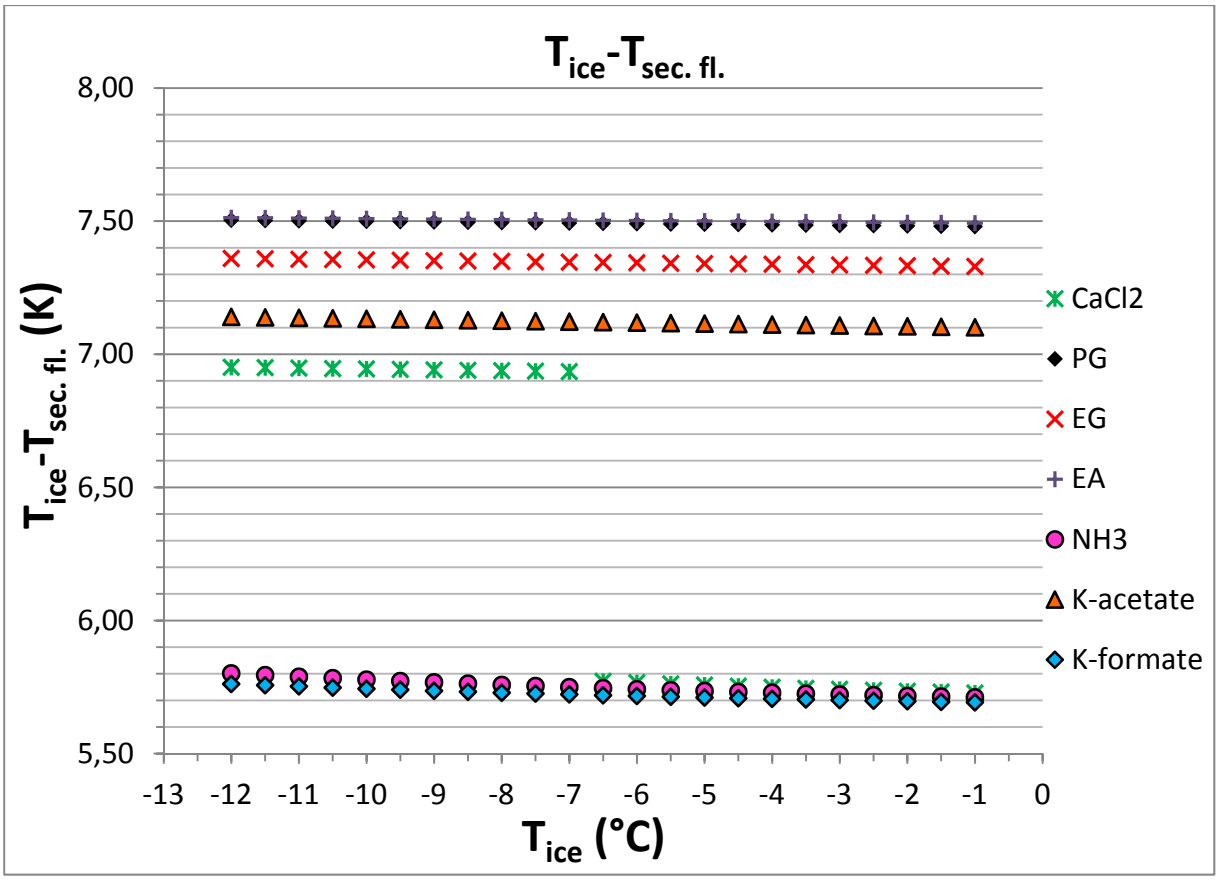

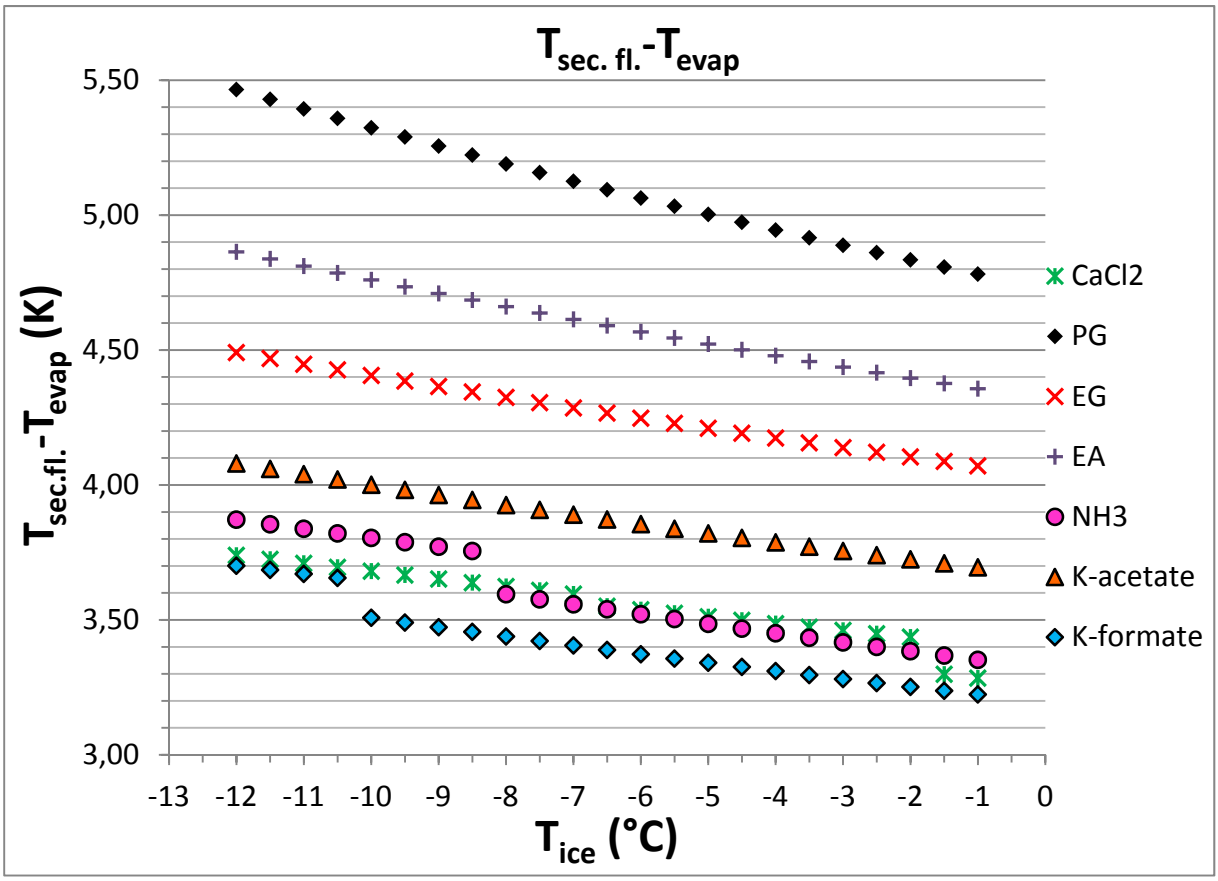

Results / Charts (CC = 200 kW; F_p = -30 °C; ΔT = 2 K)

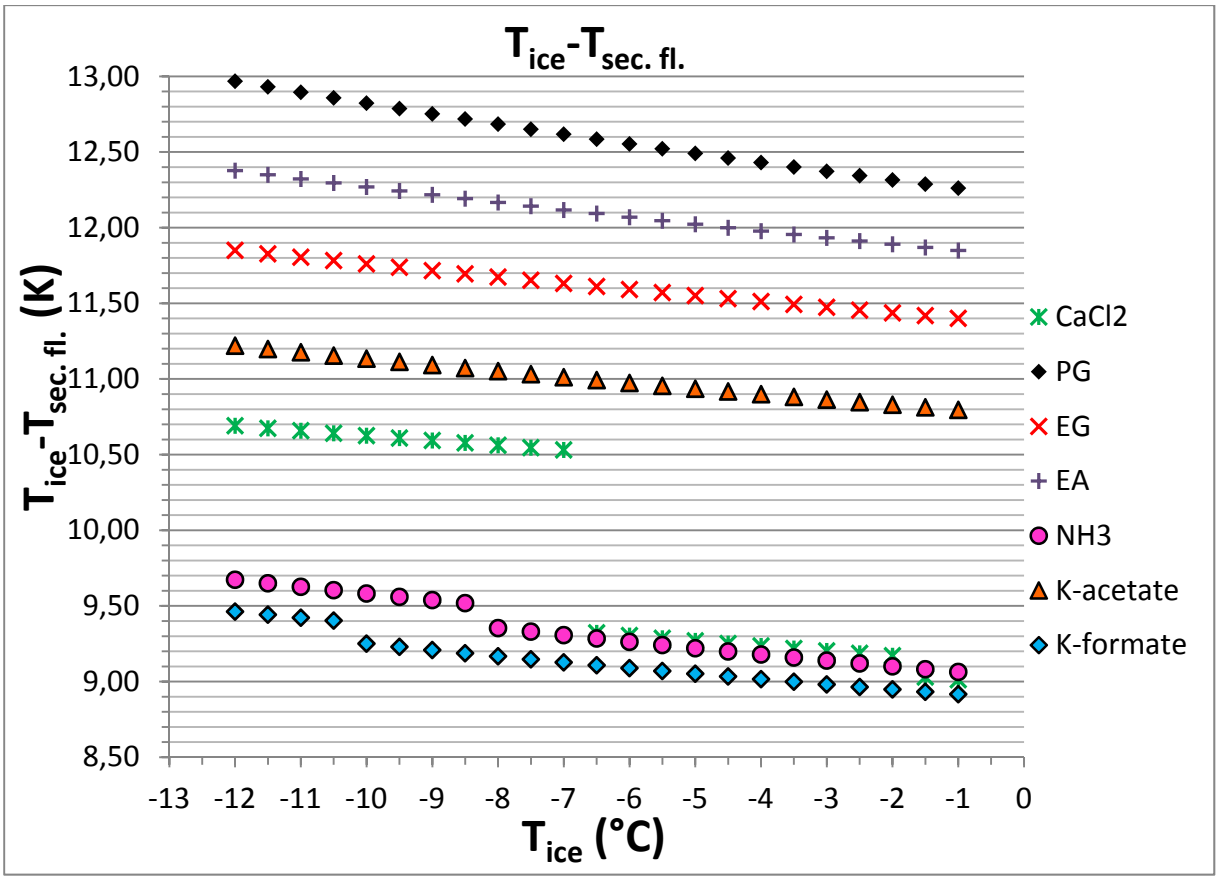

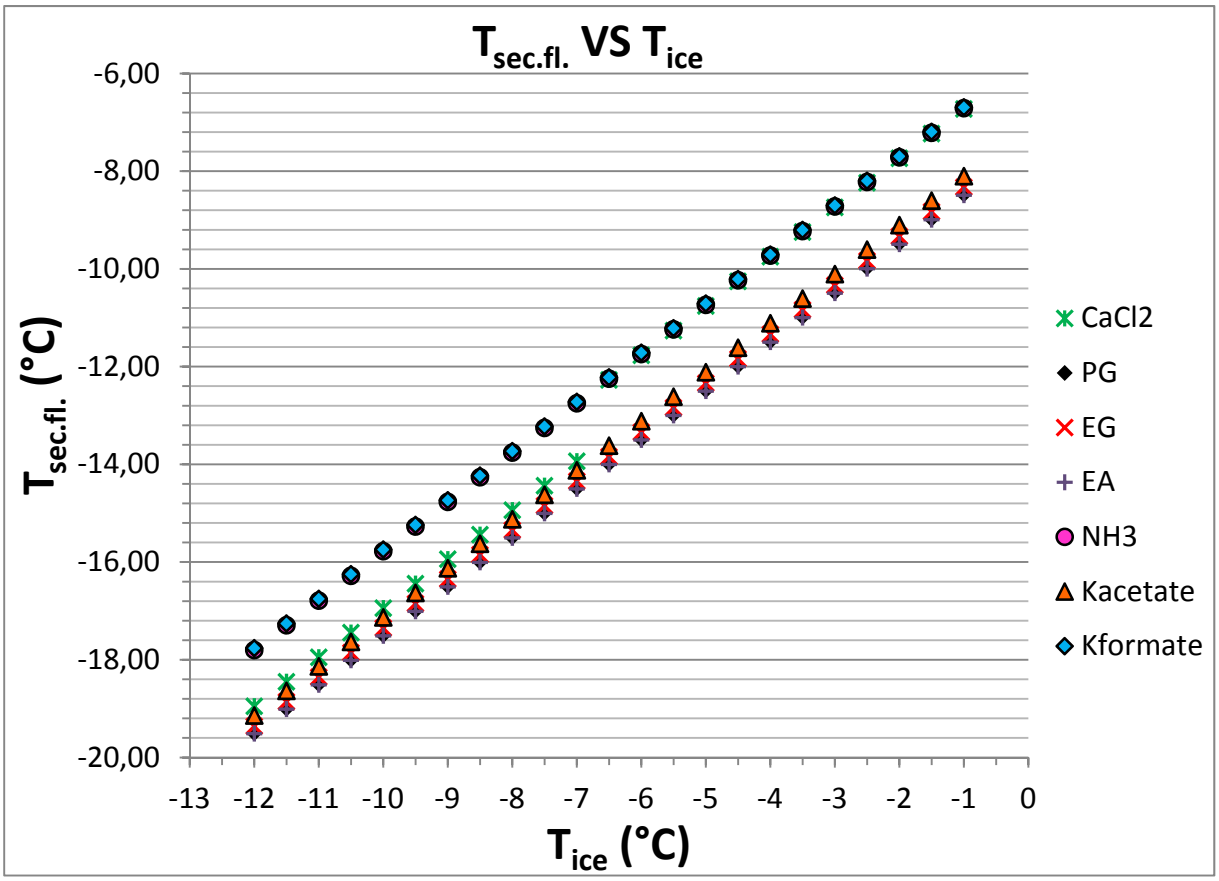

Results / Charts (CC = 200 kW; F_p = -30 °C; ΔT = 2 K)

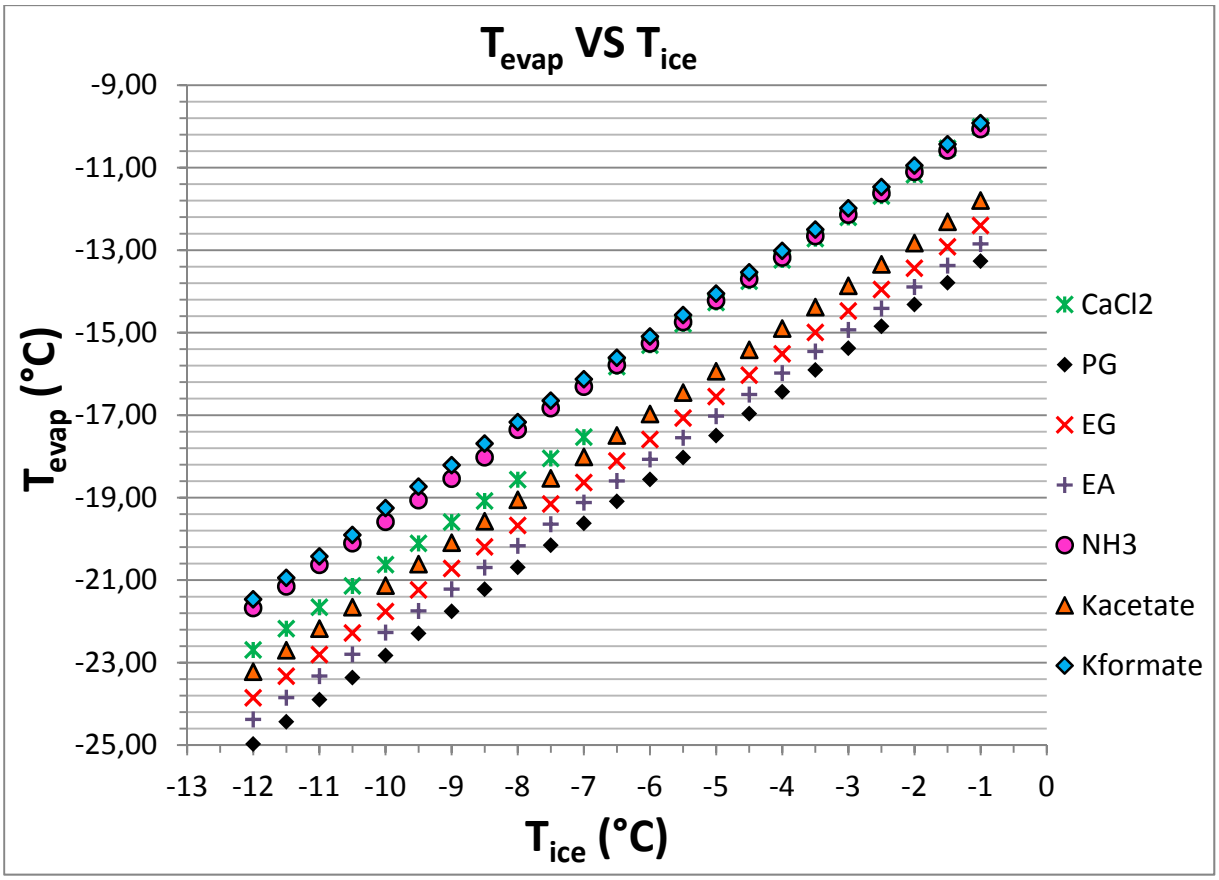

Results / Charts (CC = 200 kW; F_p = -30 °C; ΔT = 2 K)

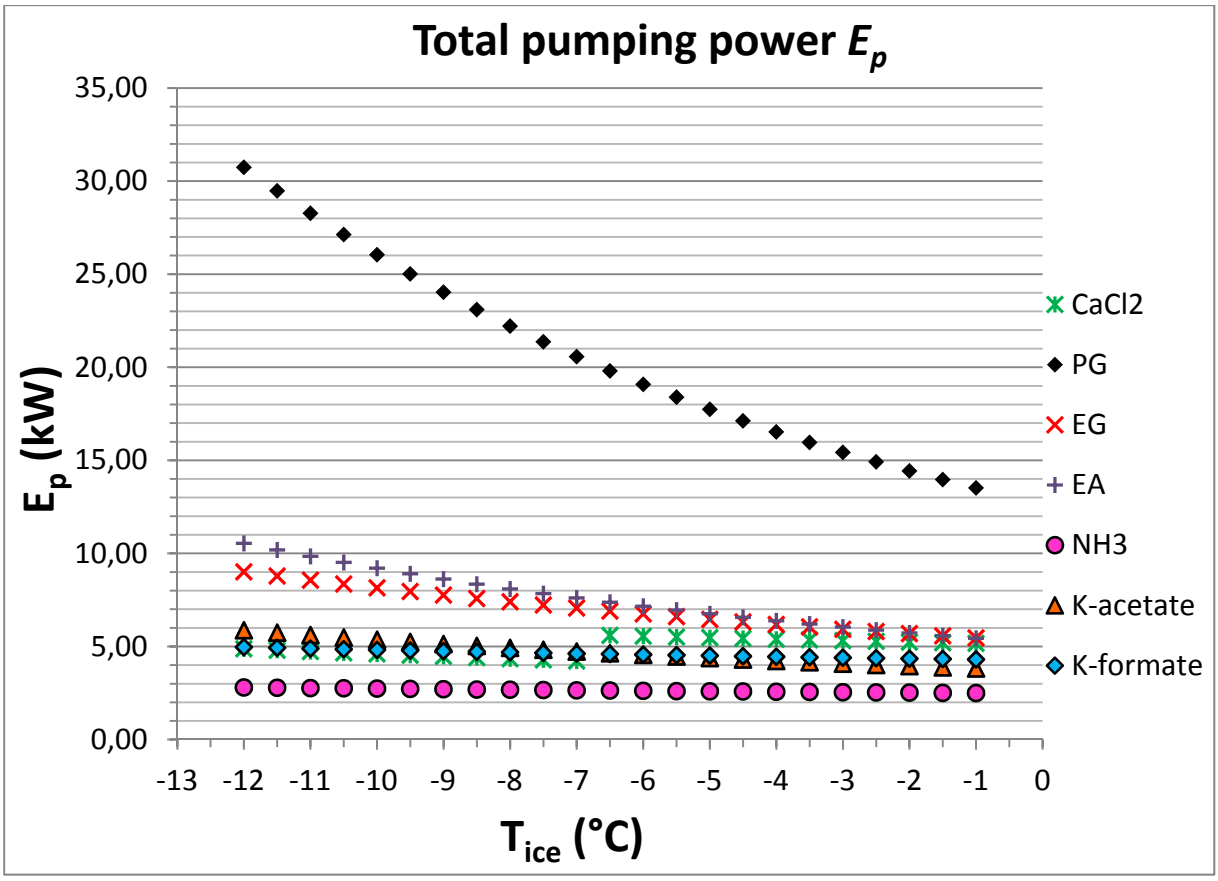

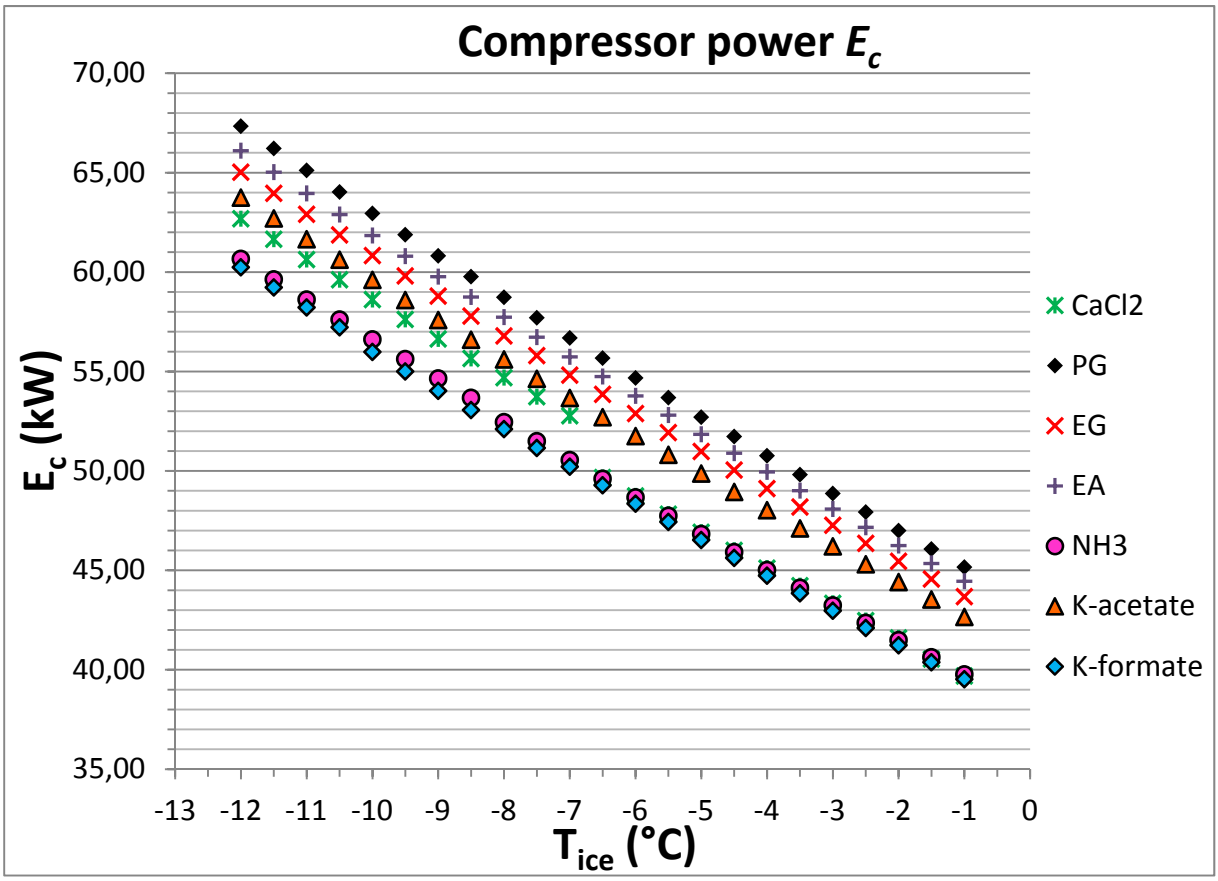

Results / Charts (CC = 200 kW; F_p = -30 °C; ΔT = 2 K)

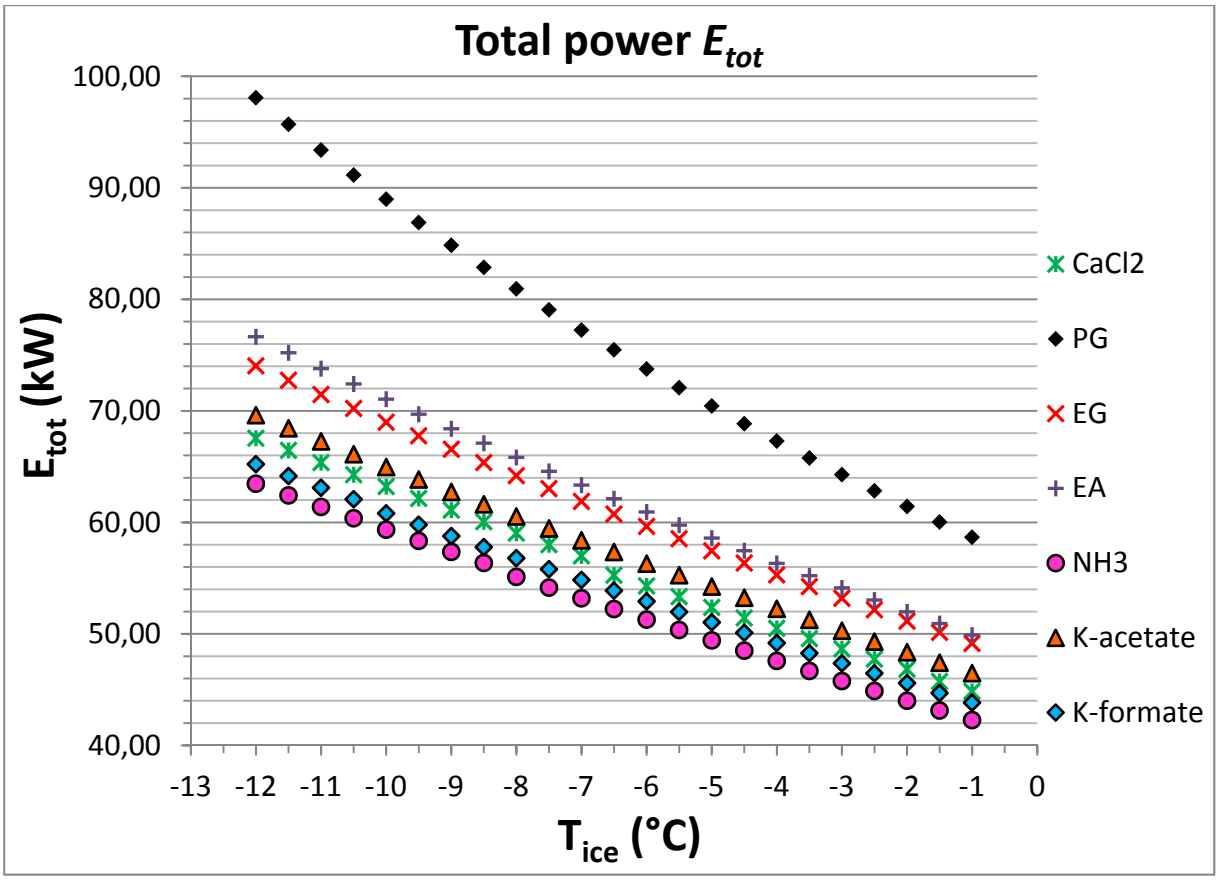

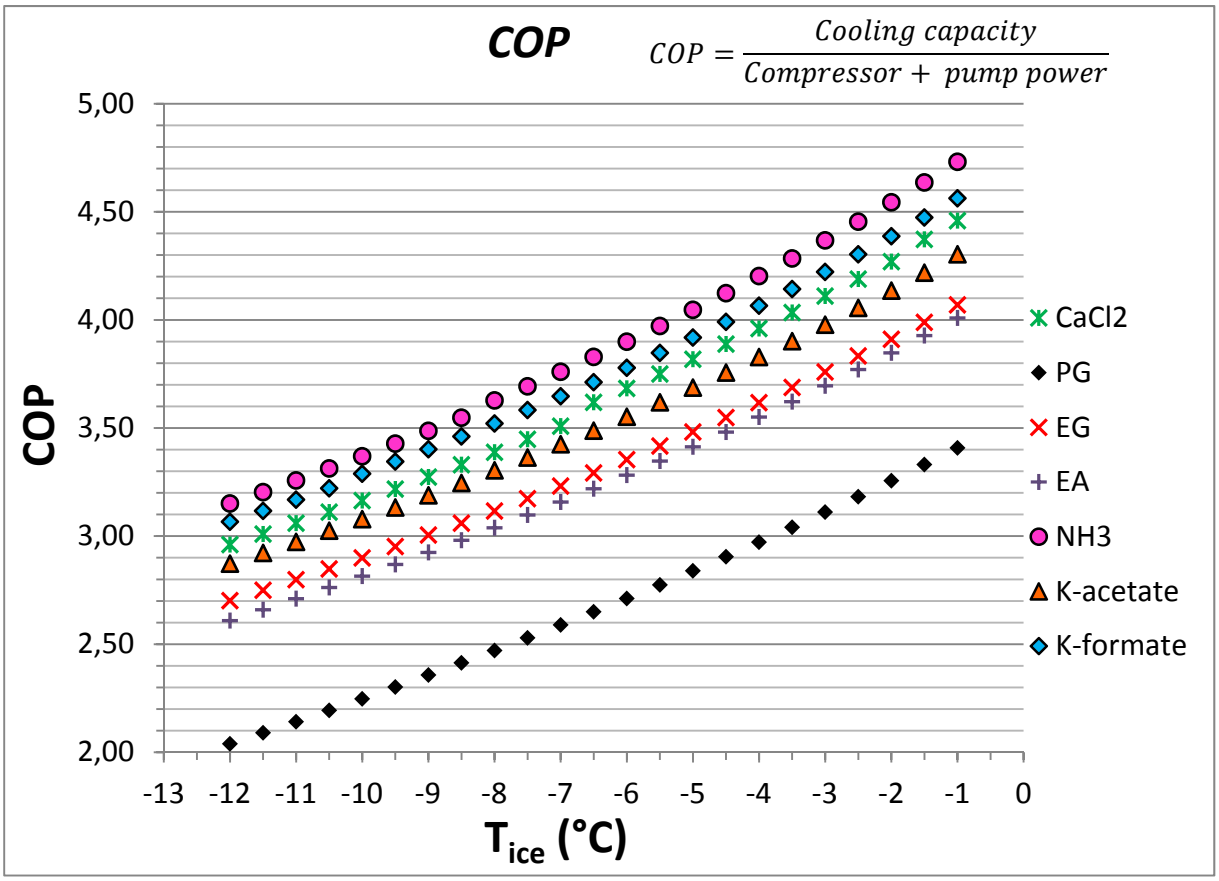

Results / Charts (CC = 200 kW; F_p = -30 °C; ΔT = 2 K)

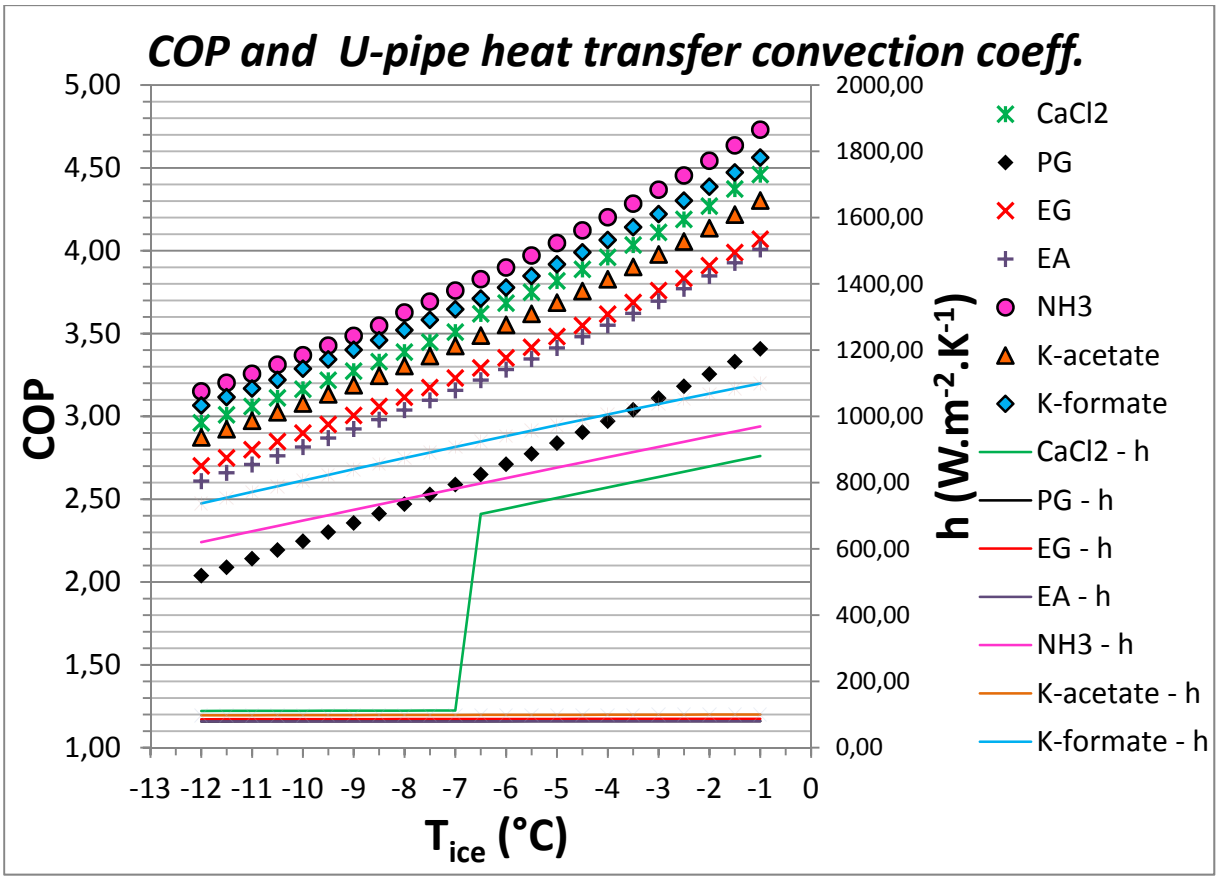

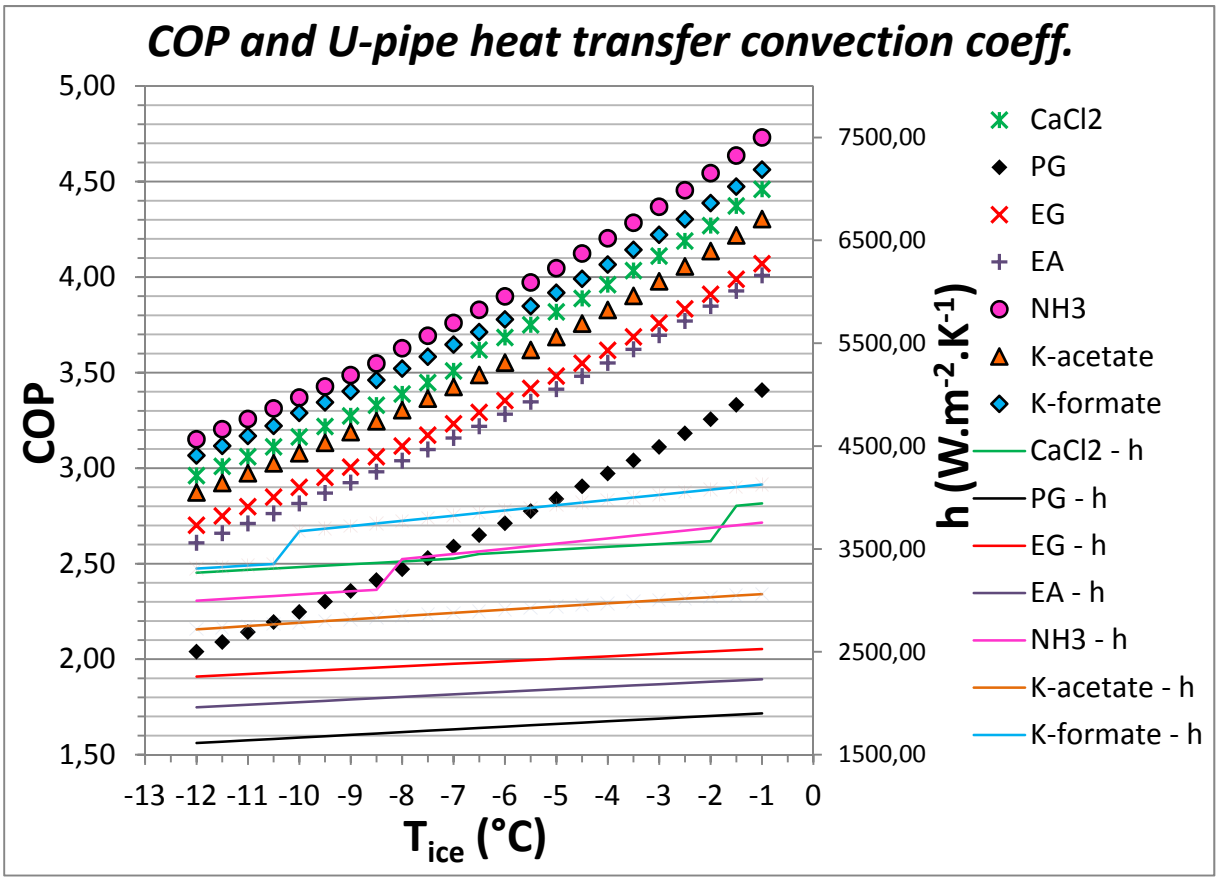

Results / Charts (CC = 200 kW; F_p = -30 °C; ΔT = 2 K)

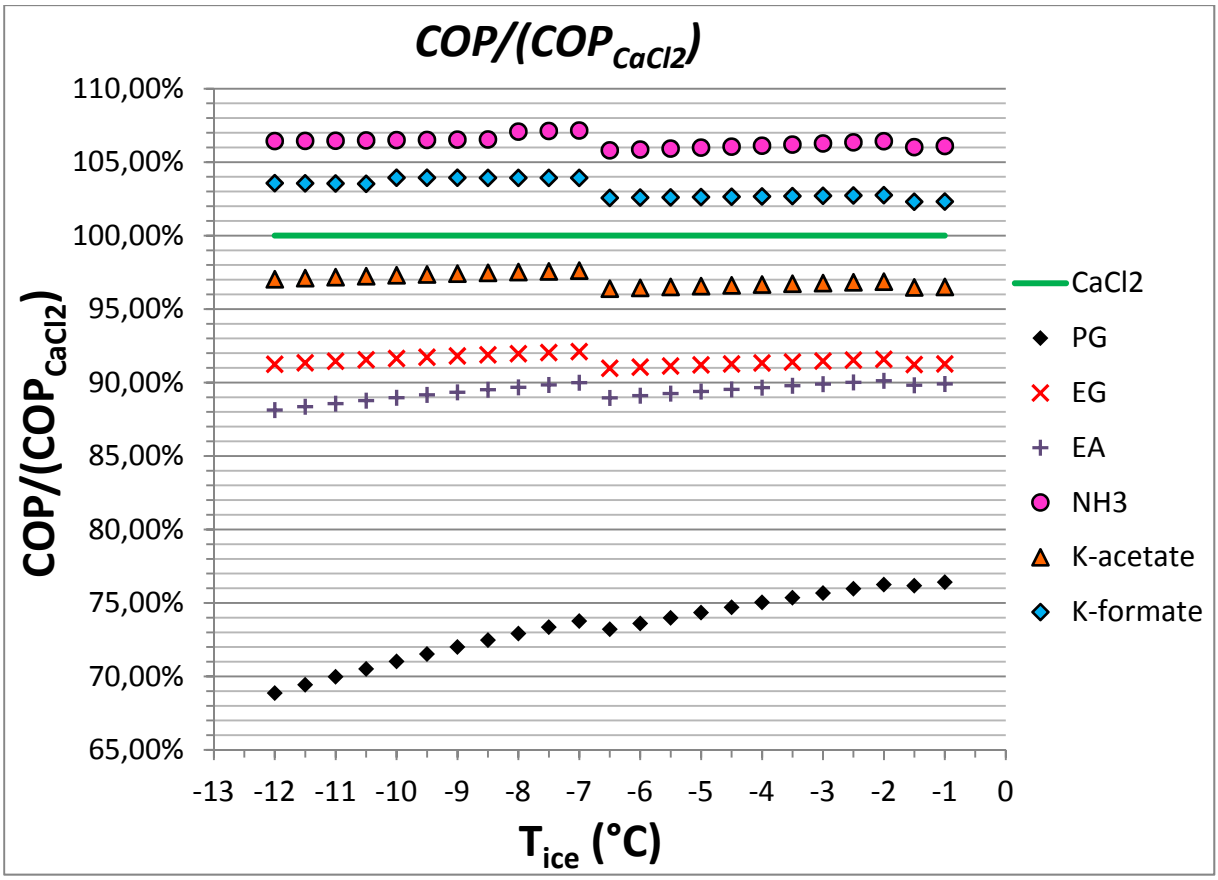

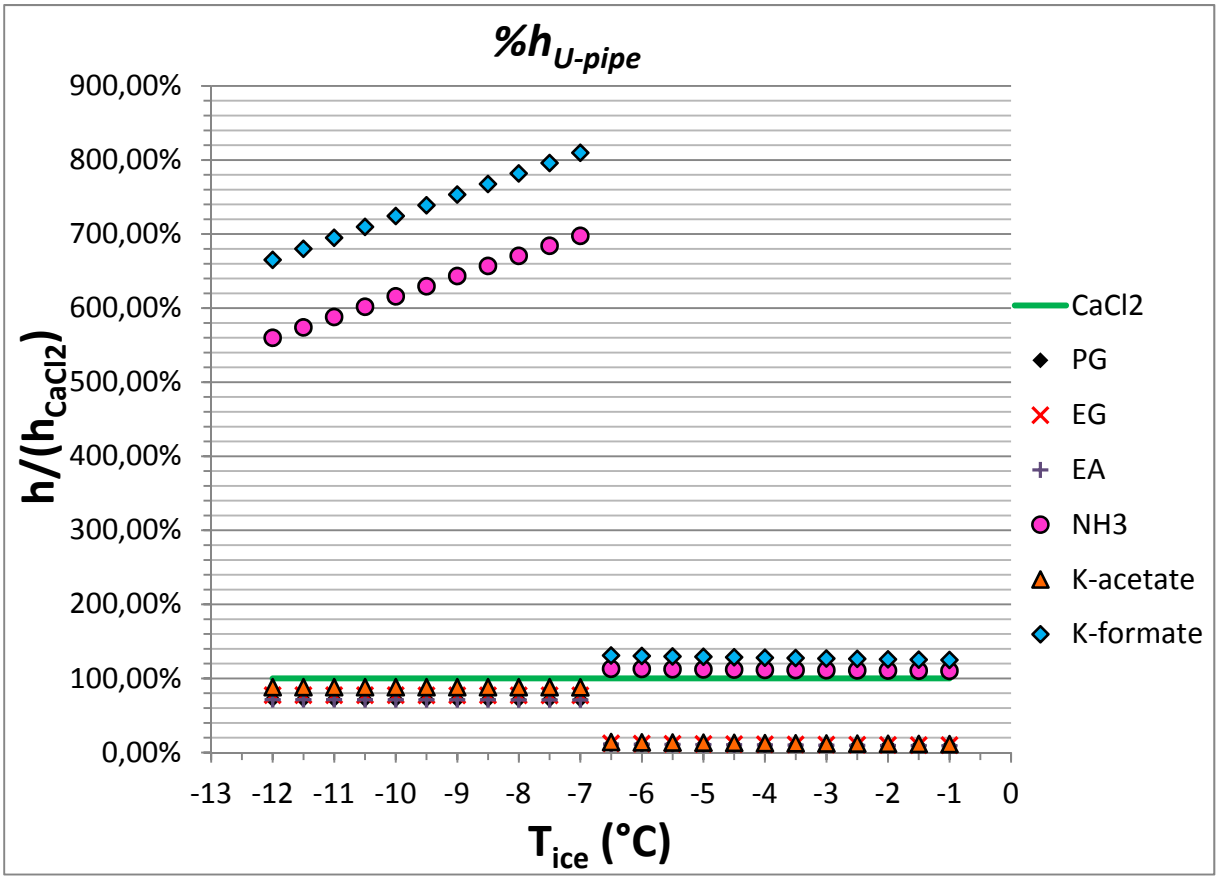

Results / Charts (CC = 200 kW; F_p = -30 °C; ΔT = 2 K)

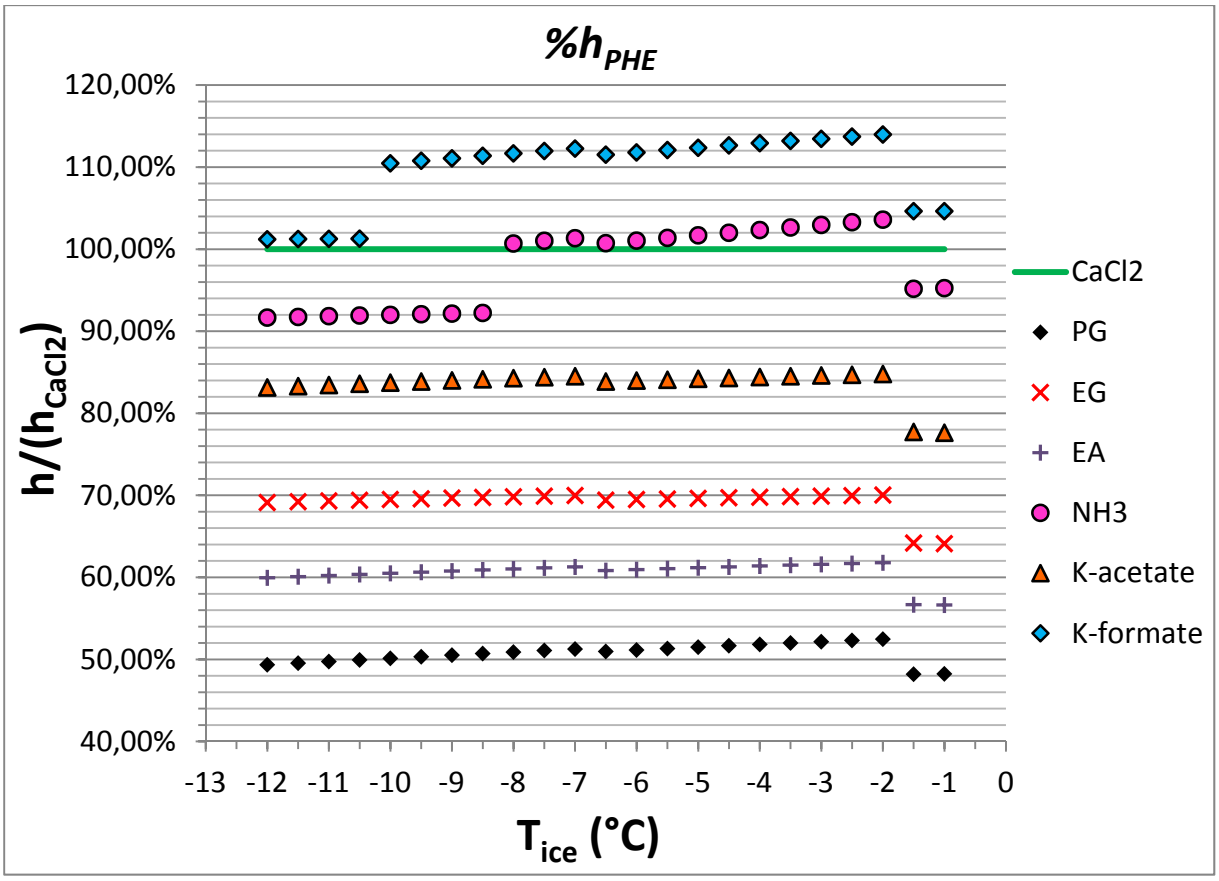

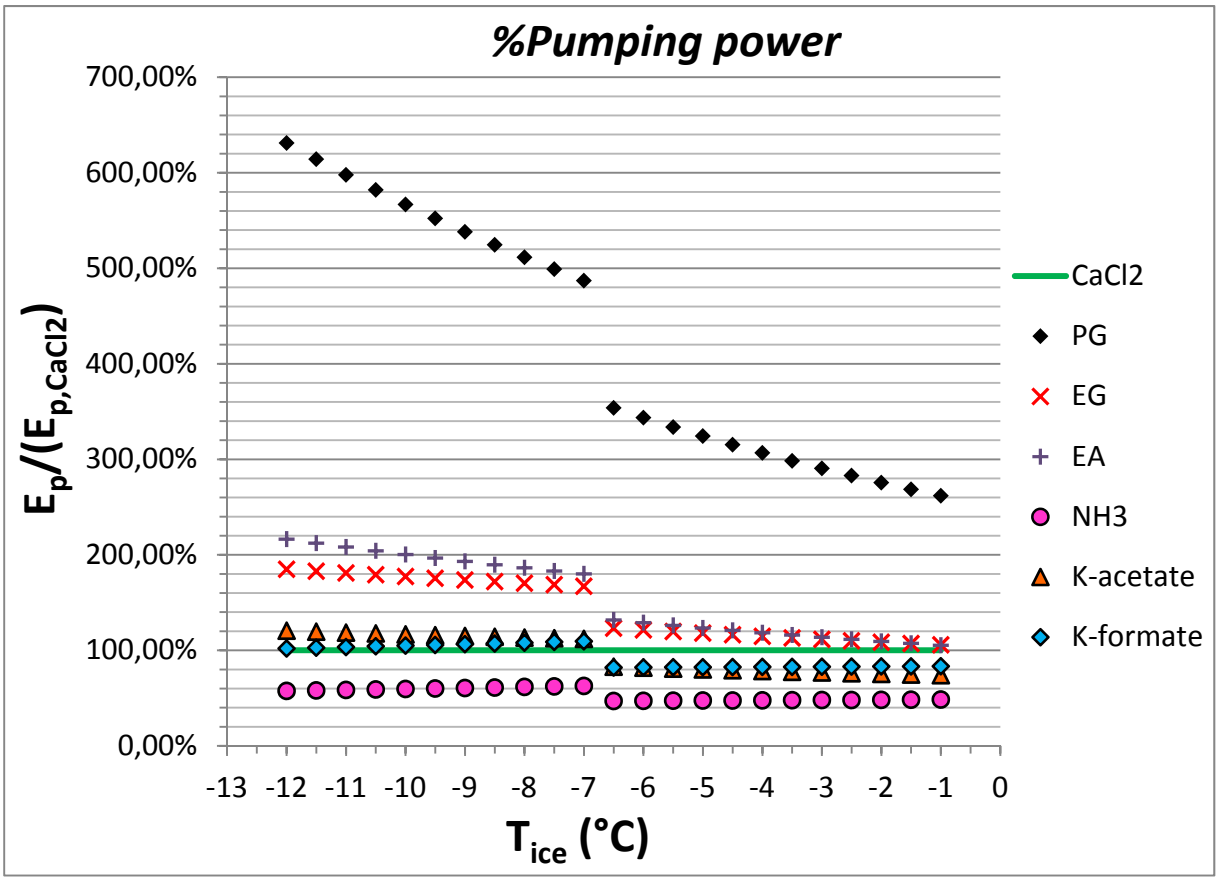

Results / Charts (CC = 200 kW; F_p = -30 °C; ΔT = 2 K)

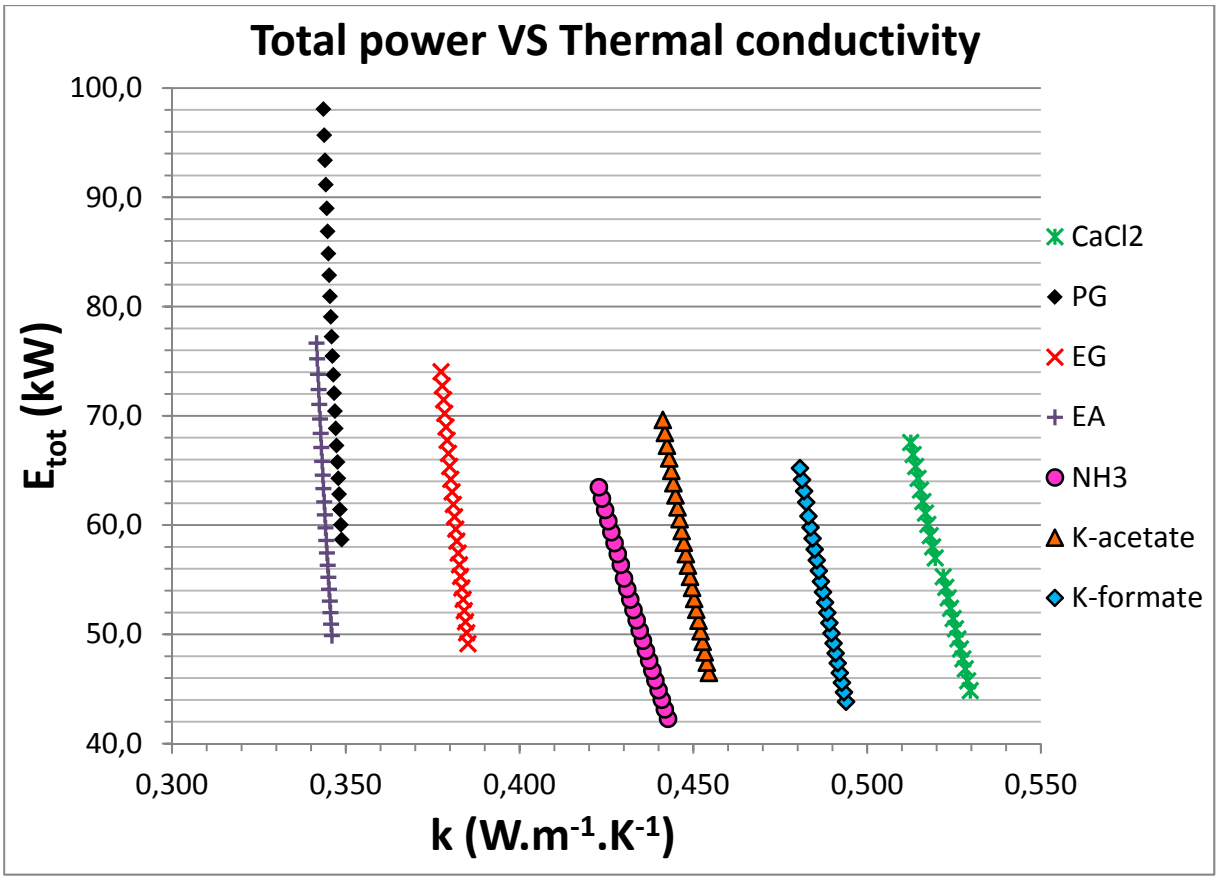

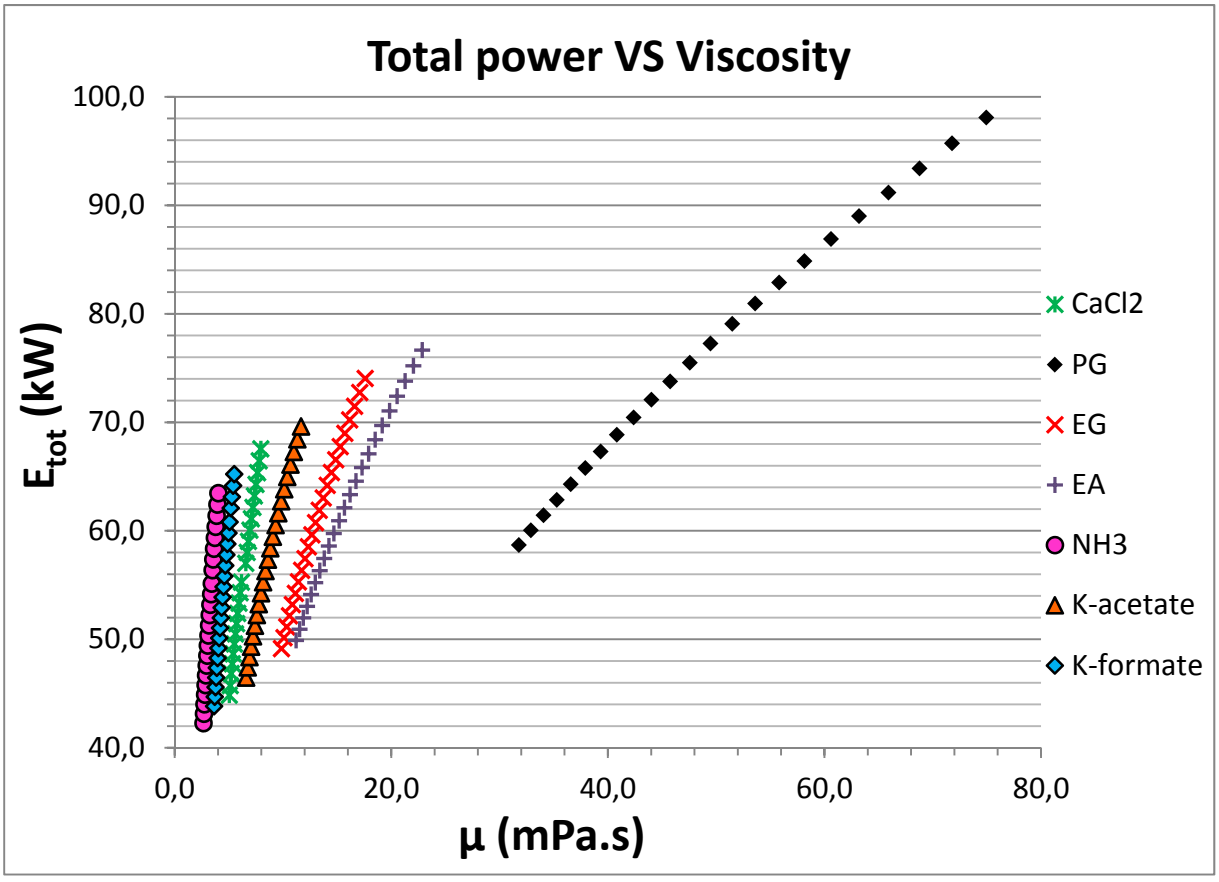

Results / Charts (CC = 200 kW; F_p = -30 °C; ΔT = 2 K)

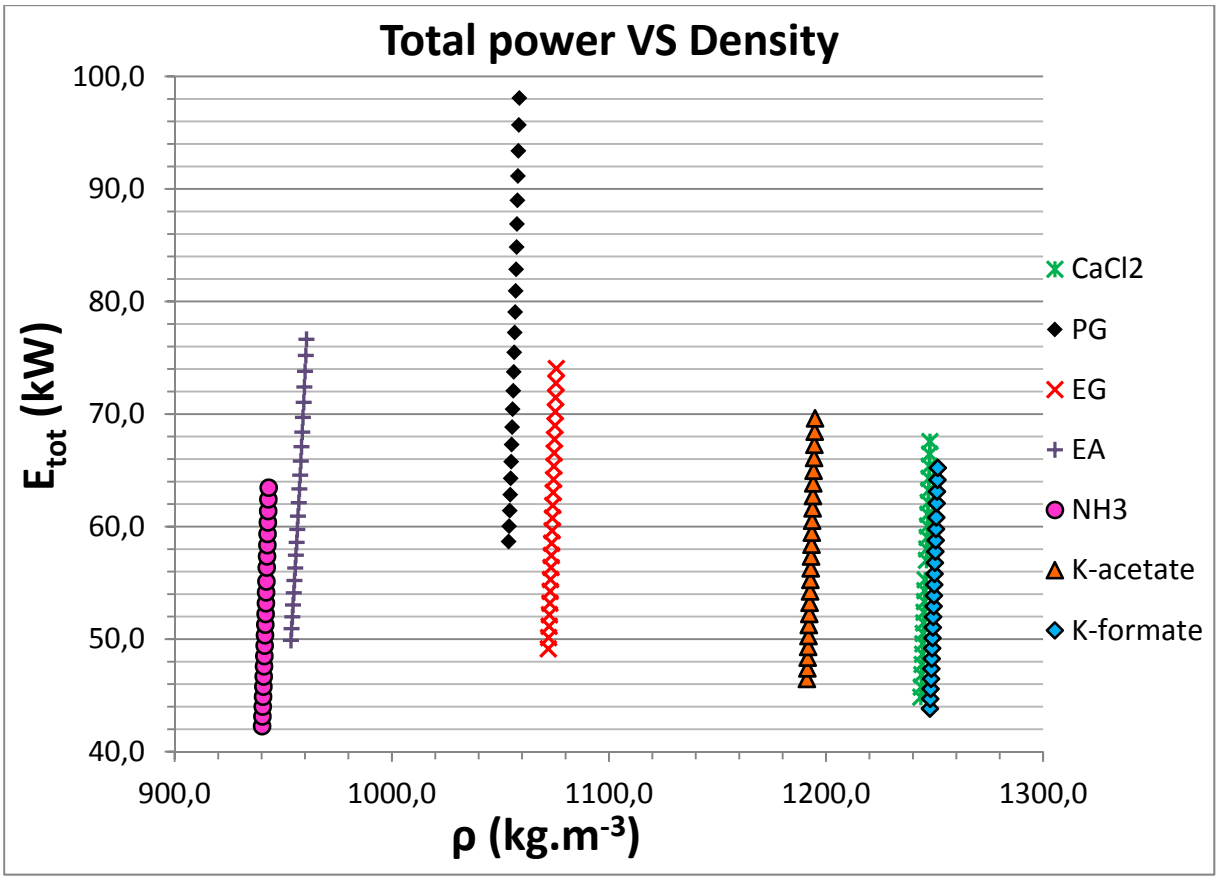

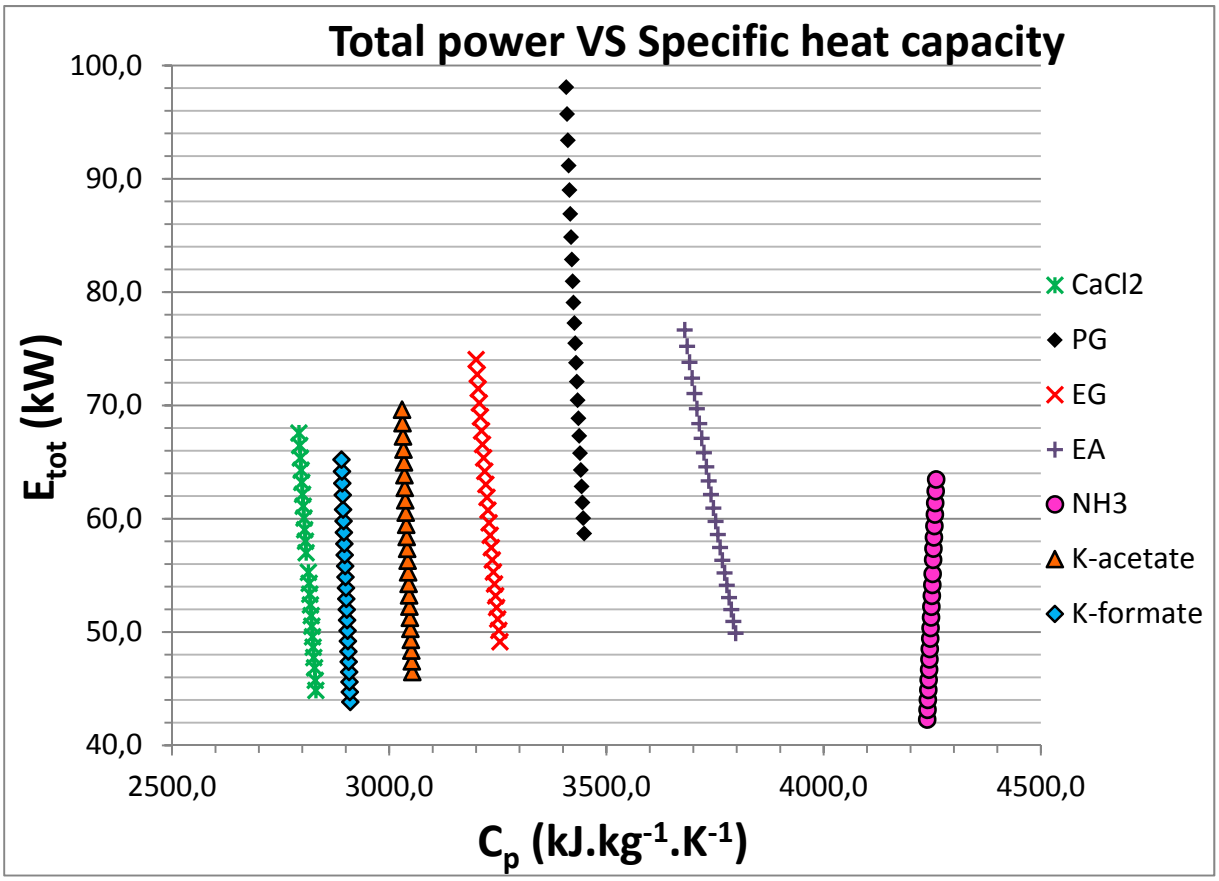

Appendix 5: Resistance value results from 2D *COMSOL Multiphysics* simulation models – Examples of temperature profile

Heat flux value	Ice top temperature (K)	Pipe inner wall average temperature (K)	Temperature difference ice-pipe	$R_{ice\text{-}pipe}$ value ($m.K.W^{-1}$)
200 W/m²	270,15	263,18	6,97	0,5592
300 W/m²	270,15	259,65	10,50	0,5586
100 W/m²	270,15	266,71	3,44	0,5611
150 W/m²	270,15	264,95	5,20	0,5598
250 W/m²	270,15	261,42	8,73	0,5589
50 W/m²	270,15	268,48	1,67	0,5650
220 W/m²	270,15	262,47	7,68	0,5591
			AVERAGE	**0,5602**

The heat flux is applied to the inner pipe wall. The heat flow mentioned in the following figures is the sum of heat loads and heat gains from the ground.

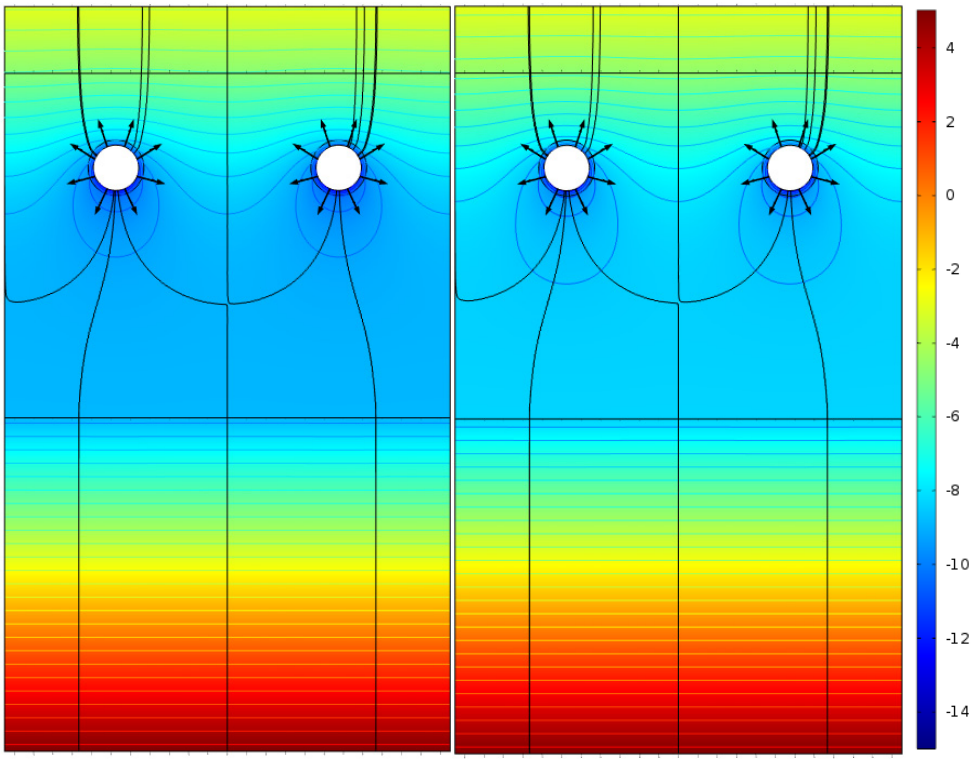

220 W/m² (Heat flow = 254 kW) **200 W/m² (Heat flow = 231 kW)**

Appendix 5: Resistance value results from 2D COMSOL Multiphysics simulation models – Examples of temperature profile

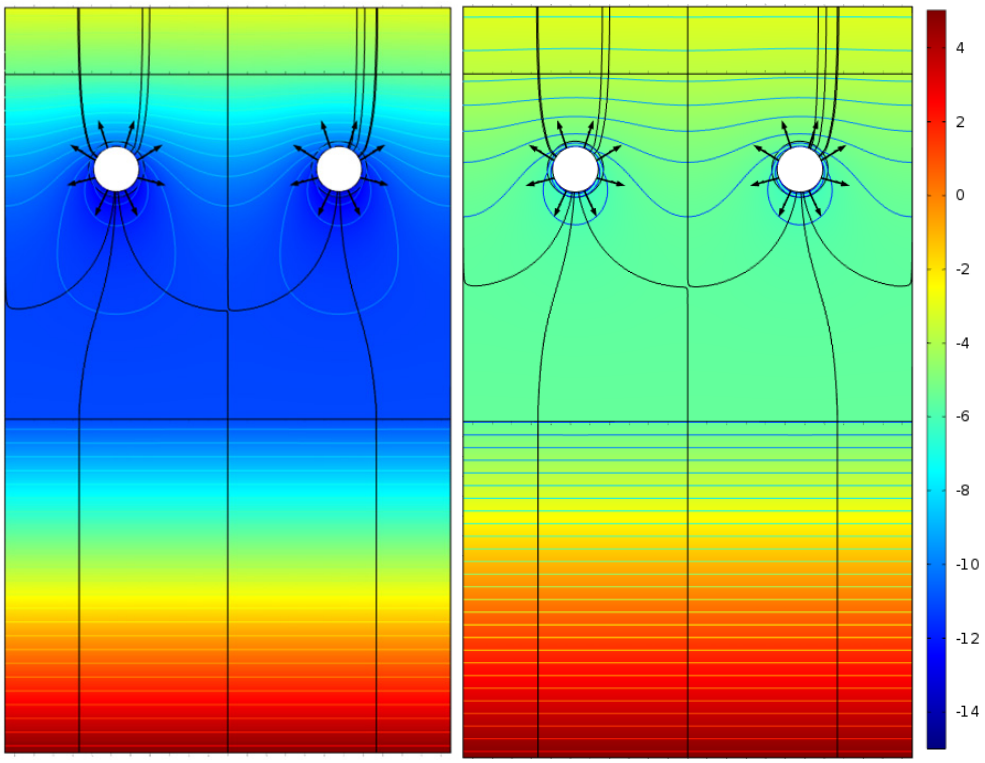

300 W/m² (Heat flow = 346 kW) **100 W/m² (Heat flow = 115 kW)**

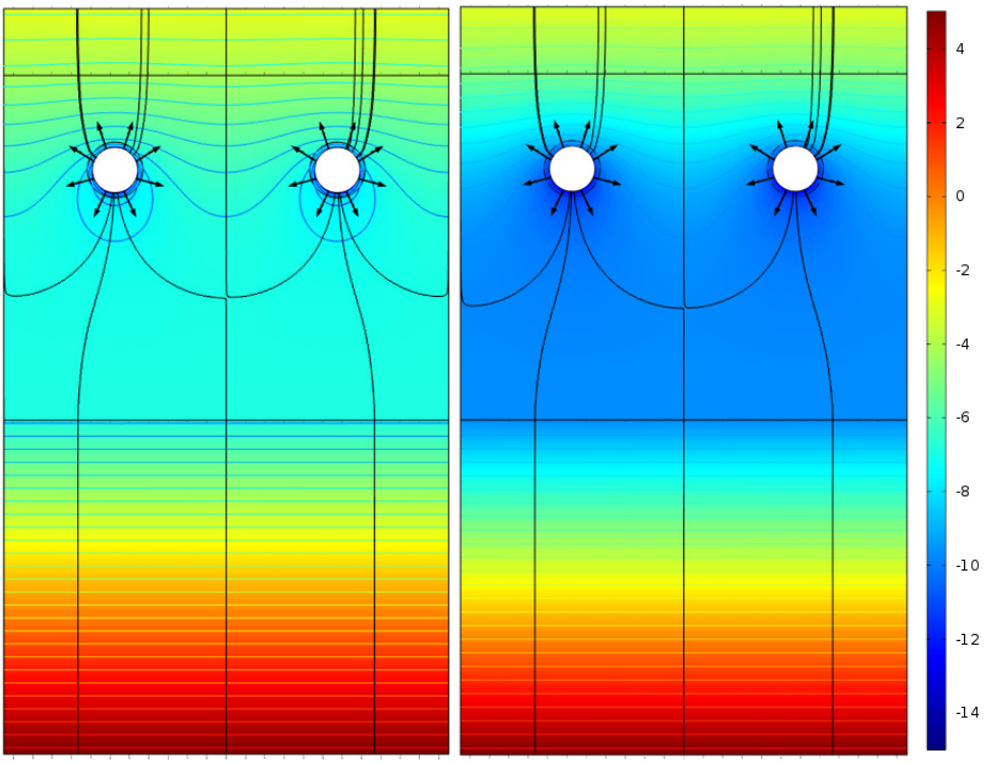

150 W/m² (Heat flow = 173 kW) **250 W/m² (Heat flow = 288 kW)**

Appendix 5: Resistance value results from 2D COMSOL Multiphysics simulation models – Examples of temperature profile

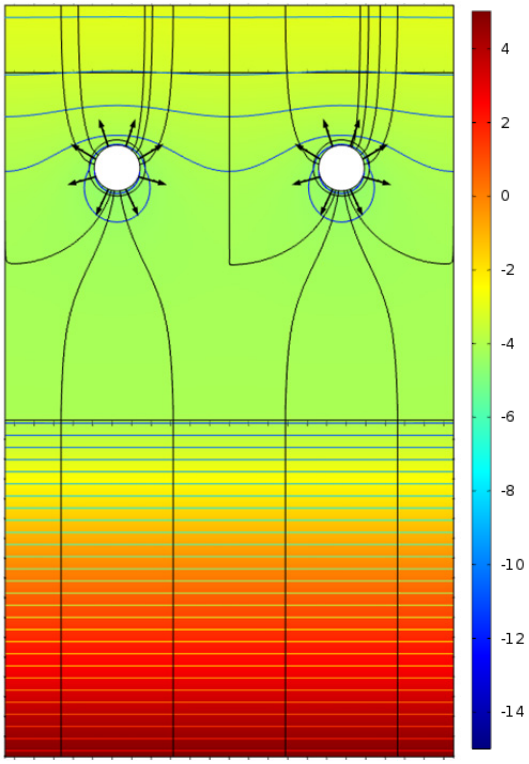

50 W/m2 (Heat flow = 58 kW)

The following figures show details for the 300 W/m² simulation.

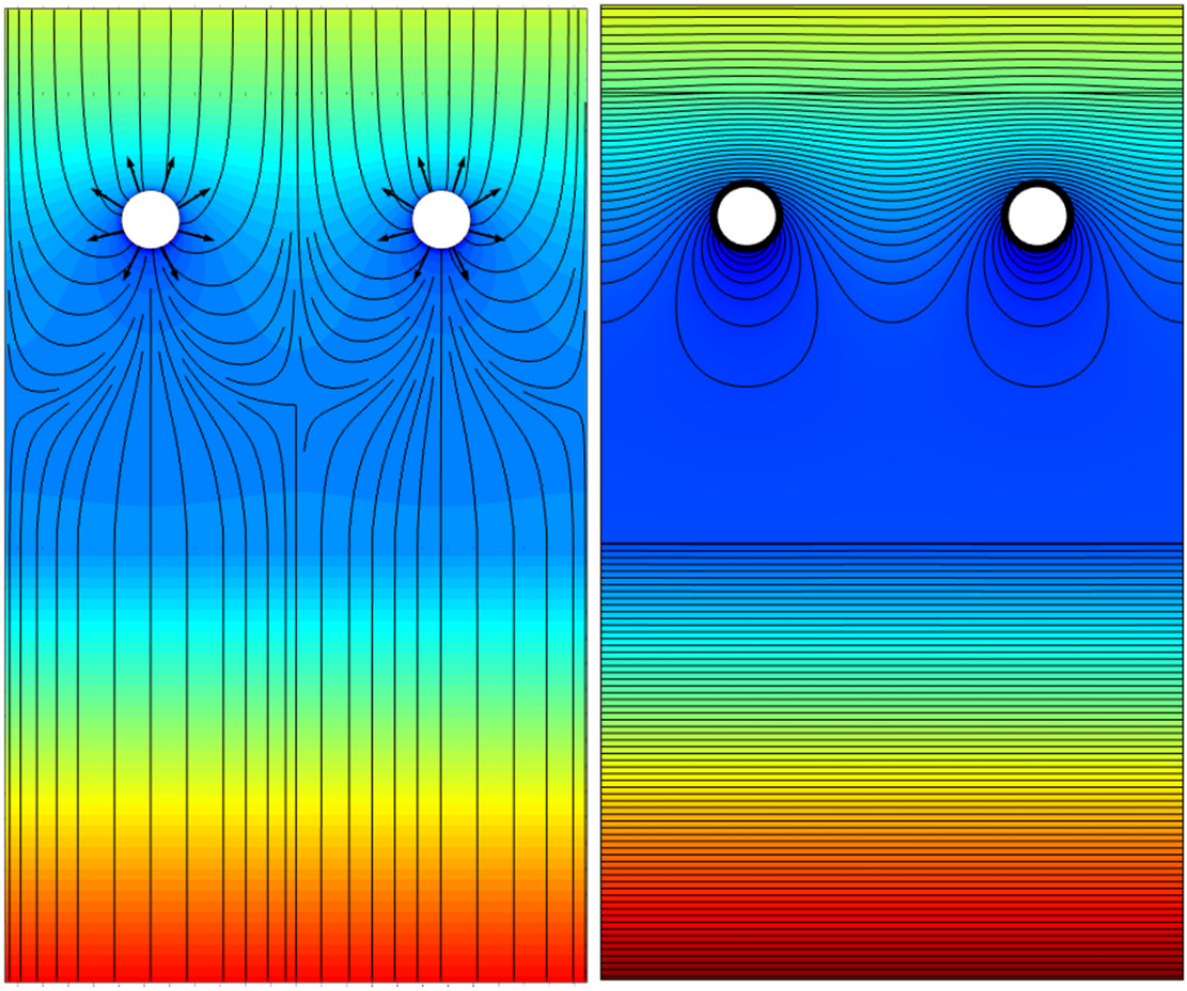

Appendix 5: Resistance value results from 2D COMSOL Multiphysics simulation models – Examples of temperature profile

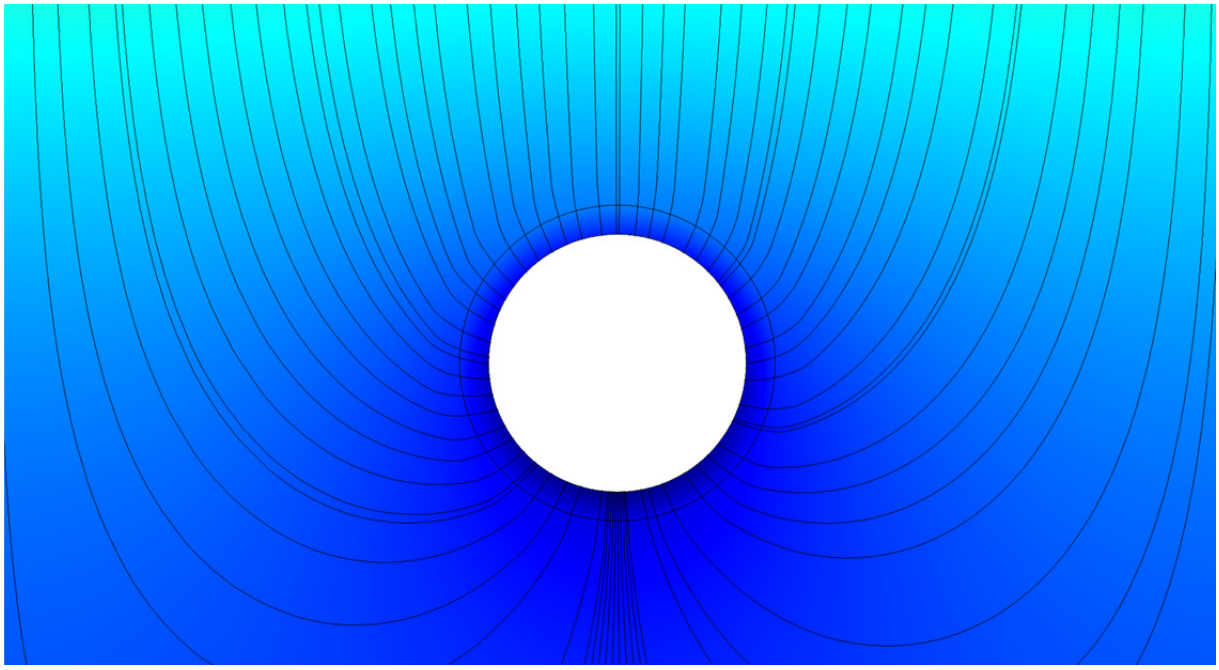

Streamlines

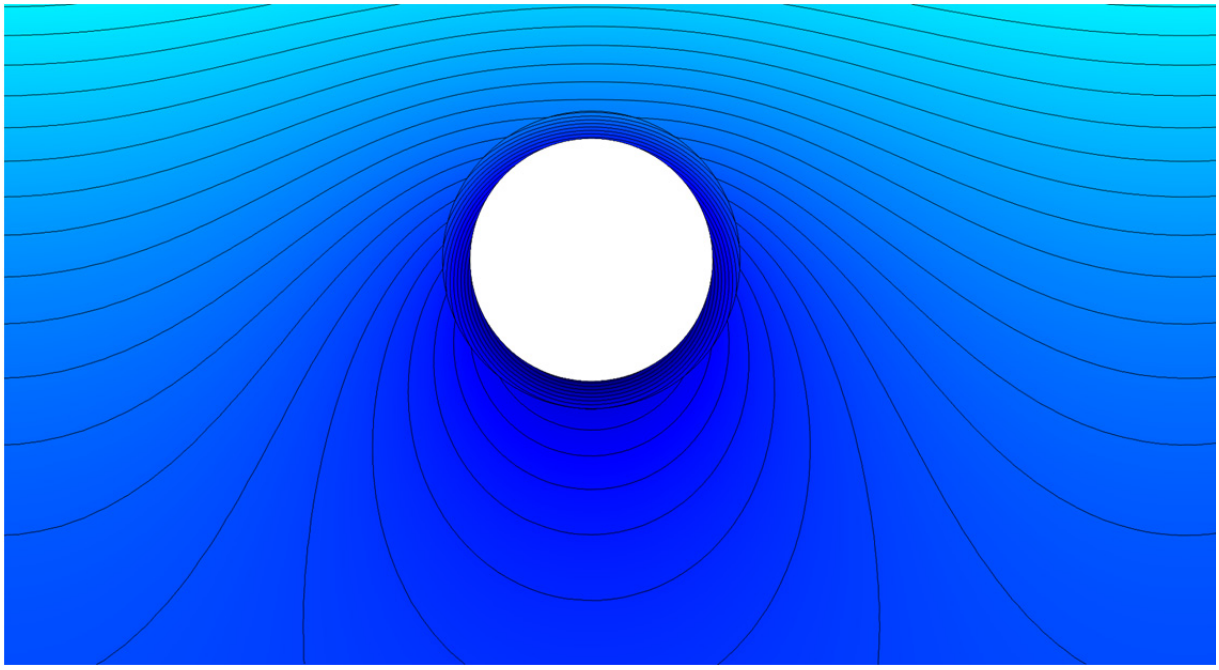

Isothermal contours

Appendix 6: Demonstration of the formula for the pumping power associated with headers

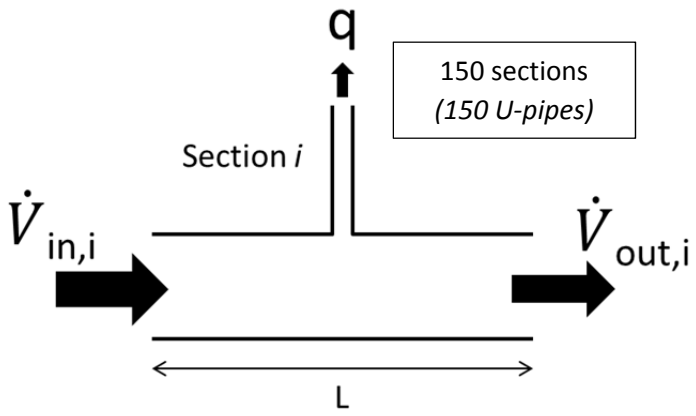

$$i \in [\![1,150]\!]$$

$$\dot{V}_{out,150} = 0$$
$$\dot{V}_{in,1} = \dot{V}_{tot}$$
$$\dot{V}_{in,i+1} = \dot{V}_{out,i}$$

$$f_{in,i+1} = f_{out,i}$$

$$q = \frac{\dot{V}_{tot}}{150} = \frac{\dot{V}_{in,1}}{150}$$

$$\dot{V}_{in,i} = \left(\dot{V}_{in,1} - (i-1)\cdot\frac{\dot{V}_{in,1}}{150}\right) = \frac{\dot{V}_{in,1}}{150}(151-i)$$

$$\dot{V}_{out,i} = \left(\dot{V}_{in,1} - i\cdot\frac{\dot{V}_{in,1}}{150}\right) = \frac{\dot{V}_{in,1}}{150}(150-i)$$

- The pumping power associated with each section is:

$$\left(E_{p,header}\right)_i = \frac{\left(\Delta p_{header}\cdot\dot{V}\right)_i}{e_{pump}}$$

where

$$\left(\Delta p_{header}\cdot\dot{V}\right)_i = \left(\Delta p_f\cdot\dot{V}\right)_{in,i} + \left(\Delta p_f\cdot\dot{V}\right)_{out,i} + \left(\Delta p_s\cdot\dot{V}_{in}\right)_i$$

- The general expression for major and minor losses is:

$$\Delta p_f\cdot\dot{V} = f\cdot\rho\cdot\frac{u^2}{2}\cdot\frac{L}{d_h}\cdot\dot{V} = 8\cdot f\cdot\rho\cdot\frac{\dot{V}^3\cdot L}{\pi^2\cdot d_h^5}$$

$$\Delta p_s\cdot\dot{V} = k\cdot\rho\cdot\frac{u^2}{2}\cdot\dot{V} = 8\cdot k\cdot\rho\cdot\frac{\dot{V}^3}{\pi^2\cdot d_h^4}$$

- Applying them in the header case gives:

$$\left(\Delta p\cdot\dot{V}\right)_i = 8\cdot\frac{\rho}{\pi^2}\left\{\frac{L}{2\cdot d_h^5}\left(f_{in,i}\cdot\dot{V}_{in,i}^3 + f_{out,i}\cdot\dot{V}_{out,i}^3\right) + k_{in,i}\cdot\frac{\dot{V}_{in,i}^3}{d_h^4}\right\}$$

- Using the expression for $\dot{V}_{in,i}$ and $\dot{V}_{out,i}$ we find:

$$\left(\Delta p\cdot\dot{V}\right)_i = 8\cdot\frac{\rho}{\pi^2}\left\{\frac{L}{2\cdot d_h^5}\cdot\left(\frac{\dot{V}_{in,1}}{150}\right)^3\left(f_{in,i}(151-i)^3 + f_{out,i}(150-i)^3\right) + k_{in,i}\cdot\left(\frac{\dot{V}_{in,1}}{150}\right)^3\frac{(151-i)^3}{d_h^4}\right\}$$

- Hence the total pumping power is given by:

$$\left(E_{p,header}\right)_{tot} = \frac{\left(\Delta p_{header}\cdot\dot{V}\right)_{tot}}{e_{pump}}$$

with

$$(\Delta p \cdot \dot{V})_{tot} = \sum_{i=1}^{150} (\Delta p \cdot \dot{V})_i$$

$$= 8\frac{\rho}{\pi^2}\frac{1}{d_h^4}\left(\frac{\dot{V}_{in,1}}{150}\right)^3 \left\{\frac{L}{2 \cdot d_h}\left(\sum_{i=1}^{150}\left(f_{in,i}(151-i)^3 + f_{out,i}(150-i)^3\right) + f_{in,1} \cdot 150^3\right) + \sum_{i=1}^{150} k_i(151-i)^3\right\}$$

- The term $f_{in,1} \cdot 150^3$ is added because it is considered that the first motif comes after a length equals to $\frac{L}{2}$, as shown here-below.

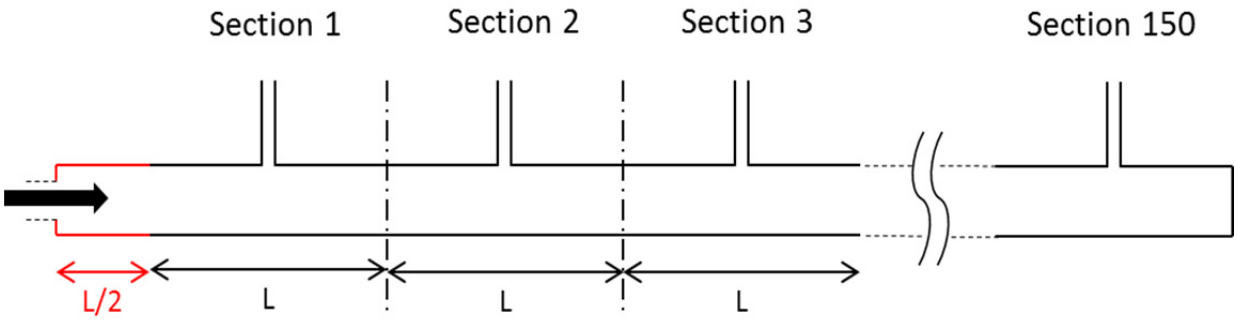

- By changing variables, $j = 151 - i$; $f'_{in,i} = f_{in,151-i}$, results

$$(\Delta p \cdot \dot{V})_{tot} = 8 \cdot \frac{\rho}{\pi^2} \cdot \frac{1}{d_h^4} \cdot \left(\frac{\dot{V}_{in,1}}{150}\right)^3 \left\{\frac{L}{d_h}\sum_{j=1}^{150}\left(f'_{in,j} \cdot j^3\right) + \sum_{j=1}^{150} k'_j \cdot j^3\right\}$$

- The minor losses' coefficient given by the Vazsonyi's equation (65) can be reduced to

$$k'_j = 0{,}37 \cdot \left(\frac{\dot{V}_{out,j}}{\dot{V}_{in,j}} - 1\right)^2 = 0{,}37 \cdot \left(\frac{j-1}{j} - 1\right)^2 = 0.37 \cdot \frac{1}{j^2}$$

which gives the final formula for the pumping power in one header

$$(\Delta p \cdot \dot{V})_{tot} = 8 \cdot \frac{\rho}{\pi^2} \cdot \frac{1}{d_h^4} \cdot \left(\frac{\dot{V}_{in,1}}{150}\right)^3 \left\{\frac{L}{d_h}\sum_{j=1}^{150}\left(f'_{in,j} \cdot j^3\right) + 0{,}37\sum_{j=1}^{150} j\right\}$$

$$(\Delta p \cdot \dot{V})_{tot} = 8 \cdot \frac{\rho}{\pi^2} \cdot \frac{1}{d_h^4} \cdot \left(\frac{\dot{V}_{in,1}}{150}\right)^3 \left\{\frac{L}{d_h}\sum_{j=1}^{150}\left(f'_{in,j} \cdot j^3\right) + 0{,}37 \cdot \frac{150 \cdot 151}{2}\right\}$$

$$(E_{p,header})_{tot} = \frac{8}{e_{pump}} \cdot \frac{\rho}{\pi^2} \cdot \frac{1}{d_h^4} \cdot \left(\frac{\dot{V}_{in,1}}{150}\right)^3 \left\{\frac{L}{d_h}\sum_{j=1}^{150}\left(f'_{in,j} \cdot j^3\right) + 0{,}37 \cdot \frac{150 \cdot 151}{2}\right\}$$

Appendix 7: ClimaCheck processed data

Due to the considerable amount of data, only a short period of time is displayed here for Järfälla's ice rink.

Time	Temp. After comp. °C	Temp. Before comp. °C	Temp. exp. valve °C	Sec.F. entering evap. °C	Sec.F. leaving evap °C	Sec.F. temp. diff. evap. K	Average temp. of sec.F. °C	MTD between ice & sec.F. K	LMTD between ice & sec.F. K
16:36:55	91,3	-8,7	22,3	-6,1	-7,2	1,1	-6,45	1,65	1,53
16:37:55	90,1	-9	22,5	-6,3	-7,4	1,1	-6,55	1,75	1,60
16:38:55	90,7	-9,3	22,8	-6,3	-7,5	1,2	-6,6	1,8	1,64
16:40:08	91,9	-9,6	23,4	-6,3	-7,5	1,2	-6,6	1,8	1,64
16:40:55	93,1	-9,7	23,8	-6,3	-7,5	1,2	-6,6	1,8	1,64
16:41:55	94,4	-9,9	24,1	-6,3	-7,6	1,3	-6,7	1,9	1,75
16:42:55	96,3	-10,5	24,3	-6,5	-7,9	1,4	-6,85	2,05	1,86
16:43:55	97,9	-10,9	24,8	-6,6	-8	1,4	-6,9	2,1	1,89
16:45:09	98,9	-11,1	25,1	-6,6	-8	1,4	-6,9	2,1	1,89
16:45:55	99,5	-11,4	25,1	-6,7	-8,1	1,4	-6,95	2,15	1,93
16:46:55	99,8	-11,6	25,1	-6,7	-8,2	1,5	-7,05	2,25	2,04
16:47:55	100	-11,7	25	-6,8	-8,2	1,4	-7,05	2,25	2,04
16:48:55	99,2	-10,4	24,3	-6,7	-7,8	1,1	-6,9	2,1	1,96
16:50:09	98,5	-9,9	23,7	-6,5	-7,4	0,9	-6,7	1,9	1,81
16:50:55	97,6	-9,6	22,9	-6,4	-7,3	0,9	-6,65	1,75	1,67
16:51:55	96,4	-9,6	20,7	-6,4	-7,3	0,9	-6,7	1,8	1,73
16:52:55	95,4	-9,4	21	-6,4	-7,3	0,9	-6,7	1,8	1,73
16:53:55	94,6	-9,4	21,4	-6,4	-7,2	0,8	-6,6	1,7	1,63
16:55:08	94,2	-9,4	21,6	-6,3	-7,2	0,9	-6,6	1,7	1,63
16:55:55	94	-9,4	21,8	-6,3	-7,2	0,9	-6,55	1,65	1,56
16:56:55	94	-9,4	22,1	-6,3	-7,2	0,9	-6,55	1,65	1,56
16:57:55	93,9	-9,3	22,3	-6,3	-7,2	0,9	-6,55	1,65	1,56
16:58:55	93,6	-9,2	22,5	-6,3	-7,2	0,9	-6,55	1,65	1,56
17:00:09	93,2	-9,1	22,5	-6,3	-7,2	0,9	-6,55	1,65	1,56
17:00:55	92,8	-9	22,5	-6,3	-7,2	0,9	-6,55	1,65	1,56
17:01:55	92,6	-9	21,9	-6,3	-7,2	0,9	-6,55	1,65	1,56
17:02:55	92,5	-8,9	22,1	-6,2	-7,1	0,9	-6,5	1,6	1,52
17:03:55	92,6	-8,8	22	-6,2	-7,1	0,9	-6,5	1,6	1,52
17:05:09	92,9	-8,7	22,1	-6,2	-7,1	0,9	-6,5	1,6	1,52
17:05:55	93	-8,7	22,3	-6,2	-7,1	0,9	-6,5	1,6	1,52

Time	Sec.F. return indoor ice rink °C	Sec.F. return outdoor ice rink °C	Outdoor temp. °C	Abs. pressure after comp. kPa	Abs. pressure before comp. kPa	Power of 1st compressor kW	Energy used for compressor 1 kWh
16:36:55	-5,7	0	5,1	936,4	281	59,93	320695,8
16:37:55	-5,7	0	5	951,8	278,4	60,31	320696,8
16:38:55	-5,7	0,1	5	960,9	278,3	60,61	320697,8
16:40:08	-5,7	0,1	5,1	969,4	278,6	60,83	320698,9
16:40:55	-5,7	0,1	5,1	975,5	278,5	61,14	320699,9
16:41:55	-5,8	0,1	5,1	1014,6	266,1	79,38	320701
16:42:55	-5,8	0,1	5	999,7	262,2	78,43	320702,3
16:43:55	-5,8	0,1	5,3	995,3	264,4	78,92	320703,6
16:45:09	-5,8	0,1	5,4	992,6	263,5	78,66	320704,9
16:45:55	-5,8	0,1	5,2	986,2	258,1	78,54	320706,2
16:46:55	-5,9	0,1	5,1	984	264,3	78,08	320707,5
16:47:55	-5,9	0,2	5,1	950,4	267,6	60,23	320708,8
16:48:55	-6	0,2	5,1	884,3	292,2	41,97	320709,6
16:50:09	-6	0,2	5,1	858,1	296,1	41,22	320710,3
16:50:55	-6	0,2	5	848,7	297,1	40,85	320711
16:51:55	-6,1	0,2	5,2	855,6	298,9	41,01	320711,7
16:52:55	-6,1	0,2	5,3	881,8	301,3	41,88	320712,4
16:53:55	-6	0,2	5,1	898,6	301,7	42,53	320713,1
16:55:08	-6	0,2	5	910,5	300,3	42,64	320713,8
16:55:55	-5,9	0,2	5	920,7	298,9	43	320714,5
16:56:55	-5,9	0,1	5	904,7	298,5	42,53	320715,2
16:57:55	-5,9	0,1	5	873,5	297,9	41,66	320715,9
16:58:55	-5,9	0,1	4,9	856,7	297,1	41,18	320716,6
17:00:09	-5,9	0,1	4,8	846,5	296,5	40,84	320717,3
17:00:55	-5,9	0,1	4,8	880,2	293	41,68	320718
17:01:55	-5,9	0,1	4,8	899,2	299,8	42,26	320718,7
17:02:55	-5,9	0,1	4,8	910,7	300,1	42,77	320719,4
17:03:55	-5,9	0,1	4,9	920,1	299,5	42,99	320720,1
17:05:09	-5,9	0,1	4,9	912,4	298,9	43,04	320720,8
17:05:55	-5,9	0,1	4,9	874,6	294,9	41,65	320721,5

Time	Power of 2nd comp. kW	Energy used for comp. 2 kWh	Power of 3rd comp. kW	Energy used for comp. 3 kWh	Total comp. power kW	Total energy used by comp. kWh	Temp.out of 1st comp. °C	After cooling oil temp. °C
16:36:55	0	1589,8	0	0	59,93	322285,6	90,5	24,5
16:37:55	0	1589,8	0	0	60,31	322286,6	93,3	26
16:38:55	0	1589,8	0	0	60,61	322287,6	96,4	25,5
16:40:08	0	1589,8	0	0	60,83	322288,7	98,1	26,2
16:40:55	0	1589,8	0	0	61,14	322289,7	99,3	27,2
16:41:55	0	1589,8	0	0	79,38	322290,8	100,3	27,5
16:42:55	0	1589,8	0	0	78,43	322292,1	102,9	28
16:43:55	0	1589,8	0	0	78,92	322293,4	103,9	28,9
16:45:09	0	1589,8	0	0	78,66	322294,7	104,2	29,3
16:45:55	0	1589,8	0	0	78,54	322296	104,6	25,4
16:46:55	0	1589,8	0	0	78,08	322297,3	104,6	23,5
16:47:55	0	1589,8	0	0	60,23	322298,6	104,4	27
16:48:55	0	1589,8	0	0	41,97	322299,4	103,7	28,1
16:50:09	0	1589,8	0	0	41,22	322300,1	102,4	27,1
16:50:55	0	1589,8	0	0	40,85	322300,8	100,2	27,6
16:51:55	0	1589,8	0	0	41,01	322301,5	98,5	28,4
16:52:55	0	1589,8	0	0	41,88	322302,2	97,8	28
16:53:55	0	1589,8	0	0	42,53	322302,9	97,9	23,1
16:55:08	0	1589,8	0	0	42,64	322303,6	98,3	22,5
16:55:55	0	1589,8	0	0	43,00	322304,3	98,7	25,8
16:56:55	0	1589,8	0	0	42,53	322305	99,3	25,9
16:57:55	0	1589,8	0	0	41,66	322305,7	98,8	25,3
16:58:55	0	1589,8	0	0	41,18	322306,4	97,7	26,1
17:00:09	0	1589,8	0	0	40,84	322307,1	96,8	26,7
17:00:55	0	1589,8	0	0	41,68	322307,8	96,4	26,9
17:01:55	0	1589,8	0	0	42,26	322308,5	96,9	27,1
17:02:55	0	1589,8	0	0	42,77	322309,2	97,4	27,5
17:03:55	0	1589,8	0	0	42,99	322309,9	98	27,9
17:05:09	0	1589,8	0	0	43,04	322310,6	98,7	24,9
17:05:55	0	1589,8	0	0	41,65	322311,3	98,3	21,6

Time	Before cooling oil temp. °C	Temp.out of 2nd comp. °C	Ice temperature °C	Temp. over ice °C	RH over ice %	Indoor temperature °C	RH indoor %
16:36:55	23,8	15,1	-4,8	1	90	5,8	67
16:37:55	22,5	15,1	-4,8	1	90	5,8	67
16:38:55	22,1	15,1	-4,8	1	90	5,8	67
16:40:08	23,7	15,2	-4,8	1	89	5,8	67
16:40:55	24,3	15,2	-4,8	1	89	5,9	67
16:41:55	24,2	15,2	-4,8	1	89	5,9	67
16:42:55	25,1	15,2	-4,8	1	89	5,9	67
16:43:55	25,9	15,2	-4,8	1,1	89	5,8	67
16:45:09	23,5	15,2	-4,8	1,1	89	5,9	67
16:45:55	17	15,2	-4,8	1	89	5,8	67
16:46:55	20,7	15,2	-4,8	1	89	5,8	67
16:47:55	25	15,2	-4,8	1,1	89	5,8	67
16:48:55	23,5	15,2	-4,8	1,1	89	5,8	67
16:50:09	23,6	15,2	-4,8	1,1	89	5,8	67
16:50:55	25,5	15,2	-4,9	1,1	89	5,9	67
16:51:55	26,1	15,2	-4,9	1,1	89	5,8	67
16:52:55	21,2	15,3	-4,9	1,1	89	5,8	67
16:53:55	16,3	15,2	-4,9	1,1	88	5,8	67
16:55:08	21,8	15,3	-4,9	1,1	88	5,8	66
16:55:55	24,1	15,3	-4,9	1,1	88	5,8	66
16:56:55	22,1	15,3	-4,9	1,1	88	5,9	66
16:57:55	22,8	15,3	-4,9	1,1	88	5,8	66
16:58:55	24,2	15,3	-4,9	1,1	88	5,9	66
17:00:09	24,6	15,3	-4,9	1,1	88	5,8	66
17:00:55	24,6	15,3	-4,9	1,1	88	5,8	66
17:01:55	25,1	15,3	-4,9	1,1	88	5,8	66
17:02:55	25,5	15,3	-4,9	1,1	88	5,8	66
17:03:55	25,1	15,3	-4,9	1,1	88	5,8	66
17:05:09	17,6	15,3	-4,9	1,1	88	5,8	66
17:05:55	18,6	15,3	-4,9	1,1	88	5,8	66

Time	Evap. temp. °C	Cond. temp. °C	Evap.-Cond. temp. diff. K	Oil cap. cool. kW	COP cool -	Cool. cap. kW	COP heat -	Heat. cap. kW	Super-heating K	Sub-cooling K
16:36:55	-10,83	22,78	33,61	0,56	5,07	303,6	5,99	358,78	2,13	0,48
16:37:55	-11,06	23,3	34,36	2,79	4,93	297,21	5,81	350,51	2,06	0,8
16:38:55	-11,07	23,61	34,68	2,71	4,88	295,9	5,77	349,56	1,77	0,81
16:40:08	-11,04	23,89	34,93	1,99	4,85	295,11	5,75	349,69	1,44	0,49
16:40:55	-11,05	24,09	35,14	2,31	4,75	290,27	5,64	344,82	1,35	0,29
16:41:55	-12,16	25,37	37,53	2,63	4,75	376,8	5,64	448	2,26	1,27
16:42:55	-12,51	24,89	37,4	2,31	4,62	362,6	5,52	433,23	2,01	0,59
16:43:55	-12,31	24,74	37,05	2,39	0	0	0,99	78,41	1,41	-0,06
16:45:09	-12,39	24,65	37,04	4,62	4,3	338,2	5,17	406,74	1,29	-0,45
16:45:55	-12,89	24,45	37,34	6,69	4,14	325,1	4,98	391,46	1,49	-0,65
16:46:55	-12,32	24,37	36,69	2,23	0	0	0,99	77,61	0,72	-0,73
16:47:55	-12,02	23,26	35,28	1,59	4,36	262,8	5,27	317,22	0,32	-1,74
16:48:55	-9,87	20,97	30,84	3,66	4,15	174,21	4,99	209,59	-0,53	-3,33
16:50:09	-9,55	20,02	29,57	2,79	4,29	176,79	5,15	212,34	-0,35	-3,68
16:50:55	-9,46	19,68	29,14	1,67	4,47	182,45	5,36	218,77	-0,14	-3,22
16:51:55	-9,32	19,93	29,25	1,83	0	0	0,99	40,69	-0,28	-0,77
16:52:55	-9,12	20,88	30	5,41	0	0	0,9	37,53	-0,28	-0,12
16:53:55	-9,08	21,47	30,55	5,41	4,18	177,58	4,98	211,72	-0,32	0,07
16:55:08	-9,2	21,89	31,09	0,56	4,79	204,32	5,71	243,41	-0,2	0,29
16:55:55	-9,32	22,24	31,56	1,35	4,71	202,35	5,6	240,98	-0,08	0,44
16:56:55	-9,35	21,69	31,04	3,03	0	0	0,96	40,88	-0,05	-0,41
16:57:55	-9,4	20,58	29,98	1,99	4,61	192,21	5,5	228,96	0,1	-1,72
16:58:55	-9,46	19,97	29,43	1,51	4,7	193,36	5,59	230,14	0,26	-2,53
17:00:09	-9,51	19,6	29,11	1,67	0	0	1	40,92	0,41	-2,9
17:00:55	-9,81	20,82	30,63	1,83	0	0	1	41,5	0,81	-1,68
17:01:55	-9,24	21,49	30,73	1,59	0	0	1	42,31	0,24	-0,41
17:02:55	-9,22	21,9	31,12	1,59	4,76	203,76	5,66	241,95	0,32	-0,2
17:03:55	-9,27	22,22	31,49	2,23	4,69	201,77	5,57	239,52	0,47	0,22
17:05:09	-9,32	21,96	31,28	5,81	0	0	0,89	38,32	0,62	-0,14
17:05:55	-9,65	20,62	30,27	2,39	0	0	0,98	40,85	0,95	-1,68

Time	LMTD Tevap & sec.F. K	MTD between Tevap & sec.F. K	Absolute resistance of evap. K.W^{-1}	Transfer coefficient in the evap. W.K^{-1}	LTMD between sec.F. & ice K	Heat rate at which ice is cooled down kW
16:36:55	4,16	4,18	1,37E-05	73055,14	1,529318172	303,6
16:37:55	4,19	4,21	1,41E-05	71001,99	1,602455398	297,21
16:38:55	4,14	4,17	1,40E-05	71455,09	1,638430608	295,9
16:40:08	4,11	4,14	1,39E-05	71788,07	1,638430608	295,11
16:40:55	4,12	4,15	1,42E-05	70438,13	1,638430608	290,27
16:41:55	5,18	5,21	1,38E-05	72701,24	1,748218779	376,8
16:42:55	5,28	5,31	1,46E-05	68685,99	1,856104013	362,6
16:43:55	4,98	5,01	-	-	1,891414236	0
16:45:09	5,06	5,09	1,50E-05	66867,71	1,891414236	338,2
16:45:55	5,46	5,49	1,68E-05	59540,83	1,926423248	325,1
16:46:55	4,83	4,87	-	-	2,038166436	0
16:47:55	4,48	4,52	1,71E-05	58613,22	2,038166436	262,8
16:48:55	2,58	2,62	1,48E-05	67495,76	1,964442002	174,21
16:50:09	2,57	2,60	1,46E-05	68687,58	1,81068069	176,79
16:50:55	2,58	2,61	1,42E-05	70609,51	1,666327937	182,45
16:51:55	2,44	2,47	-	-	1,731234049	0
16:52:55	2,24	2,27	-	-	1,731234049	0
16:53:55	2,26	2,28	1,27E-05	78700,13	1,626900379	177,58
16:55:08	2,42	2,45	1,19E-05	84353,18	1,626900379	204,32
16:55:55	2,54	2,57	1,26E-05	79555,19	1,560794526	202,35
16:56:55	2,57	2,60	-	-	1,560794526	0
16:57:55	2,62	2,65	1,37E-05	73241,57	1,560794526	192,21
16:58:55	2,68	2,71	1,39E-05	72017,41	1,560794526	193,36
17:00:09	2,74	2,76	-	-	1,560794526	0
17:00:55	3,04	3,06	-	-	1,560794526	0
17:01:55	2,46	2,49	-	-	1,560794526	0
17:02:55	2,54	2,57	1,25E-05	80109,54	1,521959284	203,76
17:03:55	2,59	2,62	1,29E-05	77782,42	1,521959284	201,77
17:05:09	2,64	2,67	-	-	1,521959284	0
17:05:55	2,98	3,00	-	-	1,521959284	0

Appendix 7: ClimaCheck processed data

Time	Pumping power for rink floor kW	Secondary fluid thermal conductivity $W.m^{-1}.K^{-1}$	Secondary fluid viscosity mPa.s	Secondary fluid density $kg.m^{-3}$	Secondary fluid specific heat capacity $J.kg^{-1}.K^{-1}$	Secondary fluid volume flow $m^3.h^{-1}$
16:36:55	18,16	0,4916	4,7894	1234,6	2823,1	197,417756
16:37:55	18,16	0,4914	4,7984	1234,7	2822,8	197,374386
16:38:55	18,16	0,4913	4,8029	1234,7	2822,7	197,352764
16:40:08	18,16	0,4913	4,8029	1234,7	2822,7	197,352764
16:40:55	18,16	0,4913	4,8029	1234,7	2822,7	197,352764
16:41:55	18,16	0,4911	4,8119	1234,7	2822,4	197,309646
16:42:55	18,16	0,4908	4,8254	1234,8	2822,0	197,245284
16:43:55	18,16	0,4907	4,8299	1234,8	2821,8	-
16:45:09	18,16	0,4907	4,8299	1234,8	2821,8	197,223914
16:45:55	18,16	0,4905	4,8343	1234,8	2821,7	197,202586
16:46:55	18,16	0,4903	4,8433	1234,8	2821,4	-
16:47:55	18,16	0,4903	4,8433	1234,8	2821,4	197,160056
16:48:55	18,16	0,4907	4,8299	1234,8	2821,8	197,223914
16:50:09	18,16	0,4911	4,8119	1234,7	2822,4	197,309646
16:50:55	18,16	0,4912	4,8074	1234,7	2822,5	197,331184
16:51:55	18,16	0,4911	4,8119	1234,7	2822,4	-
16:52:55	18,16	0,4911	4,8119	1234,7	2822,4	-
16:53:55	18,16	0,4913	4,8029	1234,7	2822,7	197,352764
16:55:08	18,16	0,4913	4,8029	1234,7	2822,7	197,352764
16:55:55	18,16	0,4914	4,7984	1234,7	2822,8	197,374386
16:56:55	18,16	0,4914	4,7984	1234,7	2822,8	-
16:57:55	18,16	0,4914	4,7984	1234,7	2822,8	197,374386
16:58:55	18,16	0,4914	4,7984	1234,7	2822,8	197,374386
17:00:09	18,16	0,4914	4,7984	1234,7	2822,8	-
17:00:55	18,16	0,4914	4,7984	1234,7	2822,8	-
17:01:55	18,16	0,4914	4,7984	1234,7	2822,8	-
17:02:55	18,16	0,4915	4,7939	1234,6	2822,9	197,39605
17:03:55	18,16	0,4915	4,7939	1234,6	2822,9	197,39605
17:05:09	18,16	0,4915	4,7939	1234,6	2822,9	-
17:05:55	18,16	0,4915	4,7939	1234,6	2822,9	-

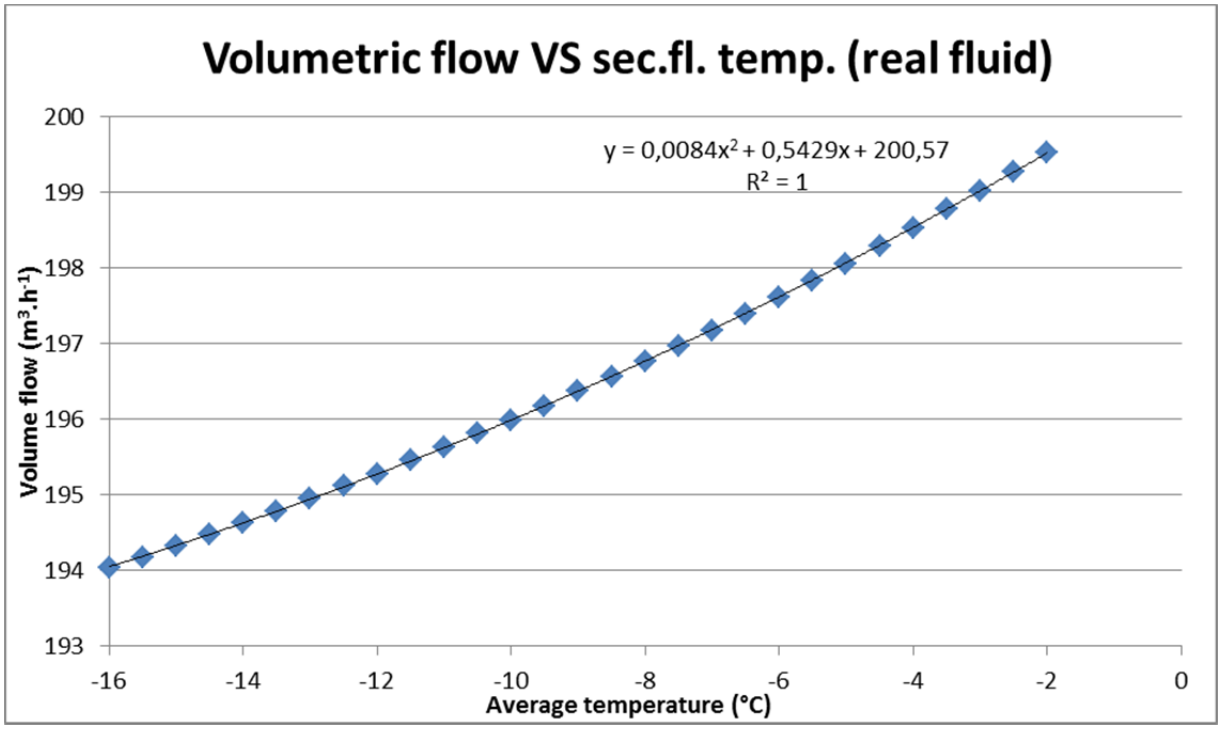
Volumetric flow VS sec.fl. temp. (real fluid)
y = 0,0084x² + 0,5429x + 200,57
R² = 1
Volume flow (m³.h⁻¹)
200
199
198
197
196
195
194
193
-16
-14
-12
-10
-8
-6
-4
-2
0
Average temperature (°C)

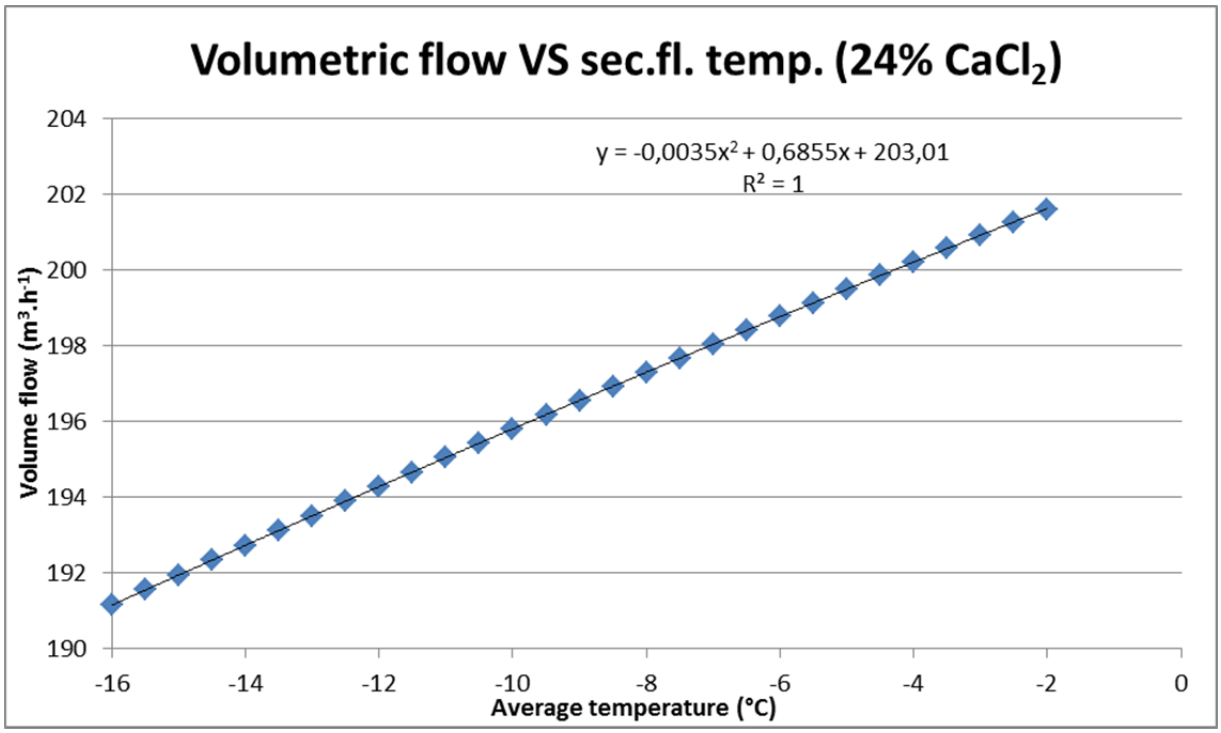
Volumetric flow VS sec.fl. temp. (24% CaCl2)
y = -0,0035x² + 0,6855x + 203,01
R² = 1
Volume flow (m³.h⁻¹)
204
202
200
198
196
194
192
190
-16
-14
-12
-10
-8
-6
-4
-2
0
Average temperature (°C)

Charts for Järfälla ice rink

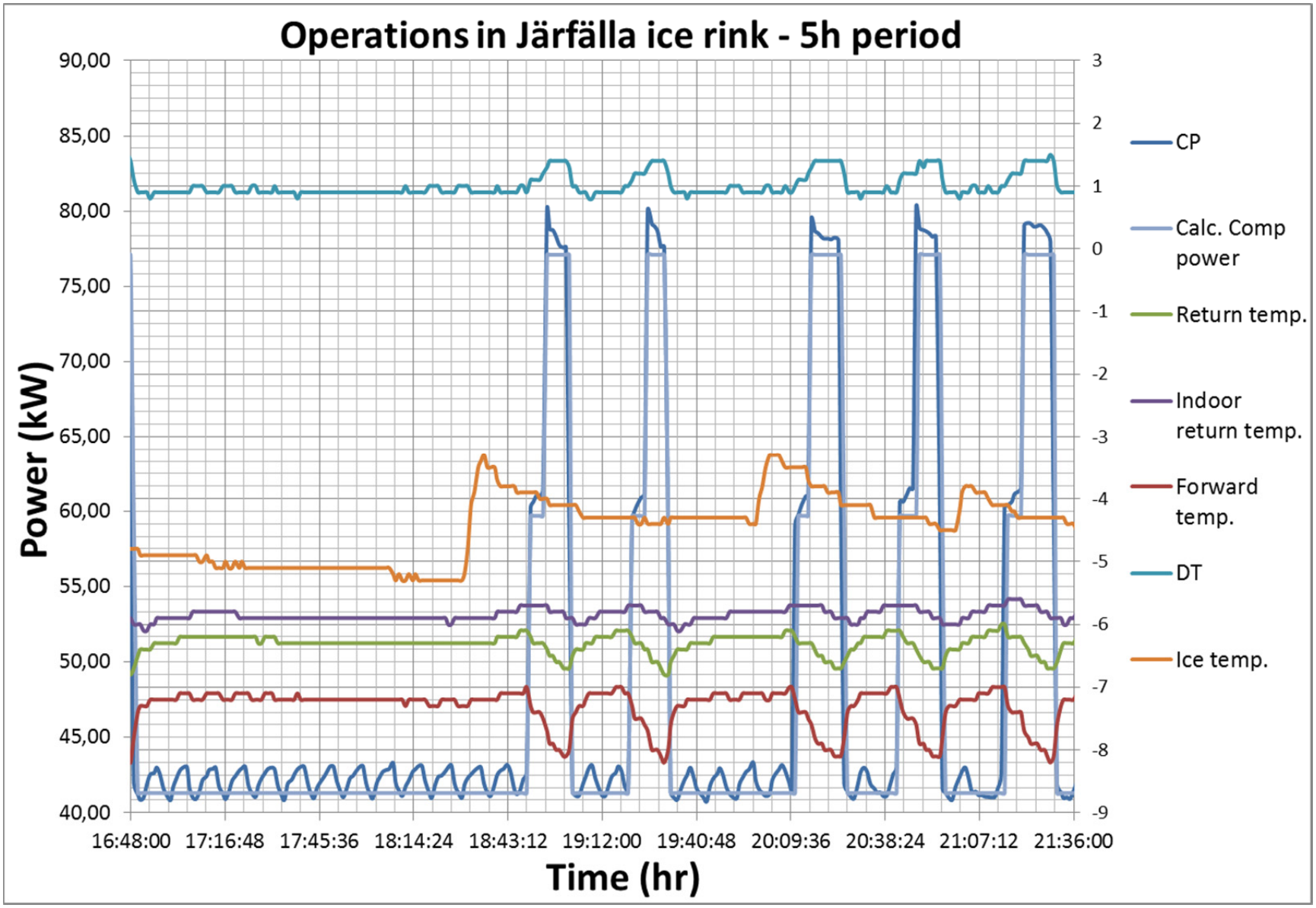
Operations in Järfälla ice rink - 5h period
Power (kW)
90,00
85,00
80,00
75,00
70,00
65,00
60,00
55,00
50,00
45,00
40,00
3
2
1
0
-1
-2
-3
-4
-5
-6
-7
-8
-9
16:48:00
17:16:48
17:45:36
18:14:24
18:43:12
19:12:00
19:40:48
20:09:36
20:38:24
21:07:12
21:36:00
Time (hr)
CP
Calc. Comp power
Return temp.
Indoor return temp.
Forward temp.
DT
Ice temp.

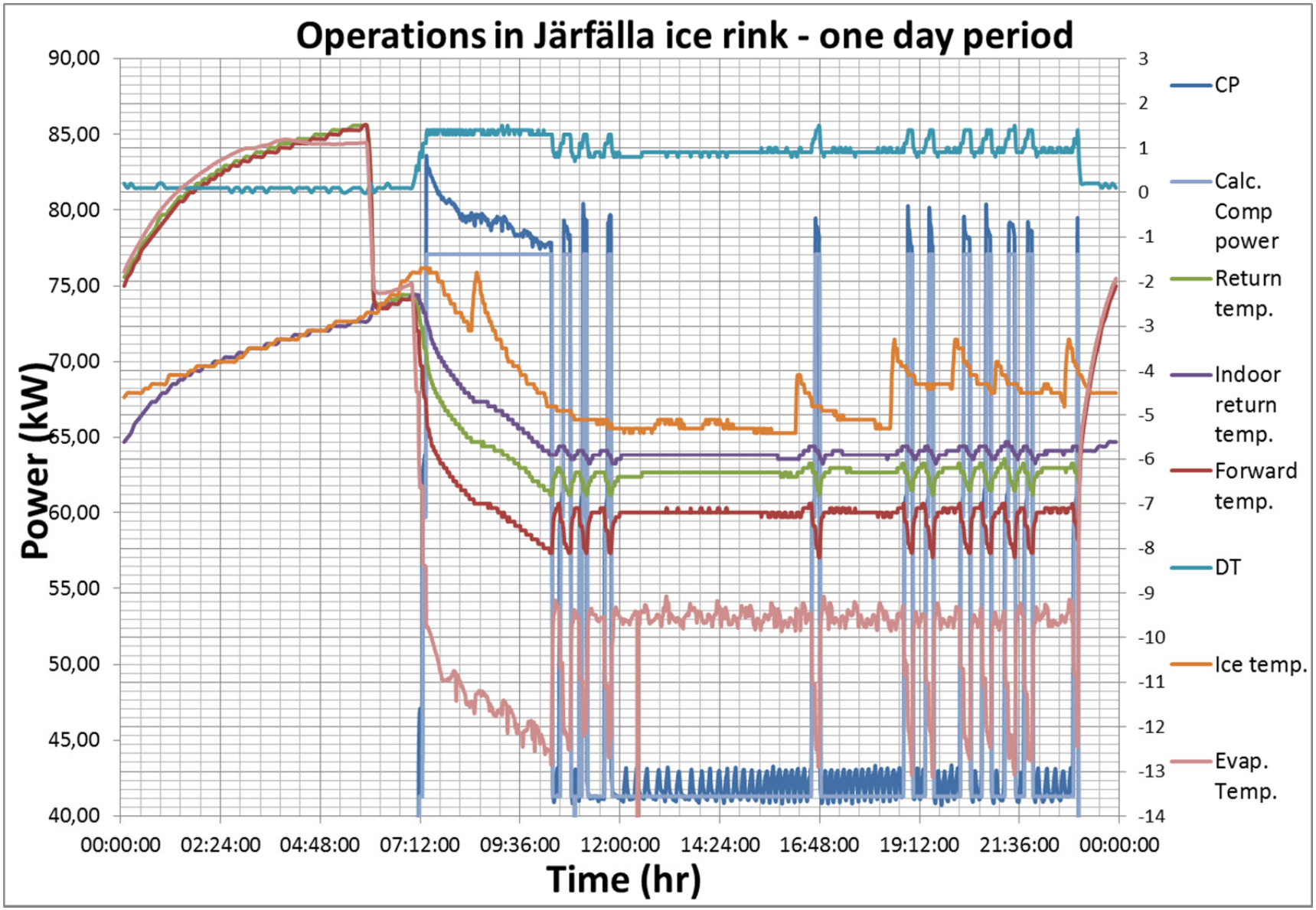
Operations in Järfälla ice rink - one day period
Power (kW)
90,00
85,00
80,00
75,00
70,00
65,00
60,00
55,00
50,00
45,00
40,00
3
2
1
0
-1
-2
-3
-4
-5
-6
-7
-8
-9
-10
-11
-12
-13
-14
00:00:00
02:24:00
04:48:00
07:12:00
09:36:00
12:00:00
14:24:00
16:48:00
19:12:00
21:36:00
00:00:00
Time (hr)
CP
Calc. Comp power
Return temp.
Indoor return temp.
Forward temp.
DT
Ice temp.
Evap. Temp.

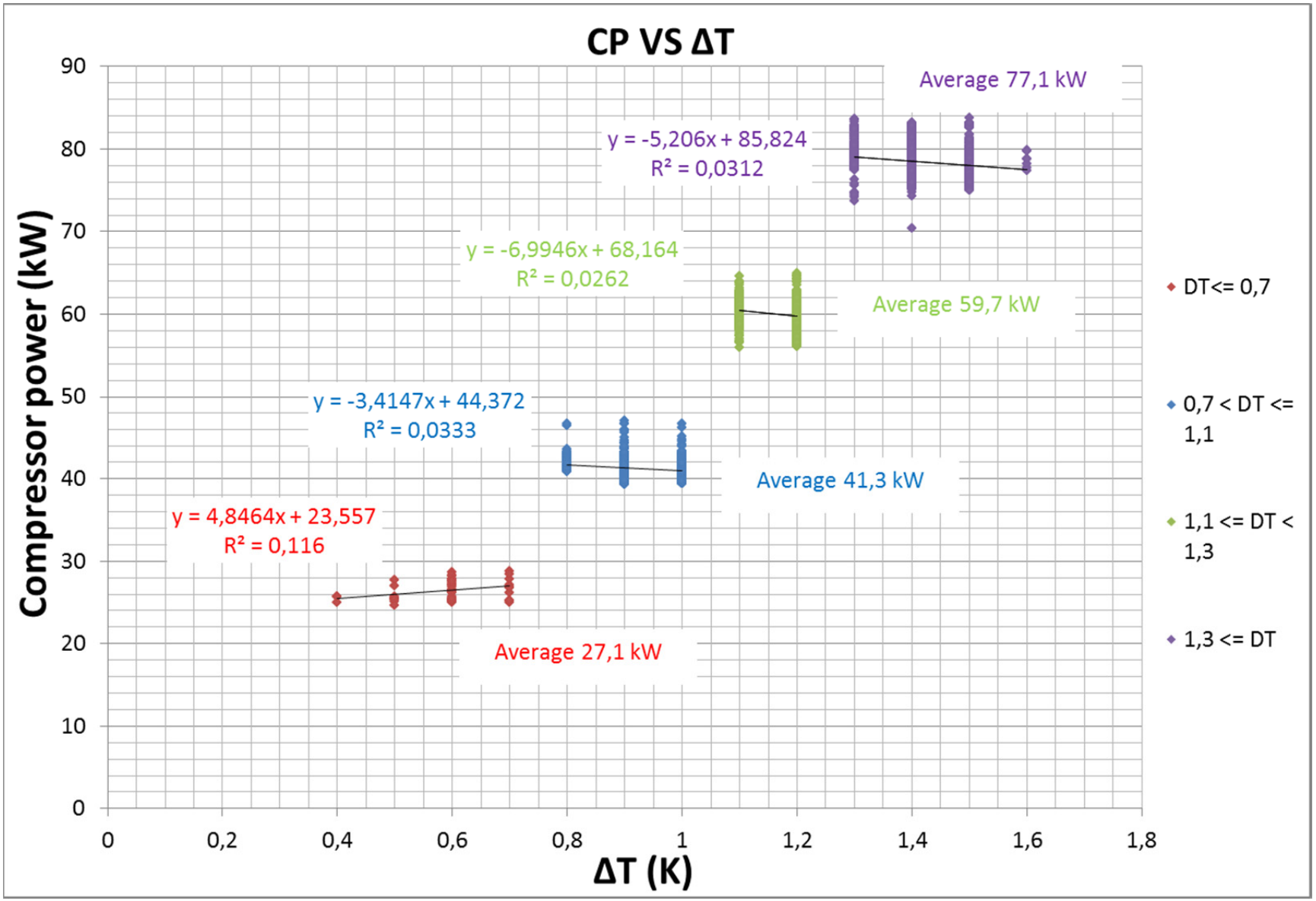
CP VS ΔT
Compressor power (kW)
ΔT (K)
Average 77,1 kW
y = -5,206x + 85,824
R² = 0,0312
y = -6,9946x + 68,164
R² = 0,0262
Average 59,7 kW
y = -3,4147x + 44,372
R² = 0,0333
Average 41,3 kW
y = 4,8464x + 23,557
R² = 0,116
Average 27,1 kW
DT<= 0,7
0,7 < DT <= 1,1
1,1 <= DT < 1,3
1,3 <= DT

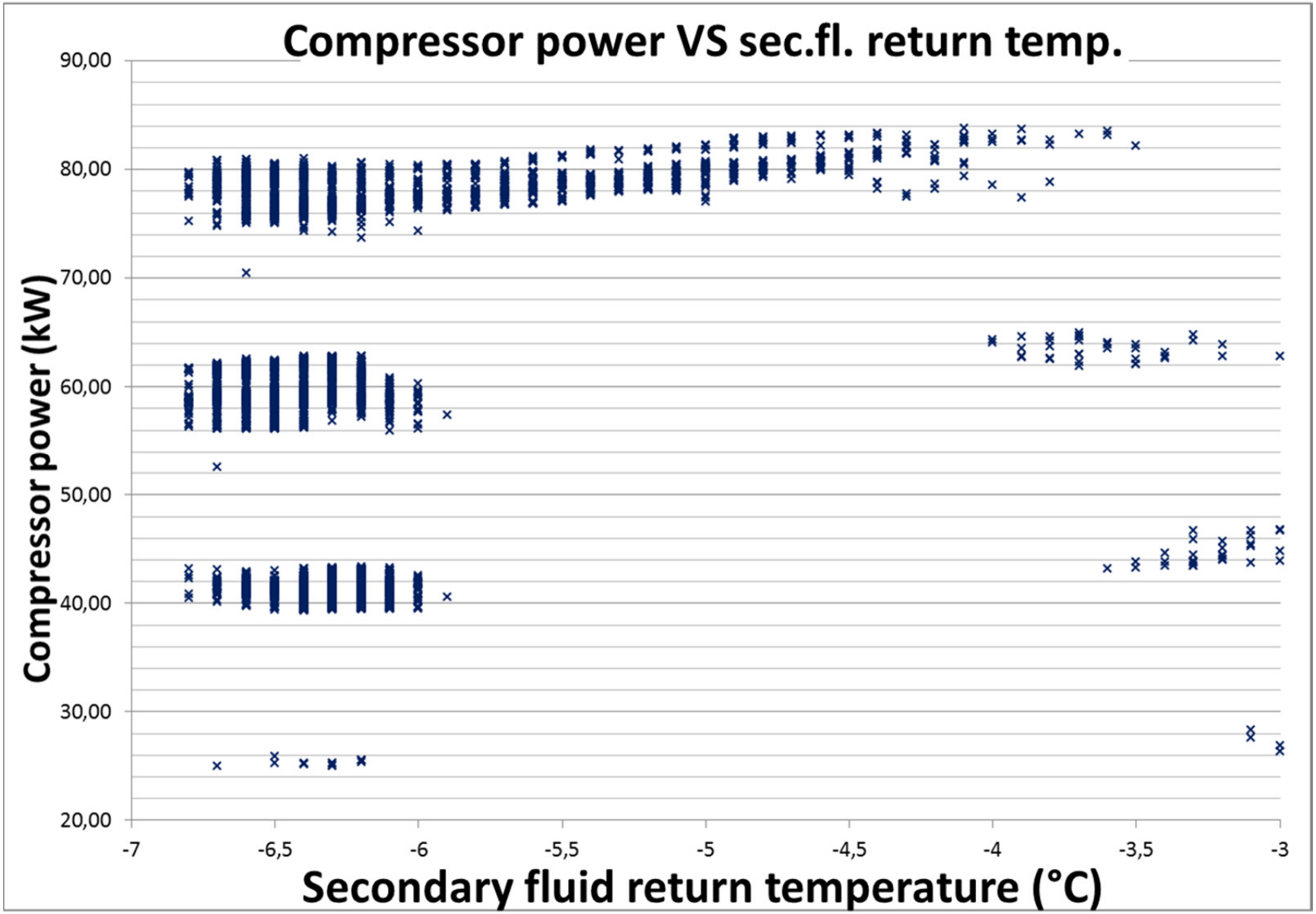
Compressor power VS sec.fl. return temp.
90,00
80,00
70,00
60,00
50,00
40,00
30,00
20,00
Compressor power (kW)
-7
-6,5
-6
-5,5
-5
-4,5
-4
-3,5
-3
Secondary fluid return temperature (°C)

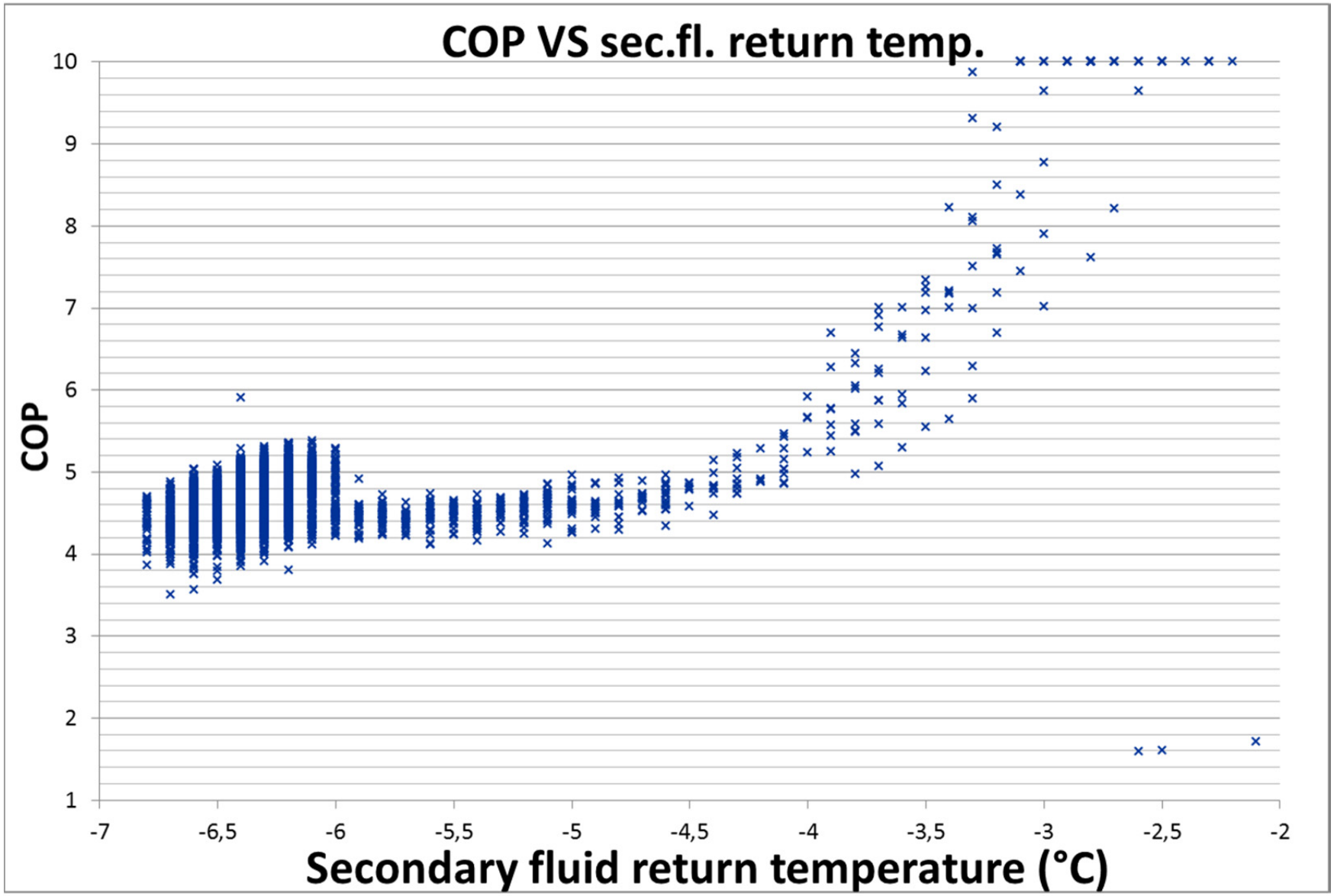
COP VS sec.fl. return temp.
COP
10
9
8
7
6
5
4
3
2
1
-7
-6,5
-6
-5,5
-5
-4,5
-4
-3,5
-3
-2,5
-2
Secondary fluid return temperature (°C)

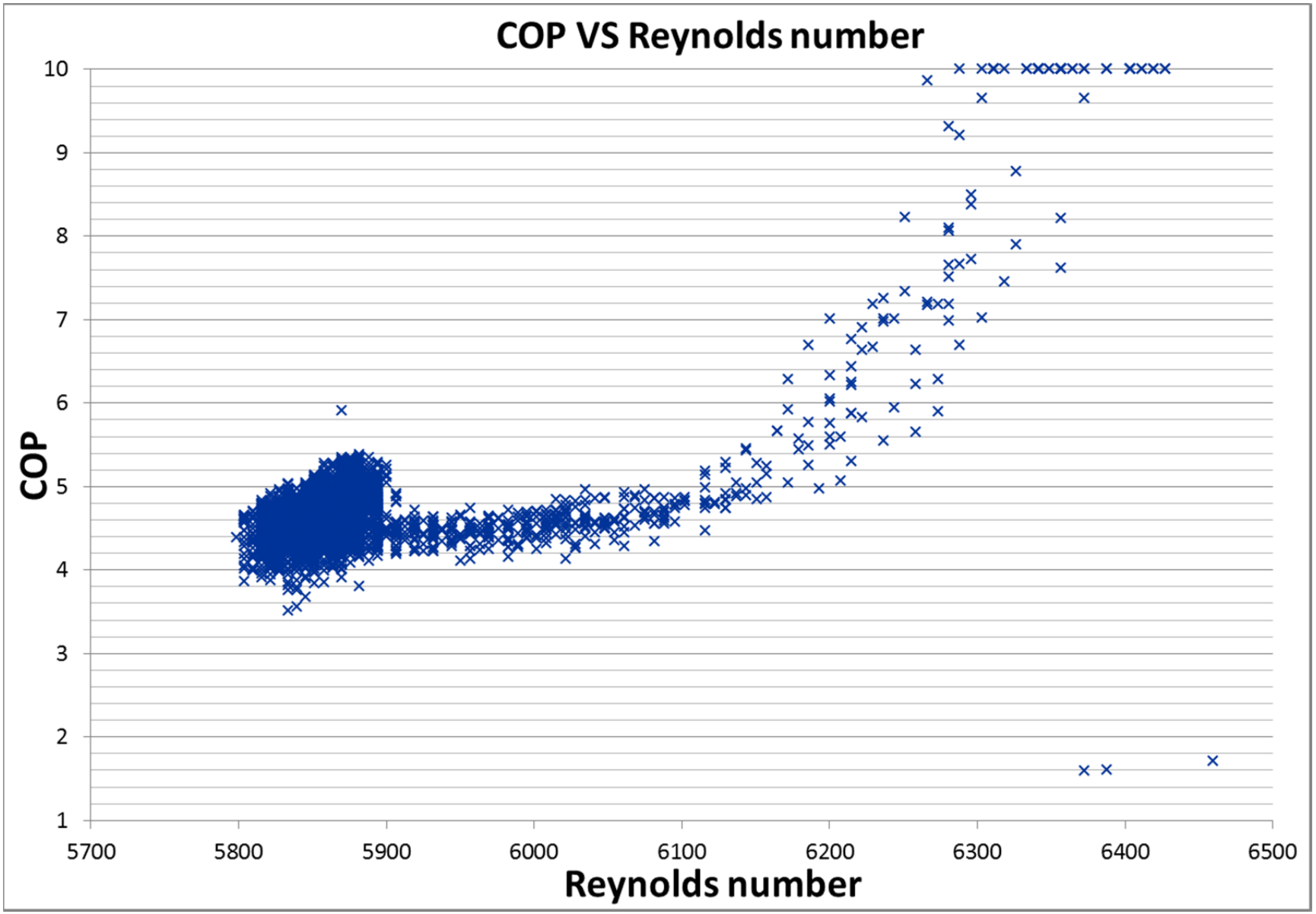
COP VS Reynolds number
COP
Reynolds number
10
9
8
7
6
5
4
3
2
1
5700
5800
5900
6000
6100
6200
6300
6400
6500

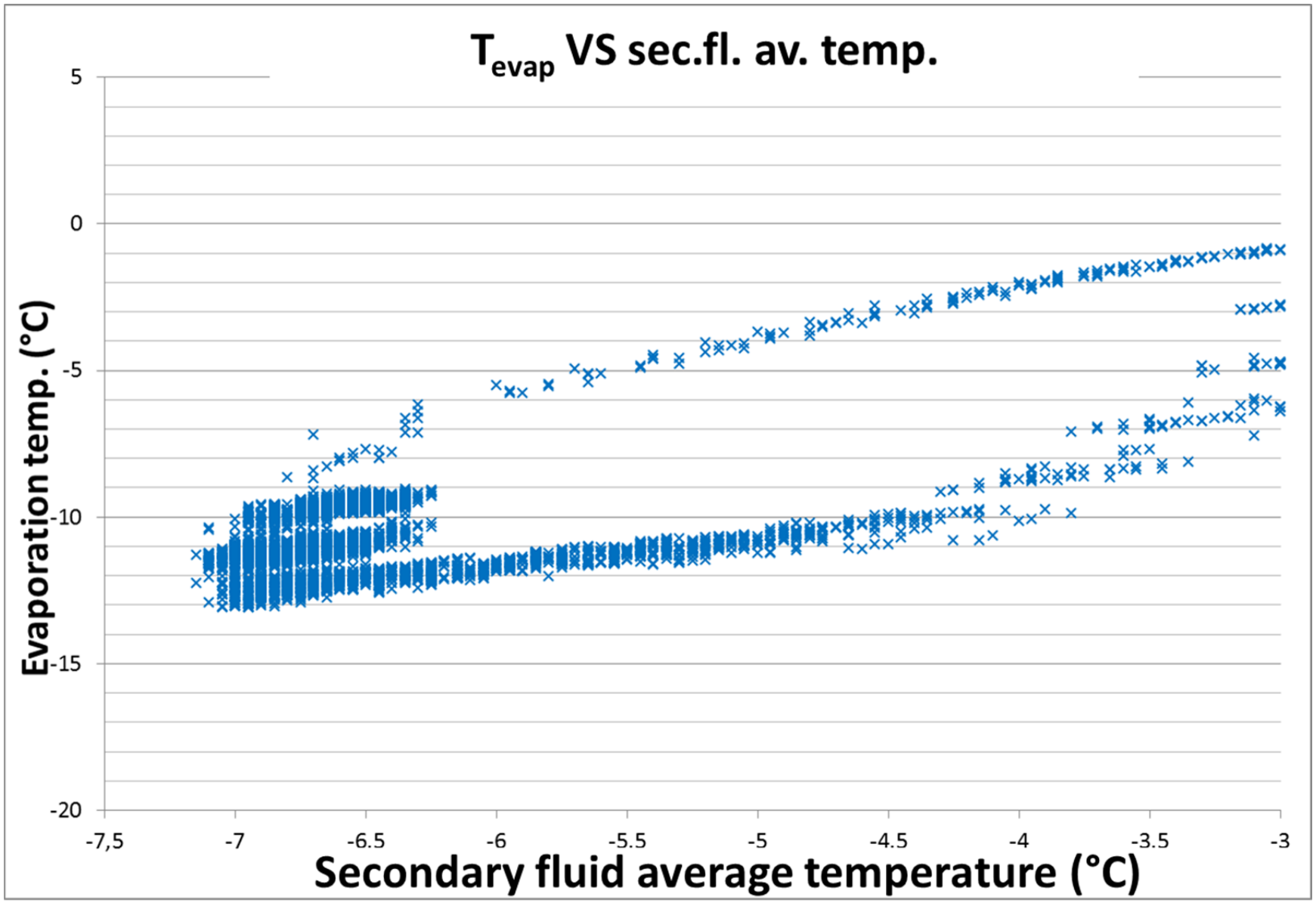
T_{evap} VS sec.fl. av. temp.
Evaporation temp. (°C)
5
0
-5
-10
-15
-20
-7,5
-7
-6.5
-6
-5.5
-5
-4.5
-4
-3.5
-3
Secondary fluid average temperature (°C)

Charts for Nacka ice rink

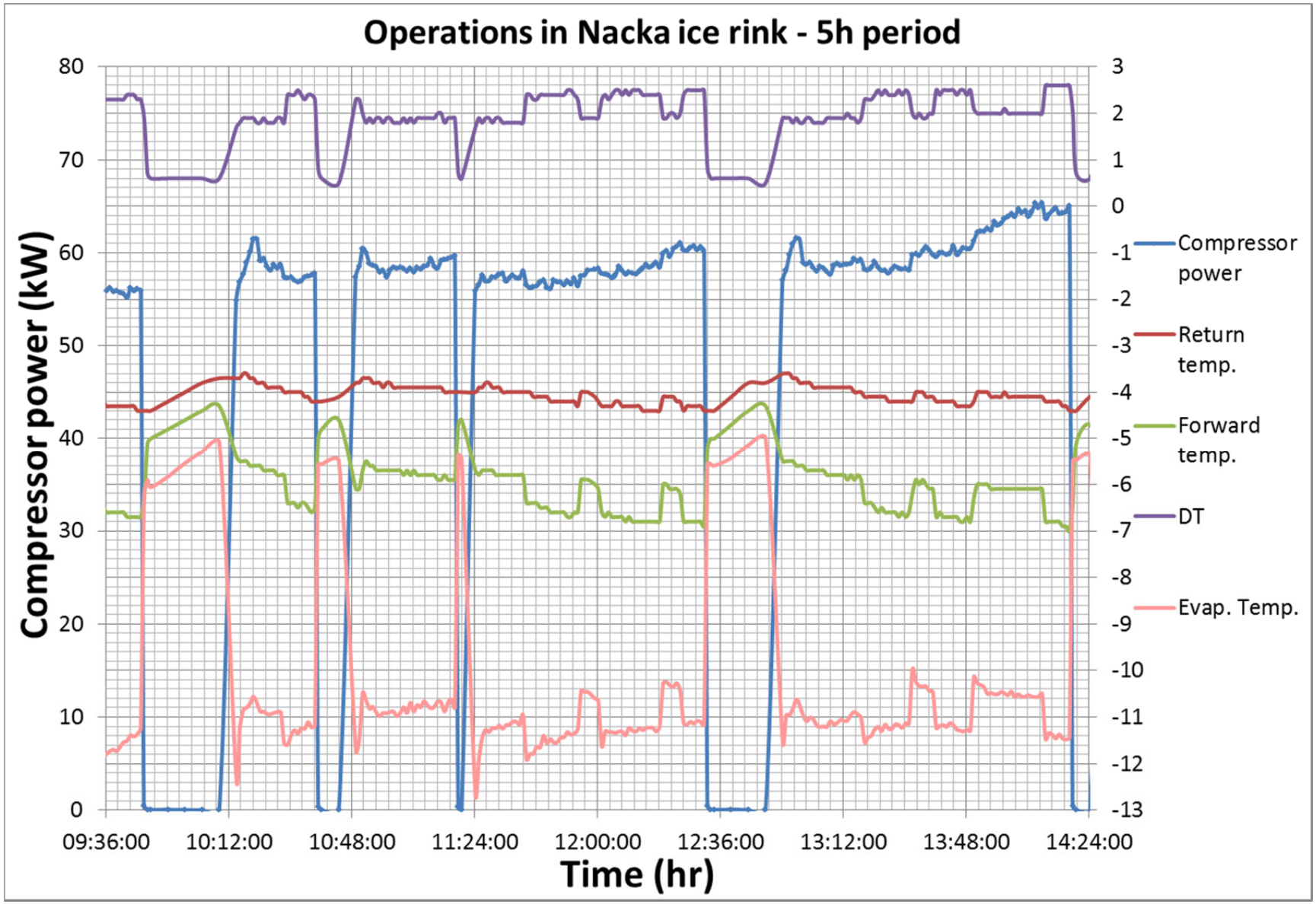
Operations in Nacka ice rink - 5h period
Compressor power (kW)
80
70
60
50
40
30
20
10
0
3
2
1
0
-1
-2
-3
-4
-5
-6
-7
-8
-9
-10
-11
-12
-13
09:36:00
10:12:00
10:48:00
11:24:00
12:00:00
12:36:00
13:12:00
13:48:00
14:24:00
Time (hr)
Compressor power
Return temp.
Forward temp.
DT
Evap. Temp.

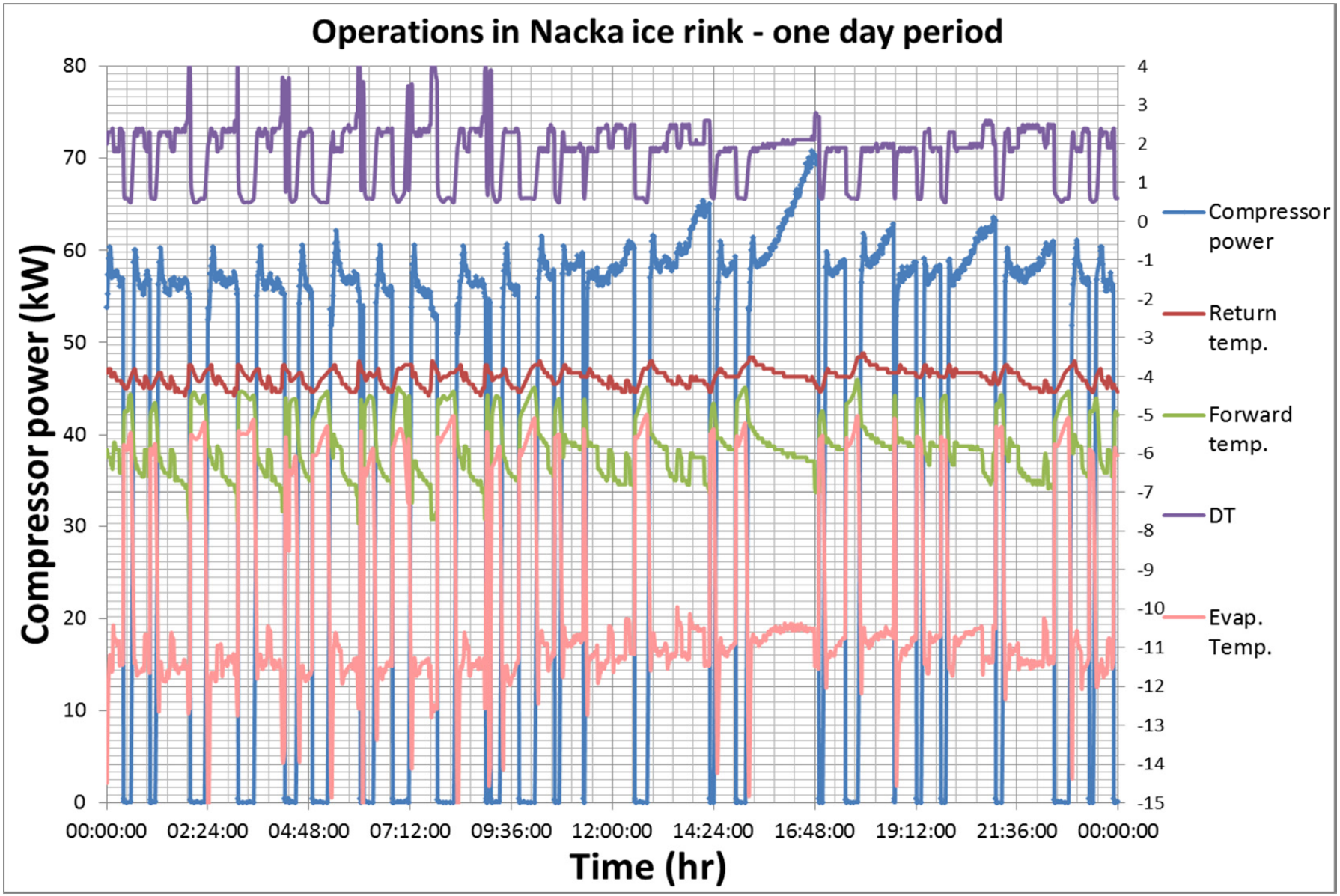
Operations in Nacka ice rink - one day period
Compressor power (kW)
80
70
60
50
40
30
20
10
0
4
3
2
1
0
-1
-2
-3
-4
-5
-6
-7
-8
-9
-10
-11
-12
-13
-14
-15
00:00:00
02:24:00
04:48:00
07:12:00
09:36:00
12:00:00
14:24:00
16:48:00
19:12:00
21:36:00
00:00:00
Time (hr)
Compressor power
Return temp.
Forward temp.
DT
Evap. Temp.

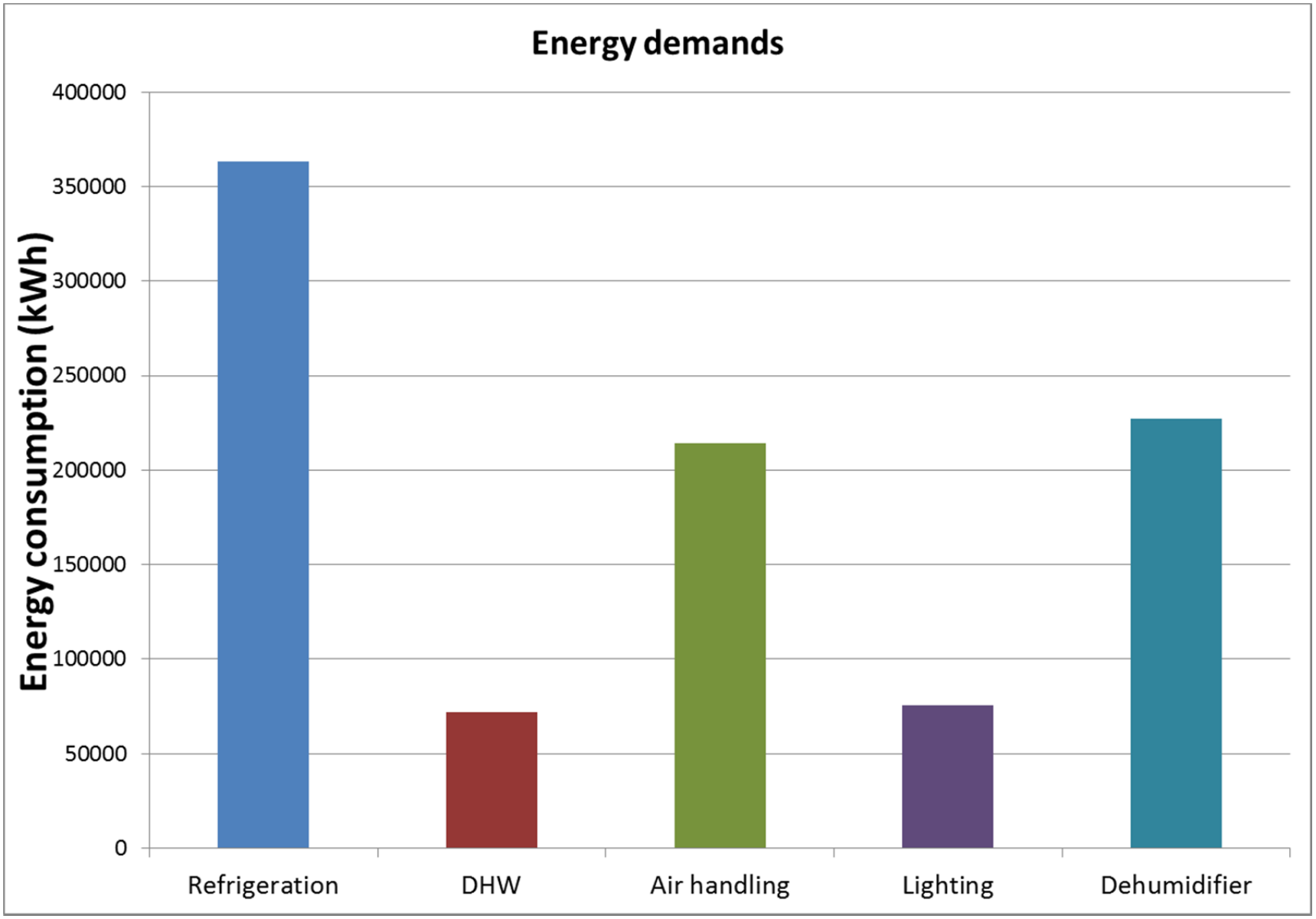
Energy demands
Energy consumption (kWh)
400000
350000
300000
250000
200000
150000
100000
50000
0
Refrigeration
DHW
Air handling
Lighting
Dehumidifier

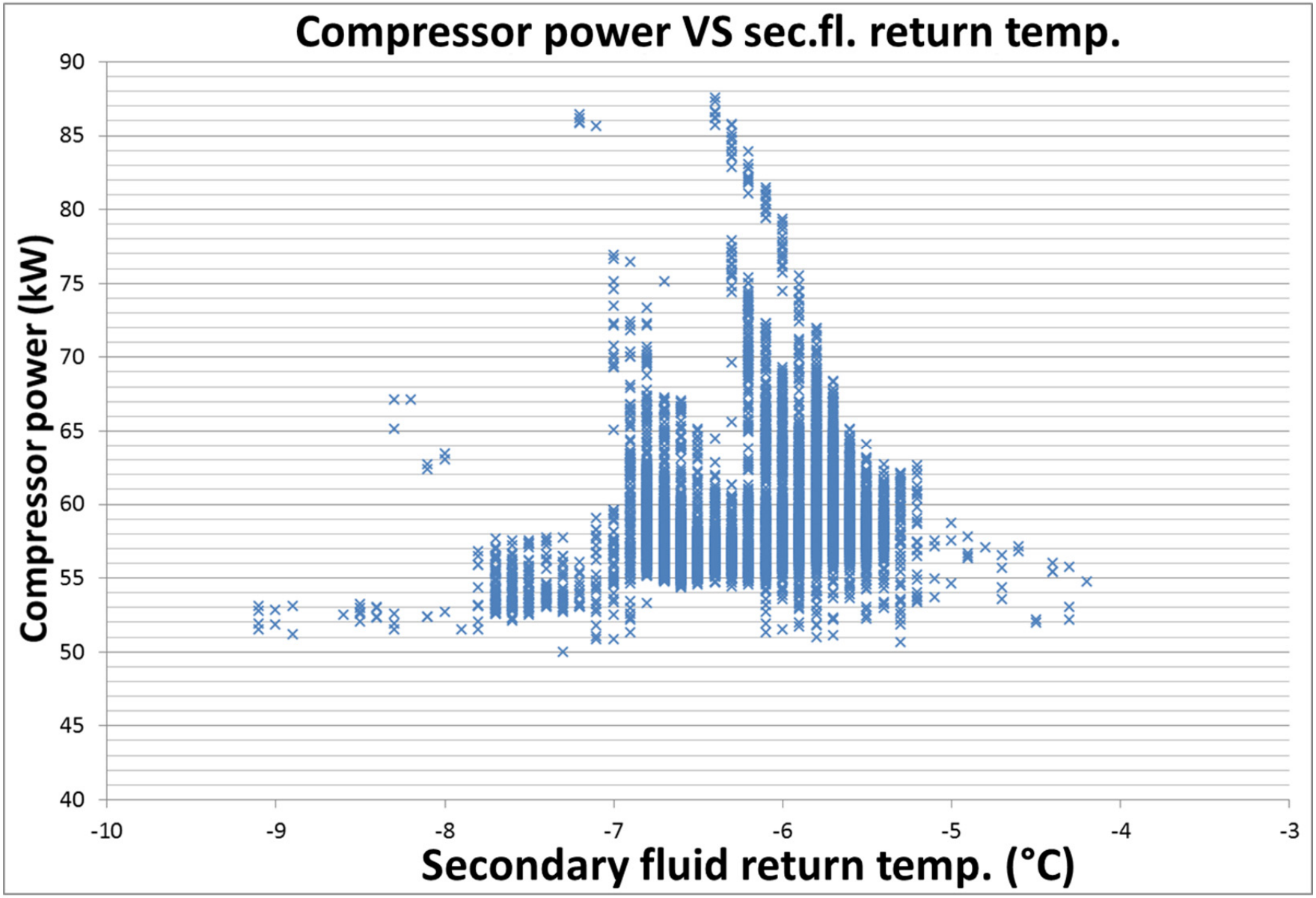
Compressor power VS sec.fl. return temp.
Compressor power (kW)
90
85
80
75
70
65
60
55
50
45
40
-10
-9
-8
-7
-6
-5
-4
-3
Secondary fluid return temp. (°C)